UNIVERSIDAD EAFIT

Engineering School

Design Engineering Research Group (GRID)

Influencing the performance of a Building Integrated low-Concentration Photovoltaic (BICPV) system by adapting an Anti-Reflective Coating (ARC) with a pyramidal texture.

Ing. Santiago Bernal del Río

ADVISOR:

Gilberto Osorio-Gomez, PhD.

February 2021

Abstract

The generation of electric energy from photovoltaic solar energy brings a new opportunity to reduce generation costs, in addition to reducing the emission of greenhouse gases. This type of generation has positioned itself as the most important for renewable energies, especially because of the impact it has had on generation on an industrial scale. However, in the residential sector, different strategies are proposed within the framework of the best use of the available area in order to reduce costs, as is the case of low-concentration photovoltaic concentration systems. This document proposes the development of an Anti-Reflective Coating (ARC) with a pyramidal texture in two dimensions for a V-Trough type photovoltaic concentrator, specifically for a Building Integrated low-Concentration Photovoltaic (BICPV), with the aim of increasing the light capture of these systems due to the loss caused by the rays coming from incidence angles different from the normal surface. For this, a methodology is executed where the concentrator is designed, the material for the Anti-Reflective Coating is determined, the design of the geometry of the texture, and, later, simulations are carried out by means of ray tracing, and experimental validation, where finally data is taken in real time of the generation of the CPV with the texture, and, it is checked how the application of this texture affects in a positive way the generation of the photovoltaic system, with increases of more than 3% in the normalized efficiency.

Keywords: V-Trough, Pyramidal Texture, Anti-Reflective Coating, Ray Tracing, BICPV.

Resumen

La generación de energía eléctrica a partir de energía solar fotovoltaica trae una nueva oportunidad de reducir los costos de generación, además de disminuir la emisión de gases de efecto invernadero. Este tipo de generación se ha posicionado como la mas importante para las energías renovables, sobretodo por el impacto que ha tenido en la generación a escala industrial. Sin embargo, en el sector residencial se proponen diferentes estrategias enmarcadas en el mejor aprovechamiento del área disponible para así disminuir los costos, como es el caso de los sistemas de concentración fotovoltaica de baja concentración. Este documento propone el desarrollo de una Capa Anti Reflectiva (ARC) con textura piramidal en dos dimensiones para un Concentrador fotovoltaico tipo V-Trough, específicamente para un sistema integrado a construcción de baja concentración fotovoltaica (BICPV), con el objetivo de aumentar la captación de luz de estos sistemas debido a la perdida que ocasionan los rayos que provienen de ángulos de incidencias diferentes a la normal de la superficie. Para esto, se ejecuta una metodología en donde se diseña el concentrador, se determina el material para la Capa Anti Reflectiva, el diseño de la geometría de la textura y posteriormente se realizan simulaciones por medio de trazado de rayos y validación experimental en donde finalmente se toman datos en tiempo real de la generación del CPV con la textura y se comprueba como la aplicación de esta afecta de manera positiva la generación del sistema fotovoltaico, con aumentos superior a 3% en la eficiencia normalizada.

Palabras Clave: V-Trough, Textura Piramidal, Capa Anti-Reflectiva, Trazado de Rayos, BICPV.

Personal publications

A scientific article was generated and published during the development process of this research project:

Conference:

- Torres-Madroñero, J. L., Tamayo-Avendaño, J. M., Bernal-del Río, S., Sierra-Pérez, J., Nieto-Londoño, C., Mejía-Gutiérrez, R., & Osorio-Gómez, G. (2020). Formulation and simulation of a hybrid solar PV-wind generation system with photovoltaic concentration for non-interconnected areas to the energy grid. In E3S Web of Conferences (Vol. 181, p. 02002). EDP Sciences.

Acknowledgements

This research has been developed in the framework of the “ENERGETICA 2030” Research Program, with code 58667 in the “Colombia Científica” initiative, funded by The World Bank through the call “778-2017 Ecosistema Científico”, managed by the Colombian Ministry of Science, Technology and Innovation (Minciencias), with contract No. FP44842-210-2018.

Contents

List of Figures

List of Tables

Chapter 1

Introduction

The increase in the demand for electrical energy in the world, added to the questioning of energy generation sources based on fossil fuels, leads humanity to a major challenge and that is to diversify the sources of generation from environmentally friendly means, since, in the world, more than 60% of the energy that is generated comes from polluting sources [EEA, 2013]. However, fossil fuels can produce both economic and environmental problems, because they are limited sources on an anthropogenic scale, in addition to causing phenomena such as climate change, acid rain and damage to the ozone layer [Manzano-Agugliaro et al., 2013]. However, the introduction of NCSRE (Non-Conventional Sources of Renewable Energy) on a global scale in the energy matrix, shows a solution to these sources of electricity and thermal power generation that seeks to reduce the environmental impact from the reduction of greenhouse gases, a problem that can be seen directly related to the emission of gaseous pollutants such as CO_2, methane, etc, or also by means of effects on the ecosystems which can be linked to the destruction of the biosphere, whether marine or terrestrial.

Within the NCSRE we can mention wind, solar, geothermal, biomass and small hydroelectric energy, among others, which have very interesting potentials in different regions of the world, and whose costs have experienced a drastic decrease in the last ten years, [IRENA, 2020], turning them into real alternatives for electricity supply at different scales. Of the different NCSRE, the most widespread, due to their cost-benefit ratio (see Fig 1.1), are solar and wind energy.

Of these two sources, solar energy, in particular, as a fundamental part of the world's sustainable development plans for the immediate future, has become one of the main energy alternatives, given that it is the most abundant source of energy available [Kannan and Vakeesan, 2016]. Furthermore, it can be said that the rest of the energies such as wind and water, among others, are a consequence of solar energy [Hantula, 2010]. In addition, when converting energy into a consumable form, solar energy is the one that requires the least subsequent processes, implying fewer efficiency losses, whether due to mechanical, thermal or chemical factors [Hantula, 2010]. Finally, this resource can be used anywhere on the planet, due to the solar presence in different areas, where clearly for countries located in the tropics represents a source with very high potential [Clifton et al.,

2018].

One of the most important advances that solar energy has had, is that the decrease of its costs is the highest compared to any other type of energy, about 90% since 2009 [IRENA] (See Fig. 1.1).

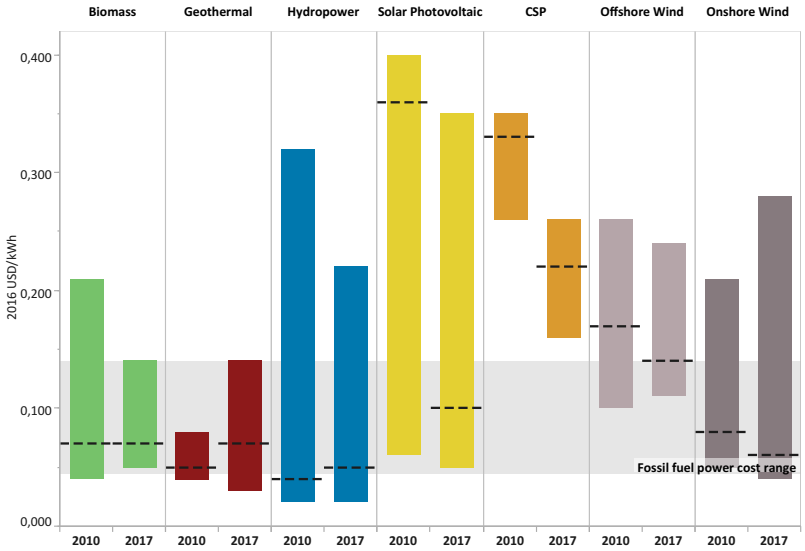

Figure 1.1: *Global levelised cost of electricity from utility-scale renewable power generation technologies 2010-2017 [IRENA, 2018]*

However, the decrease in costs of this is not proportional in all photovoltaic applications, as for the Utility market, i.e. industrial scale cost reduction has been high enough to compete today with traditional sources of generation [Fu et al., 2018]. (see Fig. 1.2). In the commercial and residential market, costs are still high because the "Soft Costs" associated with the value of the land, taxes, appliances such as investors, etc. They do not allow to diminish the costs to arrive at level of Utility [Fu et al., 2018]. One of the main reasons for this is that the effective area of solar gain in a residence is limited by the size of the roof or garden, which does not happen in Utility-Scale, which is directly related to the amount of generation and the costs of the system.

One of the advantages that solar energy has over other generation systems is that passive areas such as urban and rural buildings can be used for the installation of photovoltaic panels to generate electricity more quickly and directly to the end consumer [Fogaing et al., 2019]. This is called BIPV (Building Integrated Photovoltaics) and BAPV (Building Applied Photovoltaics) , so, photovoltaic systems can be implemented integrated into buildings, that is, the design of the photovoltaic system is part of the aesthetics of the building input (Figure 1.3(a)) or applied to buildings, where conventional photovoltaic systems are used and simply assembled in some way to the construction, (Figure 1.3(b)). This is justified by the fact that the area available in cities from buildings, demonstrate an opportunity for solar use as they are large areas without any productive use, which brings a new aesthetic challenge for solar energy.

However, one of the biggest problems with this type of arrangement is the small area and solar time

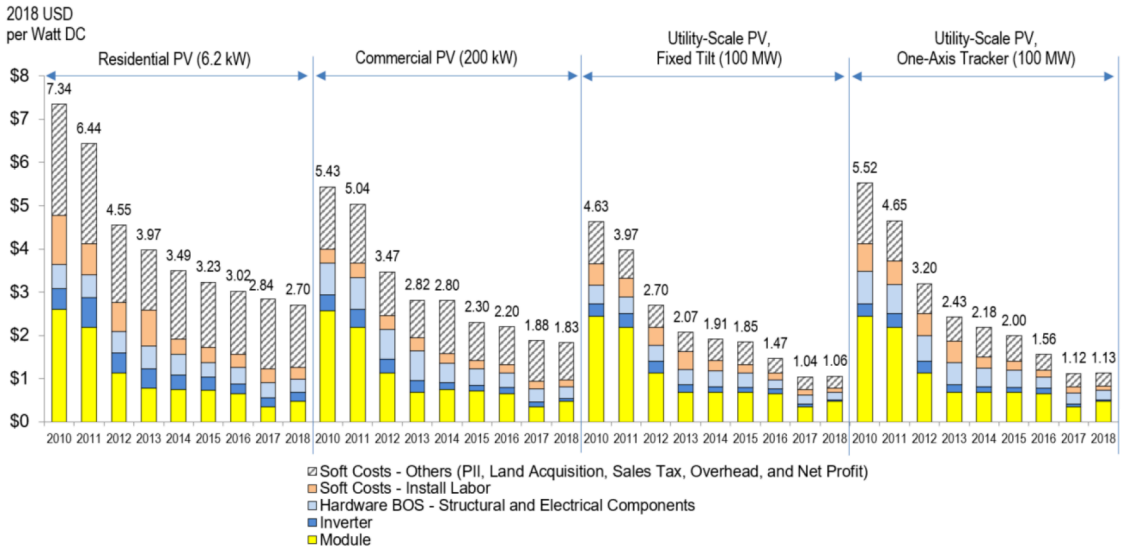

Figure 1.2: *NREL PV system cost benchmark summary (inflation adjusted), 2010–2018 [Fu et al., 2018]*

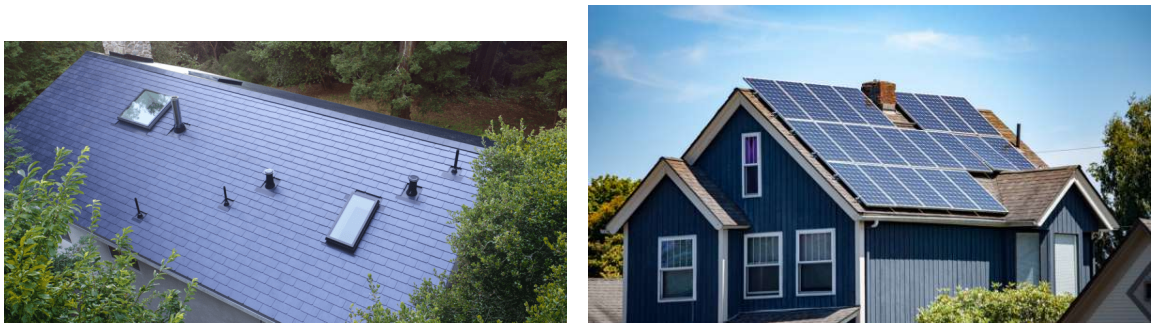

(a) BIPV (b) BAPV

Figure 1.3: *BIPV and BAPV photovoltaic implementation*

available, as in the case of horizontal facades or roofs, where for some cases the amount of solar obstacles can reduce the generation time during the day (see Figure 1.4(b)) and vertical facades where only half a day is solar (See Figure 1.4(a)), which affects generation compared to industrial-scale solar farms. For this reason, CPV (Concentrated Photovoltaics) systems become an attractive option when looking to increase solar gain in places such as building facades or warehouse roofs [Fogaing et al., 2019]. This is because they are able to increase the rate of solar radiation incident through optical materials, which are less expensive than photovoltaic material, allowing to generate more energy with a lower cost [Andrés Arias-rosales, 2017].

Then, there is a need to obtain cost-effective solutions for BICPV and BACPV systems, that is, integrated solutions or applied to buildings with photovoltaic systems, but also adding CPV systems. There is research related to the implementation of BICPV, where emphasis is placed on the development of geometries, that is, different reflector configurations, either using different materials or shapes, or on the design of concentrators

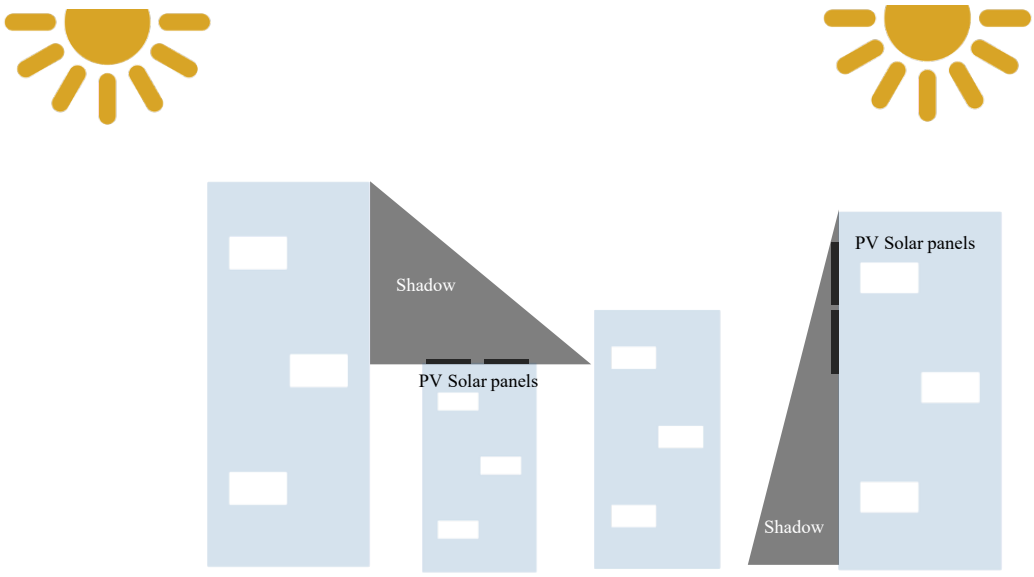

(a) Shadow in horizontal solar panel

(b) Shadow in vertical solar panel

Figure 1.4: *Shadows in different solar applications*

so that they are aesthetic and functional when implemented on facades or roofs [Li et al., 2020]. One of the opportunities found in this research is related to the improvement in the generation in systems of low photovoltaic concentration, because these systems tend to have the best cost-benefit relation, but also those that have less optical effectiveness [Hadavinia and Singh, 2019b].

Consequently, there are different strategies to improve the CPV for installations in buildings [Li et al., 2020], such as thermal use strategies, which is one of the most studied in this field [Lu et al., 2018]. One of the strategies being studied is the dissipation of heat due to high temperatures that have the cells by the concentrators (especially medium and high concentration, meaning concentration factors greater than 10 suns) using this heat as an additional energy source in some cases, for this, several strategies are used, such as pipes that pump water to dissipate the heat from the cell [Xu et al., 2017, Zheng et al., 2016, Xiaodi et al., 2010] or different fluids that allow heat dissipation and usage [Singh and Othman, 2009]. Another strategy is the use of light both to generate electrical energy and to illuminate spaces with natural light, called BICPV/D (Building integrated concentrating photovoltaic/ daylighting) , where it focuses on the design of the reflectors, as is the case of the "Smart Window" which is a window that allows the passage of sunlight to the interior, but that a portion of the light that passes through a thermo-tropic material is redirected to the PV cells [Wu et al., 2016]. Another proposal is found in the facades in which parabolic compound geometries are used, where a percentage of light is allowed to pass to illuminate spaces [Xuan et al., 2019a,b]. Finally, there are works related to optical improvements in the reflectors of the CPVs, where the concentrators are encapsulated in plastic materials with the aim of obtaining improvements in the capture of light by means of optical phenomena such as Total Internal

Reflection [Mammo et al., 2013, Sarmah and Mallick, 2015].

This research is devoted to the application of ARC (Anti Reflective Coating) with pyramidal textures to increase the amount of rays reaching the photovoltaic surface, which are redirected by the concentrators, in order to increase electricity generation and decrease the losses that photovoltaic systems have, due to the direction coming from the rays of the reflectors (See Fig. 1.5).

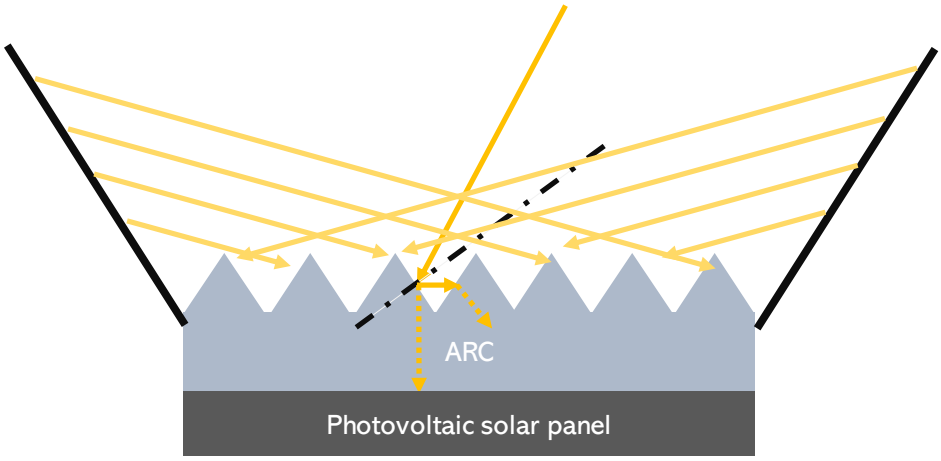

Figure 1.5: *Research proposal*

1.1 Theoretical Background

1.1.1 Irradiance

Power per unit area (W/m^2). This is the magnitude used to describe the incident power per unit area of all types of electromagnetic radiation. In the field of solar energy, normally in peak hours of energy the irradiance at the surface of the earth is approximately 1000W/m^2 with a standard AM 1.5 (Air mass, where the sun is about 41° above the horizon), which refers to the irradiance of the earth at a temperature of 25ºC at sea level [Hernandez, 2014] .

1.1.1.1 Direct Irradiation

It is the one that comes directly from the sun. It refers to the rays that travel in a linear manner without any type of interruption from the sun until they impact the earth. This type of radiation has the highest amount of energy available measured in W/m^2 [Hernandez, 2014] .

1.1.1.2 Diffuse Irradiation

It is the one that comes from the atmosphere by dispersion of the gases that compose it or from the obstacles where the light bounces. On the sunniest days without the presence of clouds this type of irradiation can account

for approximately 15% of the overall irradiation, but on cloudy days, when the amount of direct irradiation is reduced, this type of irradiation increases considerably. The phenomenon of diffuse irradiation is completely stochastic, i.e. random. [Hernandez, 2014]

1.1.2 Solar Spectrum

The solar spectrum is the energy coming from the sun in the form of electromagnetic waves which, depending on their length and frequency, represent a color in the solar spectrum. The longer the wavelength, the less energy it carries. Silicon solar cells are designed to capture wavelengths between 400-700 nm which is known as visible light. [Hasan et al., 2018]

1.1.3 Reflection

Reflection is the change of the direction of the light in the same angle of incidence coming from the same medium. An example is the duplication of images when light hits a mirror and see the reflection of what is in front of it. The equation 1.1 describes the phenomenon according to Snell's laws, where Θ_1 is the angle of incidence of the light rays coming from the source and Θ_2 is the angle of the reflected ray.

$$\Theta_1 = \Theta_2 \tag{1.1}$$

1.1.4 Total internal reflection

Total internal reflection is a consequence of Snell's law where at certain angles (Θ_c), called angles of acceptance, the ray experiences a behavior of total reflection on the material, where n_1 and n_2 are the refractive indexes for the different materials through which the light flows. Described in the equation 1.2.

$$\Theta_c = arcsin(\frac{n_1}{n_2}) \tag{1.2}$$

1.1.5 Refraction

Refraction is the physical phenomenon in light that allows waves to pass through a material (change of medium) and depending on the properties of this, change the angle of light, where Θ_1 is the angle of incidence of the light rays coming from the source and Θ_2 is the angle of the refractive ray. In Snell's law the equation 1.3, is what describes this phenomenon.

$$n_1 sin\Theta_1 = n_2 sin\Theta_2 \tag{1.3}$$

1.1.6 Anti-Reflective Coating (ARC)

The Anti-Reflective Coating (ARC) is responsible for reducing losses by reflection of the solar cell, this because the silicon is a semi-conductor material that has a refractive index of 3.4 which causes that when the rays hit the cell, these are reflected, generating losses in the absorption of light rays. To solve this problem, an ARC Silicon Nitrate layer is used with a refractive index of 1.9, which according to RayLeigh's Law explained in the Equation 1.4 complies with a refractive index indicated to be an ARC, where n_o and n_s are the refractive indexes of the first and second medium respectively and n_1 is the refractive index of the ARC.

$$n_1 = \sqrt{n_o n_s} \tag{1.4}$$

1.1.7 Texturing

Texturing is a process that is done to the material of the solar panels, either the solar cell or the laminate of it, to reduce the losses by reflectance, since there can be losses by reflection of about 40% of the photons that arrive at the cell. These losses essentially affect the device by reducing the short circuit current [LA, 2011].

Texturing processes that are carried out on the laminated or encapsulating layer of the photovoltaic system seek to allow the rays to enter more perpendicularly to the cell, and thus reduce the loss of efficiency that the system has when using completely flat surfaces. This happens because when a ray passes from one medium (air) to another medium (encapsulating material), depending on some variables, it changes its angle.

1.1.8 Concentrated Photovoltaics (CPV)

Photovoltaic concentration tries to replace the cost of large panels with cheap lenses or mirrors, decreasing the area, which lowers the cost in silicon or semiconductor to be used [Andrés Arias-rosales, 2017]. PV systems, as mentioned above, are systems that use optical devices to increase the density of irradiation that reaches the photovoltaic panel [McConnell et al., 2012]. These systems normally work under two principles, reflectance and refractance and are categorized depending on the rate of concentration of irradiation that is capable of emitting into the PV cell, thus dividing into systems of low, medium and high concentration PV, see Table 1.1.

V-Trough Concentrators are low concentration systems, see Fig. 1.6, which use simple optics as mirrors to concentrate the rays towards the photovoltaic surface. This system can be used manually or actuated, which allows for great versatility in terms of implementation costs [Arias-Rosales, 2017].

1.1.9 Ray Tracing

Ray tracing is a technique that allows the generation of computer-simulated images, either by creating 2D or 3D images [Glassner, 1989]. For the specific case of this research, this method allows to see the discrete behavior of each ray simulating the sun, to see its behavior in reflection and refraction, meaning geometric optics.

Name	Optical characteristics			Concentration Ratio			Shape
	Refractive (Coating)	Refractive(TIR)	Reflective	Low	Medium	High	
Fresnel Lens	•			•	•		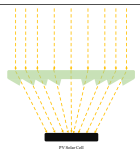
V-trough			•	•			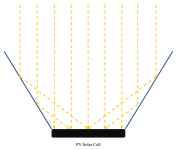
Compound parabolic concentrator			•	•			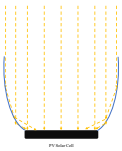
Parabolic dish/trough			•		•	•	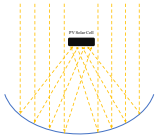
Flat reflector			•	•	•		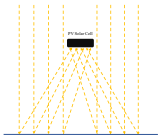
Light-Guide panel			•		•	•	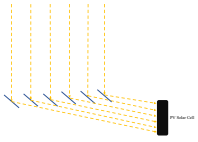
Luminescent/quantum dot	•	•		•			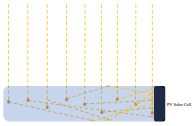

Table 1.1: *Concentrator characterisation table*

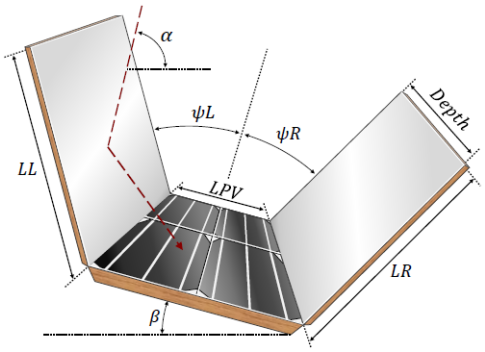

Figure 1.6: *V-Trough [Andrés Arias-rosales, 2017]*

1.2 Research question

What is the effect on electricity generation of a V-Trough BICPV system, implementing an anti-reflective coating with a two-dimensional pyramidal texture on the photovoltaic module?

The focus of this question highlights the application of CPVs in buildings because, as it is presented the introduction, urban contexts, surrounded by buildings or obstacles that prevent the passage of light, limit their generation capacity, representing a problem when implementing concentrating systems. Therefore, the aim is to improve the applications of CPVs in both vertical and horizontal facades, in order to capture as much light as possible.

For these applications, a possible solution could be the pyramidal texturing in two dimensions, since it is a process that in principle is not expensive to adapt to a system like these. Besides, it also complies with the optical principle implemented in solar cells at the manufacturing scale, which is to achieve through the phenomenon of light trapping, reduce the losses by reflection, and try to capture more rays coming at angles of incidence different from those perpendicular to the solar cell.

1.3 Objectives

1.3.1 General objective

To carry out a comparative analysis considering the application or not of an anti-reflective layer, with a pyramidal texture in two dimensions, on a photovoltaic module with a V-trough concentration, through simulation and experimental validation, to determine the effect on electricity generation.

1.3.2 Specific objectives

- To analyze the field of photovoltaic concentration, related to the strategies to increase efficiency using textures with ARC, through a literature review, in order to obtain relevant information about the variables

to be measured and taken into account in the research.

- To determine the characteristics that the textured ARC and the CPV of the case study should have, by means of material selection, manufacturing process and geometry definition, through analysis, simulation and experimentation.
- To represent the behavior of the selected ARC texture in the case of study, by means of ray tracing simulation, to demonstrate its behavior at different angles of incidence of the sun.
- To identify the impact of the integration of ARC textures in CPV systems, based on data collected through experiments and simulations, in order to determine the effect they have on power generation.

1.4 Research Scope

The scope of this project aims to validate the use of an ARC with pyramidal texture on a prototype of a CPV/V-Trough , using a research approach. Simulations of ray tracing and materials research will be developed, and after this, it will be experimentally validated on real prototypes.

1.5 Research Approach

This research was conducted with a focus on a functional product and how to improve its performance. That's why the methodology proposed by Horvath as Research for Inclusive Design [Horvath, 2008] was used. This approach, allows us to understand the context of implementation of the product, determining a design and performing an experimental validation, see Fig. 1.7.

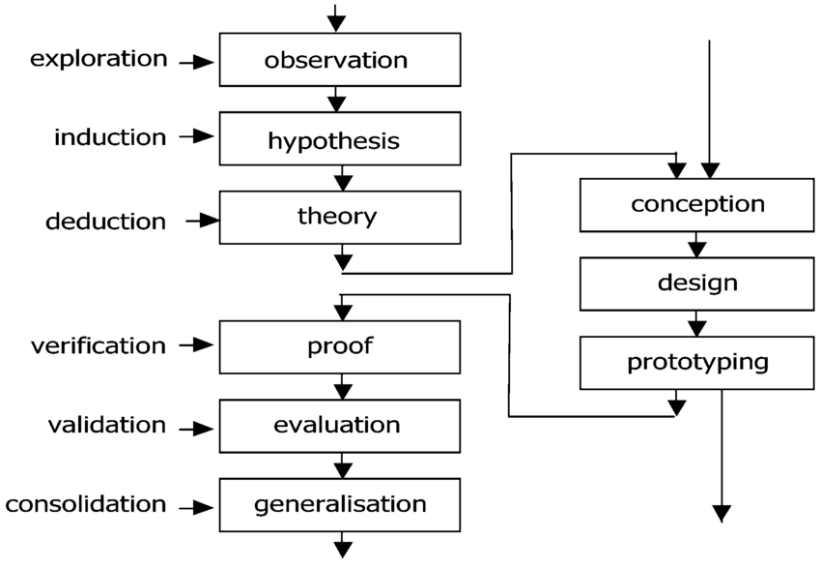

Figure 1.7: *Major phases of design inclusive research [Horvath, 2008]*

1.6 Thesis organization

The structure of this research study is organized in three different phases:

1. First phase. The background, the formulation of the problem, the theoretical framework, the review of the literature, the proposal and the objectives for carrying out the study, are presented in Chapters 1 and 2.

2. Second phase. The formulation of the research proposal, that is, the simulation, formulation and implementation of the proposal, the experimental research, the selection of the sample, the design of the experiment, the execution of the tests, the collection and storage of the data, are presented in the Chapter 3.

3. Third phase. Analytical phase, in which the research is validated through the approach validation, including the analysis results, presented in the Chapter 4.

Finally, conclusions are presented in the Chapter 5.

Chapter 2

State of the Art

Research related to the present work will be analyzed in this chapter, and divided into the following sections.

- Section 2.1. Building Integrated Concentrated Photovoltaics (BICPV): It presents an overview of the state of these technologies and how more efficient devices are reached, specifically related to optical system improvements.
- Section 2.2. Textured: The implementation of textures related to photovoltaic systems and their different applications are considered, including geometries, processes and materials.
- Section 2.3. Ray Tracing: This is a summary look at the ray tracing software and the implementations that have been made with the TracePro software for CPV.
- Section 2.4. State of the Art Conclusions: General conclusions from the literature review and research opportunity are presented.

The literature review of this work are focused on the implementation of arrays that improve the optical efficiency of concentrators, improving the amount of effective rays that reach the solar cells using concentration systems.

2.1 Building Integrated Concentrated Photovoltaics (BICPV)

BICPV systems are devices that can be integrated into the design of facades, roofs, glass, etc. in buildings. These have had a great impact in recent years because CPV systems are very important in conditions where the size or area of implementation is reduced. This is justified by the energy consumption in the construction sector, where it is estimated that about 30% of the electricity consumption comes from this sector [Li et al., 2020]. For Li [2019], an important reason that supports the use of CPV in buildings is the fact that it moves from using a purely functional or architectural structure to a multifunctional that delivers electricity. Around

the developments in this field, most of the concentration systems are focused on low concentration systems without solar tracking systems [Sarmah and Mallick, 2015], where the main type of concentrators are VT and CPC (Compound parabolic concentrator) [Chemisana, 2011].

Li et al. [2015] proposes a mathematical model of a Lens-Walled CPC pattern for a PV/T (Photovoltaic/Thermal) application, where a comparison between simulation and experiments is made. For this, the CPC is designed with an optical arrangement in which a lens is proposed to generate TIR (Total Internal Reflection), with the aim of reducing optical losses and at the same time increasing optical efficiency. These lenses were manufactured in PMMA (polymethylmethacrylate), as can be seen in Fig. 2.1.

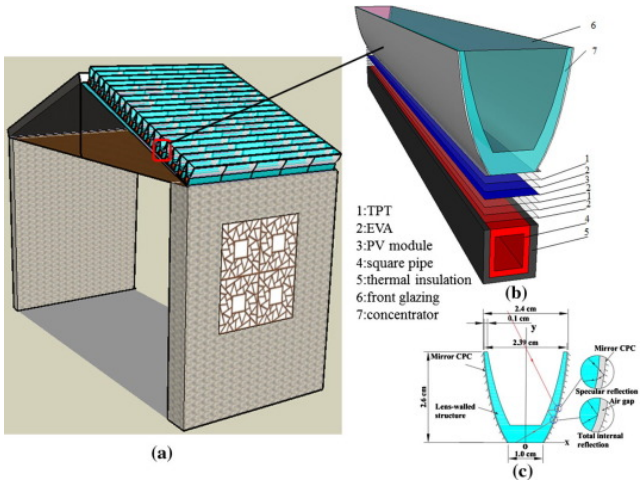

Figure 2.1: *Schematic diagram of the lens-walled CPC for building application [Li et al., 2015]*

After this, Li [2019] proposes the redesign of the "Lens-Walled PC" with a change of the geometry of the concentrator, indicating that usually the PCV systems require the implementation of solar tracking, which has caused that the implementation in buildings is not compatible in most occasions. For this reason, attention has been focused on making smaller scale applications that allow implementation in buildings, Xuan et al. propose the design and development of a "Lens-Walled CPC" with asymmetric geometry [Xuan et al., 2017], where, from the implementation of these asymmetrical lenses, they can achieve greater angles of solar acceptance and also a better distributed flow on the PV cell. In addition, with this type of development, solutions can be achieved with the use of sunlight for indoor lighting. The type of asymmetrical CPC used in the previous illustration has a greater concentration radius with respect to a traditional CPC. This is because the total internal reflection occurs on the curved surface and thus the losses are reduced, where a layer of air is also generated between the lens and the reflector (Fig. 2.2).

Sharma et al. [2015] explains that the BICPV has three main benefits in building integration, the first being generating electricity at the point of use; secondly it allows an efficient use of light within the building on and finally provide thermal management. This research seeks to maintain the operating temperature of the cell and improve its performance by Phase-Changing Materials (PCM). Results in energy conversion efficiency for the

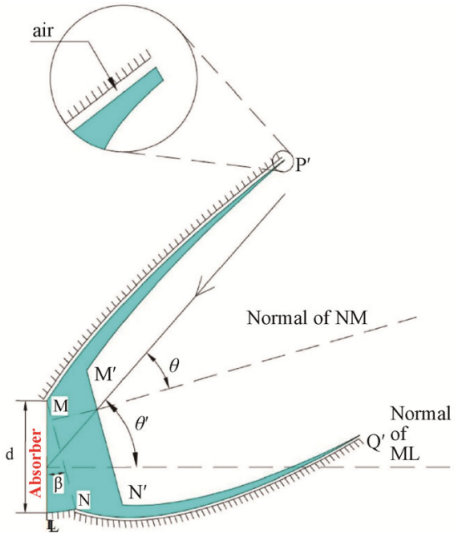

Figure 2.2: *Improved asymmetrical lens-walled CPC [Xuan et al., 2017]*

module without PCM resulted in 7.82% while PCM usage increased by 9.07%, showing a relative increase of 15.9% in comparison, and in turn a reduction in temperature of 5.2°C was observed when the BICPV module was integrated with PCM containment. For this system, a CPC was used where a dielectric material (liquid Crystal Clear® 200 Clear Urethane Casting Resin) was used, which is a super-clear optical material, bonded to the Sylgard® cell envelope to improve optical efficiency. Sarmah and Mallick [2015] proposes the development of a stationary CPV, for which a truncated concentrator is developed with a dielectric material that allows for great durability without affecting the optical losses of the system. For this, smooth-on brand polyurethane was used, which has a refraction index (η) of 1.5, For this, a comparison experiment was conducted between the CPC array and a flat panel system, which yielded results where the CPC was up to 2.27 times more efficient than the flat panel, which shows as a viable option demonstrating increases in generation but also an excellent performance of the dielectric material at different environmental conditions. Xuan et al. [2019c] attempts to validate an efficient form of a low CPV system integrated into a roof, with the aim of collecting maximum solar energy. For this, a comparison is made of a static concentrating photovoltaic/daylighting (CPV/D) in 2D, where the system was designed to leave the bottom of the external parabolas near the base area uncoated to form a "natural light window", against a conventional CPV, the development of the reflector lens was made with PMMA, where the experiment showed gains in energy generation but also in the use of light for the interior lighting of the building.

Hadavinia and Singh [2019a] report an experimental model and analysis of low concentration systems for BIPV /BAPV systems where VT and CPC were simulated with geometric equivalents (See Fig 2.3). It was studied the effect of truncation of CPC and the angles of the side wall of the VT. The light capture improved far beyond the designed acceptance angle compared to the original CPC design and the VT-shaped features exceed the acceptance angles of the original design.

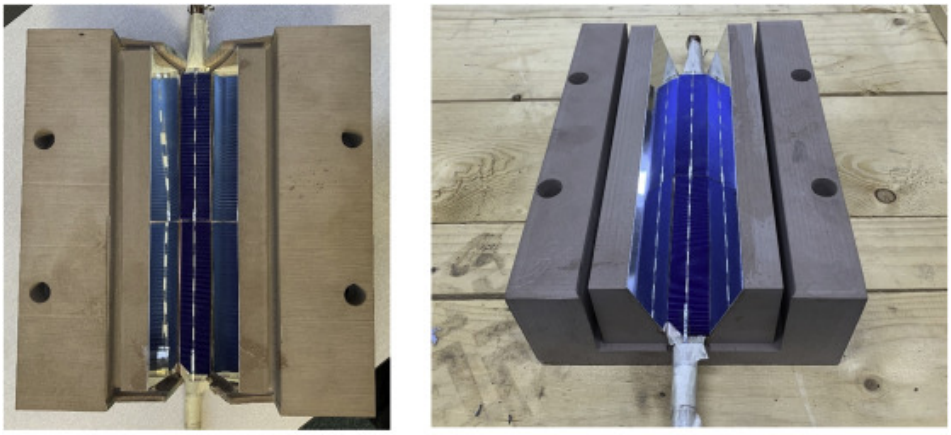

(a) CPC final setup (b) V-trough final setup

Figure 2.3: *Manufactured concentrators with solar cell, copper pipe, heat transfer copper plate and bus-bar junction: (a) CPC and (b) V-trough. [Hadavinia and Singh, 2019a]*

The truncated CPCs showed an optical efficiency equal to conventional CPCs, but a lower concentration ratio due to an equivalent reduction in the size of the entrance opening, i.e. the light entry. The experimentally measured data showed a good correlation with the ray tracing simulation. Researchers conclude that CPC and VT are good candidates for concentrator implementation in BIPV/BAPV applications, due to the cost reduction of these systems, which do not need to track the sun. Both experimental and ray tracing analyses showed that the truncated CPC concentrator achieved 2.4% higher power output compared to the VT design, and that the VT had less incident lightning loss compared to a conventional CPC. Torres-Madroñero et al. [2020] present a case study of the integration of wind generators and photovoltaic systems for a rural area in Colombia. In this case, the generation of the photovoltaic system is optimized by means of a CPV type VT, which as such seeks to reduce the area of generation with the implementation of flat reflectors and in turn increase the electrical generation of the system. In addition, Andrés Arias-rosales [2017] presents a design method for CPV type VT in which he uses genetic algorithms with different objective functions, seeking to minimize costs, maximize generation or minimize space. He uses as case studies applications for small locations. One of the important arguments for this is that he has concluded that the VT concentrators are the most cost efficient, due to the ease of replacing the mirrors and its easy implementation, both in terms of installation and accessibility.

Hamid et al. [2014] propose a system of thermal and photovoltaic use in which it uses CPV/VT with a single reflector for the roof, where they adapt a sheet of aluminum to increase solar radiation in the cell and at the same time have a more uniform flow, because the photovoltaic cell is inclined. The diffuse aluminum reflector shows an increase in solar radiation of over 50%, indicating an increase in the system's electricity generation of 25-35%. In addition to showing it as a cost-effective and easy-to-build solution. Baig et al. [2015] present a polyurethane encapsulated concentrator, which has good light transmission and dielectric properties. For this, a ray tracing and some tests in solar simulator were carried out, where the reflection, refraction and IRR

behavior was looked for. For this, a peak power of 3.7 times was determined with respect to a conventional generation. Mammo et al. [2013] developed a 3D CPC in which they reported an optical efficiency of about 75% experimentally and 94.6% in the simulation. For this purpose, they propose the development of the CPV with a reflector with 96% efficiency and only 4% of losses, and they also implement a superior glass with an anti-reflective layer to reduce the losses.

Something important that can be seen in the analysis carried out so far is that both CPCs and VTs are a good option to be implemented on the roofs of homes or other buildings. One option that could be implemented in the walls of all kinds of buildings located in areas with the necessary features for CPV would be the asymmetric CPCs, which according to Li's design could also be applied to the walls, opens up the possibilities of applying the concept of asymmetry to other CPV systems [Li, 2019].

Another type of implementation of concentrators with an important development in the optical system, are the windows. For example, Connelly et al. [2016] build a "smart window" system (BICPV) consisting of PV integrated in a thermo-tropic layer. It is treated as a glass facade electricity generator. This depends largely on the relationship between the transmittance/reflectance properties and the composition of the thermotropic layer. So, Connelly et al. [2016] propose a polymer of Hydroxypropyl Cellulose (HPC) and hydrogel membrane based rubber with different compositions. For the analysis, benefits in light transmittance and cell temperature were observed. Zhu et al. [2018] designed a window with CPV that allows light to pass through to illuminate interiors, based on Fresnel lenses, where the design focuses on the secondary lens that receive light and transmit it to the cell. For this, a simulation is made by means of the TracePro software, for the ray tracing, and the aim is to reduce the ray deviation with this second concentrator with a prismatic shape.

Based on the analysis of the literature for photovoltaic concentrators, a summary of the main articles analyzed is presented in the table 2.1.

Authors and year	Concentrated type			Concentrator Type			ARC	Textured	BICPV	Model	Simulation	Experiments
	Low	Medium	High	FLC	CPC	V-TC						
Andrés Arias-rosales [2017]	X					X				X	X	X
Shanks et al. [2019]	X				X		X		X		X	X
Al-Shohani et al. [2016]	X					X					X	
Hadavinia and Singh [2019a]	X				X	X			X		X	X
Baig et al. [2015]	X				X		X		X			X
Xuan et al. [2019c]	X				X				X		X	X
Apostoleris et al. [2016]		X		X					X	X		
Burhan et al. [2019]			X	X					X	X	X	
Hamid et al. [2014]	X				X	X			X		X	X
Torres-Madroñero et al. [2020]	X					X			X	X		

Table 2.1: *Analysis BICPV*

It can be analyzed that in most cases low concentration photovoltaic systems are used for applications in construction, this due to temperature issues and because they do not need solar tracking strategies. It is also evident that the most widely used concentrators are the CPC and the VT, this because of the ease in terms of manufacturing and fabrication. Something that should be highlighted is the implementation of new materials to generate lenses concentrators as one of the most implemented improvement strategies and that most strategies

perform simulations either electrical or ray tracing and experimentation for validation.

2.2 Textured

The geometry of a textured cell allows increasing the amount of light that the cell can finally absorb, since the reflection of the rays phenomenon depends on it. This is of great relevance when designing because it defines the angle at which the rays will bounce. It is also important since the rays that bounce off the cell and are reflected can be returned to the cell generating a phenomenon called "Light trapping" [Pociask-Bialy et al., 2018] which happens due to a phenomenon called Total Internal Reflection (TIR).

From the evaluation of the state of the art, it is seen that there is a trend to use as a textured geometry the pyramid shape, this due to manufacturing factors and increased efficiency Takumi et al. [2019], Tsai et al. [2014], Verma et al. [2011], Grunow et al. [2005], Ingenito et al. [2015], Ulbrich et al. [2013], Nam et al. [2008], Escarre et al. [2012], Pociask-Bialy et al. [2018], Campbell and Green [1987], Blieske et al. [2003], ADAM [2014], JOSEF [2004], ZHONGMING [2010], ANDREAS [2016], MIKA [2003] (Ver tabla 2.2).

	Geometry				
Authors and year	Pyramid	Inverted Pyramid	Semi-sphere	Amorphous	Cones
Takumi et al. [2019]				X	
Tsai et al. [2014]		X	X		
Verma et al. [2011]				X	
Grunow et al. [2005]	X				
Ingenito et al. [2015]	X				X
Ulbrich et al. [2013]					X
Nam et al. [2008]			X		
Escarre et al. [2012]	X				
Pociask-Bialy et al. [2018]	X				
Campbell and Green [1987]	X				
Blieske et al. [2003]	X				
ADAM [2014]	X				

Table 2.2: *Analysis of texture geometry*

Tsai et al. [2014] propose the development of an epoxy resin surface as an anti-reflective layer to reduce reflection losses and improve light absorption in solar cell modules. From the simulated results, both the inverted pyramid and the micro-lens structure can improve anti-reflective characteristics of the surface. However, they concluded that the textured pyramid structure can improve the anti-reflection rate by up to 13% compared to non-textured cells, while textures with micro-lenses or semi-spheres can improve the anti-reflection rate by 10% compared to non-textured, under a 15 degree light incidence angle. Blieske et al. [2003], developed a glass for the front cover of the photovoltaic system, allowing a significant reduction of optical losses at the glass-air interface. They used pyramids at 45° where from annual measurements an increase in power generation efficiency of 6% could be determined. In addition, for the relative transmission gain between a flat surface

and a surface with inverse pyramids an increase of 8.1% for diffuse irradiation and 6.1% for direct irradiation is calculated.

In the article of Pociask-Bialy et al. [2018], by means of a chemical treatment, an amorphous textured pattern was made in which the optical properties of eleven glass samples were studied (density of the inclusions, their profile and depth of the etching holes). They were used as a protective layer for the crystalline silicon solar cells. Obtaining a relative increase of 2% of the efficiency of the solar cell for the glass sample of zero incidence degree, demonstrates the improvement of the light retention properties of the studied glass.

Takumi et al. [2019] propose a low cost texture based on a Polydimethylsiloxane polymer with the aim of generating an anti-reflective layer, which allows to increase the current density. For this, the short circuit current density is measured, where increments of up to 21% are observed with 30º incident light. (See Fig. 2.4)

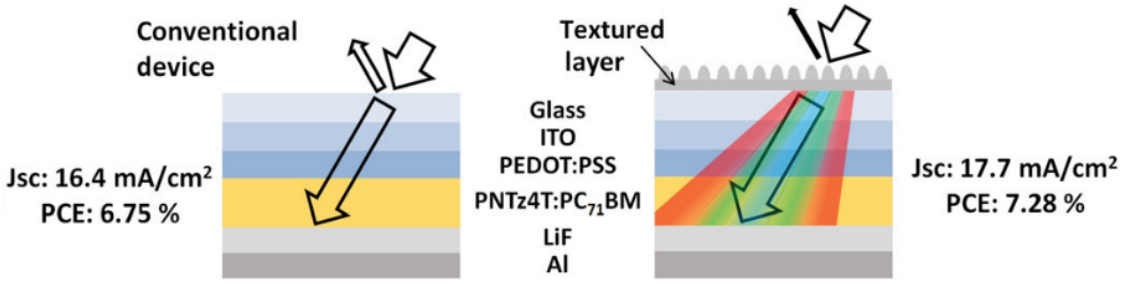

Figure 2.4: *Schematic representations of transmitted light for bare and PDMS-covered PSCs. [Takumi et al., 2019]*

2.2.1 Materials

Tsai et al. [2014] used the epoxy resin for a surface development with anti-reflective coating to reduce reflection losses and improve light absorption in the solar cell modules. The use of glass is very common as different textures are created in combination with flat and textured glass and the corresponding annual energy yields are calculated using a modified data set for hourly irradiation data, which takes into account the angle dependency [Grunow et al., 2005]. A front cover glass was also developed for all types of photovoltaic modules, allowing a significant reduction of optical losses at the glass-air interface Blieske et al. [2003]. Deubener et al. [2009] created a glass for solar protection, containing energy and environmental amortization materials, with adequate compatibility for sustainable energy concepts. Pociask-Bialy et al. [2018] studied the optical properties of eleven samples of chemically treated low iron glass using different texture patterns.

Nam et al. [2008] proposed a lithographic technique for the manufacture of solar cells made of textured crystalline silicon using ordered polymer micro spheres. Takumi et al. [2019] manufactured self-assembled templates to produce textured polydimethylsiloxane (PDMS), that is silicon from which textured coatings can be made. Jalaly et al. [2019] proposed and designed a polymer-based anti-reflective layer (See Fig. 2.5), which can be customized to operate optimally under a specific incidence angle.

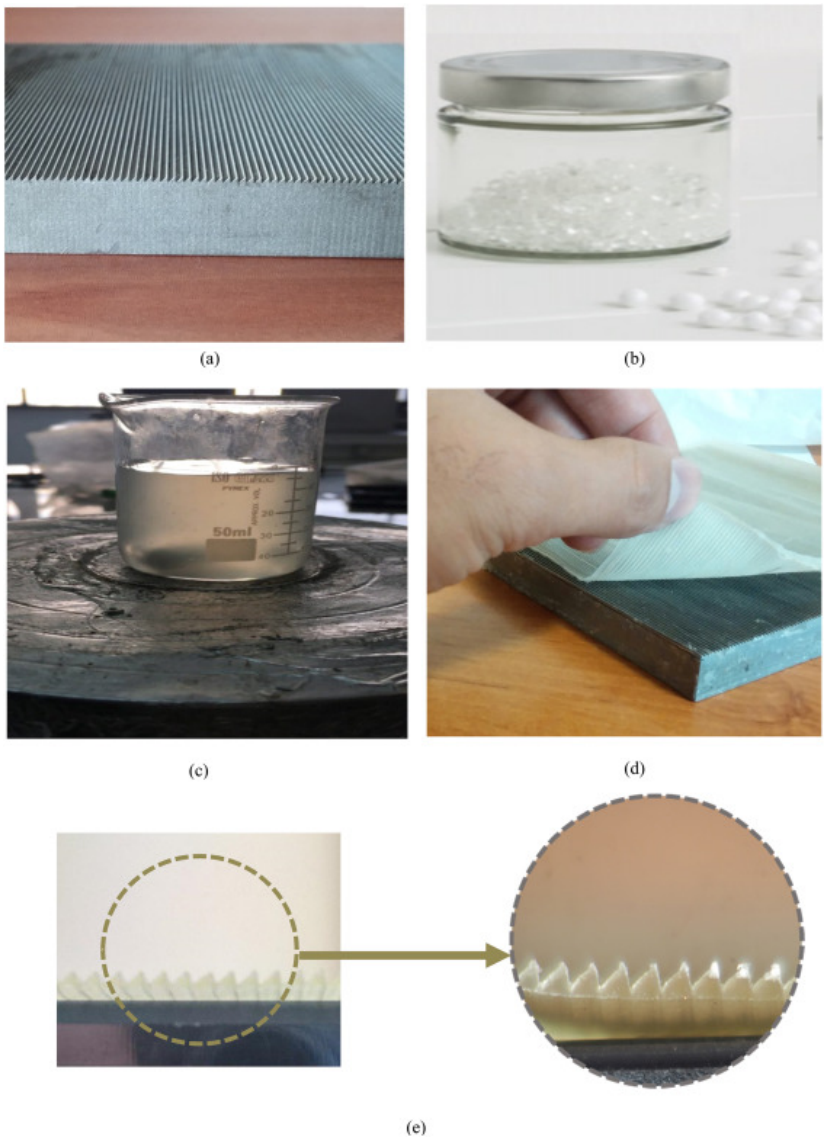

Figure 2.5: *Photos of the fabrication process of the polymer-based periodic ARC: (a) Fabricated metallic mold, (b) TPU granules, (c) The PU solution on the magnetic stirrer, (d) Separation of the PU film from the cooled mold and (e) Final form of the fabricated PU film. [Jalaly et al., 2019]*

The designed coating is manufactured using polyurethane (PU) as a transparent polymer in a low cost process. The performance of this material was verified under outdoor test conditions, where the Anti-Reflective Coating (ARC) was used to improve the conversion efficiency of a glass-covered silicon solar cell. The experiments show an increase of 5.6% in the electrical generation under outdoor conditions of a glass-covered silicon (Si) solar cell equipped with the ARC design under the target incidence angle (30°). This was compared to a cell with an ARC of the same material, but without texturing.

2.2.2 Processes used for texturing

This section presents a summary of the processes used to create textured surfaces, considering that not all of them are reported. Most of them are carried out through chemical processes. It is important to emphasize that the processes where molds are used to deposit the material and to give form to the texture are less common, nevertheless there are several works that explain them.

Blieske et al. [2003] reported the manufacture of a glass by means of an industrial melting process with extra white glass material, which allows an annual improvement of 3.1% with an incidence angle of 90°, and, of 9.4% with an angle of 60° with respect to a flat glass. In addition, this was tested in a silicon cell for 9 months without any problems. Since the texturing process shows significant evidence of increased efficiency of photovoltaic systems, the industry has begun to offer this type of product for implementation in solar panels.

Pociask-Bialy et al. [2018] proposed the experiment of texturing glass from a chemical process, using an Anti-Reflective Glass provided by D.A.Glass Company, Poland. The Anti-Reflective characteristics achieved by this glass are not achieved by applying more layers, but by the chemical treatment given to the glass itself, thus achieving an increase in efficiency of up to 2%.

Saint Gobain Glass, is a glass company which also has products aimed at the solar photovoltaic industry, some of these have texturing processes to increase the efficiency of such systems. Grunow et al. [2005] made an evaluation of the influence of textured surfaces with this type of glass in cells and photovoltaic modules. They report an increase of 3.5% of the efficiency. In addition, a search was made for the characteristics of the glass, which are called Securit Albarino S and Securit Albarino, which obviously have characteristics designed for photovoltaic systems as pyramids ranging from 1mm to 2mm wide, also, they handle a thickness of glass of 3 mm which is normally used and they say that they have products of high transmittance.

Based on the analysis of the literature for texturizing, a summary of the main articles analyzed is presented in the table 2.3. This software has been selected for the development of this research.

Authors and year	Texture Shape				2D	Material	Symmetrical	ARC	Model	Simulation	Experiment	BIPV
	Shpere	Pyramid	Amorphous	Other								
Tsai et al. [2014]	X	X				EPOXY	X	X		X		
Takumi et al. [2019]			X			PDMS		X		X	X	
Jalaly et al. [2019]		X			X	TPU		X			X	X
Pociask-Bialy et al. [2018]				X		GLASS				X	X	
Verma et al. [2011]			X			GLASS				X	X	
Nam et al. [2008]	X					PDMS		X		X	X	
Escarre et al. [2012]		X				GLASS				X	X	
Grunow et al. [2005]				X		GLASS	X				X	

Table 2.3: *Texture analysis*

From the analysis summarized in the table 2.3, it is mainly found that the textures are made on the photovoltaic glass of the panels and that in the cases where they are implemented, it is on high cost solar panels. There is no evidence of any work related to using textures to improve the optical efficiency of the solar panel when concentrators are used.

2.3 Ray Tracing

This section contains an analysis of articles using the TracePro software for the ray tracing method, summarized in the table 2.4.

Authors	CPV Simulations	PV Simulations
Hosseinzadeh et al. [2019]	X	
Zhu et al. [2020]	X	X
Antonini et al. [2013]	X	
Bodhanker et al. [2016]	X	
Gong et al. [2017]	X	
Nicol [2016]	X	
Pavlovic et al. [2014]	X	
Jafrancesco et al. [2018]		X

Table 2.4: *Tracepro Simulations*

Hosseinzadeh et al. [2019] performed the simulation of a CPV/Collector Plate with the aim of evaluating the optical complexity of the system,using the software TracePro, where a study of physical parameters in the receiver cavity was made, showing positive results related to the optical performance of the system. Zhu et al. [2020] studied the behavior of a BICPV evaluating, by means of ray tracing, the effect that the glass that encapsulates the concentrator has on the performance of the concentrator. For this, they made a transmittance analysis and compare it to a system with CPV, obtaining as a result a better performance in the use of CPV. Antonini et al. [2013] performed a simulation on a 3D CPC with the aim of determining the uniformity of the flow, and proposing different solutions related to increase the angular tolerances of the system.

Bodhanker et al. [2016] described an experimental setup, for which a collection of real solar irradiance data was performed for a solar panel with and without a mirror, and, then, a simulation was performed in TracePro to determine the distribution of the reflected irradiation on the panel. The results show a correlation in the area of the panel where there is more irradiance and suggest the implementation of panels with reflective mirrors (See Fig. 2.6).

Pavlovic et al. [2014] simulated a parabolic concentrator composed of PMMA, where a receiver is modeled in order to study the influence of the cavity. For this purpose, a light path is determined, simulating the path of the sun during the day, in order to calculate the power obtained by the receiver.

From the observed studies, it is determined that the software TracePro is able to make a ray tracing analysis as a goal of this research. Among some of the studies it is evident the importance of correctly simulating the properties of different materials, geometries and complex systems of CPV.

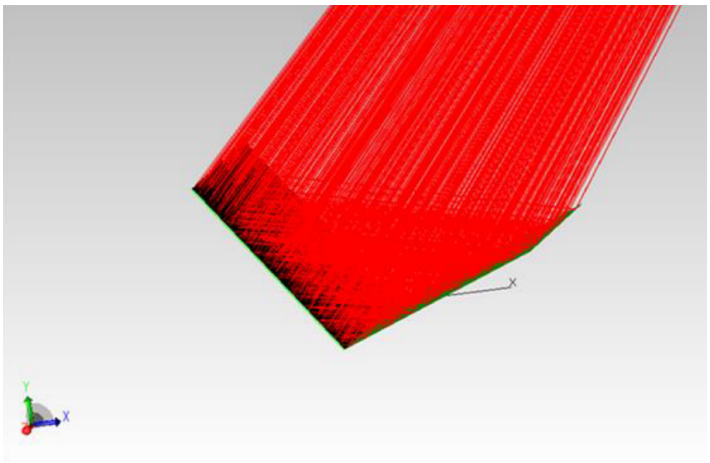

Figure 2.6: *Raytrace of Mirror Augmented Photo-Voltaic with point source sun. [Bodhanker et al., 2016]*

2.4 General conclusions for the State of the Art

- There are no studies relating the influence of textured in ARC on PV concentration as a strategy to increase the generation of PV systems, showing that it is a relevant research topic, since it is seen the importance of implementing BICPV systems and identifying improvements in these systems.
- About 80% of the articles of textures, speak of this method applied to glass and not to ARC.
- 90% of the concentrators used for BIPV are low concentrated photovoltaics systems of which CPC is 70% and V-trough is 30%.
- The measurement variables identified in the state of the art for experiments with texture iare related to current density and for simulation the power flux.
- The TracePro software is determined to be a valid tool for the simulation of the proposed problem for this research, due to its repeated use in different scientific articles and in some VTs.

Chapter 3

Proposed Approach

The aim of this chapter is to present the model that is going to be simulated and experimented, proposing the adaptation of an ARC with pyramidal texture on the solar panel of a CPV/VT. For this reason, the selection of the type of concentrator and the principle governing textured ARC is explained below. The methodology in the Fig. 3.1 is presented to validate the behavior of textures in the concentrators.

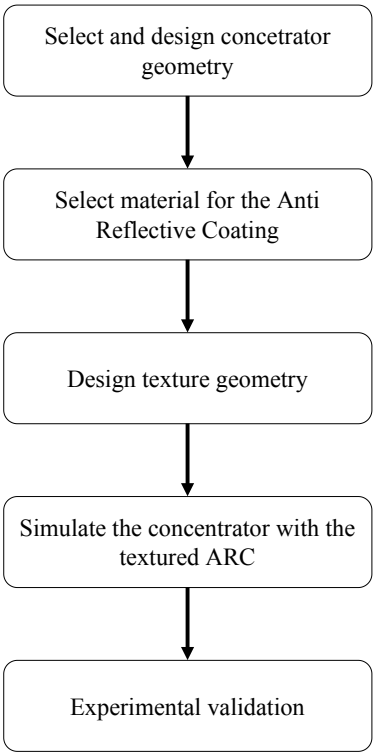

Figure 3.1: *Proposed method*

This chapter is organized as follows:

- Section 3.1 Select and design concentrator geometry: the geometry of the concentrator is selected according to the different applications it is intended for and the tools used to design it.
- Section 3.2 Select material for the Anti-reflective Coating: the properties of different materials that can be suitable for the use in the ARC are explored, in addition to a brief explanation of the functionality of the Anti-Reflective Coating.
- Section 3.3 Design texture geometry: different iterations of pyramidal textures are generated, with the aim of determining the angle of the geometry, using the method of ray tracing and taking into account the properties of different materials.
- Section 3.4 Simulate the concentrator with the textured ARC: description of the parameters required to perfom the simulation of ray tracing for CPVs with the textured ARC, in order to evaluate the effect that textures have on the concentrator.
- Section 3.5 Experimental validation: the construction of the prototypes, the design of the experiment and how the data collection is carried out.

3.1 Select and design concentrator geometry

For this work, the V-Through concentrator was selected because, as it was analyzed in Chapter 2, this is the CPV with the best cost-benefit ratio, its parts are easy to replace, and, being a low concentration system, it does not affect the temperature of the cell as much as other concentrators [Maiti et al., 2012, Bahaidarah et al., 2015, Fraidenraich, 1992, 1998].

At the time of the design or arrangement of the mirrors of the concentrator, it was done from the design of a horizontal and a vertical concentrator system, since the problem is focused on the residential sector, where both surfaces have applicability for this proposal. Therefore, different iterations were made in the angle of the mirrors with respect to the panel, as well as in the use of discreet solar tracking of 3 positions (that is, without motor for movement), with the objective of determining a cost efficient design that can be applied to the residential sector[Andrés Arias-rosales, 2017].

Then, the first step is to perform the geometric design of the concentrator in the VTdesign®software, where certain features are defined as inputs for the software. Among the most important entries to define in the design software are the length of the panel (I_{PV}), the length of the right (L_R) and left (L_L) mirrors, the tilt angle of the right (M_R) and left (M_L) mirrors, the elevation angle of the PV panel ($\beta = 0$) for horizontal, the costs of the panel (taken from the supplier), the costs of the glass and the structure [Sangani and Solanki, 2007], all this in dollars per square meter (USD/m^2), the elevation path of the sun on site ($0 < \alpha < 180$), the reflection index of the mirror ($\rho = 0.92$), and, finally, adjusting the system to certain times of the day if manual sun tracking is to be used, where (β_i) is the starting angle, ($\beta_{\alpha s}$) is the step in α, and, (β_s) is the variation in degrees of each step.

Later, to determine or select the concentrator, different iterations are performed with different dispositions of the angles of the mirrors, see Table 3.1 for the horizontal concentrator, and, Table 3.2 for the vertical concentrator. The aim is to find the best value for each of the applications in terms of profitability or cost efficiency index (I_{COE}), and, also, values related to usable area and effective concentration, which refers to the real value of irradiation that is reaching the cell.

Horizontal V-Trough Iterations

- **Iref.** It is the reference panel without any type of concentrator or solar tracking system.
- **Ia.** It is the panel with the V-Trough concentrator with the mirrors at 25°, but without the solar tracking system.
- **Ib.** It is the panel with the V-Trough concentrator with the mirrors at 30°, but without the solar tracking system.
- **Ic.** It is the panel with the V-Trough concentrator with the mirrors at 45°, but without the solar tracking system.
- **Id.** It is the reference panel without any type of concentrator and with solar tracking in three positions.
- **Ie.** It is the panel with the V-Trough concentrator with the mirrors at 25°, but with the solar tracking system.
- **If.** t is the panel with the V-Trough concentrator with the mirrors at 30°, but with the solar tracking system.
- **Ig.** It is the panel with the V-Trough concentrator with the mirrors at 45°, but with the solar tracking system.

Parameters horizontal VT						
Set-up	$I_{PV}(m)$	$L_L(m)$	$L_R(m)$	$M_L(^\circ)$	$M_R(^\circ)$	$\beta_i, \beta_{\alpha s}, \beta_s(^\circ)$
$Iref$	1	0	0	0	0	No Tracking
Ia	1	1	1	25	25	No Tracking
Ib	1	1	1	30	30	No Tracking
Ic	1	1	1	45	45	No Tracking
Id	1	0	0	0	0	60,60,-60
Ie	1	1	1	25	25	60,60,-60
If	1	1	1	30	30	60,60,-60
Ig	1	1	1	45	45	60,60,-60

Table 3.1: *VTDesign horizontal parameters CPV*

Vertical V-Trough Iterations

- **IrefV.** It is the vertical reference panel without any concentrator

- **IaV.** It is the panel with the V-Trough hub, with the right mirror at 80° and the left one at -15°
- **IbV.** It is the panel with the V-Trough hub, but completely at 90°.
- **IcV.** It is the panel with the V-Trough hub, with the right mirror at 80° and the left mirror at 0°

Something important in terms of the iterations for the vertical concentrator, is that the position of the concentrator was defined always fixed, this because as it is thought for a vertical disposition, there are no possibilities of follow-up not any angles of inclination of the system.

Parameters vertical VT						
Set-up	$I_{PV}(m)$	$L_L(m)$	$L_R(m)$	$M_L(^\circ)$	$M_R(^\circ)$	$\beta(^\circ)$
$IrefV$	0.156	0	0	0	0	90
IaV	0.156	0.156	0.156	80	-15	90
IbV	0.156	0.156	0.156	25	25	90
IcV	0.156	0.156	0.156	80	0	90

Table 3.2: *VTDesign vertical parameters CPV*

3.2 Select material for the Anti-Reflective Coating

For the selection of materials, an investigation of different optical properties and weathering resistance of different materials is made in order to determine which of these is the right one to implement in the texture, this because the ARC has the ability to reduce the losses by reflection that has the PV panels [Stapiński et al., 2012]. This selection is made taking into account the Anti-Reflective coating phenomenon (see Fig. 3.2), which is calculated with the equation 3.1, where the ideal materials to generate an ARC must have a refractive index similar to the reference, since finding a material with the exact value is difficult especially for the manufacturing phase; for this it is understood that n_1 is the refractive index of the ARC, n_0 the refractive index of air, and, n_s the refractive index of PV glass.

$$n_1 = \sqrt{n_0 n_s} \tag{3.1}$$

To validate this effect, it is necessary to determine the characteristics that the texture to be implemented in the photovoltaic panel must have, based on the selection of the ARC material through analysis, simulation and experimentation.

3.3 Design texture geometry

In this section an iteration of different texture angles is performed to determine the best geometries by testing them in a commercial panel by means of ray tracing software, in order to find the best angles to implement in the ARC. For this, a ray tracing analysis was carried out considering the textures presented in the Fig. 3.3.

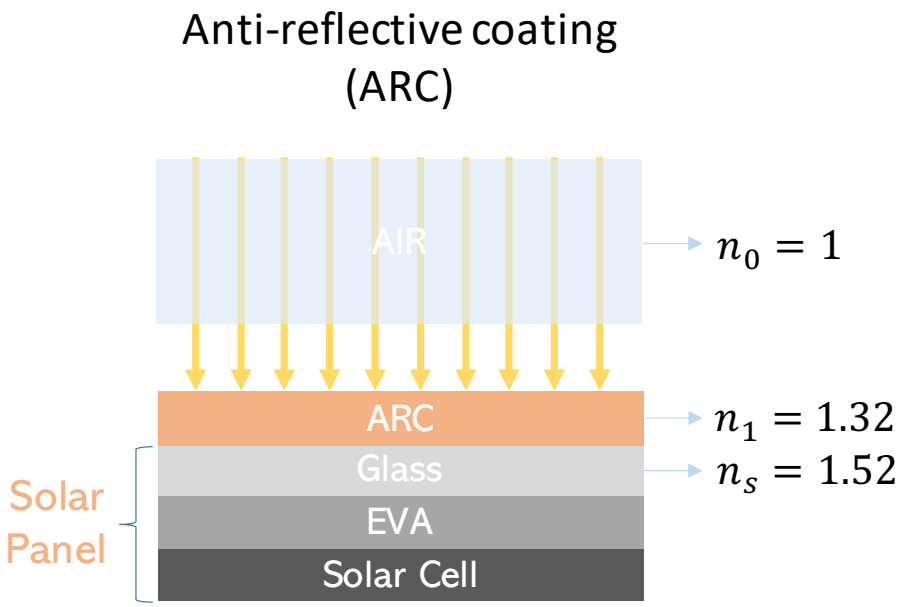

Figure 3.2: *Diagram of Anti-reflective, considering the different layers of a photovoltaic panel (Solar Cell, EVA (Ethylene-vinyl acetate) and Glass).*

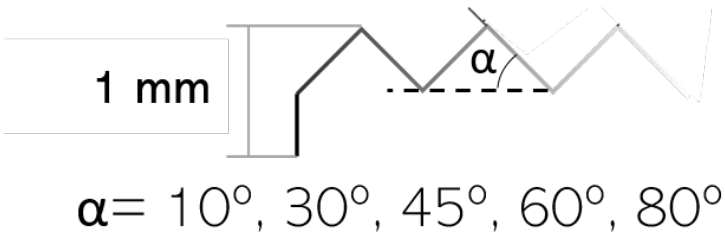

Figure 3.3: *Simulated textures by ray tracing*

Simulation for texture design

For the definition of the geometry of the texture, the ray tracing method is used, which allows to calculate the behavior of the rays, by means of geometric optics with the properties of the materials and the shapes of the geometry. To do this, multiple softwares could be used, but in this research the software TracePro, from Lambda Research, is used. This is a software that as explained in the state of the art, is frequently used for problems related to photovoltaic systems. For the simulation, a model with the real layers of a solar panel is proposed, as it is shown in the Fig. 3.4.

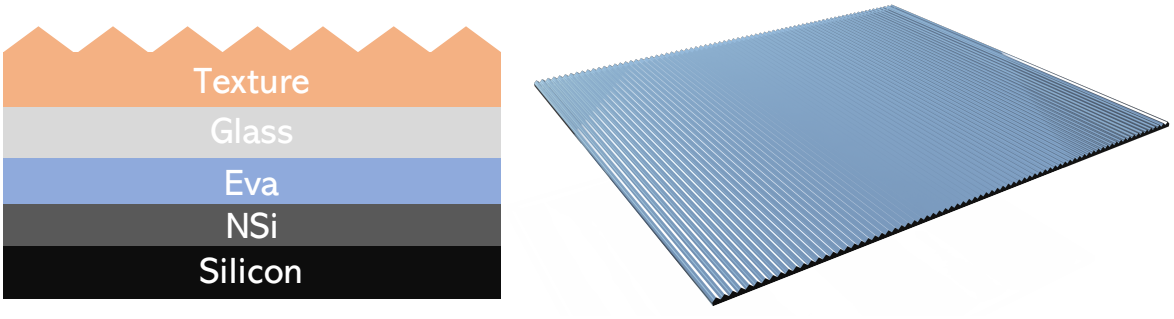

Figure 3.4: *Model used to simulate texture*

After this, a simulation is performed with the objective of comparing the best texture of the ARC with the chosen materials, compared to an ARC without texture but with the chosen materials, in order to determine the influence of texturing the ARC.

3.4 Simulation of the concentrator with the textured ARC

This section explains how the simulations of the CPV and the textures with different materials and configurations were carried out in the software TracePro®. The characteristics that the materials to be simulated must have, are determined according to the components presented in the Fig. 3.5.

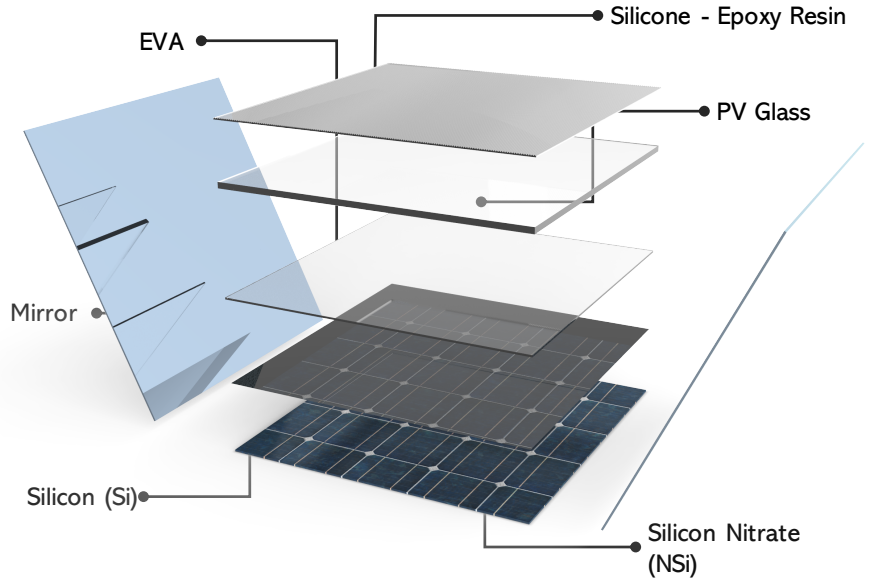

Figure 3.5: *Exploded view of the simulation model*

The firs step is to determine the characteristics of the materials for the wavelengths of the visible spectrum, where the corresponding ranges of 0.4μm - 0.7μm, with a step of 0.05μm, are determined. For this, the refractive indices of silicon [Aspnes and Studna, 1983], silicon nitride (NiS) [Vogt, 2016], ethylene-vinyl acetate (EVA) [Vogt et al., 2016, Vogt, 2016], PV glass [Vogt et al., 2015, TREHARNE et al., 2011], and, ARC materials (Silicone and Epoxy Resin) [Schneider et al., 2009] were found, as it could be observed in the table 3.3.

	Refractive Index						
Wavelenght (μm)	**Silicon**	**Silicon Nitrate**	**EVA**	**Photovoltaic Glass**	**Epoxy**	**Rtv_ Silicone**	**Sylgard_ Silicone**
0,4	5,62	2,18	1,50	1,52		1,44	1,44
0,45	4,63	2,15	1,50	1,51		1,44	1,44
0,5	4,28	2,12	1,49	1,51		1,43	1,43
0,55	4,07	2,10	1,49	1,51	1,49	1,43	1,43
0,6	3,93	2,09	1,49	1,5		1,42	1,43
0,65	3,83	2,08	1,48	1,5		1,42	1,42
0,7	3,76	2,07	1,48	1,5		1,42	1,42

Table 3.3: *Refractive index table*

Two types of silicones were used for this, since according to the literature there are different types of silicones with good optical properties.

After the selection of materials, the simulation conditions are determined, where they must define the parameters to simulate the irradiance. For this, the dimensions that the sun would have with respect to the concentrator and the height of simulation are determined, as it is observed in the Fig. 3.6. This should be considered because it must ensure that, for the inclination of the sun, simulating the path during the day, all rays always make contact with all surfaces of the concentrator, i.e. the mirrors and cells.

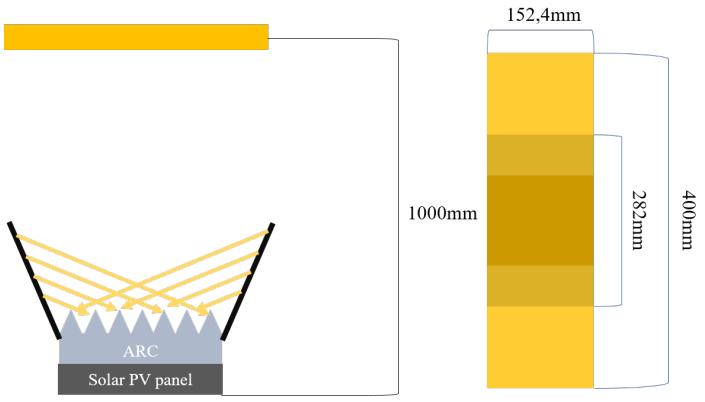

Figure 3.6: *Photovoltaic concentrator and sun measurements*

After obtaining the measurements of the sun with respect to the CPV, an analysis of the amount of rays is made to determine which is the ideal value of rays where the results are not affected by noise. For this, the

simulation with the conditions described above in a range between $10 - 1,000,000$ of rays is carried out in order to find the value of power in Watts where the curve begins to converge, as it is observed in the Fig. 3.7.

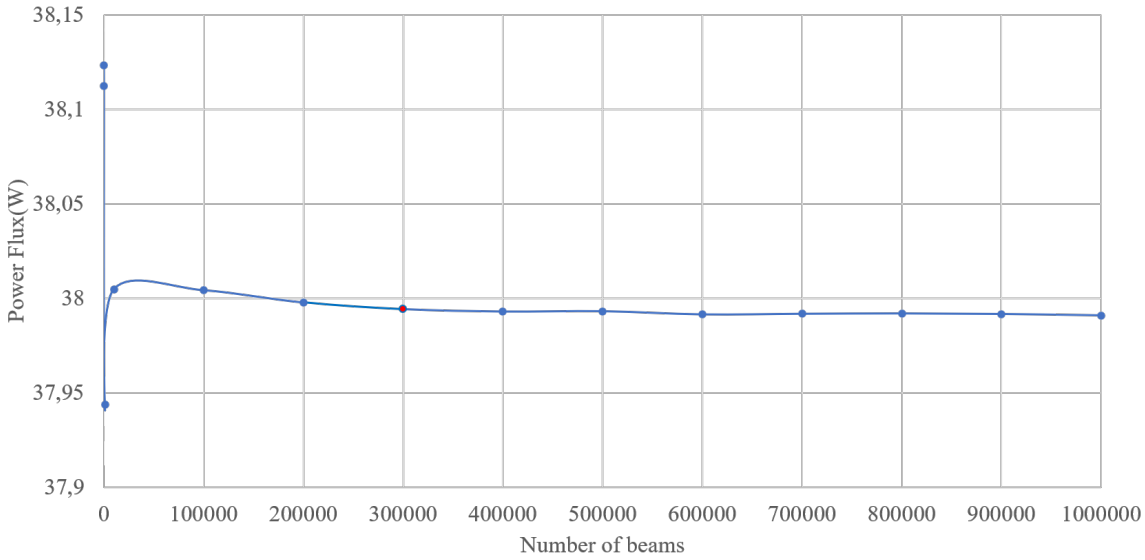

Figure 3.7: *Convergence curve of beams*

The Fig. 3.8 illustrates the variation with the increase in the number of lightning strikes, and the simulation with 300,000 rays, the one surrounded with the blue line box, is the one that, according to what it is observed in the Fig. 3.7, the curve converges, and a much more uniform flow distribution is observed, therefore this value is determined to perform the simulations.

Finally, it is determined to make the simulation for the visible light spectrum, because this portion of the spectrum is the one that mostly uses the silicon PV panels [Ali et al., 2014]. Therefore, the solar spectrum is extracted, and, from a moving average, the values between 400nm and 700nm are determined with a step of 25, as it is observed in the Fig. 3.9.

From this, a weighting of the wavelengths determined by the moving average is made, giving a weight to each value being 550 the value 1, since it is the greater, and the rest of values calculated with respect to this, as it is seen in the Table 3.4. This allows to obtain the discrete spectrum to enter it within the software TracePro, in ordet to make the simulation with values of standard irradiation of 1000 W/m^2.

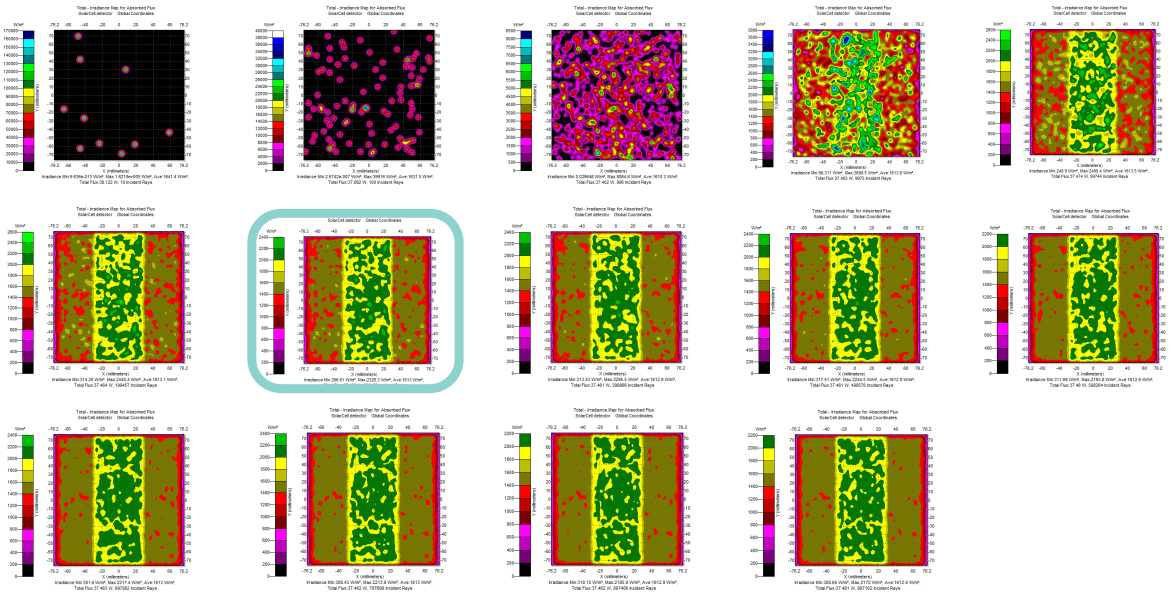

Figure 3.8: *Lightning Flow Distribution Illustration*

Wavelength (nm)	Mobile average	Weight
400	5.1403E-01	0.380
425	9.2482E-01	0.684
450	1.1596E+00	0.857
475	1.3048E+00	0.964
500	1.3377E+00	0.989
525	1.3295E+00	0.983
550	1.3529E+00	1.000
575	1.3458E+00	0.995
600	1.3224E+00	0.977
625	1.3140E+00	0.971
650	1.2842E+00	0.949
675	1.2579E+00	0.930
700	1.1775E+00	0.870

Table 3.4: *Wavelength weighting*

After determining the parameters for the simulation of direct irradiation, a simulation with diffuse irradiation is also performed where a dome is generated for a cloudy sky, as it is observed in the Fig. 3.10. This dome is calculated from the equation 3.2, which describes the intensity of illumination ($\frac{L_{oc}}{L_{zoc}}$) for each incidence angle (θ) of the generated dome.

$$\frac{L_{oc}}{L_{zoc}} = \frac{1+2sin(\theta)}{3} \tag{3.2}$$

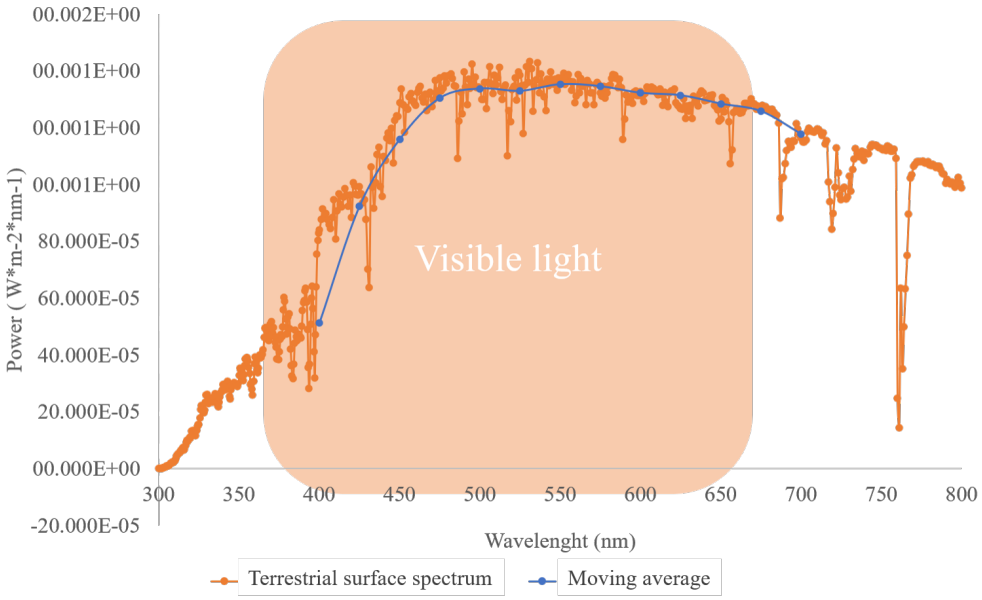

Figure 3.9: *Concentrator measurements*

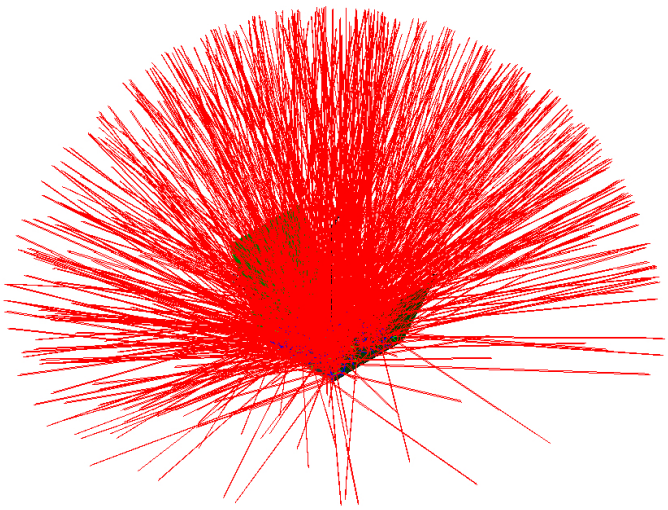

Figure 3.10: *Diffuse irradiation dome*

From the equation 3.2, the values for each angle of incidence are obtained, as they can be seen in the Table 3.5, describing the emissivity for the polar angles, of TracePro and real angle, and the azimuth angle. A standard temperature of 300ºK, equal to 26ºC, is used.

Temperature (K)	Wavelength (um)	Polar Angle TracePro (deg)	Polar Angle (deg)	Azimuth Angle (deg)	Emissivity
300	0,5	0	90	0	1,000
300	0,5	5	85	0	0,997
300	0,5	10	80	0	0,990
300	0,5	15	75	0	0,977
300	0,5	20	70	0	0,960
300	0,5	25	65	0	0,938
300	0,5	30	60	0	0,911
300	0,5	35	55	0	0,879
300	0,5	40	50	0	0,844
300	0,5	45	45	0	0,805
300	0,5	50	40	0	0,762
300	0,5	55	35	0	0,716
300	0,5	60	30	0	0,667
300	0,5	65	25	0	0,615
300	0,5	70	20	0	0,561
300	0,5	75	15	0	0,506
300	0,5	80	10	0	0,449
300	0,5	85	5	0	0,391
300	0,5	90	0	0	0,333

Table 3.5: *Emissivity for each angle of incidence*

It can be seen how the emissivity decreases as the polar angle decreases, that is, each time it gets closer to the horizontal. With these values the simulations for the horizontal and vertical concentrator are made.

3.5 Experimental Validation

The following test protocol shows the sequence of steps that must be performed in a logical and coherent order to build a CPV unit with a textured ARC at the top to make more efficient use of solar energy and reduce energy losses. Therefore, all the items to be taken into account and the manufacturing steps of components to be able to perform the experiment are explained.

3.5.1 Security Issues

The following safety issues should be considered for the test: Checking electrical connections, mouthpiece for volatile materials, gloves, eyeglasses, and lab coat.

3.5.2 Prerequisites

The following prerequisites should be considered for the test: Calibration of measuring equipment, check that external instruments are available, check that the data measurement formats are printed, and, have all the

elements ready.

3.5.3 Materials and equipment for testing

The required materials and equipment are summarized in the Table 3.6.

Equipment	Quantity	Description	Annotations	Supply
Test object	2	Photovoltaic panel		EAFIT
Test object	4	Texture	2 Textures of 45º and 2 Textures of 60º	EAFIT
Materials	2	Mold		EAFIT
Security	3	Mask		EAFIT
Security	6	Gloves		EAFIT
Security	3	Glasses		EAFIT
Security	3	Lab coats		Team
Validation	2	Equipment	Multimeter	EAFIT
Validation	2	Equipment	Thermometer	EAFIT
Validation	1	Equipment	Level of incilination	EAFIT
Validation	1	Equipment	Camera	Team
Validation	1	Notebook		Team
Validation	1	Equipment	Amprobe Solar 600	UPB
Validation	1	Equipment	Electronic load	EAFIT
Validation	2	Equipment	Pyranometer	EAFIT

Table 3.6: *Materials and equipment required for the test*

3.5.4 Pre-test

The following steps should be executed in advance in order to verify the right conditions:

1. Have all materials available and close to the work site.
2. Adapt the Test Bench and verify that the sensors are placed correctly.
3. Place the experiment in a surface and place where it can be at least 24 hours.
4. Place the experiment on a clean surface free of environmental materials.

3.5.5 Procedure

The test procedure considers the configuration of the cells, the assembly of the test stand, and capturing the results. More detail is presented next.

Configure the cells:

1. Test continuity
2. Characterize the panels at standard irradiation

3. Select the 2 most similar panels for the test

Test stand assembly:

1. Manufacture the test prototype (2 CPV)
2. Adapt the electronics to the prototype (Panels, Temperature Sensors, Wattmeters, Pyranometers)
3. Locate the prototypes at the test site
4. Adjust the tilt angle of the panels, according to the latitude of the location.

Results capture:

1. Connect the panels to the electronic box that measures the power of the systems.
2. Collect irradiation data through the pyranometers

3.6 Experimental design

An experiment design is carried out considering the defined texture as an input variable, and the output variable is the power, which is measured with an electronic system, with two levels of treatment, that is, with texture and without texture, and trying to perform the experiment for at least 3 days for each of them, that is, for each texture selected. In this case textures of 45° and 60°. As a second experiment, the data collection is made during several days with a solar characterizer Solar Amprobe 600 [Amprobe], with which V-I curves can be drawn, with the aim of comparing in a short instant of time how the curve changes when there is and there is not texture.

Single-factor design

- Dependent Variable item is continuous: Power.
- Independent Variable item is categorical or binary: Treatment 1 (not textured), Treatment 2 (textured). Two equivalent devices are placed in all directions except for the treatment: one with textured, the other without textured. In all other aspects they will have to be the same:
- Similar PV panels.
- Same reflective material.
- Same electrical circuit.
- Same type of sensors.
- Same angular position.
- Same sun exposure.

- Same load.

The only variable that changes is the treatment, that is, it has texture or no texture. Then, having those two devices equivalent in every way except for treatment, as many measurements of the dependent variable as possible are taken in as many weather conditions as possible. In the end, two sets of continuous measurement data would be reached, one group comes from Treatment 1, the other from Treatment 2. The average is taken from each group, compared, and that gives the magnitude of the difference.

The statistical question is: **Is the difference between the two groups significant in terms of the dependent variable?**

Chapter 4

Validation of the proposed approach

In this chapter the analysis and data collection is carried out with respect to the approach proposed in the Chapter 3. First, the results obtained from the simulations are analyzed, and decisions are made to perform and analyze the experimental data.

4.1 Concentrator design and selection

Based on the iterations and characteristics presented in the section 3.1, results are obtained for concentrators with horizontal and vertical configurations. Remember that the aim of the analysis is to find the best value for each of the applications in terms of profitability or cost efficiency index (I_{COE}),the percentage reduction or increase in area ($Area(\%)$) compared to a conventional panel and, also, values related to usable area and effective concentration (CR_e), which refers to the actual value of the irradiance reaching the cell, taking into account that for a conventional panel on a clear day, the CR_e would be 1.

The Table 4.1 presents the results for the concentrator in horizontal configuration.

Results			
Set-up	CR_e	I_{COE}	$Area(\%)$
Iref	0.7661	1	0
Ia	0.7898	0.8394	-3
Ib	0.7931	0.8429	-3.4
Ic	0.8016	0.8519	-4.4
Id	0.9608	1.2541	-20.3
Ie	1.5075	1.6022	-49.2
If	1.4705	1.5628	-47.9
Ig	1.1478	1.2199	33.3

Table 4.1: *Results of the different applications of horizontal concentrators*

It is determined that for the horizontal solution to be cost-efficient this is given by adding 3 positions of manual solar tracking or for places where the sun does not have an incidence of 180 degrees if not less, as would be the case of the city of Medellin, but especially in urban applications where to a large extent the buildings can generate light obstacles, which affects the solar generation of a conventional system and that the CPV has a better performance.

From the obtained results it is determined that for the configurations Ie, If and Ig, the values of cost efficiency, I_{COE}, are bigger than 1, that is, they are more cost efficient than a normal panel without concentration and without solar tracking. In addition, according to these results for the configuration Ie the reduced area with respect to a commercial configuration is of 49.2% supposing this a saving in the space, important subject for the implementation of PV systems in residences.

Table 4.2 presents the results for the concentrator in vertical configuration.

Resultados			
Set-up	CR_e	I_{COE}	Area (%)
$IrefV$	0.6351	1.0	0%
IaV	1.0139	1.2998	-37.4%
IbV	0.6236	0.7995	+1.8%
IcV	0.97	1.2486	-34.8%

Table 4.2: *Results of the different applications of vertical concentrators*

For the vertical solution, the IaV iteration represents an improvement in all the indicators with respect to the reference; this because the CR_e is greater than 1, it has a better indicator of I_{COE}, and, in addition, the area is reduced by 37.4%.

From the previous, the iterations Ia and Ie are chosen, for the horizontal configuration. They are the same geometrically, only that Ia does not have discreet solar tracking, and Ie has it.

The Fig. 4.1 presents the implementation of both iterations in horizontal, and the iteration IaV for the implementation in vertical.

4.2 Material definition for Anti-Reflective Coating

From the equation 3.1 for determining the ARC shown in section 3.2, this step starts with a database search to find the materials for the textured coating. Therefore, prior to the simulation and experimentation phase, a filtration of materials was carried out on the CES Edupack®software, until approximately five materials that met the requirements and properties. Of 4026 materials were found, including metals, ceramics, polymers, among others. A filtration process begins with the following parameters: Refractive Index and transparency, as it is presented in the Fig. 4.2.

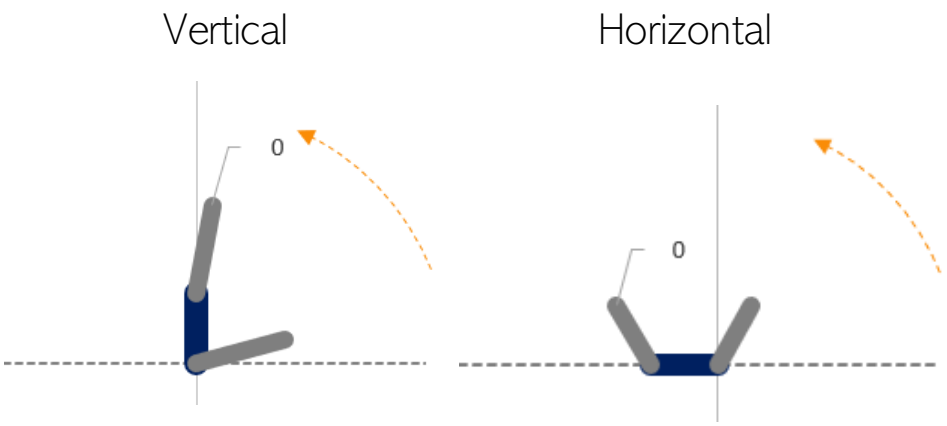

Panel length	1	Panel length	1
Mirror length I	1	Mirror length I	1
Mirror length D	1	Mirror length D	1
Mirror Angle I	80	Mirror Angle I	30
Mirror Angle D	-15	Mirror Angle D	30
Panel Tilt	90	Panel Tilt	0
Material Reflection	0.92	Material Reflection	0.92

Figure 4.1: *Geometric final design*

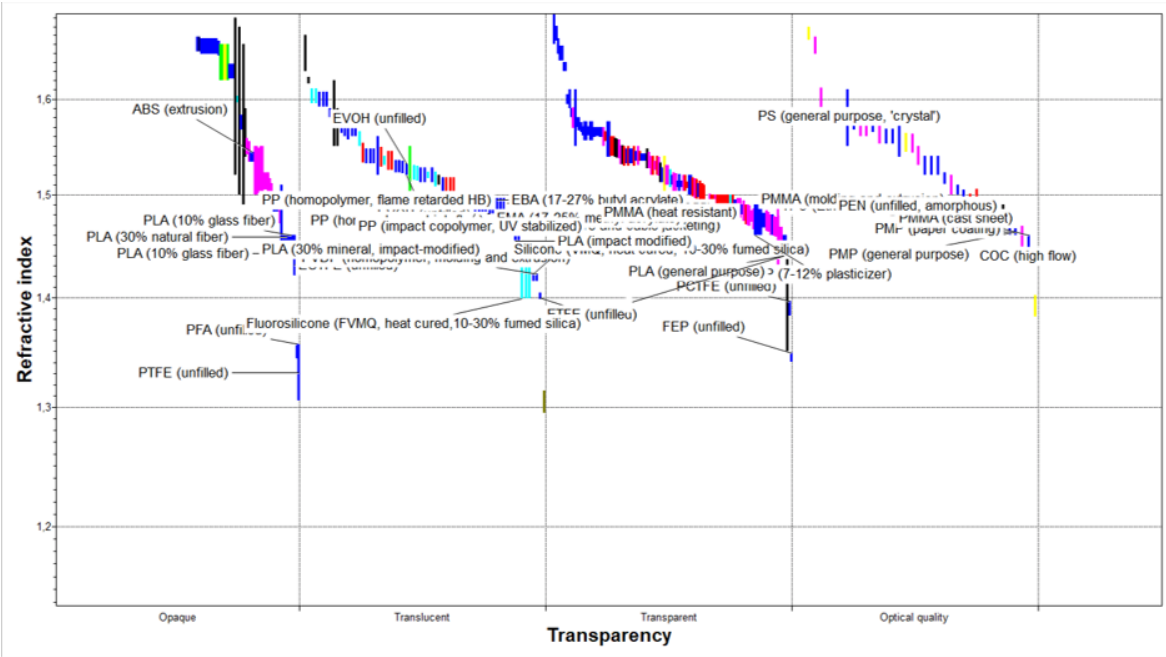

Figure 4.2: *Best materials with requirements in transparency and refraction index*

For the criterion of refraction index a range between 1.13 to 1.51 was determined. These values are given by the refraction index of glass that is 1.52, considering that these materials are searched with refraction index

below this value. Then for the transparency, the program categorizes them in 4 levels (Opaque, translucent, transparent and optical quality materials).

From the previous filter, 365 materials are obtained, and then, a second filtering process is performed, adding a requirement of Service Temperture (°C) > 80, as it is presented in the Fig. 4.3.

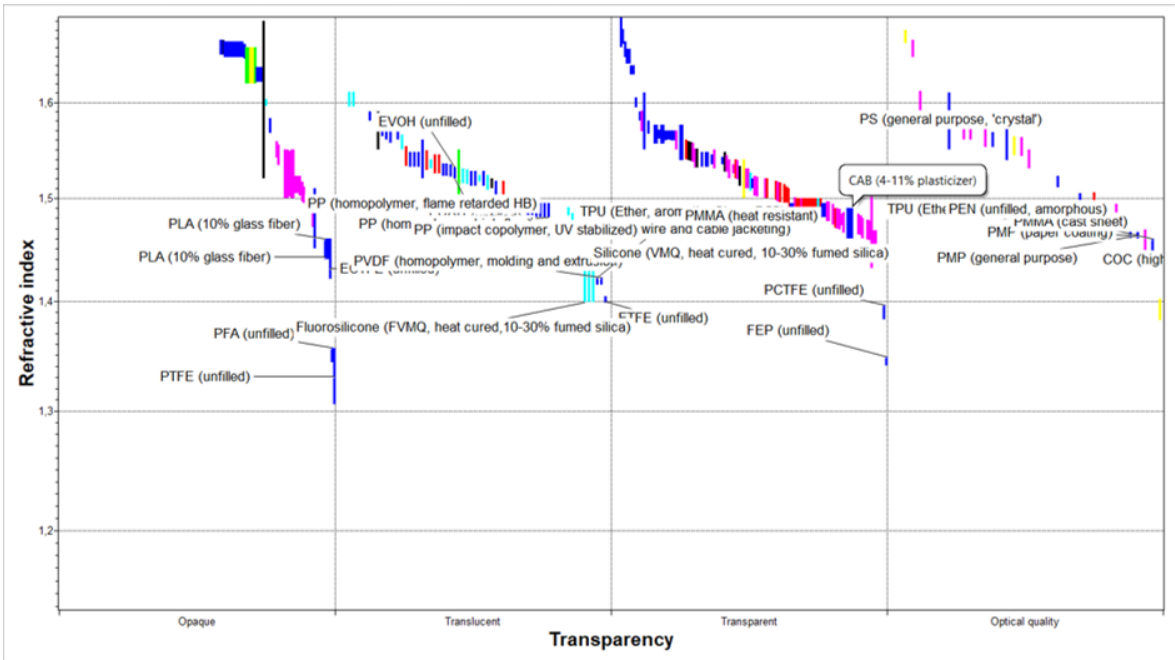

Figure 4.3: *Best materials with requirements in transparency, refraction index and temperatures over 80ºC*

This, in order to ensure that the selected material can withstand high temperatures, considering that studies are reported that CPV/VT reaches temperatures higher than the value specified above [Solanki et al., 2008].

After this, 18 materials that meet all parameters are reached, after adding requirements related to water resistance and UV radiation, which can degrade some materials [Acevedo-Gómez et al., 2017], since these materials will be exposed to rainwater and radiation from the Sun. So, it is intended to ensure durability over time without affecting the optical properties. This last filtering is presented in the Fig. 4.4.

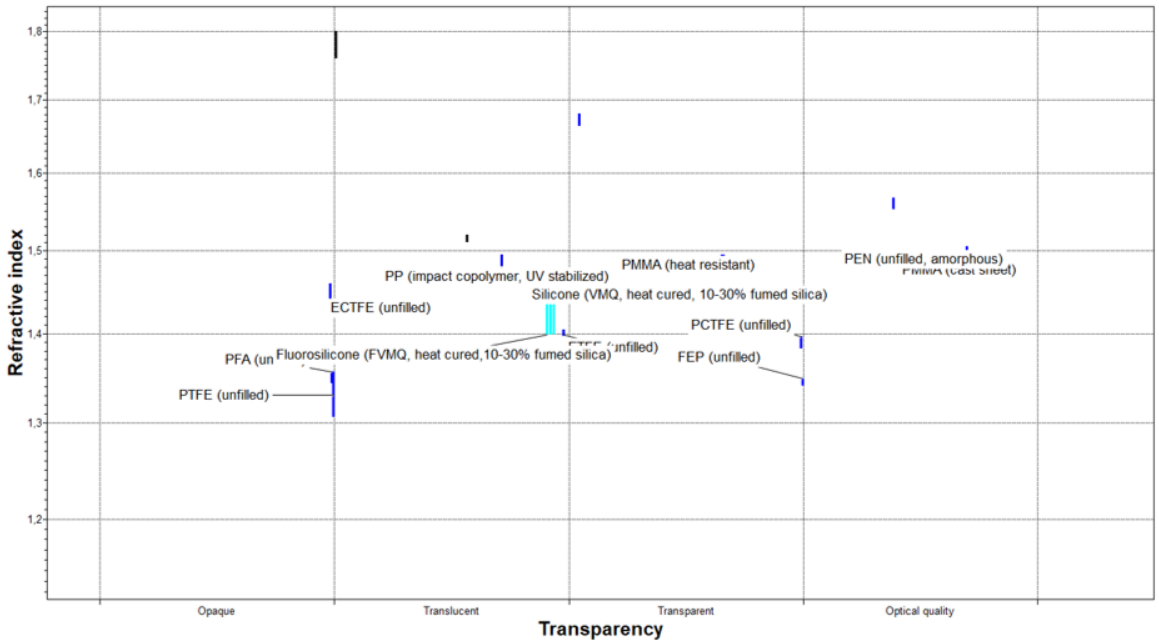

Figure 4.4: *Best materials with requirements in transparency, refraction index, water resistance, UV radiation and temperatures over 80ºC*

Finally, 7 materials indicated for the tests are obtained, as it is shown in the table 4.3.

	Material						
	PEN	PMMA	PCTFE	FEP	ETFE	SILICONE	EPOXY
Refractive index(n)	1,5	1,49-1,5	1,38-1,4	1,34-1,35	1,4	1,4	1,48
Proceso	Injection and extrusion	Thermoforming and mechanized	Thermoforming	Injection and extrusion	Injection and extrusion	Injection and extrusion	Injection and extrusion
Precio (COP/kg)	9,2e3-1,5e4	8,4e3-8,8e3	3,0e5-4,0e5	7,0e4-8,1e4	6,1e4- 9,5e4	9,7e3-1,8e4	6.9e3-8.9e3

Table 4.3: *Materiales seleccionados*

However, the Silicone and the Epoxy Resin are selected, because these materials are easily accessible and comply with the optical properties indicated to generate the ARC.

4.3 Texture design

According to section 3.3, the analysis of the simulation results in TracePro is presented, where it is revealed which angles should be chosen for the design, as it is presented in the Fig. 4.5, and the Table 4.4, where **Ref Without_text** refers to the simulation performed without ARC textured, and **Text (10°, 30°, 45°, 60°, 80°)** refers to the simulation with the textures at the specified angle. For this purpose, the simulated model has been made with the real layers that a solar panel has, and that are presented in the Fig. 3.4.

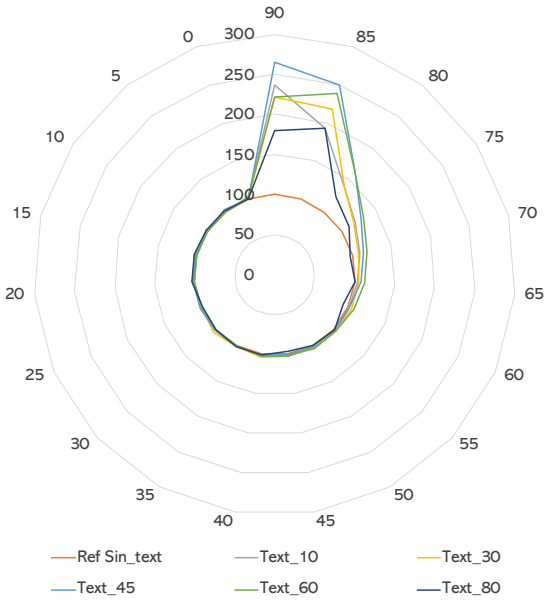

Figure 4.5: *Polar graph of the different textures*

Standardized efficiency for different angles of the textures						
Angle(°)	Ref Without_text (%)	Text 10° (%)	Text 30° (%)	Text 45° (%)	Text 60° (%)	Text 80° (%)
90	0	136,78	121,27	164,24	121,87	79,15
85	0	92,50	118,72	150,09	139,83	93,32
80	0	39,80	41,49	63,68	62,23	23,10
75	0	20,12	17,65	29,10	31,98	10,95
70	0	9,93	8,49	13,31	18,75	-3,69
65	0	2,96	4,69	7,51	12,15	0,18
60	0	1,81	4,78	1,82	7,92	-6,73
55	0	3,02	2,63	0,95	3,82	1,66
50	0	3,90	3,80	0,66	2,22	-0,81
45	0	1,11	2,53	0,62	2,12	-3,28
40	0	1,12	3,78	0,53	2,14	1,59
35	0	1,12	1,97	0,63	0,27	0,79
30	0	1,05	4,23	0,72	0,04	-0,35
25	0	1,03	0,12	1,16	0,01	-1,78
20	0	1,02	2,33	2,24	0,13	3,81
15	0	0,98	2,58	2,02	0,20	3,23
10	0	0,93	0,75	0,34	-0,06	2,58
5	0	0,92	0,69	3,21	-0,28	1,68
0	0	0,90	0,71	0,12	2,58	0,11
Mean	**0**	**16,89**	**18,06**	**23,31**	**21,47**	**10,82**

Table 4.4: *Standardized efficiency for different angles of textures*

The Table 4.4 shows the amount of power transmitted by the simulated rays that pass through the model and reach the cells of the different textures. For this, the simulation was made corresponding to the trajectory of the sun during half a day, discretized in 19 angles ranging from 0º to 90°, where 0º is 12:00 pm, and 90º is 6:00 pm. Observing the Table 4.4 it can be analyzed that the best results belong to the 45° texture with an average in its efficiency of 23.31W of flow, and, the 60° texture with an average of 21.47W, both being the highest results in this simulation. In addition, the Fig. 4.5 shows how the peaks of efficiency begin from 55°, and for textures of 45° and 60° these are the ones that are usually above the rest.

Therefore, it is determined that textures of 45° and 60° are the most efficient and demonstrate a significant amount of rays that enter the system, so these two are considered for the next steps of the proposed method.

From the results previously obtained, a simulation is made with textures of 45 ° and 60 ° comparing them with a non-textured ARC, in order to validate whether the fact that the ARC has texture increases efficiency, as it is observed in the Fig. 4.6.

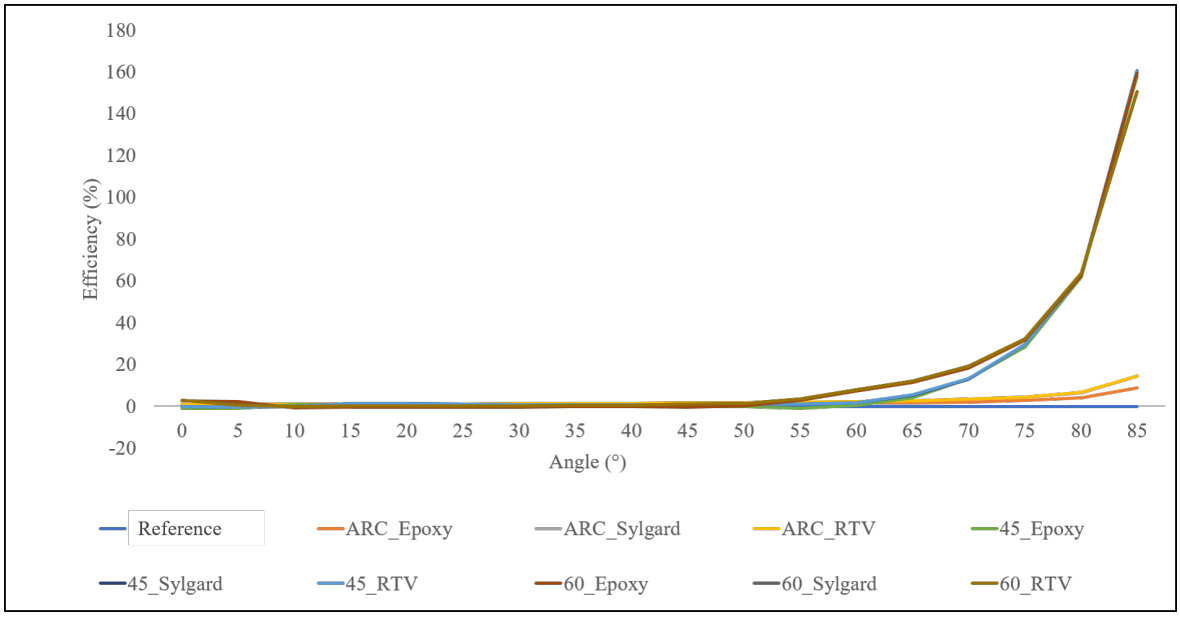

Figure 4.6: *Comparison of ARC with and without texture*

Fig. 4.6 shows the influence of textures when the angle of incidence is greater than 45°, but for other values, the efficiency usually has values very similar to the ARC, always greater than the reference, which would be a commercial PV panel. This shows that the implementation of the texture in the ARC generates increased performance of the system.

4.4 Simulation results

Taking into account all the parameters defined in the section 3.4, the next step is the simulation with the software TracePro®, where a total of 72 simulations are made for the horizontal concentrator, and 144 for the vertical concentrator, as it is presented in the Table 4.5.

	Horizontal CPV	Vertical CPV
Texture's Angles	45º & 60º	45º & 60°
Sun's incidence angle	0º, 5º, 10º, 15º, 20º, 25º, 30º, 35º, 40º	0º, 5º, 10º, 15º, 20º, 25º, 30º, 35º, 40º, 45º, 50º, 55º, 60º, 65º, 70º, 75º, 80º, 85º, 90º
Materials	No Material, Epoxy Resin, Qsil 216 and RTV Silicone	No Material, Epoxy Resin, Qsil 216 and RTV Silicone
Wavelenght	Visible Spectrum (400-700nm)	Visible Spectrum (400-700nm)

Table 4.5: *Simulations*

For both concentrators the simulation is done with the textures of 45° and 60°, with a step of 5° for the position of the sun, and also testing the selected materials, that is, Silicone RTV, Sylgard Silicone, Epoxy Resin, and without ARC. The normalized efficiency (EFE) was used for the analysis of the results according to the equation (4.1), where $n_{Reference}$ is the Power flux of the conventional solar panel.

$$EEF = \frac{n_{material} - n_{Reference}}{n_{Reference}} \times 100 \tag{4.1}$$

An illustration of the simulation of the horizontal CPV is shown in the Fig. 4.7.

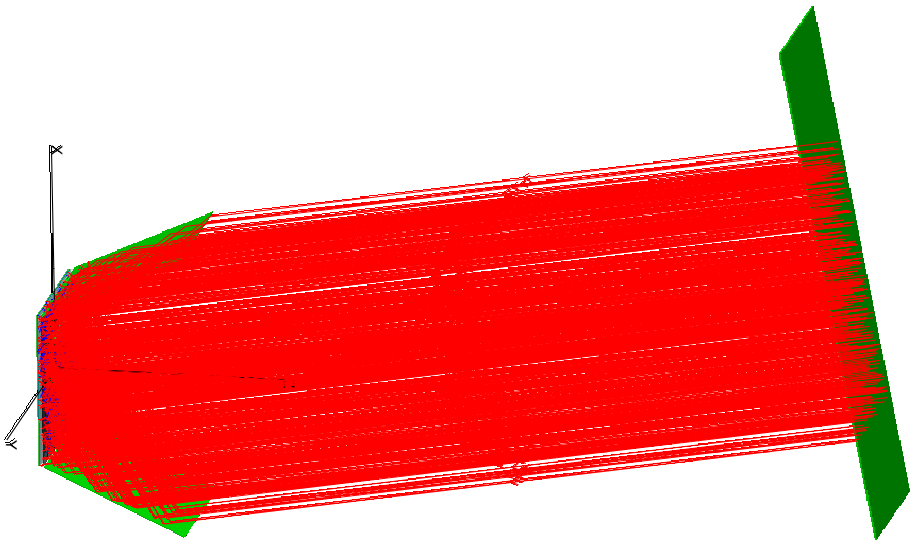

Figure 4.7: *Illustration of the simulation*

In order to perform a correct simulation, Appendix B shows the process and step by step of the different models that were used for the simulations, as well as the use of different materials to find the best results.

The following treatments are defined for the simulation results:

- Reference: It refers to the simulations carried out without any type of textured ARC
- Texture_Epoxy_Resin: It refers to the simulation where ARC with epoxy resin texture is used
- Texture_Epoxy_Resin_WithoutCPV: It refers to the simulation where ARC with Epoxy Resin texture is used, without using concentrators.
- Texture_Sylgard_Silicone: It refers to the simulation where ARC is used with Sylgard Silicone texture.
- Texture_Sylgard_Silicone_WithoutCPV: It refers to the simulation where ARC with Sylgard Silicone texture is used, without using Concentrators.
- Texture_RTV_Silicone: It refers to the simulation where the RTV Silicone texture is used.
- Texture_RTV_Silicone_WithoutCPV: It refers to the simulation where the RTV Silicone texture is used, without using Concentrators.

4.4.1 45° texture simulation in horizontal CPV

The simulation is carried out with the software TracePro®, for the concentrator with the texture of 45°, in angles of 0-40°, being 0° the 12:00 pm of the day, that is the point of greater irradiance, and, 40° approximately the 2:00 pm. The results are presented in the Table 4.6.

45° Texture Horizontal CPV								
	Total Flux [W]				Normalized Efficiency [%]			
Angle (°)	Reference	Epoxy	Sylgard	RTV	Reference	Epoxy	Sylgard	RTV
0	32,03	32,46	32,14	32,15	0,00	1,35	0,36	0,36
5	31,88	31,89	32,60	32,60	0,00	0,04	2,24	2,26
10	30,01	30,18	30,23	30,24	0,00	0,56	0,75	0,76
15	26,68	27,17	27,57	27,59	0,00	1,84	3,36	3,42
20	23,12	23,94	24,26	24,25	0,00	3,53	4,91	4,86
25	19,55	20,70	20,83	20,82	0,00	5,89	6,53	6,49
30	15,97	17,15	17,32	17,33	0,00	7,40	8,47	8,54
35	12,30	13,22	13,34	13,34	0,00	7,46	8,46	8,49
40	9,27	9,24	9,33	9,33	0,00	-0,30	0,66	0,68

Table 4.6: *Textured Concentrator 45°*

From the Table 4.6, the RTV silicone is the one that has the best performance with the texture of 45°, being, in the highest amount of incidence angles, the one that obtained the highest efficiency, similar to the Sylgard type silicone. In addition, the Epoxy Resin, in spite of having a lower performance, obtained results above the

reference. Something that can be noticed in the table is that when reaching 40º the drop in efficiency is very high, insomuch that for the epoxy resin the value is already negative below the reference.

Then, an efficiency comparison is carried out between the results of the textures implemented in the CPV, and the Normalized Efficiency (EFE) for the same textures, but without CPV. In the Figure 4.8, it can be observed that all the materials that were used when there was concentration, show a considerable increase in efficiency with respect to the implementation without CPV.

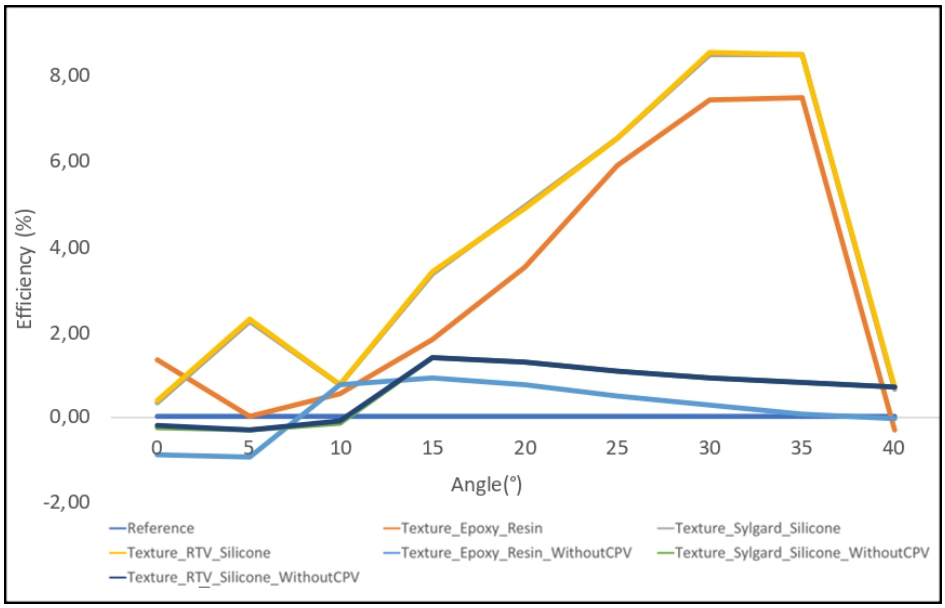

Figure 4.8: *Texture implementation comparison of 45° over CPV vs. no CPV*

An irradiance analysis is carried out for a specific angle of incidence. Figure 4.9 presents the irradiance maps for the angle of 25º, equivalent to 1:30 pm, for which it was simulated with 661.19 W/m^2, which is the average of radiation of the last 5 years for the city of Medellin, in that hourly interval.

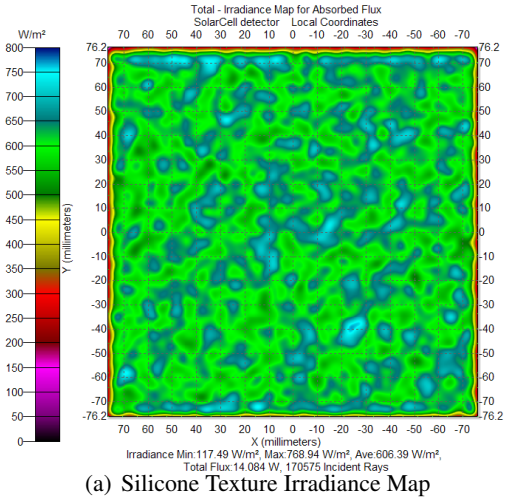

(a) Silicone Texture Irradiance Map

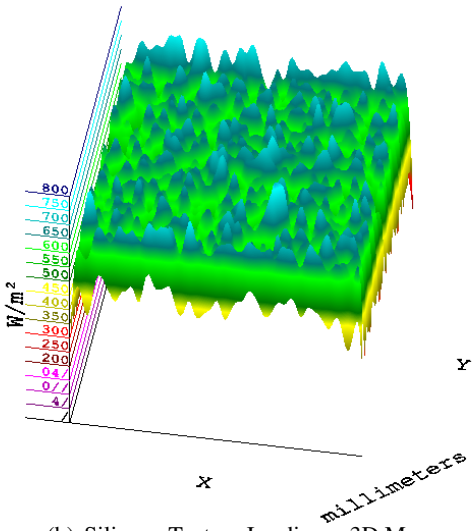

(b) Silicone Texture Irradiance 3D Map

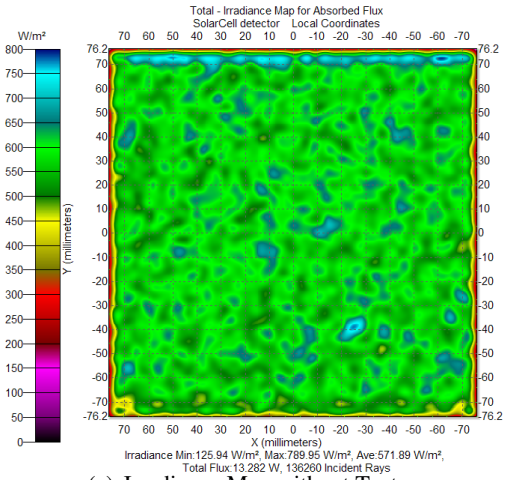

(c) Irradiance Map without Texture

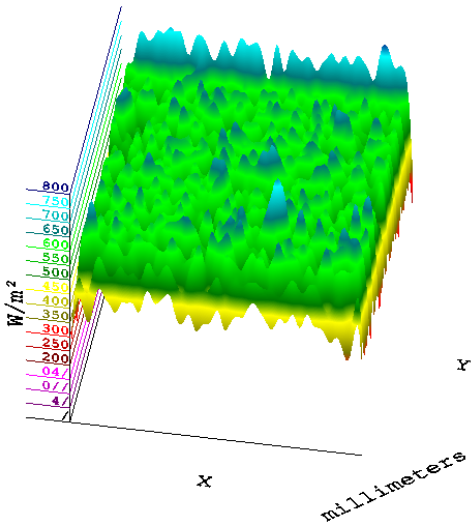

(d) Irradiance 3D Map without Texture

Figure 4.9: *Irradiance maps at 25º for the 45° texture*

This map shows the results for the RTV Silicone and for the Non-Textured treatment. The results obtained for this case, show that the power flow for the Silicone was 14.37W, while for the treatment without texture it was 13.54W, showing a 6.11% efficiency of the silicone superior to the reference. This result is evidenced by looking at Fig. 4.9(a) and 4.9(b) for the silicone, where a greater number of blue peaks are observed with respect to the non-textured one, since these are of greater energy. But, it can also be observed that they are more uniform in the 3D maps, showing a benefit of the use of a silicone texture, for the distribution or balance of the current within the photovoltaic panel.

4.4.2 60° texture simulation in horizontal CPV

For the 60° texture, the simulation is carried out with the same parameters as the 45° texture, and the results are presented in the Table 4.7.

60° Texture Horizontal CPV								
	Total Flux [W]				Normalized Efficiency [%]			
Angle (°)	Reference	Epoxy	Sylgard	RTV	Reference	Epoxy	Sylgard	RTV
0	32,03	32,68	32,88	32,90	0,00	2,04	2,65	2,71
5	31,88	32,36	32,31	32,32	0,00	1,51	1,34	1,38
10	30,01	30,58	30,79	30,80	0,00	1,92	2,62	2,64
15	26,68	27,42	27,58	27,58	0,00	2,79	3,38	3,40
20	23,12	24,04	24,19	24,20	0,00	3,97	4,63	4,65
25	19,55	20,61	20,75	20,75	0,00	5,41	6,11	6,13
30	15,97	17,10	17,21	17,21	0,00	7,10	7,81	7,83
35	12,30	13,38	13,25	13,25	0,00	8,77	7,73	7,74
40	9,27	9,40	9,47	9,48	0,00	1,37	2,21	2,22

Table 4.7: *Textured Concentrator 60°*

From the Table 4.7, the RTV silicone is the one that has a better performance with the 60° texture, being, in the greater amount of incidence angles, the one that obtained greater efficiency, similar to the Sylgard type silicone. In addition, the Epoxy Resin, in spite of having a lower performance, obtained results above the reference. In contrast to the texture of 45º, to the slope of 40º, although the efficiency falls, the texture of 60º still shows better results than the reference, so much so that for epoxy resin efficiency is 1.37%, while for silicones the efficiencies are above 2%.

Then, an efficiency comparison is carried out between the results of the textures implemented in the CPV and the Normalized Efficiency (EFE) for the same textures, but without CPV. From the Figure 4.10, it can be observed that all the materials that were used when there was concentration, show a considerable increase in efficiency with respect to the implementation without CPV. This is a similar result for the 45º texture.

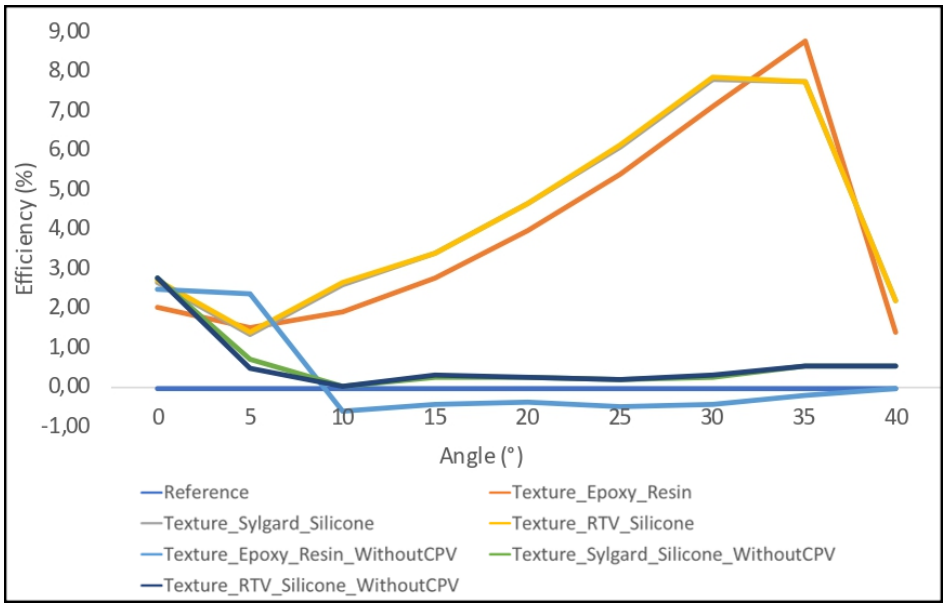

Figure 4.10: *Texture implementation comparison of 60° over CPV vs. no CPV*

An irradiance analysis is carried out for a specific angle of incidence. The Figure 4.11 presents the irradiance maps for the angle of 110º, equivalent to 1:30 pm, with the same conditions of the simulation explained for the 45º texture.

This map shows the results for the RTV Silicone and for the Non-Textured treatment. The results obtained for this case, show that the power flow for the Silicone was 14.27W, while for the treatment without texture it was 13.54W, showing a 5.43% efficiency of the silicone superior to the reference. This result is evidenced by looking at Fig. 4.11(a) and 4.11(b) for the silicone, where a greater number of blue peaks are observed with respect to the non-textured one, since these are of greater energy, but it can also be seen that they are more uniform in the 3D maps, showing a benefit of the use of silicone texture for the distribution or balance of the current within the photovoltaic panel.

From the data obtained previously, a statistical group analysis is performed to determine from the EFE, which of the configurations represents a better statistical group by comparing the textures in CPV and without CPV, for the angles of incidence evaluated. The results of this analysis are presented in the Table 4.8 and the Figure 4.12.

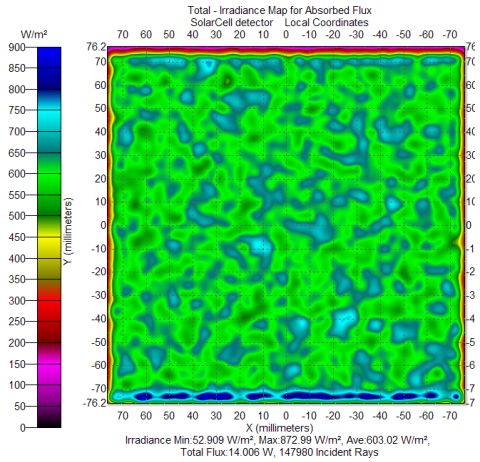

(a) Silicone Texture Irradiance Map

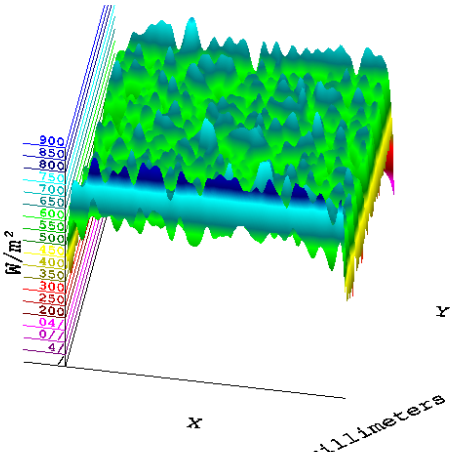

(b) Silicone Texture Irradiance 3D Map

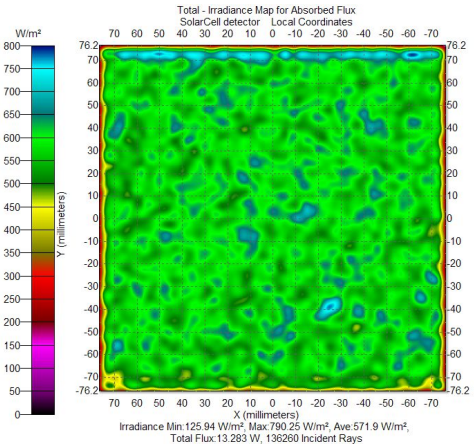

(c) Irradiance Map without Texture

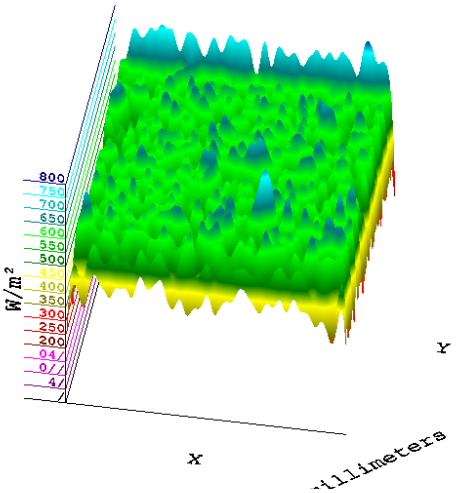

(d) Irradiance 3D Map without Texture

Figure 4.11: *Irradiance maps at 25º for the 60° texture*

Test of statistical groups		
Treatment	Efficiency	Groups
RTV_60	4,62	a
Sylgard_60	4,62	a
Resina_60	4,19	ab
RTV_45	3,91	abc
Sylgard_45	3,89	abc
Resina_45	3,31	abcd
Sylgard_60_No_CPV	0,63	bcd
RTV_60_No_CPV	0,62	bcd
RTV_45_No_CPV	0,61	bcd
Sylgard_45_No_CPV	0,60	bcd
Resina_60_No_CPV	0,30	cd
Resina_45_No_CPV	0,19	cd
Reference	0,00	d

Table 4.8: *Test Tukey for simulations in the horizontal configuration*

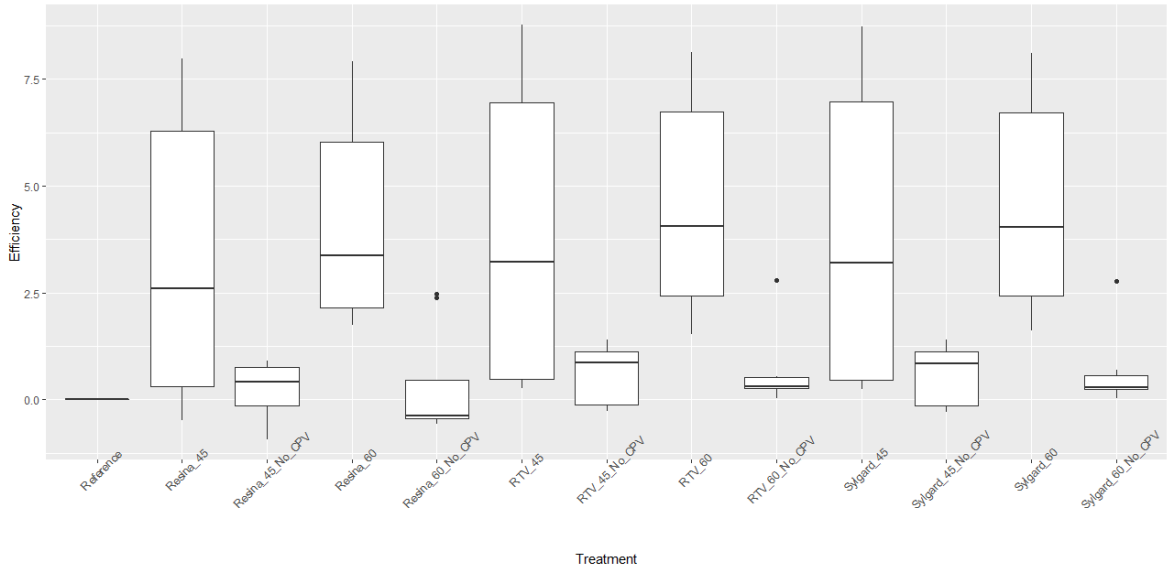

Figure 4.12: *Boxplot analysis for the different treatments in the horizontal configuration*

4.4.3 45° texture simulation in vertical CPV

The simulation is carried out with the software TracePro®, for the concentrator with the texture of 45°, in angles of 0-90°, being 0° the 12:00 pm of the day, that is the point of greater irradiance, and 90° approximately the 6:00 pm. The results are presented in the Table 4.9.

From the Table 4.9, the RTV silicone is the one that has the best performance with the texture of 45°, being, in the highest amount of incidence angles, the one that obtained the highest efficiency, similar to the Sylgard type silicone. In addition, the Epoxy Resin, in spite of obtaining a lower performance, obtained results above the reference. It can also be observed that the lower the angle, the greater the effect of the texture in the case of verticality, showing for the highest angles, negative values, with the lowest being 0.92% for the Epoxy Resin, and 9.14% for the RTV Silicone.

Then, an efficiency comparison is carried out between the results of the textures implemented in the vertical CPV and the Normalized Efficiency (EFE) for the same textures, but without the reflectors or concentrators. In the Figure 4.13, it can be observed that the results "_SinCPV" show a better effect than those applied in CPV, that is, when the panel is in a vertical location, the textures have much more effect on the performance in the absence of photovoltaic concentrators.

Texture 45º Vertical CPV								
	Total Flux [W]				Normalized efficiency [%]			
Angle (°)	Reference	Epoxy	Sylgard	RTV	Reference	Epoxy	Sylgard	RTV
0	1,98	2,13	2,16	2,16	0,00	7,65	9,09	9,14
5	6,88	7,13	7,22	7,23	0,00	3,60	4,93	5,01
10	11,89	12,26	12,38	12,38	0,00	3,10	4,13	4,16
15	16,11	17,03	17,35	17,36	0,00	5,71	7,68	7,74
20	20,68	21,76	21,88	21,89	0,00	5,20	5,80	5,83
25	25,55	26,27	26,55	26,56	0,00	2,84	3,92	3,95
30	29,94	30,63	30,83	30,84	0,00	2,30	2,97	3,00
35	28,69	29,41	29,80	29,82	0,00	2,51	3,89	3,94
40	26,18	26,34	26,52	26,53	0,00	0,60	1,31	1,33
45	26,23	26,39	26,57	26,57	0,00	0,64	1,31	1,33
50	25,99	26,17	26,33	26,33	0,00	0,67	1,28	1,30
55	25,51	25,67	25,84	25,84	0,00	0,64	1,29	1,31
60	24,84	25,02	25,06	25,07	0,00	0,70	0,89	0,91
65	23,96	24,07	24,21	24,21	0,00	0,44	1,02	1,04
70	22,87	23,04	23,16	23,17	0,00	0,76	1,28	1,29
75	21,62	21,83	21,94	21,94	0,00	0,98	1,48	1,49
80	20,42	20,60	20,41	20,42	0,00	0,91	-0,02	-0,01
85	19,09	18,91	19,03	19,03	0,00	-0,92	-0,30	-0,28
90	17,35	17,21	17,31	17,32	0,00	-0,81	-0,18	-0,16

Table 4.9: *Vertical photovoltaic concentrator with 45º texture*

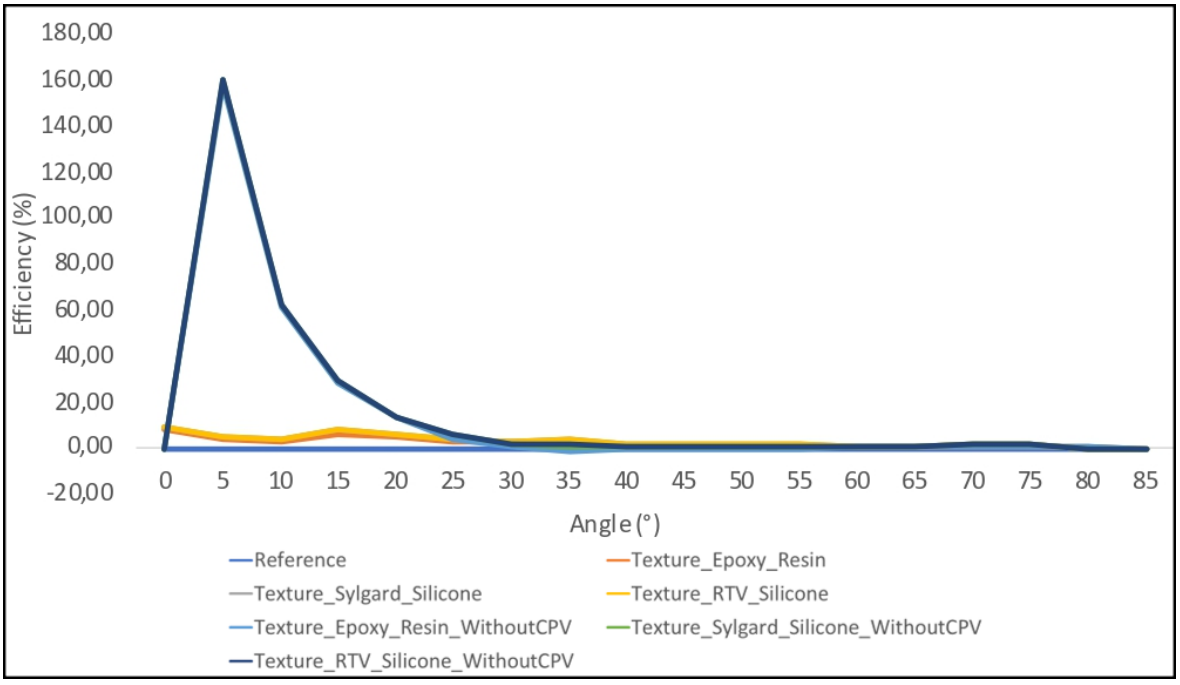

Figure 4.13: *Texture implementation comparison of 45° over CPV vs. no CPV*

4.4.4 60° texture simulation in vertical CPV

For the 60° texture, the simulation is carried out with the same parameters as the 45° texture, and the results are presented in the Table 4.10.

Texture 60º Vertical CPV								
	Total Flux [W]				Normalized efficiency [%]			
Angle (°)	Reference	Epoxy	Sylgard	RTV	Reference	Epoxy	Sylgard	RTV
0	1,98	2,35	2,36	2,36	0,00	18,73	19,05	19,04
5	6,88	7,68	7,73	7,73	0,00	11,54	12,24	12,23
10	11,89	12,96	13,03	13,03	0,00	9,06	9,63	9,64
15	16,11	17,62	17,75	17,75	0,00	9,37	10,15	10,17
20	20,68	22,11	22,30	22,31	0,00	6,90	7,83	7,85
25	25,55	26,90	27,11	27,11	0,00	5,28	6,10	6,11
30	29,94	31,43	31,64	31,64	0,00	4,98	5,67	5,68
35	28,69	29,90	30,11	30,12	0,00	4,23	4,97	4,99
40	26,18	26,25	26,48	26,48	0,00	0,26	1,14	1,16
45	26,23	26,19	26,49	26,49	0,00	-0,13	1,00	1,02
50	25,99	26,06	26,21	26,21	0,00	0,24	0,83	0,85
55	25,51	25,53	25,70	25,70	0,00	0,08	0,75	0,77
60	24,84	24,81	24,98	24,98	0,00	-0,13	0,55	0,57
65	23,96	24,05	24,10	24,11	0,00	0,35	0,58	0,60
70	22,87	22,92	23,06	23,06	0,00	0,21	0,81	0,83
75	21,62	21,60	21,72	21,72	0,00	-0,09	0,44	0,44
80	20,42	20,35	20,46	20,47	0,00	-0,35	0,22	0,23
85	19,09	19,59	19,27	19,23	0,00	2,64	0,93	0,74
90	17,35	17,82	17,87	17,87	0,00	2,74	3,01	3,01

Table 4.10: *Vertical photovoltaic concentrator with 60º texture*

From the Table 4.10, the RTV silicone is the one that has a better performance with the 60° texture, being, in the greater amount of incidence angles, the one that obtained greater efficiency, similar to the Sylgard type silicone. In addition, the Epoxy Resin, in spite of obtaining a lower performance, obtained results above the reference. It is worth highlighting that for the 60º texture, the silicones never present negative values.

Then, an efficiency comparison is carried out between the results of the textures implemented in the vertical CPV and the Normalized Efficiency (EFE) for the same textures, but without the reflectors or concentrators. From the Fig. 4.14, it can be observed that the results are similar to the simulation of vertical concentration with 45º texture. This means that the "_SinCPV" treatments show a better effect than those applied in CPV, that is, when the panel is in a vertical location, the textures have much more effect on performance in the absence of photovoltaic concentrators.

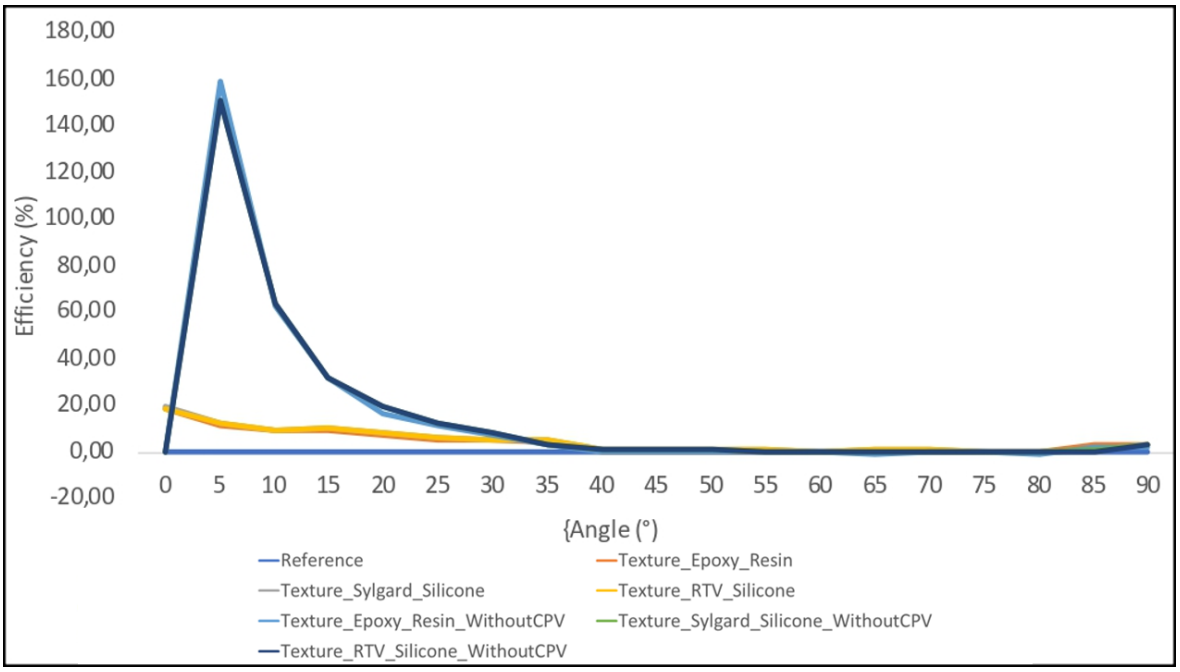

Figure 4.14: *Texture implementation comparison of 60° over CPV vs. no CPV*

From the data obtained previously, a statistical group analysis is carried out to determine from the EFE, which of the configurations represents a better statistical group by comparing the textures in CPV and without CPV, for the angles of incidence evaluated. The results of this analysis are presented in the Table 4.8 and the Figure 4.15.

Test of statistical groups		
Treatment	Efficiency	Groups
RTV_60_NO_CPV	16.522778	a
Sylgard_60_NO_CPV	16.518889	a
Resina_60_NO_CPV	16.355556	a
Sylgard_45_NO_CPV	15.667778	a
RTV_45_NO_CPV	15.648333	a
Resina_45_NO_CPV	14.814444	a
RTV_60	4.522632	a
Sylgard_60	4.521053	a
Resina_60	3.995263	a
RTV_45	2.753684	a
Sylgard_45	2.724737	a
Resina_45	1.974737	a
Reference	0	a

Table 4.11: *Statistical group test for the vertical concentrator*

The results obtained show that the implementation of the Silicone textured CPV at 60°, it is clear that when the panel is vertical, the statistical groups for all the configurations are the same, that is to say that the use or

non-use of textures has no effect on the CPV.

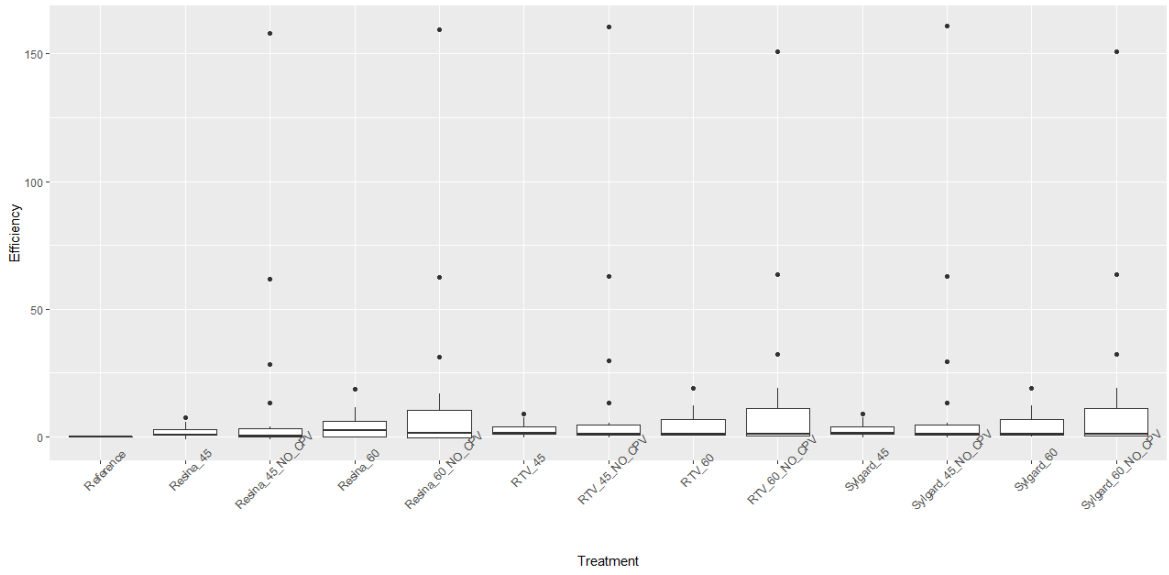

Figure 4.15: *Boxplot analysis for the different treatments in the vertical configuration*

4.4.5 Diffuse irradiation results

With the parameters defined in the section 3.4, the simulation is carried out with the maximum value of irradiation of 100 W/m^2, which refers to the maximum value of a cloudy sky, for the same considerations mentioned above, that is, a horizontal and vertical concentrator with textures of 45° and 60°. The results of this analysis are presented in the Table 4.12.

	Diffuse radiation in Horizontal CPV (W)							Standardized Efficiency in Diffuse Radiation for Horizontal CPV (%)						
		Textured 45			Textured 60				Textured 45			Textured 60		
	Reference	Epoxy	Sylgard	RTV	Epoxy	Sylgard	RTV	Reference	Epoxy	Sylgard	RTV	Epoxy	Sylgard	RTV
Total Flux	0,926	0,957	0,964	0,964	0,964	0,974	0,974	0,00	3,42	4,11	4,12	4,14	5,21	5,22
Incident Rays	78511	96256	94936	94874	108092	105659	105568	0,00	22,60	20,92	20,84	37,68	34,58	34,46
	Diffuse radiation in Vertical CPV (W)							Standardized Efficiency in Diffuse Radiation for Vertical CPV(%)						
		Textured 45			Textured 60				Textured 45			Textured 60		
	Reference	Epoxy	Sylgard	RTV	Epoxy	Sylgard	RTV	Reference	Epoxy	Sylgard	RTV	Epoxy	Sylgard	RTV
Total Flux	0.869	0.905	0.91319	0.913	0.918	0.925	0.925	0.00	4.17	5.13	5.13	5.69	6.47	6.48
Incident Rays	75820	91091	89449	89388	102344	99814	99744	0.00	20.14	17.98	17.90	34.98	31.65	31.55

Table 4.12: *Diffuse radiation results*

In the Table 4.12 it is observed that, in diffuse irradiation, positive results are obtained for both textures and that these textures continue to increase the efficiency of the concentrator, in addition to the fact that a marked trend continues to be seen with silicone, achieving the best results. Besides, it can be seen that the 60º texture is the one that has the best result being for the silicones in the horizontal concentrator, with an increase of efficiency of 5,21% for the Sylgard Silicone, and 5,22% for the RTV Silicone. However, in the vertical concentrator, a better effect of the texture in diffuse irradiation is seen, with an increase of efficiency of 6,47% for the Sylgard Silicone and 6,58% for the RTV Silicone.

Taking into account the previous results, the experimentation is carried out on the horizontal CPV, because in the statistical group test, differences were detected in groups for the use of textures that can increase the CPV performance.

4.5 Experimental results

The results obtained experimentally are explained next, showing the manufacturing process to achieve the texture, the construction of the concentration prototype, the assembly of the experiment with each of its devices, including their design and selection, and, finally, the data obtained and the main results.

4.5.1 Texture Manufacturing

Molds in aluminum were manufactured in order to obtain a better finish in the texture, besides, the aluminum is resistant to corrosion, is waterproof, is also a recyclable material, and, finally, is a material that allows a very good finish regardless of the heat or the speeds at which the tool that intervenes Valenciana [2014]. See the drawings of the molds in Annex C

A series of steps were carried out to manufacture the final texture in silicone.

- For the preparation of the material for the tests, two types of silicone with good optical characteristics and with good results in previous simulations were chosen. The first material was silicone Qsil [silicones, 2017], to prepare it a 10 to 1 ratio of silicone and its catalyst is needed, and then stirred until a homogeneous mixture is obtained. The second material was RTV silicone Esquim, with a ratio of 1 to 1.33gr of each material, is prepared so that it covers the desired volume, and the texture can be left with 1mm thickness, as it is observed in the Figure 4.16(a).

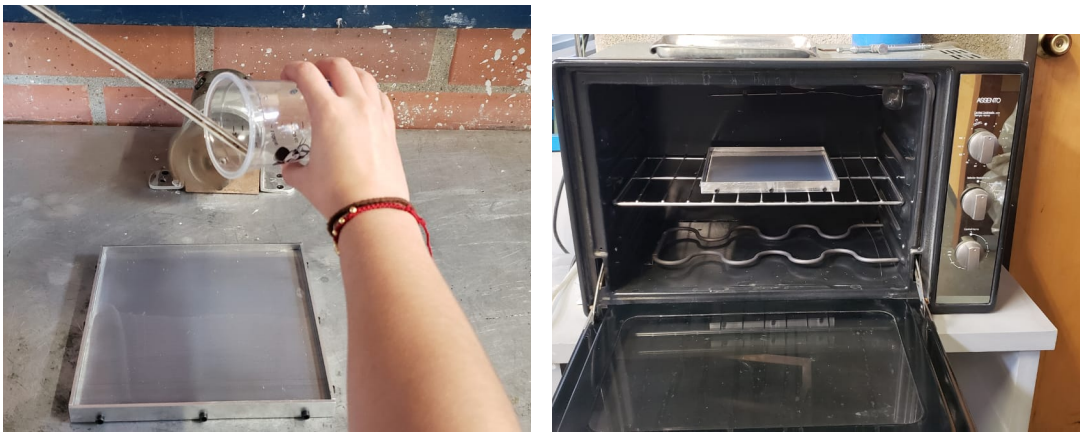

(a) Silicone casting in the mold

(b) Mold inside the oven

Figure 4.16: *Texture fabrication*

- The pieces are placed in an oven for 1 hour at a temperature of 120°C, for the correct gelling of the piece, until it is in a solid piece, as it is observed in the Figure 4.16(b).

- Afterwards, the piece is taken out of the oven and the edges of the silicone material are carefully peeled off until it is completely taken out of the mold, as it is observed in the Figure 4.17(a).

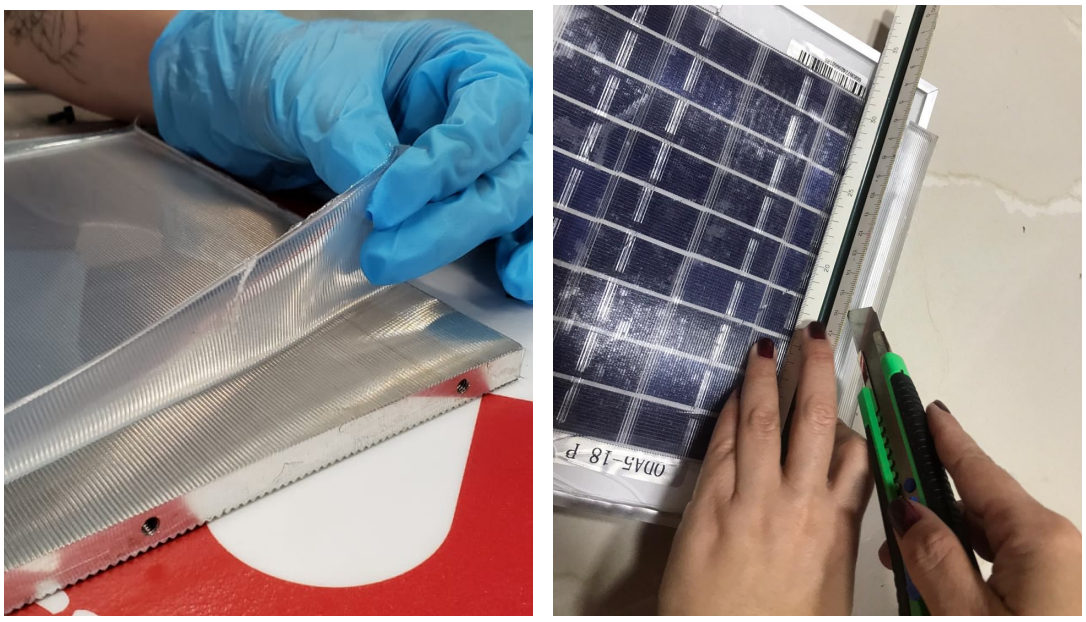

(a) Textured demoulding (b) Texture cutting

Figure 4.17: *Textured fabrication*

- After making the silicone piece, the next step is to place it on the panel. The first step is to cut the ends to fit exactly into the panel and then clean the panel very well so that there is no particulate material that creates layers of air, as it is observed in the Figure 4.17(b).

- A dimensional and geometrical measurement is carried out with a microscope at the angles of each peak of the textures with the objective of determining if they were correctly manufactured. For this, in the Figure 4.18(a) it is possible to see how the texture was made of 45°, fulfilling the desired inclination value, and, the Figure 4.18(b) shows the results for the texture of 60°.

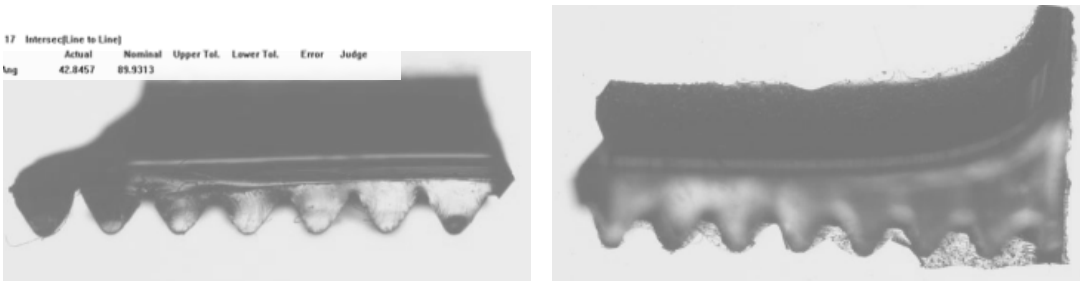

(a) 45º Texture (b) 60º Texture

Figure 4.18: *Texture photography on the microscope*

- Two samples were made with the silicones mentioned above, where they are tested by means of a spectrophotometer, as it is observed in the Figure 4.19.

Figure 4.19: *Spectrophotometer and Xenon lamp*

A Xenon lamp is put as light source, because it is the source that has a spectrum more similar to the sun, in what concerns the visible spectrum. Then, it is measured how much of this light reaches the

spectrophotometer, measuring for each wavelength, as it is observed in the Figure 4.20.

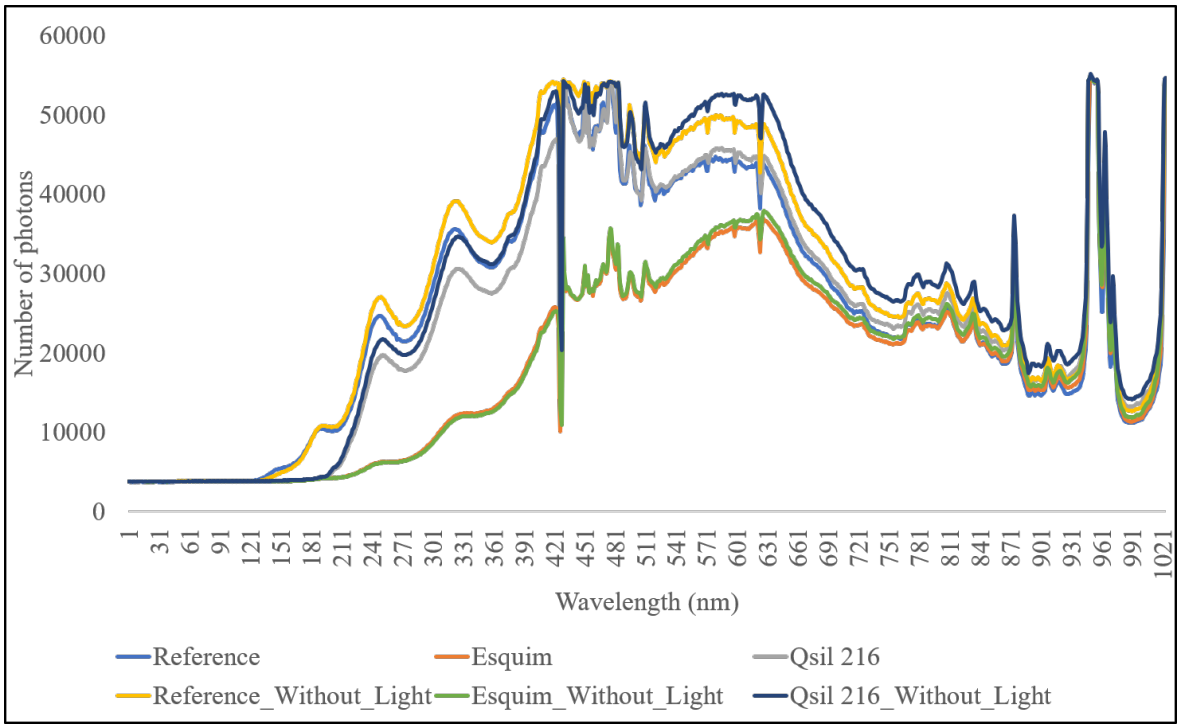

Figure 4.20: *Light transmittance results*

In this test, two measurements were made, one with the light of the room and another without light in the room, to avoid noise from external sources. The data is analyzed within the visible light spectrum. The dark blue and light gray lines show that Qsil 216 silicone has a better light transmittance, that is, the number of photons that passes through the material and reaches the spectrophotometer.

Preliminary tests for the fabrication of textures, which were validated in a solar simulator, are presented in Appendix A.

4.5.2 Manufacture of the test prototype

For the development of the CPV prototype, a series of requirements were established, in order to allow the reflective material to be placed on the concentrator, to be rotated in order to change the angle, in addition to being able to place a solar panel of 19 x 20.5 cm, for which commercial 5W electronic panels were used [Electrónicas], with the following characteristics:

- Optimum voltage (Vmp): 18.36V
- Open circuit voltage: 22V
- Maximum power: 5W

- Full panel efficiency: 8.74%
- Optimal operating current: 0.27A
- Short circuit current (Isc): 0.29A
- Number of cells: 36
- Temperature: - 40°C 85°C
- Panel dimensions: 260 x 220 x 18mm
- Weight: 0.8Kg

The prototype was made of laser-cut MDF wood and assembled with nails, wooden columns, and screws, from a concept modeled and generated in 3D, as it is presented in the Figure 4.21.

Figure 4.21: *Prototype 3D Model*

The physical prototype is showed in the Figure 4.22(c). This prototype allows the panel to be placed in the central part; on the side surfaces it is possible to place any reflective material, and rotate it at an angle every 5° from 0° to 105° thanks to the holes made at that distance. After cutting and assembling the prototype, the necessary angles are verified by means of a digital level, as it is presented in the Figure 4.22(a), to confirm that they correspond to those needed for the experiment. Considering the azimuth angle for the test, two additional prototypes had to be used, as it is presented in the Figure 4.22(b). These had to be conditioned to place the photovoltaic concentration prototype on them, to use them as it is observed in the Figure 4.22(c).

(a) Reflector angle validation

(b) Azimuth prototype

(c) Prototype built without panel

Figure 4.22: *Prototype concentrator manufactured*

Considering that the case study is carried out in Medellin, Colombia, the concentrator is given a tilt of 10°

4.5.2.1 Development of the electronic system

An electronic device was designed to take generation data, which is composed of an Arduino as a microcontroller, 2 Wattmeters, two PWM regulators for the PV panel, a 12V battery, two temperature sensors and an electronic load. This was done with the objective of being able to measure the output power of two photovoltaic concentrators for a sample each second. In addition, an electronic load was used with the aim of draining a constant current to the system, and, thus, ensure that the difference in generation of the panels is due to the texture that has a concentrator with respect to the other. This electronic device is presented in the Figure 4.23.

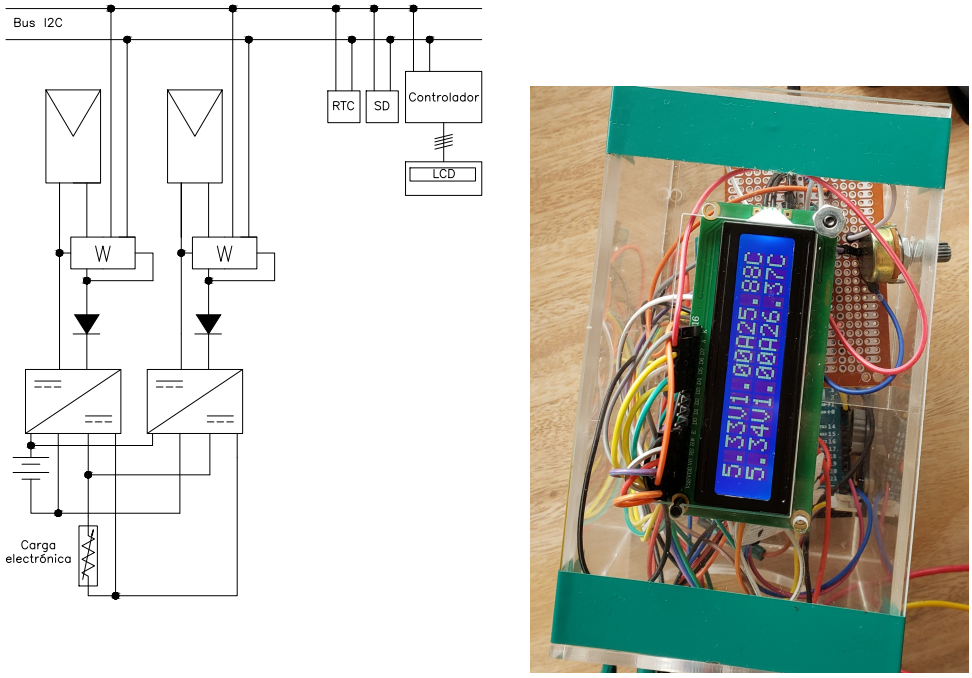

(a) Electronic sheet (b) Electronic circuit assembly

Figure 4.23: *Electronic device*

4.5.3 Location

The experiment was set up on the terrace of a building at EAFIT University, Medellín, Colombia. To carry out the experiment, this place was defined because there are no building obstacles for the light emitted by the sun, which makes the rays arrive directly within the time interval defined for the tests. The experimental setup is presented in the Figure 4.24.

Figure 4.24: *Experimental setup*

4.5.4 Data Collection

This section shows how the data collection was done for the days in which the tests were performed, for which an example of a data collection day is shown in the Figure 4.25, where can be seen, in general, that the panel 2, which has the texture (45° and 60°), is usually above the panel 1 which means no texture.

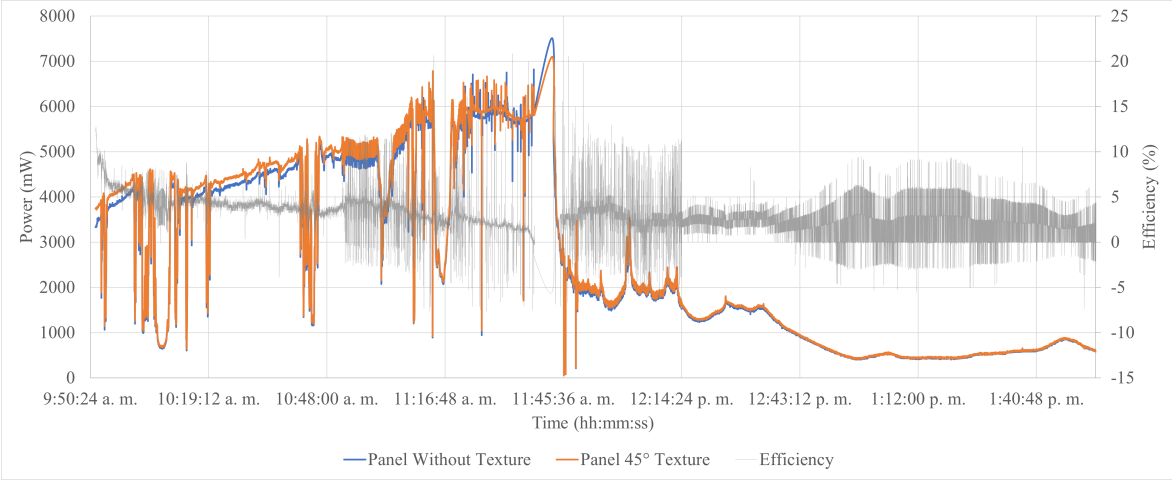

(a) 45° texture data

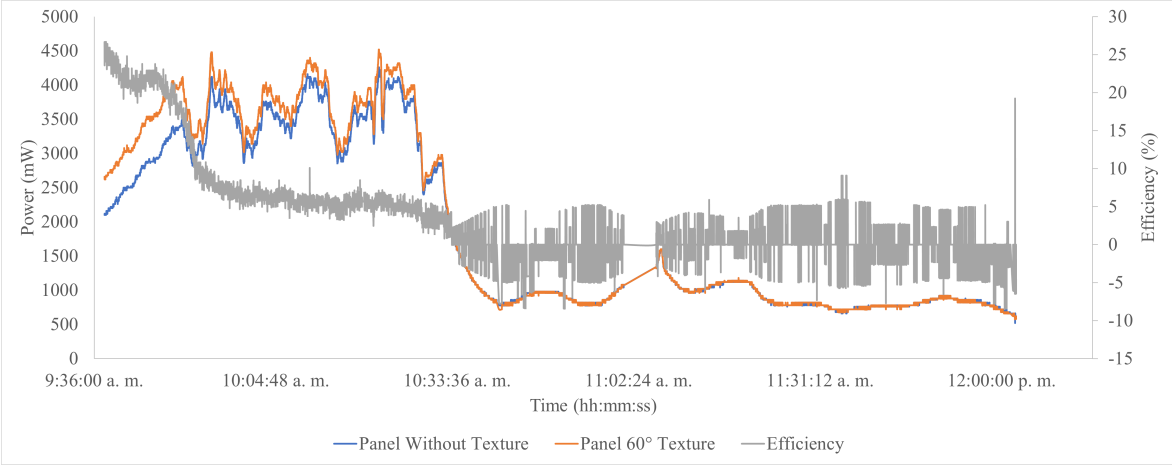

(b) 60° texture data

Figure 4.25: *Collected data respecting energy generation*

For data collection, data are taken every second during different days, at times from 9:30 am to 2:30 pm, in order to collect as much data as possible, and these times are selected because the inclination of the designed concentrators generates shadows before 10:00 am and after 2:00 pm.

A data filtering is performed in order to determine the data that can be analyzed, considering that about 416,000 data were collected. To do this, a day is determined as a control day, that is, a day where both concentrators are placed without any texture to collect data, this is because between both panels there is a

difference of factory, which can affect the results. Therefore, a relation of panels is taken between panel 2 and panel 1, always understanding that panel 2 is the one that takes the texture, either of 45º or of 60º, for all the days of tests, except the control day where none takes texture, as explained previously. From the above, the intercepts where the control day intersects with any of the other days where there was presence of textures were found. Figure 4.26(a) presents the intercepts with the texture of 45º, and Figure 4.26(b) presents the intercepts with the 60º texture.

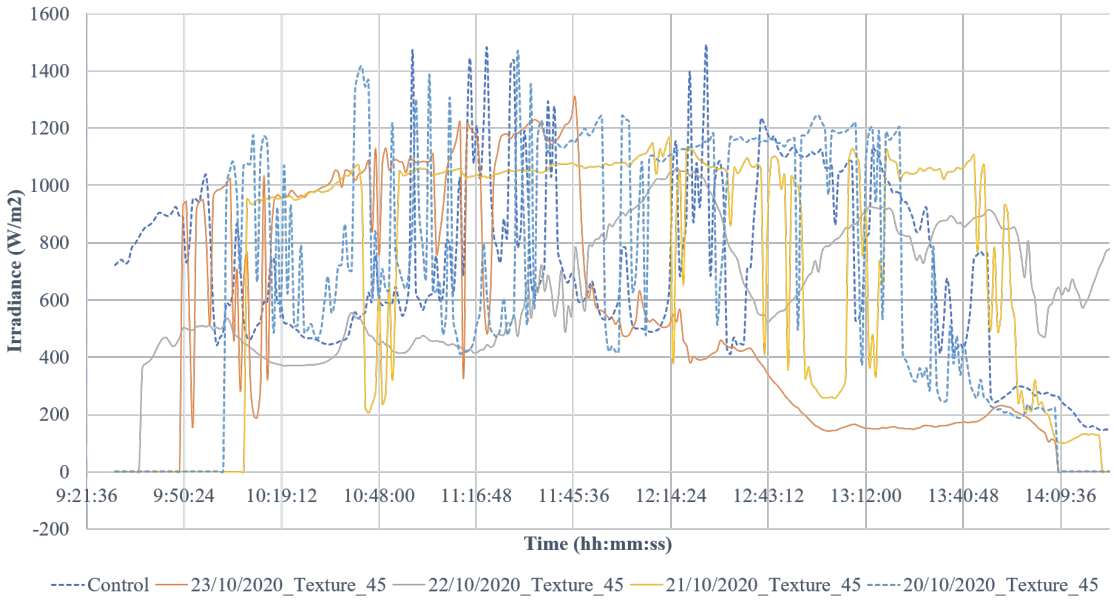

(a) 45° texture data

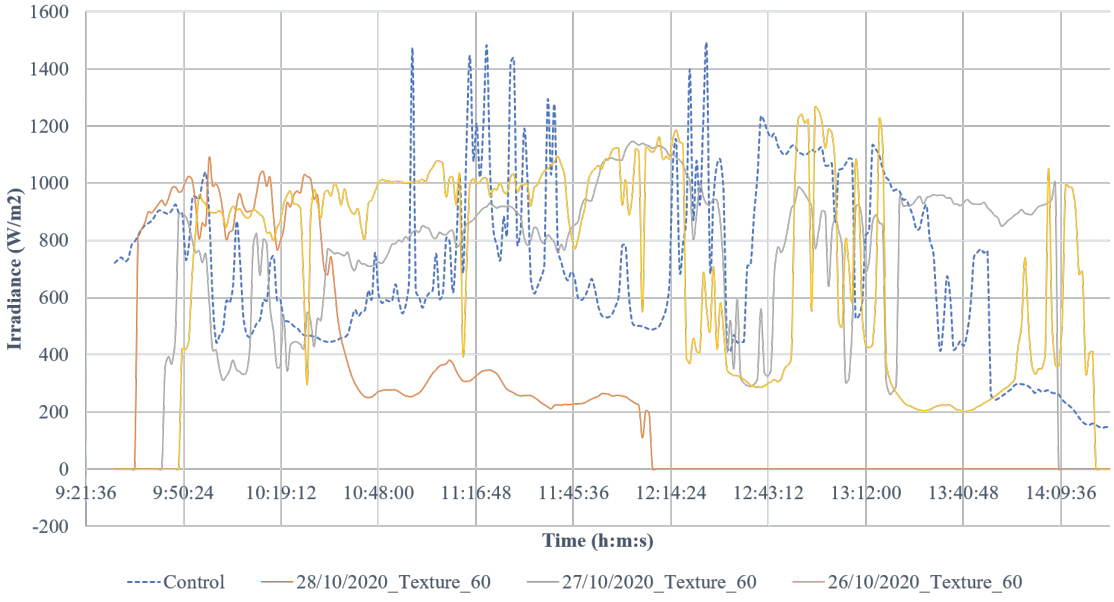

(b) 60° texture data

Figure 4.26: *Intercepts for data collection days with respect to the control day*

This is intended for looking for the points that relate the same time and radiation to the test days with a tolerance of +- 20W, in such a way that the data are really comparable between the control and the intercepts of the other days, since the time of day is completely linked to the angle of incidence of solar irradiance.

From the intercepts found, the comparable data are determined to be able to perform the data analysis. Figure 4.27 shows a day with the data already filtered for the 60º texture. These data are evaluated by means of an analysis of variance for both textures separately, where for the 45º texture a total of 30 coincidences or points were obtained where there were intercepts and for the 60º texture, 18 points, being thus sufficient points to perform an analysis with amount of representative data.

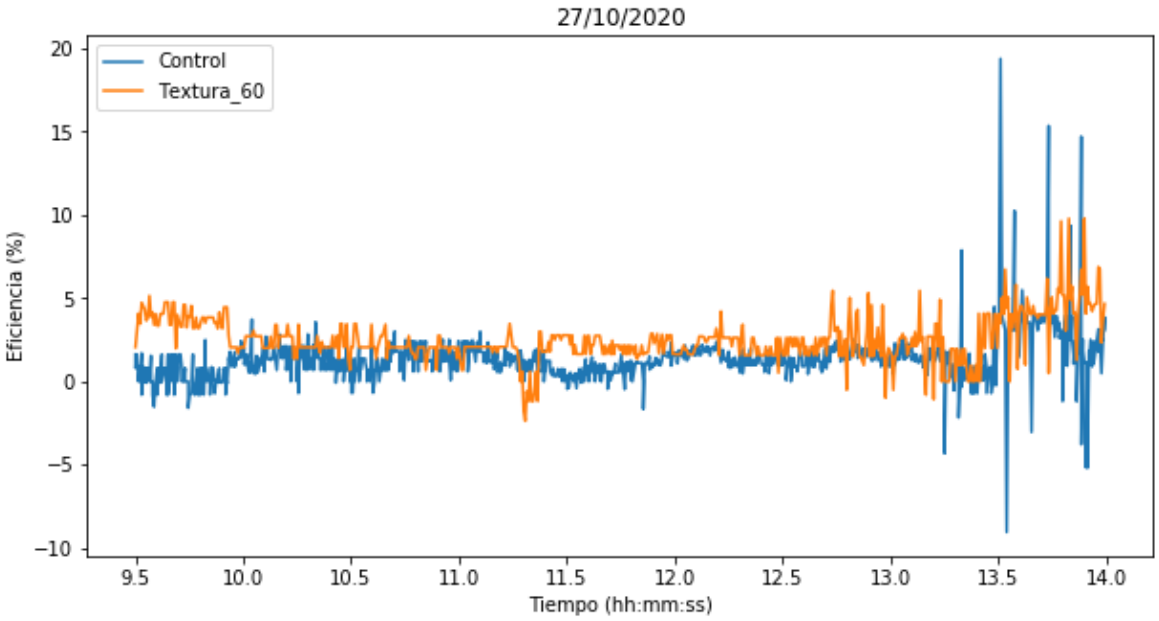

Figure 4.27: *Filtered data.*

After having all the data, a Boxplot diagram is made and presented in the Figure 4.28, to see how is the behavior of the texture contrasting the panel without texture for all the days where intercepts were found. From this graphical analysis it is evident that the average of the values of the relationship texture 45º, are usually above the values of the control relationship, as it is observed in the Figure 4.28(a), and, for the 60º texture the same behavior is observed in the Figure 4.28(b). This shows a first evidence that for both cases, the CVPs with texture usually improve their performance with respect to no texture.

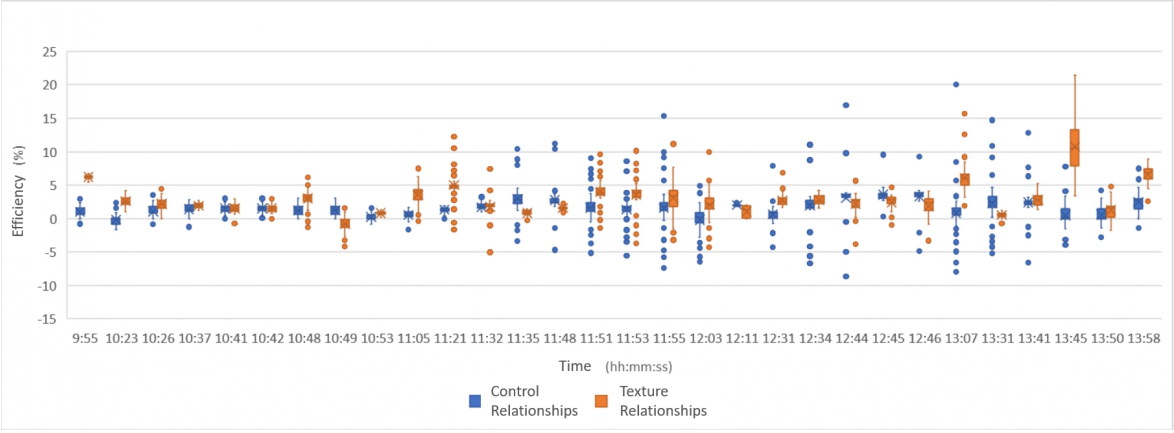

(a) Data hours texture 45° versus panel without texture

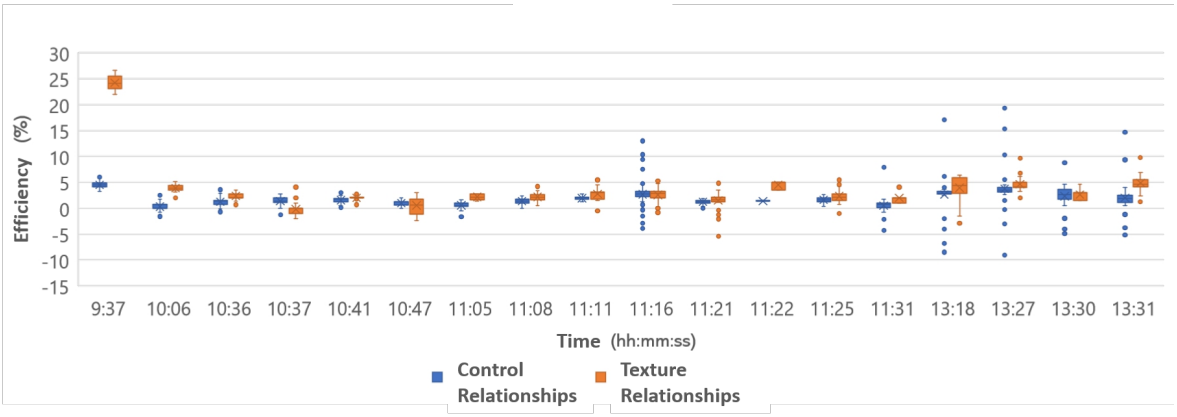

(b) Data hours texture 60° versus panel without texture

Figure 4.28: *Intercepts for data collection days with respect to the control day.*

An ANOVA (Analysis of Variance) is carried out in order to verify that the assumptions of the ANOVA are fulfilled for both experiments, and with the objective of validating if the normal distribution of the data is fulfilled, guaranteeing that the experiment was well conducted, with an alpha minus of 0.5. Two tests were performed for these, the Tukey test and the LCD test. The assumptions of the ANOVA for each hourly interval used for the analysis can be found in Appendix D.

For the 45º texture, as it is observed in the Figure 4.29 and the Table 4.13, it is evident that they belong to different statistical groups where the texture has a higher average than the control, which shows that the implementation of silicone textures of 45° generates an increase in efficiency.

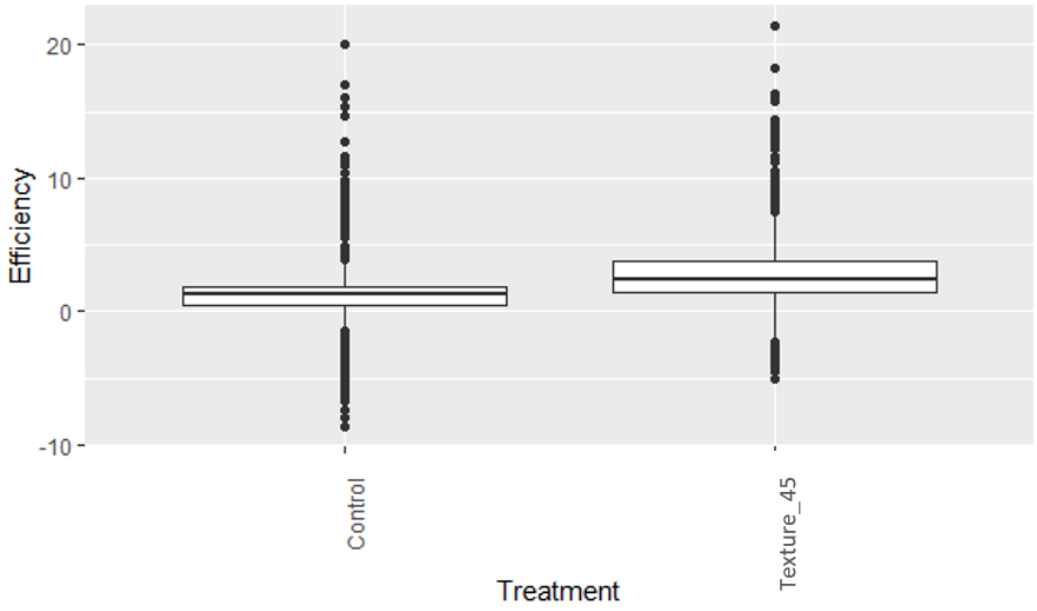

Figure 4.29: *Statistical Group Analysis for 45° Texture*

Test Fisher LSD			Test Tukey		
Treatment	Efficiency	Groups	Treatment	Efficiency	Groups
Texture_45	2.865144	a	Texture_45	2.865144	a
Control	1.253732	b	Control	1.253732	b

Table 4.13: *Test Fisher and Tukey for 45° texture*

Also in the table 4.14 it is possible to observe that it complies with the p-value less than alpha, that is to say that the null hypothesis is rejected.

Analysis of Variance Table					
Response:	Efficiency				
	Df	Sum Sq	Mean Sq	F Value	Pr(>F) Value
Treatment	1	10988	10988.1	333.98	2.20E-16
Residuals	3298	108506	32.9		

Table 4.14: *45º Texture Anova*

For the 60º texture, as it is observed in the Figure 4.30 and the Table 4.15, it is evident that they belong to different statistical groups where the texture has a higher average than the control, which evidences that the implementation of textures in silicone of 60° generates an increase in efficiency.

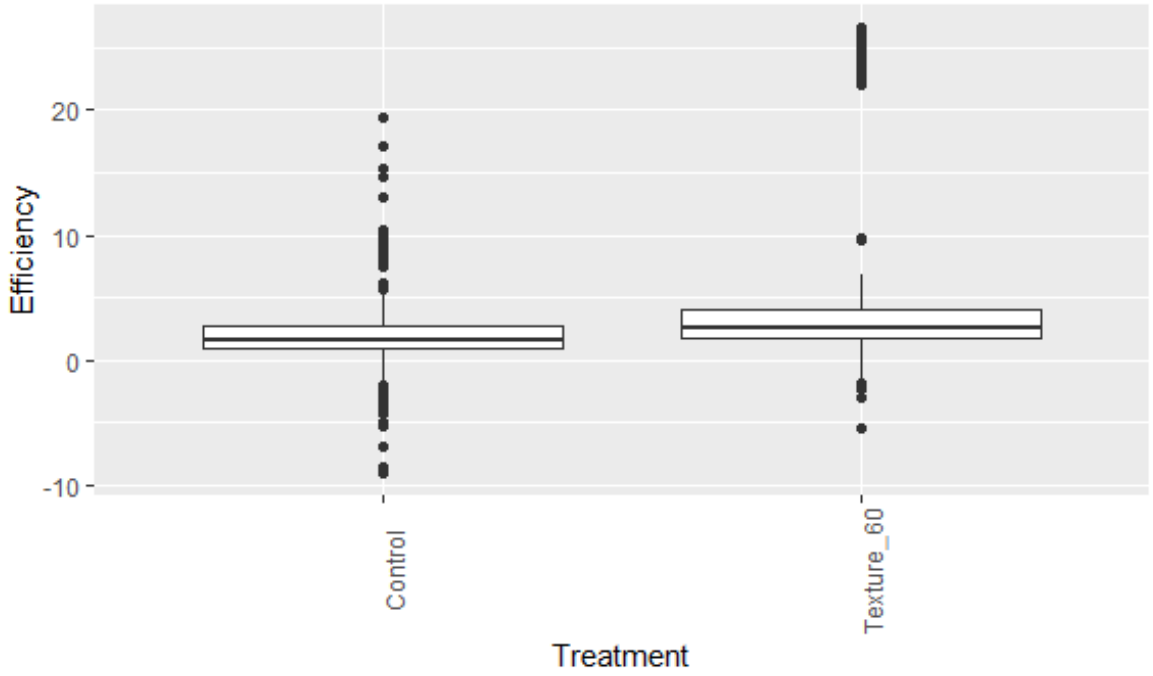

Figure 4.30: *Statistical Group Analysis for 60º Texture*

Test Fisher LSD			Test Tukey		
Treatment	Efficiency	Groups	Treatment	Efficiency	Groups
Texture_60	5.590247	a	Texture_60	5.590247	a
Control	1.940744	b	Control	1.940744	b

Table 4.15: *Test Fisher and Tukey for 60° texture*

From the table 4.15, it can be seen that the average efficiency of the 60º texture is about 5.5% while that of the control is 1.9%, showing an increase of more than 3% caused by the 60º texture. In addition, it complies with the p-value lower than the alpha, as it can be observed in the Table 4.16.

Analysis of Variance Table					
Response:	Efficiency				
	Df	Sum Sq	Mean Sq	F Value	Pr(>F) Value
Treatment	1	10988	10988.1	333.98	2.20E-16
Residuals	3298	108506	32.9		

Table 4.16: *60º Texture Anova*

Finally, a statistical group analysis is performed for each of the hours where the texture and control relationships were comparable, in order to determine when the texture worked better, and, when it was equal or worse than the control. To do this, a Tukey test is also performed for both textures, where the results can be seen in the Figure 4.31 and the Figure 4.32.

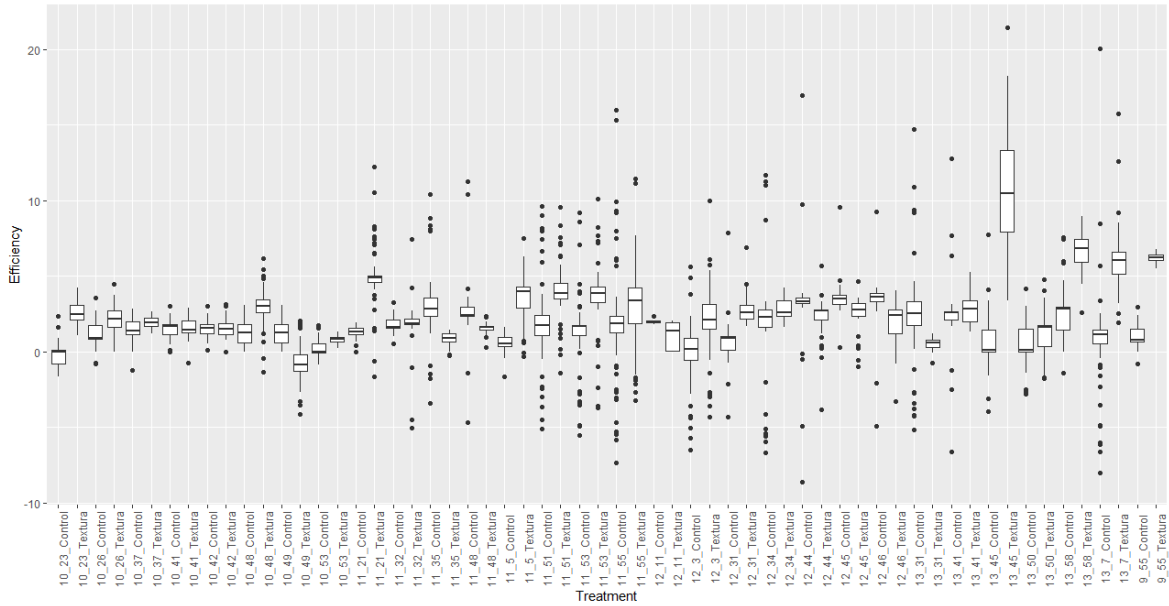

Figure 4.31: *Statistical groups for each hour in 45º texture*

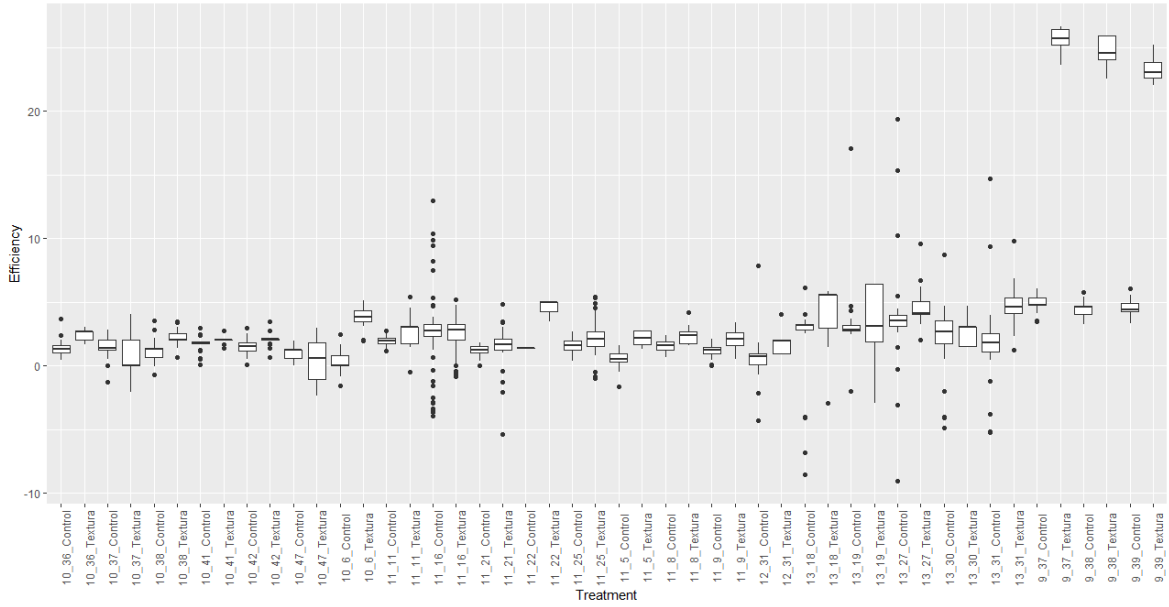

Figure 4.32: *Statistical groups for each hour in 60º texture*

For the texture of 45°, in the 60% of the cases, it was a better statistical group than the control, and, for the texture of 60°, more than the 80% of the groups obtained better results.

Subsequent to the results obtained by the method described above, an analysis is performed by means of a current and voltage curve tracer. For this, the concentrator with the texture that obtained the best result previously, i.e. 60º, is used, and the texture in the concentrator is measured with the tracer for periods of time

of less than 1 minute, in such a way that the available solar resource does not change, and, then, the texture is removed as quickly as possible, and the curve is traced on the concentrator without texture again, in order to ensure that the solar resource is the same for both implementations. In order to perform this test, it must be carried out during several days due to the high level of cloudiness at the test site, so that data remains throughout the day between 9:30 am and 2:00 pm.

For the test with the solar characterization, some data could be compared during 3 days, giving as a result an increase of 1.45% of efficiency when the texture is implemented, but also giving a higher energy value, as it can be seen in the Table 4.17.

Maximum Power Point				
Time	60° Texture (W)	No Texture (W)	Irradiance (W/m^2)	Efficiency
9:20	1,289	1,275	270	1,1%
10:11	2,44	2,352	780	3,74%
10:45	1,387	1,316	300	5,4%
11:17	1,348	1,337	270	0,82%
11:45	6,401	6,529	1200	-1,96%
12:11	5,836	6,039	1050	-3,36%
12:28	5,686	5,745	1050	-1,02%
12:40	5,621	5,542	1050	1,42%
13:50	3,843	3,79	890	1,39%
14:02	2,754	2,573	870	7,03%
Energy (Wh)	**36.605**	**36.498**		1,45%

Table 4.17: *Tests with IV Characterizer*

Something important to emphasize is that as the sun moves away from noon the efficiency increases, as it is observed in the Figure 4.33.

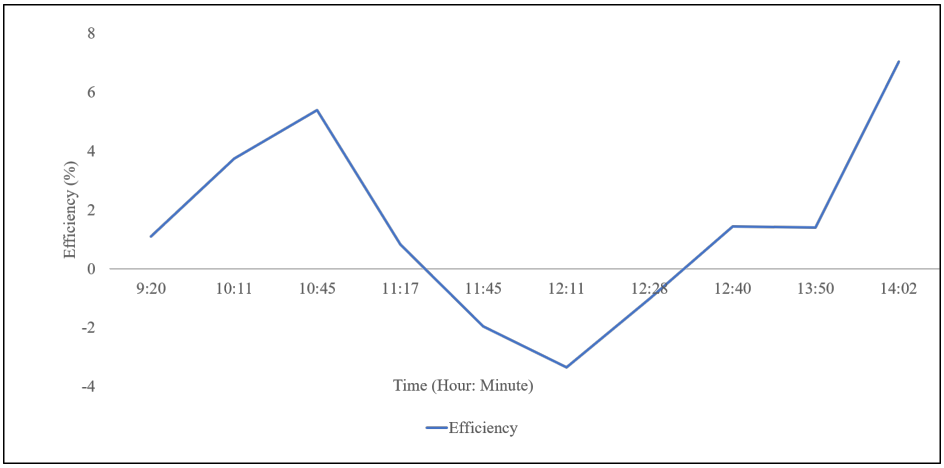

Figure 4.33: *Efficiency curve with characterizer for different moments of the day*

The losses at midday may be partly due to the adhesion that the texture has on the panel, since for some

cases too many air bubbles were found which can directly affect the efficiency of these, as it can be observed in the Figure 4.34. This was corrected by using glass cleaner, since this liquid allows to remove grease and dirt that may be in the photovoltaic panel so that when the texture is adhered, it is better assembled, but avoiding 100% of the bubbles is impossible due to the rigidity of the silicone and the finish that has the photovoltaic glass. Also, as the day passed by, the corners of the manufactured texture began to detach the silicone, generating a greater amount of bubbles which directly affect the performance of the texture due to the generation of small layers of air when light passes through it, trying to pass to the air and being a medium close to a refractive index of 1, light rays or photons in a large amount of point are reflected as the difference in magnitude between the two media is large.

Figure 4.34: *Air bubbles due to adhesion between texture and CPV*

Chapter 5

Conclusions

The primary thing that this work allows to observe is that, although different studies present how to improve the efficiency of photovoltaic concentrators, either for industry or for the residential sector, and, multiple strategies to include texture in photovoltaic arrays, either from the components closest to silicon or in the encapsulating materials that make up the photovoltaic panels, there is no evidence of work that seeks to improve the optical performance of V-Trough type photovoltaic concentrators, with the use of anti-reflective layers with pyramidal textures, which opens an important avenue of research because it proposes solutions that seek, above all, a cost efficiency, that allows the implementation of renewable energy in a sustainable and efficient manner.

The proposed method allows to validate in a coherent way the use of the textures for photovoltaic concentration, in this one can be seen of explicit way as it is the process of design and manufacture of the textures and of the prototypes of the CPV, with the aim to come to a proposal of experimental validation supported in the simulations previously realized. For the manufacture of the texture, an important research was carried out regarding materials that had adequate optical properties to generate an anti-reflective layer, taking into account their refraction index. In this, Silicone for its properties and Epoxy Resin for the ease of obtaining the material, being a material easy to handle and abundant in the industry, stood out for the selection of material for the texture. However, during the research, materials with quite low refraction indexes were evidenced, close to the value of ideal anti-reflective layer, which leaves open the possible implementation of other types of materials in future research, which, thus, allow to seek to improve even more the efficiency of the systems, either by means of anti-reflective layers or by encapsulating the panels in this type of materials.

Another important objective achieved in this work was the manufacture of the texture where, through different aluminum molds, silicone layers with textures of 45 ° and 60 ° quite close to the proposed CAD models were generated. For this, CNC machinery was used. But, it also allowed to experiment with different types of silicones where it could be verified that the properties of light transmittance vary depending on the silicone used, as it was shown in the tests made with the spectrophotometer, where it was found that the Qsil silicone obtained values superior to 90% of amount of photons that passed to the spectrophotometer, unlike the

RTV silicone of the Esquim brand, which was in some points below 80% in the light transmittance.

In the simulation section it was possible to validate the operation of the TracePro software, carrying out an iterative process of simulations where the parameters were changed and improved to arrive at a model similar to that of a commercial photovoltaic panel (See appendix B). For this one, obtained results show an indication of the operation of the textures in the photovoltaic concentrator where the simulation with silicone texture at 45º increases on average 4.4%, while that of 60° increases 4.5% in the horizontal photovoltaic concentrator, obtaining punctual values in the simulation of increases of up to 8.5% in the case of RTV silicone for an incidence angle of 30°. For the case of the simulation carried out in the photovoltaic concentrator in a vertical position, an average increase of 2.75% is found for the 45º texture, as opposed to the 60 texture where an average value of 4.52% was reached for the silicone RTV. In this simulation significant differences were found between both textures, where for the highest values the 60º texture obtained improvements of 19.04%, however for the 45º texture for the angles from 40º to 90º the efficiency increases were close to 0%.

Something important to add in the simulations is that the realization of the tests with continuous diffuse irradiance showing a positive behavior, where it was obtained that for the 60° texture an increase in the efficiency above 5% in the case of the Silicones applied to the horizontal concentrator. However, for the vertical panel values above 6% were obtained. With all the previous data analyzed, a statistical group test was carried out, which showed that for the simulations in the horizontal concentrator, the textures mainly with silicone showed significant differences with the groups where there were no concentrators, a different case from that of the vertical panel where for all the treatments the groups showed no statistical differences, which is why the experimental phase was preceded only by the horizontal configuration. Silicone shows at least 0.5% higher performance than Epoxy Resin, for all tests performed. In the Horizontal Concentrator the effect of the texture is greater than if there were no concentrators where for angle of 30° and 35°, it can be 16 times better than if there is no concentrator. Although the texture shows an increase in yield at the vertical concentrator no different statistical groups are determined for this solution.

In the case of the results obtained by carrying out the experiment, improvements of the Normalized Efficiency more than 5% were evidenced for the 60° texture during the days in which data were obtained, for this one, behaviors above 6% were evidenced in the morning hours and close to 2: 00 pm, and similar behaviors between texture and non-texture when approaching noon; where for the 45° texture there was an average improvement of 2%, with similar behaviors in terms of the solar angle with the 60° texture. For the analysis of the data of the textures for each moment of the day where there could be measurements the 60% of the measurements with the texture of 45° were different statistical groups, being better the texture, while in the texture of 60° it was more than 80%. Also, it is important to say, that during the days of tests, there were several cloudy moments where the percentage of diffuse irradiation surpassed the direct one. However, as a main result and with an important tendency with respect to the simulations, the 60º texture obtains better performance than the 45º texture. In terms of electrical generation, the tests performed with the Amprobe characterizer show that

there is an increase in the generation for the moments in which it was evaluated during the different days, these were of 0.107W, showing an increase of 1.45% of the generation for the system, however at points where the sun had inclination angles close to the point where the reflector generates shadow, increases of up to 7.03% are found, showing a positive effect of the use of the texture. In addition, at points close to midday, the efficiency is negative, however this result is also attributed in part to the amount of air bubbles generated in the ARC-PV Panel Texture assembly, a situation that generates reflection of rays outside the PV panel.

From the results presented in the simulations and the experiments carried out, it can be concluded that the application of the texture in the concentrators demonstrates an opportunity of real implementation of these in urban contexts, where the difficulty of obtaining solar resource during the whole day in solar panels can be difficult due to the obstacles generated by large buildings. Therefore, the prominence of CPVs is seen as a solution to these needs and the adaptation of an economical optical strategy such as ARC Textures proposed in this project also allows to improve the amount of light collected by these systems. Something interesting that can come out of this type of applications is that depending on the application, i.e., if it is going to go in a clear place, with obstacles, in vertical or horizontal facade or some tilt angle, is that it allows to define different configurations that aim to increase efficiency and reduce costs, for example, as it was seen in the simulation results of the vertical CPV, including the ARC Texture did not generate a significant difference in generation, but in contexts where there is full light during the whole day, it can be a better strategy a conventional photovoltaic panel with the ARC Texture or as in the case of the Horizontal CPV, adding also the ARC Texture, demonstrates an improvement in generation.

Finally, in the realization of the experiments a factor to improve is the adhesion of the texture to the photovoltaic panel, this because during the experiments a great amount of air bubbles were evidenced that affected the performance of the textures, this because when a layer of air is generated, a medium with a refraction index similar to 1 is produced, which generates an obstacle for the passage of light and generates reflections. This was solved in a certain way by cleaning the glass of the photovoltaic panel with glass cleaners, this to remove the grease and thus make the silicone adhere better. However, in the corners as time went by, air began to get between the silicone and the glass, which began to affect the performance. From here it is determined that as a future work, different forms or mechanisms must be found to generate a better adhesion between the silicone and the glass since this directly affects the performance of the system, which allows better results to be obtained.

References

IRENA. LCOE 2010-2017, 2018. URL /Statistics/View-Data-by-Topic/Costs/LCOE-2010-2017.

Ran Fu, David Feldman, and Robert Margolis. U . S . Solar Photovoltaic System Cost Benchmark : Q1 2018. Technical Report Novmnber, 2018. URL https://www.nrel.gov/docs/fy16osti/66532.pdf.

Ricardo Mejía Andrés Arias-rosales. *Solar beam radiation modeling for design and simulation of V-Trough photovoltaic applications*. PhD thesis, EAFIT, 2017.

Imre Horvath. Differences between'research in design context'and'design inclusive research'in the domain of industrial design engineering. *Journal of Design Research*, 7(1):61–83, 2008.

Guiqiang Li, Gang Pei, Jie Ji, Ming Yang, Yuehong Su, and Ning Xu. Numerical and experimental study on a pv/t system with static miniature solar concentrator. *Solar Energy*, 120:565–574, 2015.

Qingdong Xuan, Guiqiang Li, Gang Pei, Jie Ji, Yuehong Su, and Bin Zhao. Optimization design and performance analysis of a novel asymmetric compound parabolic concentrator with rotation angle for building application. *Solar Energy*, 158:808–818, 2017.

Homan Hadavinia and Harjit Singh. Modelling and experimental analysis of low concentrating solar panels for use in building integrated and applied photovoltaic (bipv/bapv) systems. *Renewable Energy*, 139:815–829, 2019a.

Takahiro Takumi, Savanna Lloyd, Hideyuki Murata, and Varun Vohra. Low-cost light manipulation coatings for polymer solar cell photocurrent increase under various incident angles. *Materials Research Letters*, 7(2): 68–74, 2019.

S Jalaly, M Vahdani, M Shahabadi, and G Mir Mohamad Sadeghi. Design, fabrication, and measurement of a polymer-based anti-reflection coating for improved performance of a solar panel under a specific incident angle. *Solar Energy Materials and Solar Cells*, 189:175–180, 2019.

Prathusha Bodhanker, Ann Bradish, and John Kelly Kissock. Design and performance improvement of mirror augmented photovoltaic systems. *ASME 2016 10th International Conference on Energy Sustainability, ES*

2016, collocated with the ASME 2016 Power Conference and the ASME 2016 14th International Conference on Fuel Cell Science, Engineering and Technology, 1:1–7, 2016. doi: 10.1115/ES2016-59366.

EEA. Infografía — Agencia Europea de Medio Ambiente, 2013. URL https://www.eea.europa.eu/es/senales/senales-2013/infografia.

Francisco Manzano-Agugliaro, Alfredo Alcayde, Francisco G Montoya, Antonio Zapata-Sierra, and Consolación Gil. Scientific production of renewable energies worldwide: An overview. *Renewable and Sustainable Energy Reviews*, 18:134–143, 2013.

International Renewable Energy Agency IRENA. Conclusiones principales: Costos de generación de energía renovable en 2019. Technical report, 2020.

Nadarajah Kannan and Divagar Vakeesan. Solar energy for future world: - A review. *Renewable and Sustainable Energy Reviews*, 62:1092–1105, 2016. ISSN 18790690. doi: 10.1016/j.rser.2016.05.022.

Richard Hantula. *Science in the real world: How Do Solar Panels Work*. 2010. ISBN 9781604134728. URL http://www.livescience.com/41995-how-do-solar-panels-work.html.

Andrew Clifton, Bri-Mathias Hodge, Caroline Draxl, Jake Badger, and Aron Habte. Wind and solar resource data sets. *Wiley Interdisciplinary Reviews: Energy and Environment*, 7(2):e276, 2018.

IRENA. Costs. URL https://www.irena.org/costs.

Mireille B Tadie Fogaing, Hermes Gordon, Carlos F Lange, David H Wood, and Brian A Fleck. *Concentrated Photovoltaic (CPV): From Deserts to Rooftops*, volume 70. Springer International Publishing, 2019. ISBN 978-3-030-05635-3. doi: 10.1007/978-3-030-05636-0. URL http://link.springer.com/10.1007/978-3-030-05636-0.

Guiqiang Li, Qingdong Xuan, M.W. Akram, Yousef Golizadeh Akhlaghi, Haowen Liu, and Samson Shittu. Building integrated solar concentrating systems: A review. *Applied Energy*, 260:114288, feb 2020. ISSN 0306-2619. doi: 10.1016/J.APENERGY.2019.114288. URL https://www.sciencedirect.com/science/article/pii/S0306261919319750{#}f0015.

Homan Hadavinia and Harjit Singh. Modelling and experimental analysis of low concentrating solar panels for use in building integrated and applied photovoltaic (BIPV/BAPV) systems. *Renewable Energy*, 139:815–829, 2019b. ISSN 18790682. doi: 10.1016/j.renene.2019.02.121. URL https://doi.org/10.1016/j.renene.2019.02.121.

Wei Lu, Zhishan Liu, Jan-Frederik Flor, Yupeng Wu, and Mo Yang. Investigation on designed fins-enhanced phase change materials system for thermal management of a novel building integrated concentrating pv. *Applied Energy*, 225:696–709, 2018.

Rong Ji Xu, Xiao Hui Zhang, Rui Xiang Wang, Shu Hui Xu, and Hua Sheng Wang. Experimental investigation of a solar collector integrated with a pulsating heat pipe and a compound parabolic concentrator. *Energy Conversion and Management*, 148:68–77, 2017.

Wandong Zheng, Lin Yang, Huan Zhang, Shijun You, and Chunguang Zhu. Numerical and experimental investigation on a new type of compound parabolic concentrator solar collector. *Energy Conversion and Management*, 129:11–22, 2016.

Xue Xiaodi, Zheng Hongfei, He Kaiyan, Chen Zhili, Tao Tao, and Xie Guo. Experimental study on a new solar boiling water system with holistic track solar funnel concentrator. *Energy*, 35(2):692–697, 2010.

Baljit Singh and MY Othman. A review on photovoltaic thermal collectors. *Journal of renewable and sustainable energy*, 1(6):062702, 2009.

Yupeng Wu, Karen Connelly, Yuzhe Liu, Xiaowen Gu, Yanfeng Gao, and George Z Chen. Smart solar concentrators for building integrated photovoltaic façades. *Solar Energy*, 133:111–118, 2016.

Qingdong Xuan, Guiqiang Li, Yashun Lu, Bin Zhao, Xudong Zhao, and Gang Pei. Daylighting characteristics and experimental validation of a novel concentrating photovoltaic/daylighting system. *Solar Energy*, 186: 264–276, 2019a.

Qingdong Xuan, Guiqiang Li, Yashun Lu, Bin Zhao, Xudong Zhao, Yuehong Su, Jie Ji, and Gang Pei. Design, optimization and performance analysis of an asymmetric concentrator-pv type window for the building south wall application. *Solar Energy*, 193:422–433, 2019b.

Eliyas Debebe Mammo, Nazmi Sellami, and Tapas Kumar Mallick. Performance analysis of a reflective 3d crossed compound parabolic concentrating photovoltaic system for building façade integration. *Progress in photovoltaics: research and applications*, 21(5):1095–1103, 2013.

Nabin Sarmah and Tapas K Mallick. Design, fabrication and outdoor performance analysis of a low concentrating photovoltaic system. *Solar Energy*, 112:361–372, 2015.

Pedro Hernandez. Radiación directa, difusa y reflejada, 2014. URL `https://pedrojhernandez.com/`.

Ahmed Hasan, Jawad Sarwar, and Ali Hasan Shah. Concentrated photovoltaic: A review of thermal aspects, challenges and opportunities. *Renewable and Sustainable Energy Reviews*, 94:835–852, 2018.

MAESTRA EN CIENCIAS EN LA. *Texturizado de sustratos de silicio cristalino para aplicaciones en celdas solares*. PhD thesis, Instituto Nacional de Astrofísica, Óptica y Electrónica, 2011.

Robert McConnell, Vasilis Fthenakis, and V Fthenakis. Concentrated photovoltaics. *Third Generation Photovoltaics*, pages 167–182, 2012.

Andrés Arias-Rosales. *Solar beam radiation modeling for design and simulation of V-Trough photovoltaic applications*. PhD thesis, Universidad EAFIT, 2017.

Andrew S Glassner. *An introduction to ray tracing*. Elsevier, 1989.

Guiqiang Li. Design and development of a lens-walled compound parabolic concentrator-a review. *Journal of Thermal Science*, 28(1):17–29, 2019.

Daniel Chemisana. Building integrated concentrating photovoltaics: a review. *Renewable and sustainable energy reviews*, 15(1):603–611, 2011.

Shivangi Sharma, Nazmi Sellami, Asif Tahir, KS Reddy, and Tapas K Mallick. Enhancing the performance of bicpv systems using phase change materials. In *AIP Conference Proceedings*, volume 1679, page 110003. AIP Publishing, 2015.

Qingdong Xuan, Guiqiang Li, Yashun Lu, Bin Zhao, Xudong Zhao, Yuehong Su, Jie Ji, and Gang Pei. Overall detail comparison for a building integrated concentrating photovoltaic/daylighting system. *Energy and Buildings*, 199:415–426, 2019c.

José Luis Torres-Madroñero, Jorge Mario Tamayo-Avendaño, Santiago Bernal-del Río, Julián Sierra-Pérez, César Nieto-Londoño, Ricardo Mejía-Gutiérrez, and Gilberto Osorio-Gómez. Formulation and simulation of a hybrid solar pv-wind generation system with photovoltaic concentration for non-interconnected areas to the energy grid. In *E3S Web of Conferences*, volume 181, page 02002. EDP Sciences, 2020.

Suhaila Abdul Hamid, Mohd Yusof Othman, Kamaruzzaman Sopian, and Saleem H Zaidi. An overview of photovoltaic thermal combination (pv/t combi) technology. *Renewable and Sustainable Energy Reviews*, 38:212–222, 2014.

Hasan Baig, Nazmi Sellami, and Tapas K Mallick. Performance modeling and testing of a building integrated concentrating photovoltaic (bicpv) system. *Solar energy materials and solar cells*, 134:29–44, 2015.

Karen Connelly, Yupeng Wu, Jun Chen, and Yu Lei. Design and development of a reflective membrane for a novel building integrated concentrating photovoltaic (bicpv)'smart window'system. *Applied energy*, 182: 331–339, 2016.

Li Zhu, Zebiao Shao, Yong Sun, Veronica Soebarto, Feng Gao, George Zillante, and Jian Zuo. Indoor daylight distribution in a room with integrated dynamic solar concentrating facade. *Energy and Buildings*, 158:1–13, 2018.

Katie Shanks, Ashley Knowles, Adam Brierley, Hasan Baig, Henry Orr, Yanyi Sun, Yupeng Wu, Senthilarasu Sundaram, and Tapas Mallick. An experimental analysis of the optical, thermal and power to weight perfor-

mance of plastic and glass optics with ar coatings for embedded cpv windows. *Solar Energy Materials and Solar Cells*, 200:110027, 2019.

Wisam AM Al-Shohani, Raya Al-Dadah, Saad Mahmoud, and Abdulmaged Algareu. Optimum design of v-trough concentrator for photovoltaic applications. *Solar Energy*, 140:241–254, 2016.

Harry Apostoleris, Marco Stefancich, and Matteo Chiesa. Tracking-integrated systems for concentrating photovoltaics. *Nature Energy*, 1(4):16018, 2016.

Muhammad Burhan, Muhammad Wakil Shahzad, and Kim Choon Ng. Concentrated photovoltaic (cpv): From deserts to rooftops. In *Advances in Sustainable Energy*, pages 93–111. Springer, 2019.

M Pociask-Bialy, KD Mynbaev, and M Kaczmarzyk. Light trapping by chemically micro-textured glass for crystalline silicon solar cells. *Opto-Electronics Review*, 26(4):307–311, 2018.

Ming Jong Tsai, SY Chen, JW Chen, RB Huang, and TL Lin. An epoxy-based micro-structure surface for improving anti-reflection efficiency of a solar cell module. In *Applied Mechanics and Materials*, volume 598, pages 317–321. Trans Tech Publ, 2014.

Lalit K Verma, Mridul Sakhuja, J Son, AJ Danner, H Yang, HC Zeng, and CS Bhatia. Self-cleaning and antireflective packaging glass for solar modules. *Renewable Energy*, 36(9):2489–2493, 2011.

P Grunow, D Sauter, V Hoffmann, D Huljić, B Litzenburger, and L Podlowski. The influence of textured surfaces of solar cells and modules on the energy rating of pv systems. *20th EPVSEC, Barcelona*, 2005.

Andrea Ingenito, Olindo Isabella, and Miro Zeman. Nano-cones on micro-pyramids: modulated surface textures for maximal spectral response and high-efficiency solar cells. *Progress in Photovoltaics: Research and Applications*, 23(11):1649–1659, 2015.

Carolin Ulbrich, Andreas Gerber, Ko Hermans, Andreas Lambertz, and Uwe Rau. Analysis of short circuit current gains by an anti-reflective textured cover on silicon thin film solar cells. *Progress in Photovoltaics: Research and Applications*, 21(8):1672–1681, 2013.

Hye Jin Nam, Soon Cheol Jeong, Duk-Young Jung, Young Kuk Kim, Kyu Min Han, and JunSin Yi. Fabrication of textured silicon solar cell using microlens as anti-reflection layer. In *2008 Conference on Optoelectronic and Microelectronic Materials and Devices*, pages 246–248. IEEE, 2008.

Jordi Escarre, Karin Söderström, Matthieu Despeisse, Sylvain Nicolay, Corsin Battaglia, Gregory Bugnon, Laura Ding, Fanny Meillaud, Franz-Josef Haug, and Christophe Ballif. Geometric light trapping for high efficiency thin film silicon solar cells. *Solar Energy Materials and Solar Cells*, 98:185–190, 2012.

Patrick Campbell and Martin A Green. Light trapping properties of pyramidally textured surfaces. *Journal of Applied Physics*, 62(1):243–249, 1987.

U Blieske, T Doege, P Gayout, M Neander, D Neumann, and A Prat. Light-trapping in solar modules using extra-white textured glass. In *3rd World Conference onPhotovoltaic Energy Conversion, 2003. Proceedings of*, volume 1, pages 188–191. IEEE, 2003.

MODAVIS ROBERT ADAM. Photovoltaic dual textured glass, jul "31" 2014. WO Patent 2014116778A1.

WEIKINGER JOSEF. Glass pane, may "6" 2004. US Patent 20040086716A1.

LU YIWEI; ST JEAN JIM; MELLOTT NATHAN P; WANG ZHONGMING. Lighting system cover including AR-coated textured glass, and method of making the same, mar "18" 2010. US Patent 20100067223A1.

SCHIAVONI MICHELE; GAYOUT PATRICK; NOSITSCHKA WOLFGANG ANDREAS. Textured transparent plate and method of manufacturing such a plate, febr "9" 2016. US Patent 9257580B2.

KAGEYAMA JUNICHI; SATO KAZUO; KAMBE MIKA. Cover glass for a solar battery, jul "3" 2003. WO Patent 2003054974A1.

J Deubener, G Helsch, A Moiseev, and H Bornhöft. Glasses for solar energy conversion systems. *Journal of the European Ceramic Society*, 29(7):1203–1210, 2009.

J. Hosseinzadeh, A. Mohhebi, and R. Loni. Optical simulation of a solar parabolic collector and cavity receivers using ray-tracing software tracepro with native conditions of IRAN for solar dryers. *INMATEH - Agricultural Engineering*, 59(3):197–208, 2019. ISSN 20682239. doi: 10.35633/INMATEH-59-22.

Li Zhu, Jiqiang Zhang, Qingxiang Li, Zebiao Shao, Mengdong Chen, Yang Yang, and Yong Sun. Comprehensive analysis of heat transfer of double-skin facades integrated high concentration photovoltaic (CPV-DSF). *Renewable Energy*, 2020. ISSN 0960-1481. doi: https://doi.org/10.1016/j.renene.2020.07.045. URL `http://www.sciencedirect.com/science/article/pii/S0960148120311216`.

A. Antonini, M. Stefancich, J. Coventry, and A. Parretta. Modelling of Compound Parabolic Concentrators for Photovoltaic Applications. *International Journal of Optics and Applications*, 3(4):40–52, 2013. ISSN 2163-2979. doi: 10.5923/j.optics.20130304.02.

Jinghu Gong, Chenglong Wang, Chenyang Gong, Fei Liang, and Jun Ma. Study on the uniformity of high concentration photovoltaic system with array algorithm. *Solar Energy*, 153:181–187, 2017. ISSN 0038092X. doi: 10.1016/j.solener.2017.05.046. URL `http://dx.doi.org/10.1016/j.solener.2017.05.046`.

Joel Nicol. The influence of irradiance concentration using an asymmetric reflector on the electrical performance of a PVT hybrid collector with standard monocrystalline cells. (December

2016), 2016. URL https://fenix.tecnico.ulisboa.pt/downloadFile/1407770020545598/thesis{_}Joel{_}Lopez.pdf.

Sasa Pavlovic, Velimir Stefanovic, and Milorad Bojic. Optical simulation of a solar parabolic collector using ray-tracing software TracePro. *WIT Transactions on Information and Communication Technologies*, 57: 211–218, 2014. ISSN 17433517. doi: 10.2495/CCCS130251.

David Jafrancesco, Joao P. Cardoso, Amaia Mutuberria, Erminia Leonardi, Iñigo Les, Paola Sansoni, Franco Francini, and Daniela Fontani. Optical simulation of a central receiver system: Comparison of different software tools, oct 2018. ISSN 18790690. URL https://doi.org/10.1016/j.rser.2018.06.028.

Subarna Maiti, Nabin Sarmah, Pratap Bapat, and Tapas K Mallick. Optical analysis of a photovoltaic v-trough system installed in western india. *Applied optics*, 51(36):8606–8614, 2012.

Haitham M Bahaidarah, Bilal Tanweer, Palanichamy Gandhidasan, and Shafiqur Rehman. A combined optical, thermal and electrical performance study of a v-trough pv system—experimental and analytical investigations. *Energies*, 8(4):2803–2827, 2015.

Naum Fraidenraich. Analytic solutions for the optical properties of v-trough concentrators. *Applied optics*, 31 (1):131–139, 1992.

N Fraidenraich. Design procedure of v-trough cavities for photovoltaic systems. *Progress in photovoltaics: Research and Applications*, 6(1):43–54, 1998.

CS Sangani and CS Solanki. Experimental evaluation of v-trough (2 suns) pv concentrator system using commercial pv modules. *Solar energy materials and solar cells*, 91(6):453–459, 2007.

T Stapiński, K Marszałek, M Lipiński, P Panek, and W Szczepanik. Investigations of solar panels with anhanced transmission glass. *Microelectronic materials and technologies, WUPK, Koszalin*, 285, 2012.

David E Aspnes and AA Studna. Dielectric functions and optical parameters of si, ge, gap, gaas, gasb, inp, inas, and insb from 1.5 to 6.0 ev. *Physical review B*, 27(2):985, 1983.

Malte Ruben Vogt. *Development of physical models for the simulation of optical properties of solar cell modules*. PhD thesis, Technische Informationsbibliothek (TIB), 2016.

Malte R Vogt, Hendrik Holst, Henning Schulte-Huxel, Susanne Blankemeyer, Robert Witteck, David Hinken, Matthias Winter, Byungsul Min, Carsten Schinke, Ingo Ahrens, et al. Optical constants of uv transparent eva and the impact on the pv module output power under realistic irradiation. *Energy Procedia*, 92:523–530, 2016.

Malte Ruben Vogt, Harald Hahn, Hendrik Holst, Matthias Winter, Carsten Schinke, Marc Köntges, Rolf Brendel, and Pietro P Altermatt. Measurement of the optical constants of soda-lime glasses in dependence of iron content and modeling of iron-related power losses in crystalline si solar cell modules. *IEEE Journal of Photovoltaics*, 6(1):111–118, 2015.

ROBERT TREHARNE et al. *RF Magnetron Sputtering of Transparent Conducting Oxides and CdTe/CdS Solar Cells*. PhD thesis, Durham University, 2011.

Florian Schneider, Jan Draheim, Robert Kamberger, and Ulrike Wallrabe. Process and material properties of polydimethylsiloxane (pdms) for optical mems. *Sensors and Actuators A: Physical*, 151(2):95–99, 2009.

Khuram Ali, Sohail A Khan, and MZ Mat Jafri. Effect of double layer (sio2/tio2) anti-reflective coating on silicon solar cells. *Int. J. Electrochem. Sci*, 9(12):7865–7874, 2014.

Amprobe. SOLAR-600 Solar Analyzer Data Sheet. Technical report. URL `www.Amprobe.com`.

CS Solanki, CS Sangani, D Gunashekar, and G Antony. Enhanced heat dissipation of v-trough pv modules for better performance. *Solar Energy Materials and Solar Cells*, 92(12):1634–1638, 2008.

David Acevedo-Gómez, Alejandro Velásquez-López, Gilberto Osorio-Gómez, and Ricardo Mejía-Gutiérrez. Influence of epoxy resin as encapsulation material of silicon photovoltaic cells on maximum current. In *MATEC Web of Conferences*, volume 108, page 14001. EDP Sciences, 2017.

Valenciana. Ficha técnica aluminio 6061, 2014. URL `http://www.valencianadeacp.com/images/valenciana/fichas-tecnicas/aluminios/Ficha/20Tecnica/20Aluminio/20AW6061VACP.pdf`.

Quantum silicones. QSil 216. Technical report, 2017. URL `www.quantumsilicones.com`.

Esquim. ESQUIM. URL `http://www.esquimcol.com/quimicas.php{#}titulo-pro`.

Didacticas Electrónicas. Paneles: Panel solar policristalino 5W. URL `https://didacticaselectronicas.com/index.php/energia-solar/paneles/panel-solar-policristalino-5w-energ{í}a-solar-celdas-solares-paneles-solares-policristalinos-para-ene`

Daniel Cardona. Proyecto de texturizado en paneles fotovoltaicos, june "06" 2019.

Josef Weikinger. Glass Pane, may "06" 2004. US20040086716A1.

Argos. Ficha técnica. url https://colombia.argos.co/Conoce-nuestros-productos/Agregados, 2017.

Oriel. Ficha técnica. URL `https://www.newport.com/p/94063A`.

Appendix A

Appendix 1:Preliminary tests to manufacture textures

The decision of the process and the material to make the texture is a fundamental part due to the fact that in addition to the fulfillment of certain technical criteria such as refractive indexes, transmittance, shape, etc. The issue of balance between cost and efficiency becomes a crucial factor when designing the texture. For this reason, as a preliminary test, processes that are easy to implement and materials that can be obtained easily and at a good cost were proposed. This experiment was proposed by Cardona [2019] in a final project and will be explained below.

For this, a first test was performed, see figure A.1, where a resin spraying process, Sandblasting, and two CNC methods with symmetrical and asymmetrical shape were tested.

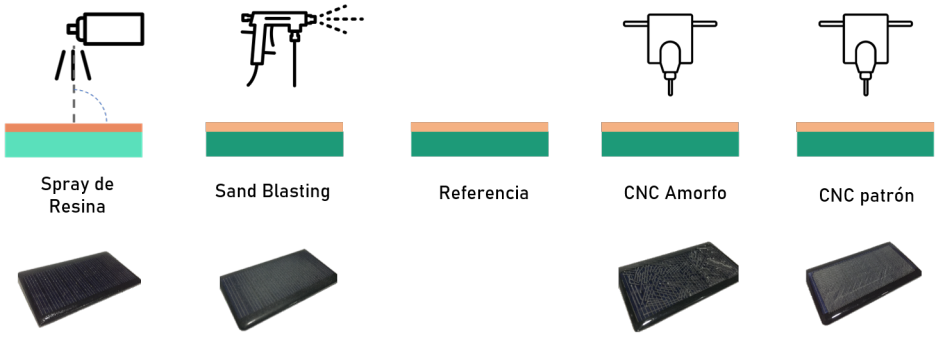

Figure A.1: *Processes of the first test.*

A.1 Epoxy resin Spray

To make hemispherical textures, the resin spray method was used because this method allows to obtain a texture similar to the spray produced by the condensation of water on the plants, which is similar to the shape mentioned above. In the different textures inventions on panel laminates, the textures do not have great difference in size and shape since many of them have pyramidal forms that are generated by means of controlled processes as can be seen in the patents of Weikinger [2004], ADAM [2014], ANDREAS [2016], these have very similar forms and their dispersion does not exceed 3 times the height or radius of these. Due to the above, it is necessary to obtain textures that meet this condition so as not to distort the results of what has been found in the industry and literature.

The process to follow consists of increasing the thickness of the panel generating a texture, since the encapsulation of this also uses resin, Acevedo-Gómez et al. [2017], this in order to check if this material deposited on the panel is capable of increasing the efficiency of the cell. The way to characterize the method was defined as shown in the Table A.1, which resulted in the texture shown in the figure A.2.

Variables	Descripción	Instrumento de medición	Unidades
Experimento de surcos semiesféricos			
Método: espray de resina			
Altura de aplicación	Estandarización del método para todos los paneles de la muestra	Flexómetro	500mm
Distancia horizontal		Flexómetro	500mm
Ángulo de aplicación		Flexómetro	45°
Número de aplicaciones		Observación	4
Nivel lumínico		Light meter	Lux
Resina		Referencia	Gemelos
		Porciones	1 resina 1 catalizador 1 de thinner
Espray (atomizador convencional para re envasar líquidos)	Diámetro interno de toma	Pie de rey	1.5mm
	Diámetro de salida boquilla	Pie de rey	0.2mm
	Compresión de cámara	Pie de rey	6mm
	Precio	-	$1500

Table A.1: *Resin Test Characteristics*

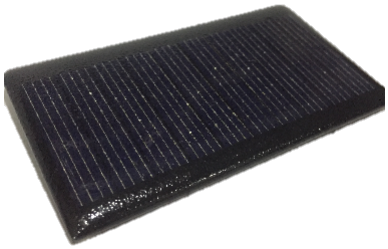

Figure A.2: *Texture with Epoxy Resin*

A.2 Sandblasting

Sandblasting is another of the methods proposed because it allows to generate a rough surface with semispheres from the blows of small sand grains, which are ejected from an air pressure gun. For the use of this method, a type of sand called glue sand is used, which comes from deposits or river alluvial, also has a set of fragments of rocks and minerals that have an approximate size of between 0.074 mm and 4.75 mm, Argos [2017], which was sifted to obtain a grain diameter not exceeding 2 mm which does not generate a very large texture. After several tests in old cells it was concluded that the amount of sand could be 175 grams as it was a favorable amount to cover the entire area and generate visual changes to convert them into an amorphous structure.

The following table A.2 shows the variables used for the application of the Sandblasting method, which resulted in the texture shown in the figure A.3.

Variables independientes	Descripción	Instrumento de medición	Unidades
Experimento para surcos irregulares			
Método: Sand Blasting			
Altura de aplicación	Estandarización del método para todos los paneles de la muestra	Flexómetro	0mm
Distancia horizontal		Flexómetro	100mm
Angulo de aplicación		Goniómetro	45°
Cantidad de arena		Mini báscula	180gr
Nivel lumínico		Light meter	Lux
Presión		Compresor	180psi
Arena	Arena de pega	Módulo de finura	Prom:3.2mm
Cantidad de arena	Peso utilizado	bascula	175 gr
Diámetro mayor de grano	Obtener granos no mayores a 2mm	Tamiz	2mm

Table A.2: *Epoxy Resin Test Features*

Figure A.3: *Sandblasting Texture*

A.3 CNC Scratching

To obtain pyramidal shapes, the CNC scratch method was used by means of a two-axis machining, in addition to a tool sharpened to 45° because the angle defined from the literature to have a more uniform generation during the day is 45°, Tsai et al. [2014], Campbell and Green [1987] . The variables that will be used to proceed with the method are expressed in the table A.3 where you can find those that were extracted from a G code generation software such as the cutting speed and revolutions, since they are directly related to the capacity of the machine. Obtaining as a result the textures that can be seen in the figure A.4.

	Descripción	Instrumento de medición	Unidades
Experimento para surcos piramidales			
Método: Rayado CNC			
Velocidad de corte	Estandarización del método para todos los paneles de la muestra	programado	200m/s
Distancia ente pasadas		Pie de rey	1mm
Profundidad de corte		Pie de rey	0.2mm
Revoluciones		programado	200rpm
Angulo de surco		galga	45°
Velocidad de corte		programado	82mm/s
Diámetro de herramienta		Pie de rey	1/4
Angulo de herramienta		Goniómetro	45°

Table A.3: *Resin Test Characteristics*

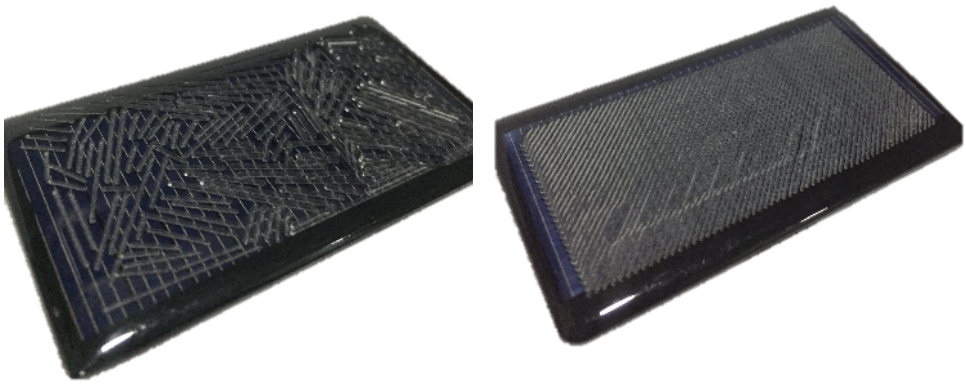

(a) Asymmetric CNC Texture (b) Symmetric CNC Texture

Figure A.4: *Textura CNC*

A.4 Results of the texturing processes

This stage is divided into two important steps, the first were the tests in the simulator and second the results obtained from these tests.

A.4.1 Simulator Testing

To perform the tests we used a sun pattern **Sol3A** from Oriel, see figure A.5 which simulates the standard irradiance (STC) of AM1.5 which is equivalent to 1000 W/m2 at 25°C ,in order to have a measure similar to the spectrum of the sun.

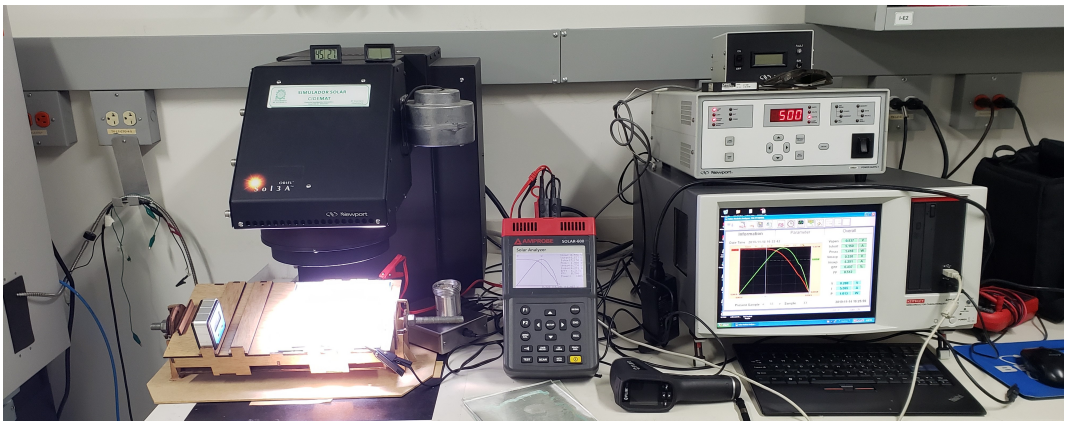

Figure A.5: *Test Bench*

In addition, a current/voltage (IV) curve characterizer from Keithley was used to measure and determine the performance of the solar panels. This can be seen on the right in the figure A.5. In order to carry out the

tests, 10 replicas of each of the treatments were used to look at the dispersion of the data and to ensure that the results obtained are statistically representative, see figure A.6.

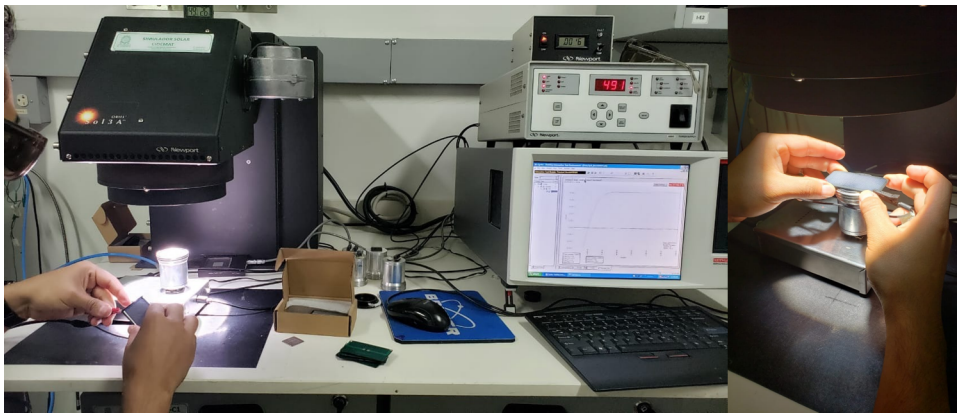

Figure A.6: *Laboratory tests*

A.4.1.1 Test results

To measure the results we opted for a **ANOVA** where it could be validated from a statistical criterion if any of the treatments had a significant increase in efficiency on a panel without texture, resulting in that although the treatment of resin spray is the one with the highest average, the variance of the data can belong to any statistical group, so the **ANOVA** in the Table A.4 and in the figure A.7 shows that there are no different statistical groups so it cannot be concluded that any of the treatments is better than the other.

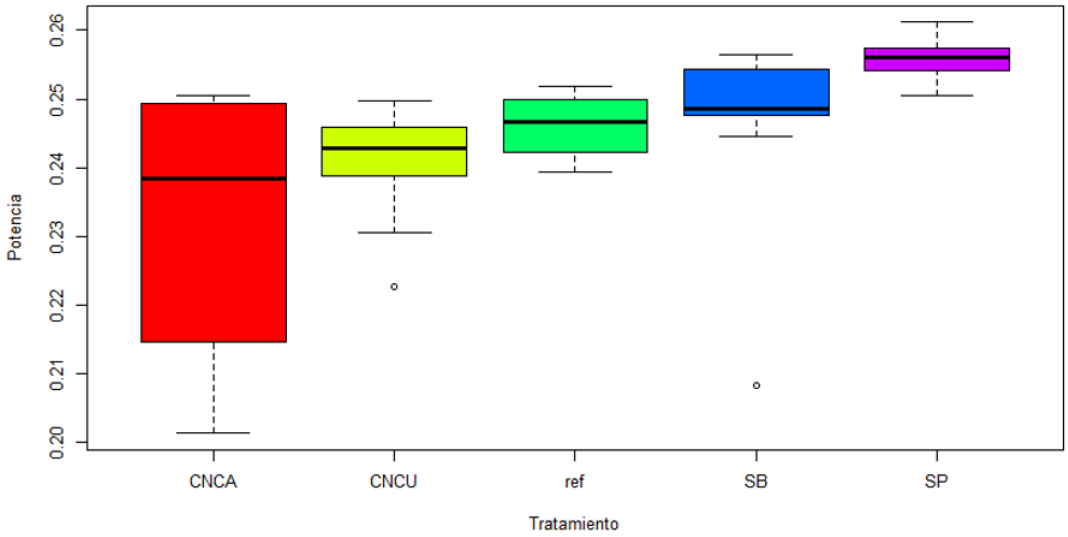

Figure A.7: *Box and Whisker Diagram*

Tratamiento	Media	Grupo Estadístico
SP	0.2558621	a
SB	0.2462813	ab
Referencia	0.2460702	abc
CNC Uniforme	0.2403345	bc
CNC Amorfa	0.2320542	c

Table A.4: *ANOVA table*

From the previous result and seeing that the epoxy resin shows a tendency to improve efficiency, an experiment was designed by means of a controlled spraying process, which allows validating if the dispersion in the data was due to the process and not to the texture. For this, it was proposed to control the distance and spraying by means of a paint gun as shown in the figure A.8(c).

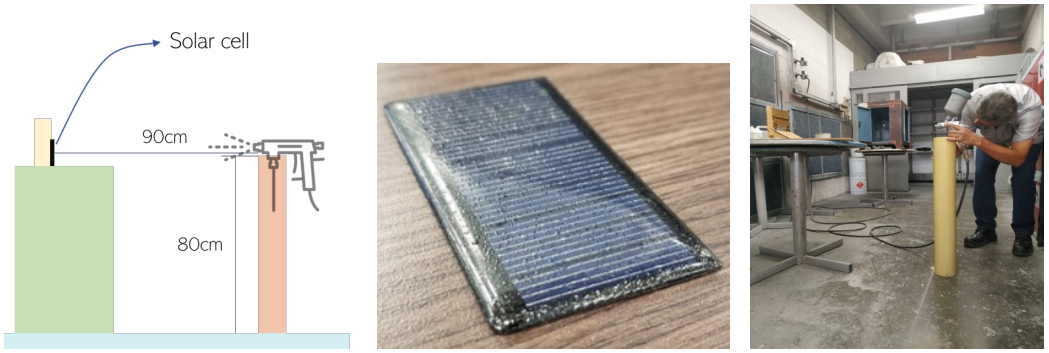

(a) Especificaciones de la prueba (b) Resultado en el panel (c) Proceso de rocío en el laboratorio

Figure A.8: *Controlled Resin Spraying*

However, the results also did not show that any group was statistically different as can be seen in the Table A.5, so it is concluded that from the methods proposed with uncontrolled processes the increase in efficiency is not significant.

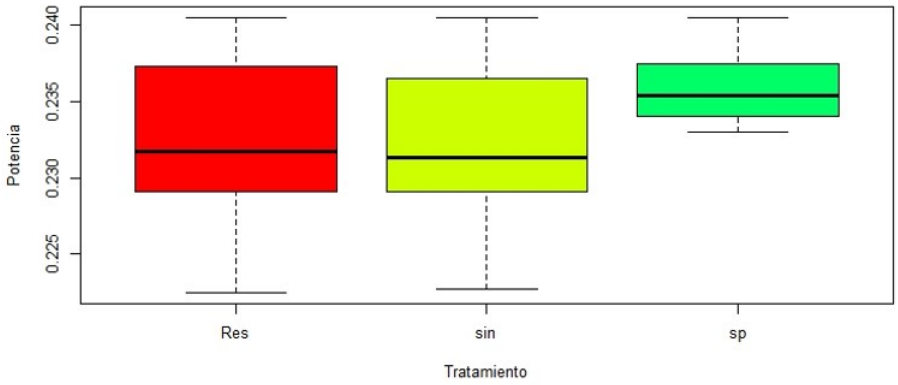

Figure A.9: *Box and Whiskers Diagram*

Tratamiento	Media	Grupo Estadístico
Sp	0.2362133	a
Res	0.2325217	a
sinRes	0.2319867	a

Table A.5: *ANOVA table*

Appendix B

Simulation Process

(a) 30° Texture (b) Asymmetrical 30º texture

Figure B.1: *Texture at 30° and at 30° asymmetrical*

(a) 45° Texture (b) Asymmetrical 45º texture

Figure B.2: *Texture at 45° and at 45° asymmetrical*

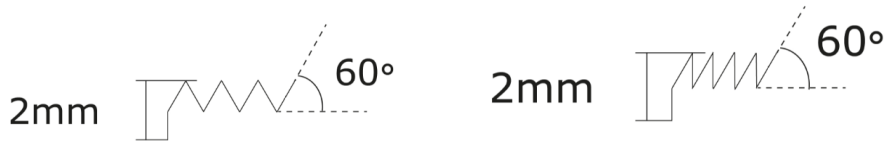

(a) 60° Texture (b) Asymmetrical 45º texture

Figure B.3: *Texture at 60° and at 60° asymmetrical*

B.0.1 30° Texture

The first simulated texture geometry was 30°, see figure B.1(a), which was simulated in angles of 0-80°, being 0° the 12 of the day that is the point of greater irradiance and 80° finishing the day.

From what can be seen in the Table B.1, the FEP material is the one that has the best performance with the texture of 30°, being in the greater amount of incidence angles the one that obtained greater efficiency. In addition, the Epoxy Resin was the material with the worst performance, although for the angle of 50°, it was the one with the best performance. However, something that can be seen is that on average all the materials obtained a performance above the reference which would be the arrangement without texture.

30º Texture												
Angle	**Reference(W)**	**PCTFE**	**FEP**	**ETFE**	**Wavelength**	**Epoxy**	**Reference (%)**	**PCTFE**	**FEP**	**ETFE**	**Wavelength**	**Epoxy**
0	22.4335	22.7827	22.8456	22.745	22.745	22.5572	0	1.55660062	1.83698487	1.38854838	1.38854838	0.55140749
10	22.1406	22.4569	22.5345	22.4274	22.4274	22.2549	0	1.42859724	1.77908458	1.29535785	1.29535785	0.51624617
20	21.2262	21.4424	21.4971	21.3984	21.3984	21.1984	0	1.01855254	1.27625293	0.81126155	0.81126155	-0.13097022
30	19.5676	20.0909	20.1294	20.0704	20.0704	19.9519	0	2.67431877	2.87107259	2.56955375	2.56955375	1.96396083
40	17.3263	17.8966	17.9205	17.8792	17.8792	17.7626	0	3.29152791	3.4294685	3.19110254	3.19110254	2.51813717
50	14.4475	14.9489	14.9592	14.9601	14.9601	14.9867	0	3.47049663	3.54178924	3.54801869	3.54801869	3.73213359
60	11.0323	11.8142	11.8048	11.8151	11.8151	11.702	0	7.08737072	7.00216637	7.09552858	7.09552858	6.07035704
70	6.66433	7.83744	7.82087	7.79123	7.79123	7.67779	0	17.6028198	17.3541826	16.9094268	16.9094268	15.2072301
80	2.56575	4.02567	4.03047	4.02032	4.02032	3.97589	0	56.9003215	57.0874013	56.6918055	56.6918055	54.9601481
							Promedios	**10.5589562**	**10.6864892**	**10.388956**	**10.388956**	**9.48762781**

Table B.1: *30º texture*

B.0.2 30º asymmetrical texture

The texture of 30° asymmetric, see figure B.1(b), was simulated in angles of 0-80°, being 0° the 12 of the day that is the point of greater irradiance and 80° finishing the day.

From what can be seen in the Table B.2, the FEP material is the one that has the best performance with the texture of 30° asymmetric, being in the highest amount of incidence angles the one that obtained the highest efficiency. In addition, the Epoxy Resin was the material with the worst performance. Something that should be highlighted is that FEP obtained the worst performance when the incidence angle was 60°, however as in almost all the other angles it was the best, in the end in the conglomerate it obtained the best performance.

30º Texture_Straight angle												
Angle	**Reference(W)**	**PCTFE**	**FEP**	**ETFE**	**Wavelength**	**Epoxy**	**Reference (%)**	**PCTFE**	**FEP**	**ETFE**	**Wavelength**	**Epoxy**
0	22.4335	22.8914	22.9407	22.8612	22.8612	22.7012	0	2.04114383	2.26090445	1.90652373	1.90652373	1.19330466
10	22.1406	22.6641	22.7323	22.6274	22.6274	22.4563	0	2.36443457	2.67246597	2.19867574	2.19867574	1.42588728
20	21.2262	21.654	21.7097	21.6183	21.6183	21.4457	0	2.01543376	2.2778453	1.84724539	1.84724539	1.03409937
30	19.5676	19.9658	20.0179	19.934	19.934	19.7723	0	2.03499663	2.30125309	1.87248308	1.87248308	1.04611705
40	17.3263	17.7843	17.8291	17.7549	17.7549	17.6144	0	2.64338029	2.90194675	2.47369606	2.47369606	1.66279009
50	14.4475	14.713	14.7402	14.8244	14.8244	14.7931	0	1.83768818	2.02595605	2.60875584	2.60875584	2.39210936
60	11.0323	11.6032	11.212	11.5742	11.5742	11.4413	0	5.17480489	1.62885346	4.91194039	4.91194039	3.70729585
70	6.66433	7.5574	7.66426	7.49508	7.49508	7.67483	0	13.400747	15.004209	12.4656192	12.4656192	15.1628146
80	2.56575	4.00761	4.04594	3.98888	3.98888	3.88074	0	56.1964338	57.690344	55.4664328	55.4664328	51.2516808
							Promedios	**9.74545143**	**9.862642**	**9.52793025**	**9.52793025**	**8.764011**

Table B.2: *30º asymmetrical texture*

B.0.3 Textura 45°

The texture of 45°, see figure B.2(a), was simulated in angles of 0-80°, being 0° the 12 of the day that is the point of greater irradiance and 80° finishing the day.

From what can be seen in the Table B.3, the FEP material is the one that has the best performance with the texture of 45°, being in the greater amount of incidence angles the one that obtained greater efficiency. In addition, the Epoxy Resin was the material with the worst performance. Something that should be highlighted is that FEP obtained the worst performance when the incidence angle was 10°, contrary to Wavelength, Epoxy Queen and EFTFE, however as in almost all the other angles it was the best, in the end in the conglomerate it obtained the best performance.

45º Texture												
Angle	**Reference(W)**	**PCTFE (W)**	**FEP (W)**	**ETFE (W)**	**Wavelength (W)**	**Epoxy (W)**	**Reference (%)**	**PCTFE (%)**	**FEP (%)**	**ETFE (%)**	**Wavelength (%)**	**Epoxy (%)**
0	22.4335	22.7903	22.832	22.7624	22.7624	22.5607	0	1.59047853	1.77636125	1.46611095	1.46611095	0.56700916
10	22.1406	22.3341	22.42	22.7514	22.7514	22.6719	0	0.87396006	1.26193509	2.75873283	2.75873283	2.39966397
20	21.2262	21.664	21.6938	21.6448	21.6448	21.538	0	2.06254534	2.20293788	1.97209109	1.97209109	1.46893933
30	19.5676	19.9519	19.9884	19.9303	19.9303	19.7827	0	1.96396083	2.15049367	1.85357428	1.85357428	1.09926613
40	17.3263	17.7213	17.7746	17.5443	17.5443	17.4354	0	2.27977121	2.58739604	1.25820285	1.25820285	0.62967858
50	14.4475	14.8261	14.8391	14.8071	14.8071	14.7125	0	2.62052258	2.71050355	2.48901194	2.48901194	1.83422737
60	11.0323	11.7491	11.7612	11.7393	11.7393	11.4991	0	6.49728524	6.60696319	6.40845517	6.40845517	4.23121199
70	6.66433	7.96502	7.99051	7.95584	7.95584	7.88594	0	19.5171908	19.8996748	19.3794425	19.3794425	18.3305749
80	2.56575	4.35996	4.37119	4.35542	4.35542	4.31984	0	69.9292605	70.3669492	69.7523141	69.7523141	68.3655851
							Promedios	**11.9261083**	**12.1736905**	**11.9264373**	**11.9264373**	**10.9917952**

Table B.3: *Textura 45°*

B.0.4 45º asymmetrical Texture

The texture of 45° asymmetric, see figure B.2(b), was simulated in angles of 0-80°, being 0° the 12 of the day that is the point of greater irradiance and 80° finishing the day.

From what can be seen in the Table B.4, the FEP material is the one that has the best performance with the texture of 45° asymmetric, being in the greater amount of incidence angles the one that obtained greater efficiency. In addition, the Epoxy Resin was the material with the worst performance. Wavelength and ETFE obtained a good performance in 70°, however in the rest of the angles they did not stand out much, the Epoxyc Resin obtained in 50° values below the reference, that is to say, losses for the system.

45º Texture _Straight angle												
Angle	**Reference(W)**	**PCTFE**	**FEP**	**ETFE**	**Wavelength**	**Epoxy**	**Reference (%)**	**PCTFE**	**FEP**	**ETFE**	**Wavelength**	**Epoxy**
0	22.4335	22.8127	22.8562	22.78	22.78	22.5929	0	1.6903292	1.88423563	1.54456505	1.54456505	0.7105445
10	22.1406	22.6315	22.7081	22.5942	22.5942	22.4046	0	2.21719375	2.5631645	2.04872497	2.04872497	1.19237961
20	21.2262	21.691	21.7512	21.6593	21.6593	21.481	0	2.18974663	2.4733584	2.0404029	2.0404029	1.20040328
30	19.5676	19.9736	20.0319	19.9424	19.9424	19.773	0	2.07485844	2.37279993	1.91541119	1.91541119	1.04969439
40	17.3263	17.7993	17.8582	17.5511	17.5511	17.4384	0	2.72995389	3.06989952	1.29744954	1.29744954	0.6469933
50	14.4475	14.5724	14.6804	14.522	14.522	14.3923	0	0.86450943	1.61204361	0.51566015	0.51566015	-0.38207302
60	11.0323	11.1583	11.2927	11.0627	11.0627	11.4123	0	1.14210092	2.36034191	0.27555451	0.27555451	3.44443135
70	6.66433	7.57288	7.43675	7.53614	7.53614	7.4336	0	13.6330284	11.5903624	13.0817351	13.0817351	11.5430959
80	2.56575	3.85897	3.93489	3.82736	3.82736	3.85147	0	50.4031959	53.3621748	49.1711975	49.1711975	50.1108838
							Promedios	**8.54943518**	**9.0320423**	**7.98785566**	**7.98785566**	**7.72403922**

Table B.4: *45º asymmetrical Texture*

B.0.5 60º Texture

The texture of 60°, see figure B.4, was simulated in angles of 0-80°, being 0° the 12 of the day that is the point of greater irradiance and 80° finishing the day.

Based on what can be seen in the Table B.5, Wavelength and ETFE obtained the best results on average with an increase of 12.34% in standardized efficiency. However, it can be seen that in most angles they obtained a normal performance, but at 80° the difference was very high compared to the rest of the materials. The Fep obtained the 4th place and finally and as a constant the Epoxy Resin with the worst performance.

60º Texture												
Angle	**Reference(W)**	**PCTFE**	**FEP**	**ETFE**	**Wavelength**	**Epoxy**	**Reference (%)**	**PCTFE**	**FEP**	**ETFE**	**Wavelength**	**Epoxy**
0	22.4335	23.565	23.5723	23.5679	23.5679	23.5611	0	5.04379611	5.07633673	5.0567232	5.0567232	5.02641139
10	22.1406	22.6401	22.6865	22.6024	22.6024	23.1819	0	2.25603642	2.46560617	2.085761	2.085761	4.70312458
20	21.2262	21.6149	21.6579	21.5911	21.5911	21.4333	0	1.83122745	2.03380728	1.71910186	1.71910186	0.975681
30	19.5676	19.9244	19.9902	19.8979	19.8979	19.5937	0	1.82342239	2.15969255	1.68799444	1.68799444	0.13338376
40	17.3263	17.597	17.63	17.5909	17.5909	17.5361	0	1.56236473	1.75282663	1.52715814	1.52715814	1.21087595
50	14.4475	14.9019	14.9244	14.8623	14.8623	14.6774	0	3.14518083	3.30091711	2.87108496	2.87108496	1.59127877
60	11.0323	11.8856	11.9172	11.865	11.865	11.7585	0	7.73456124	8.0209929	7.54783681	7.54783681	6.5824896
70	6.66433	8.05339	8.09884	8.04626	8.04626	8.00232	0	20.8432055	21.5251946	20.736218	20.736218	20.0768869
80	2.56575	4.23973	4.22883	4.31205	4.31205	4.2754	0	65.2433012	64.8184741	68.0619702	68.0619702	66.633538
							Promedios	**12.1647884**	**12.3504276**	**12.3659832**	**12.3659832**	**11.8815189**

Table B.5: *60º Texture*

B.0.6 60º asymmetrical Texture

The texture of 60° asymmetric, see figure B.3(b), was simulated in angles of 0-80°, being 0° the 12 of the day that is the point of greater irradiance and 80° finishing the day.

From what can be seen in the Table B.6, PCTFE obtained the best performance, being the best result for all angles, the Epoxy Resin obtained positive results in 0°, 10° and 40°, however at 30°, 50° and 60° was below the reference, so on average it got the worst result only above the reference. Finally, the FEP got the second best result, but at the angles of 50° and 60° it got negative values, i.e. below the reference.

60º Texture_Straight angle												
Angle	**Reference(W)**	**PCTFE**	**FEP**	**ETFE**	**Wavelength**	**Epoxy**	**Reference (%)**	**PCTFE**	**FEP**	**ETFE**	**Wavelength**	**Epoxy**
0	22.4335	23.5694	23.5377	23.5797	23.5797	23.5848	0	5.06340963	4.9221031	5.10932311	5.10932311	5.13205697
10	22.1406	22.3412	22.4599	22.2904	22.2904	23.2745	0	0.90602784	1.44214701	0.6765851	0.6765851	5.12136076
20	21.2262	21.5354	21.6042	21.4953	21.4953	21.2982	0	1.45669032	1.78081805	1.26777285	1.26777285	0.33920344
30	19.5676	19.8704	19.928	19.8471	19.8471	19.5449	0	1.547456	1.84182015	1.42838161	1.42838161	-0.1160081
40	17.3263	17.281	17.4072	17.221	17.221	17.5353	0	-0.26145224	0.46692023	-0.6077466	-0.6077466	1.20625869
50	14.4475	14.6946	13.9995	14.6423	14.6423	14.2933	0	1.71033051	-3.10088251	1.34833016	1.34833016	-1.06731268
60	11.0323	11.0399	10.6739	10.9333	10.9333	10.5137	0	0.06888863	-3.24864262	-0.89736501	-0.89736501	-4.70074237
70	6.66433	7.16711	7.30543	7.09449	7.09449	7.19928	0	7.54434429	9.61987177	6.45466236	6.45466236	8.02706349
80	2.56575	3.66652	3.77687	3.60757	3.60757	3.56856	0	42.9024652	47.2033518	40.6048914	40.6048914	39.0844782
							Promedios	**6.77090668**	**6.769723**	**6.15387055**	**6.15387055**	**5.8918176**

Table B.6: *60º asymmetrical Texture*

B.0.7 Comparison of textures

From the results obtained from the simulations presented above, an increase in efficiency behavior is evident for all the textures with all the materials used. However, as can be seen in the Table B.7, Wavelength and ETFE with an average efficiency of 12.36% with a texture of 60°, obtained the highest value of all the simulations carried out. Another important value is that the behavior of the materials in the 60° texture was superior to any other type of texture. Finally, a trend is seen in the influence of the texture when the incidence angles are higher, as can be seen in the figure B.4, that is, in the hours of lower solar irradiance.

	PCTFE	**FEP**	**ETFE**	**Wavelength**	**Epoxy**
Textura 45	11.92610834	12.1736905	11.9264373	11.9264373	10.9917952
Textura 45 Recta	8.549435176	9.0320423	7.98785566	7.98785566	7.72403922
Textura 60	12.16478843	12.3504276	12.3659832	12.3659832	11.8815189
Textura 60 Recto	6.770906682	6.769723	6.15387055	6.15387055	5.8918176
Textura 30	10.5589562	10.6864892	10.388956	10.388956	9.48762781
Textura 30 Recto	9.745451433	9.862642	9.52793025	9.52793025	8.764011

Table B.7: *Average Efficiencies*

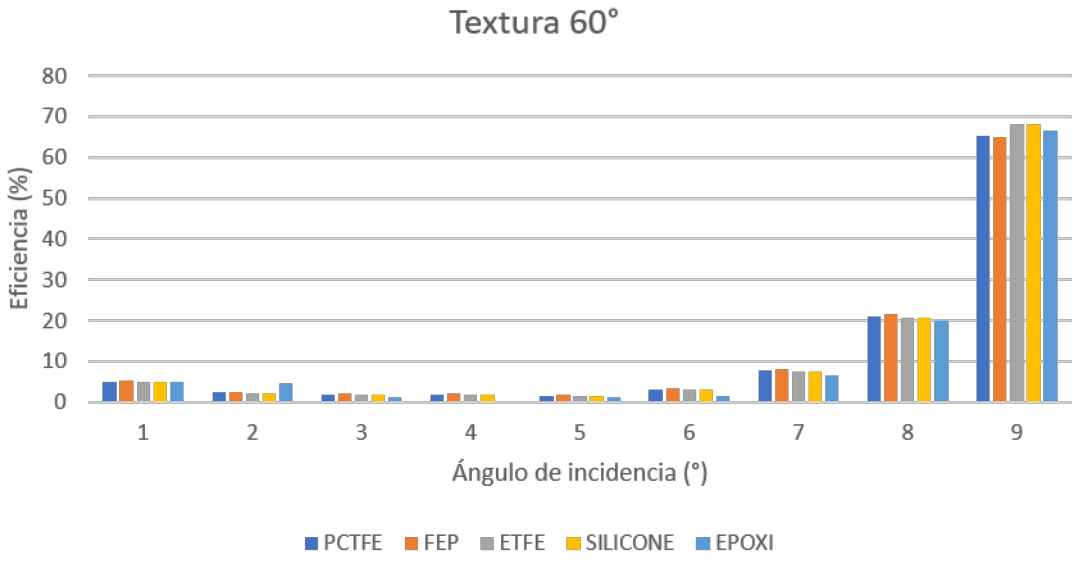

Figure B.4: *60° texture*

B.0.8 Simulation

Prior to the realization of the experimental phase, it is determined to carry out simulations of ray tracing, with the aim of validating in the first instance if the textures have an influence on the optical performance of the photovoltaic system and also to be a reference point for comparison with respect to the experimental study.

For the realization of the simulation, code is made in Visual Basics in the software, which is able to run the simulation at various angles of incidence and in which the following parameters were defined:

- **Sun** a cylinder of 200mm radius and 10mm width was defined that emits 1000W/mˆ2 with a normal angular distance to the surface.
- **Solar cell** The cell was defined with the standard measurements of 6in ^{2} and with a perfect absorbent material.
- **EVA** Encapsulated material with a refractive index of 1.49.
- **Glass** Glass was defined with a commercially based refractive index of 1.52.
- **Texture** Wavelength and Epoxy Resin were used for the texture, with refractive indexes of 1.42 and 1.49 respectively. With the texture of 45 degrees.

In the figure B.5 it can be seen how the assembly was in the simulator.

From the model, we proceed to make an evaluation of the incidence of the sun at angles of 0°, 10°, 20°, 30°, 40° because it is the maximum degree of inclination that the real simulator allows. For this, different simulations were made with different parameters.

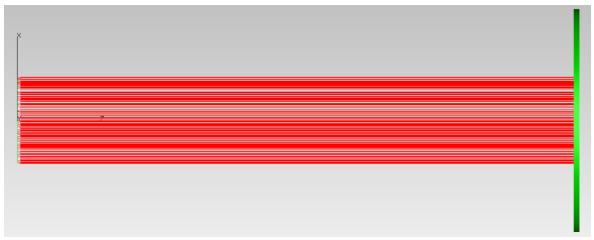

(a) Graphic simulation model

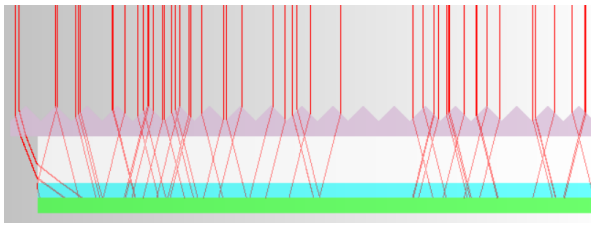

(b) Interaction of the rays with the panel and the texture

Figure B.5: *Simulation*

Parameter	Value
Source	1000 W/m2 - Irradiance type
Texture	Wavelength Material - Epoxy Resin
Wavelength	0.548 nm
Objective	Perfect Absorbent
Irradiation Type	Surface Normal
Angle of incidence	40 - 0 in 5 positions

Table B.8: *Parameters Perfect Absorbent Simulation*

B.0.8.1 Perfect Absorbent Structure Simulation

The first simulation that was carried out was based on a configuration of the cell based on the real layers that a photovoltaic panel has but, putting as an absorbent material a "Perfect Absorbent" to determine the power flow and the amount of rays that reach the cell. The parameters defined for this simulation can be seen in the Table B.8.

After defining these parameters, 3 different configurations will be determined in the structure of the photovoltaic system.

- **Commercial Structure** In the commercial structure the different texture materials are simulated with a structure that has a layer of EVA, another of glass and that of the texture material, see figure B.6 in this what is sought is to determine how would be the behavior of the texture on a commercial panel.

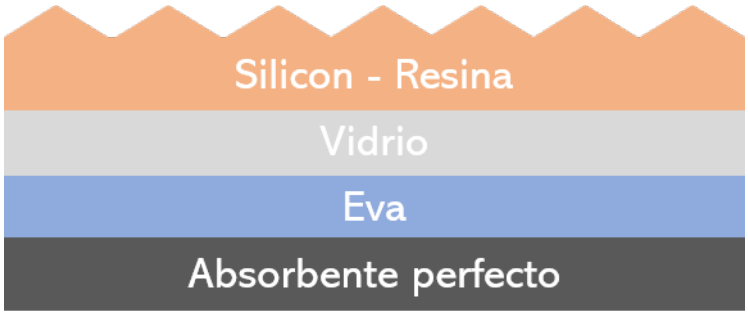

Figure B.6: *Perfectly absorbent commercial structure*

After this we proceed to perform the simulation where you can see in the table refFlux1 how the silicon for all angles maintains an increase in efficiency with respect to silicon and the reference that is the cell without texture.

Angle (°)	Reference (W)	Texture_Epoxy (W)	Texture_Wavelength (W)	Efficiency_REF (%)	Efficiency_Epoxy (%)	Efficiency_Wavelength (%)
0	22.4406	22.5359	22.6837	0	0.4246767	1.08330437
10	22.1324	22.5817	22.6727	0	2.03005548	2.4412174
20	21.1991	21.4838	21.6092	0	1.34298154	1.93451609
30	19.5127	19.7367	19.8798	0	1.1479703	1.88133882
40	17.238	17.4372	17.5954	0	1.15558649	2.07332637

Table B.9: *Power Flux*

Also in the figure B.7, it is noted how is the behavior of the texture in these angles, where it is evident that for the angles of incidence of 0, 10 and 20, the percentage of efficiency is higher with respect to those of 30 and 40.

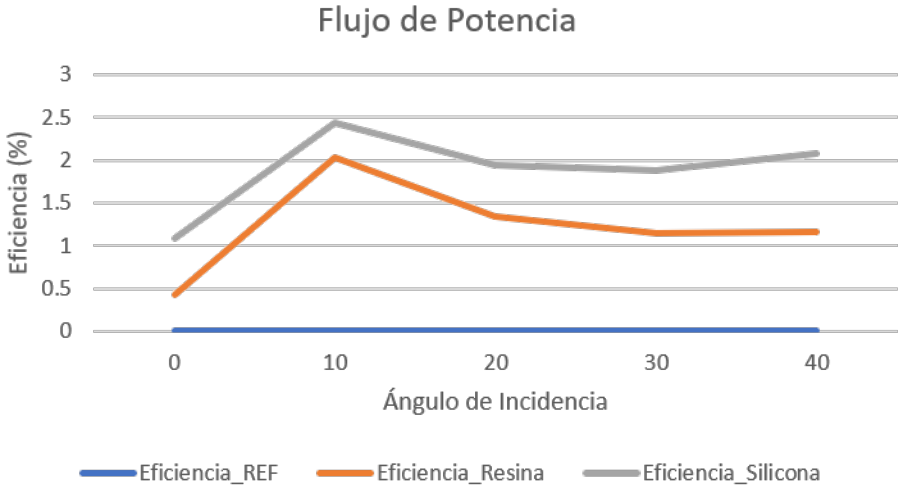

Figure B.7: *Normalized efficiency*

- **Structure without EVA** After this, the experiment is performed with the parameters mentioned above,

but without EVA encapsulating material, see figure B.8, this because for the experiments this material was not used. Therefore, it is intended to validate the behavior of the rays without the encapsulant.

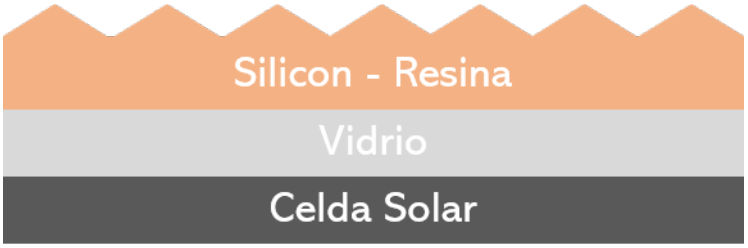

Figure B.8: *Perfectly absorbent EVA-free structure*

From the simulation carried out by means of this method a behavior very similar to the previous one can be seen, where the Wavelength continues behaving in a better way than the Epoxy Resin see Table B.10.

Angle (°)	Reference (W)	Texture_Epoxy (W)	Texture_Wavelength (W)	Efficiency_REF (%)	Efficiency_Epoxy (%)	Efficiency_Wavelength (%)
0	22.4406	22.5236	22.6773	0	0.369865333	1.054784631
10	22.1324	22.6505	22.7342	0	2.340911966	2.719090564
20	21.1991	21.5396	21.6411	0	1.606200263	2.084994174
30	19.5127	19.7456	19.8962	0	1.193581616	1.965386646
40	17.238	17.421	17.5906	0	1.061608075	2.045480914

Table B.10: *Flux Power*

In addition, the behaviors in the different angles still have the peaks in the same places, see figure B.9.

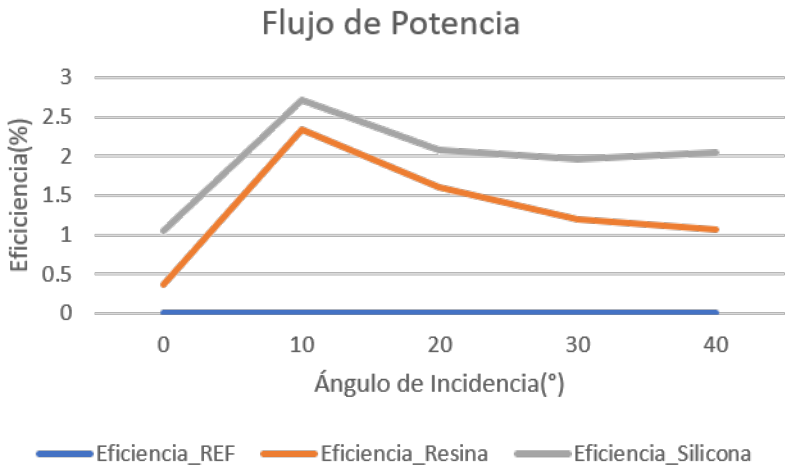

Figure B.9: *Normalized efficiency*

- **Structure without EVA and with Air** This simulation was made with the objective of validating the behavior of the radiation with the texture assuming an air layer between the cell and the glass, this because for possible experiments if EVA is not used, the taps where the current of the cell flows, would

Angle (°)	Reference (W)	Texture_Epoxy (W)	Texture_Wavelength (W)	Efficiency_REF (%)	Efficiency_Epoxy (%)	Efficiency_Wavelength (%)
0	21.4149	21.3242	21.5373	0	-0.423536883	0.571564658
10	21.0757	21.2139	21.2467	0	0.655731482	0.811360951
20	20.077	19.7912	20.1321	0	-1.42351945	0.274443393
30	18.3928	17.1214	17.6417	0	-6.912487495	-4.083663173
40	16.0671	8.98323	13.8546	0	-44.08928805	-13.77037549

Table B.11: *Flux Power*

generate a layer of air because they would not allow a contact between the glass and the cell, as can be seen in the figure B.10

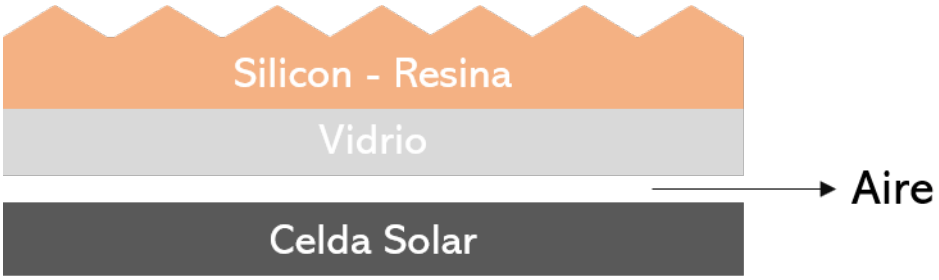

Figure B.10: *Structure without EVA and with Air*

In the Table B.11 you can see that the air layer influences negatively the text where you notice that there are more losses than increases in efficiency.

In addition, a trend is shown in the figure B.11 where each time the angle of incidence increases, the efficiency drops more.

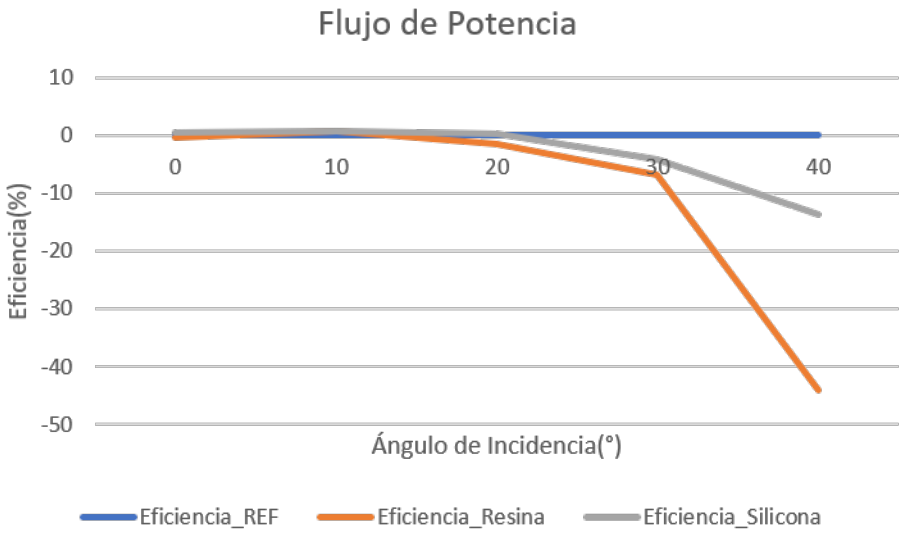

Figure B.11: *Normalized efficiency*

B.0.8.2 Structure with Absorbent Silicon

For this simulation, the tests were performed based on the inclusion of a reflective material as a "target for the rays", the rest of the parameters are the same as those used in the previous simulation, see table B.12.

Parameter	Value
Source	1000 W/m2 – Irradiance type
Texture material	Silicona - Epoxy Resin
Wavelength	0.548 nm
Objective	Absorbent 40% of refelctivity
Irradiance type	Normal to surface
Angle of incidence	40 – 0 en 5 posiciones

Table B.12: *Parameters Perfect Absorbent Simulation*

After the definition of the above-mentioned parameters, the following two simulations were carried out.

- **Structure without EVA** Se presenta el experimento sin material encapsulante EVA, ver figura B.12, esto debido a que para los experimentos este material no se utilizo. Por lo cual se pretende validar el comportamiento de los rayos sin el encapsulante.

Figure B.12: *Structure without EVA*

From the simulation made by this method it is seen that there is a positive behavior in most of the incidence angle, however for the texture with Epoxy Resin at 40° the yield was -2.95%, that is less than the reference. While the Wavelength remained above the reference yield for all angles, see Table refFlux4.

Angle (°)	Reference (W)	Texture_Epoxy (W)	Texture_Wavelength (W)	Efficiency_REF (%)	Efficiency_Epoxy (%)	Efficiency_Wavelength (%)
0	4.48812	4.987	5.49134	0	11.11556732	22.35278914
10	4.46098	5.25555	5.15431	0	17.8115571	15.54210061
20	4.35051	4.49122	4.58779	0	3.234333446	5.454073201
30	4.05144	4.10772	4.31724	0	1.389135715	6.560630294
40	3.66454	3.55631	3.68468	0	-2.953440268	0.54959149

Table B.13: *Flux Power*

In the figure B.13 the behavior of both solutions is presented, where it is seen that for the smaller angles of incidence the efficiency is greater, but then it is falling as the angle increases. In addition, the Epoxy Resin at 20° performed better than the Wavelength.

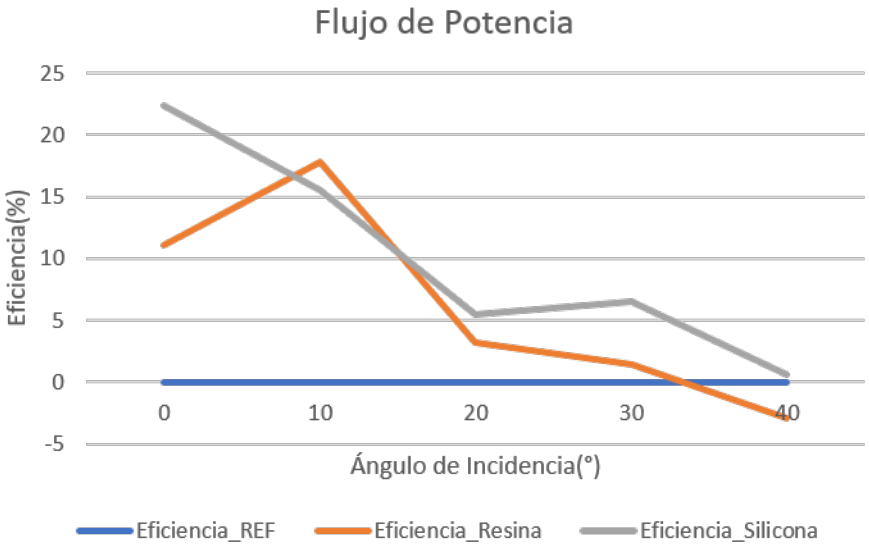

Figure B.13: *Normalized efficiency*

- **Structure without EVA and with Air** This simulation was made with the objective of validating the behavior of the radiation with the texture assuming an air layer between the cell and the glass, this because for possible experiments if EVA is not used, the taps where the current of the cell flows would generate a layer of air because they would not allow a contact between the glass and the cell, as can be seen in the figure B.14.

Figure B.14: *Structure without EVA and with Air Absorbent with reflectivity*

In the Table B.14 the behavior of this configuration is presented where the Epoxy Resin presents negative values below -5% in 30° and below -30 in 40°. The behavior of the Wavelength is not very different, although with less losses, with a minimum of -7.3% at 40°.

Angle (°)	Reference (W)	Texture_Epoxy (W)	Texture_Silicone (W)	Efficiency_REF (%)	Efficiency_Epoxy (%)	Efficiency_Silicone (%)
0	4.28	4.56	5.03	0	6.57	17.55
10	4.21	4.57	4.55	0	8.59	8.16
20	4.01	3.98	4.09	0	-0.64	1.939
30	3.67	3.48	3.58	0	-5.35	-2.49
40	3.21	2.13	2.97	0	-33.66	-7.35

Table B.14: *Flux Power*

In the figure B.15 it is seen a trend in both solutions of a drop in efficiency each time the angle of incidence increases, being much more critical for the Epoxy Resin.

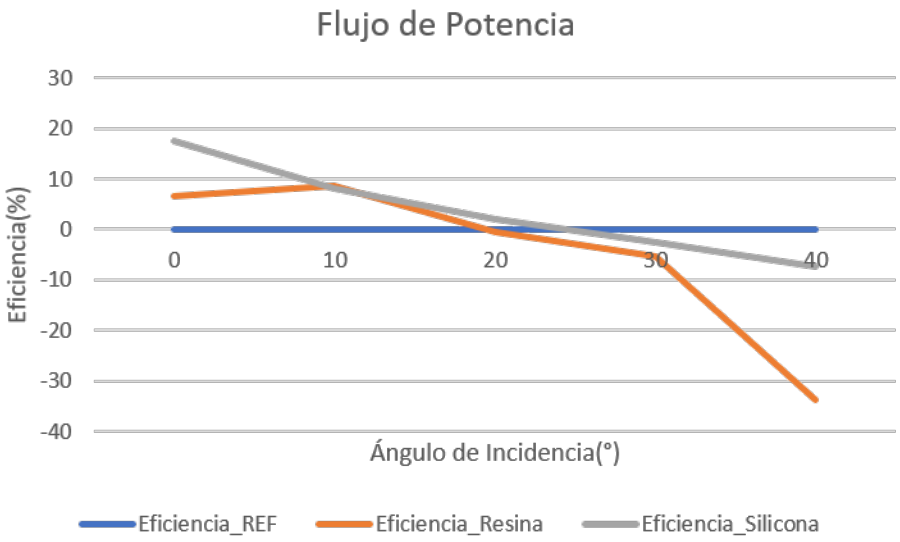

Figure B.15: *Normalized efficiency*

B.0.8.3 Structure with absorbent silicon and rounded texture in the peaks.

For this simulation the tests were carried out from the addition of a reflective material as a "target for the rays", the rest of the parameters are the same as those used in the previous simulation, see table B.15.

Parameter	Value
Source	1000 W/m2 – Irradiance type
Texture material	Silicona - Epoxy Resin- Rounded tip
Wavelength	0.548 nm
Objective	Absorbent 40% of refelctivity
Irradiance type	Normal to surface
Angle of incidence	40 – 0 in 5 positions

Table B.15: *Parameters Simulation Absorbent 40% refelctivity and with the Texture with roundings*

After the definition of the above-mentioned parameters, the following two simulations were carried out.

- **Structure without EVA** The experiment is presented without EVA encapsulating material, see figure B.16, this because for the experiments this material was not used. Therefore, the behavior of the rays without the encapsulant will be validated.

Figure B.16: *EVA-free structure with rounded texture*

From the simulation carried out by means of this method, it can be seen that there is a positive behavior at all incidence angles, with a superior tendency of the Wavelength for most incidence angles, see Table B.16.

Angle (°)	Reference (W)	Texture_Epoxy (W)	Texture_Wavelength (W)	Efficiency_REF (%)	Efficiency_Epoxy (%)	Efficiency_Wavelength (%)
0	4.48812	5.14324	5.54272	0	14.59675766	23.49758919
10	4.46098	5.24022	4.88198	0	17.46791064	9.437388197
20	4.35051	4.64514	4.66332	0	6.772309453	7.190191495
30	4.05144	4.27064	4.42375	0	5.410421973	9.189572103
40	3.66454	3.73662	3.71158	0	1.966959018	1.28365361

Table B.16: *Flux Power*

In the figure B.17 the behavior of both solutions is presented, where it can be seen that the Epoxy Resin has an important peak at 10° and the Wavelength at 10° and 30°.

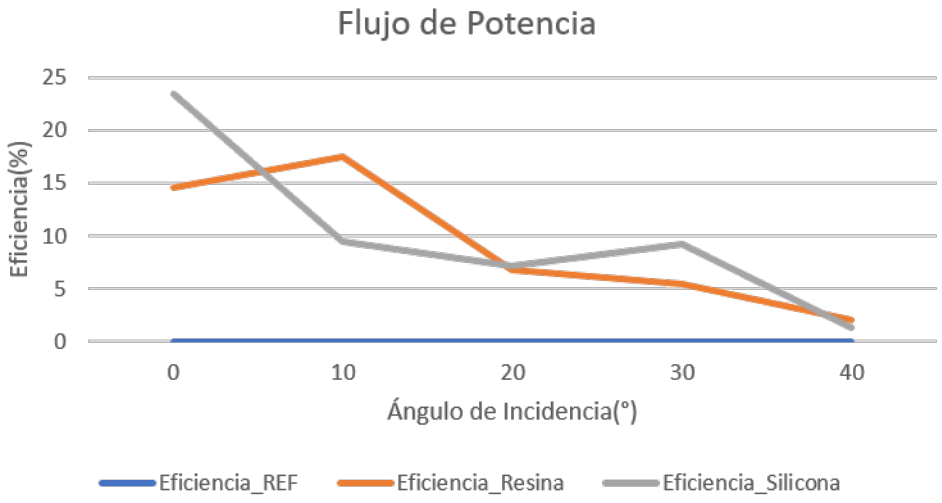

Figure B.17: *Normalized efficiency*

- **Structure without EVA and with Air** This simulation was made with the objective of validating the behavior of the radiation with the texture assuming an air layer between the cell and the glass, this because for possible experiments if EVA is not used, the taps where the current of the cell flows would generate a layer of air because they would not allow a contact between the glass and the cell, as can be seen in the figure B.18.

Figure B.18: *Structure without EVA and with Air with rounded texture*

In the Table B.17 the behavior of this configuration is presented where the Epoxy Resin presents negative values below -0% in 30° and below -20 in 40°. The behavior of the Wavelength is not very different, although with less losses, with a minimum of -2.4% at 40°.

Angle (°)	Reference (W)	Texture_Epoxy (W)	Texture_Wavelength (W)	Efficiency_REF (%)	Efficiency_Epoxy (%)	Efficiency_Wavelength (%)
0	4.28298	4.60868	5.01054	0	7.604518349	16.98723786
10	4.21513	4.59143	4.41187	0	8.927364043	4.667471703
20	4.0154	4.09138	4.17145	0	1.892214972	3.886287792
30	3.67856	3.6692	3.75752	0	-0.254447392	2.146492106
40	3.21343	2.45941	3.13502	0	-23.46464681	-2.440071824

Table B.17: *Flux Power*

In the figureB.19 you can see a trend in both solutions of a drop in efficiency every time the angle of incidence increases, being much more critical for the Epoxy Resin.

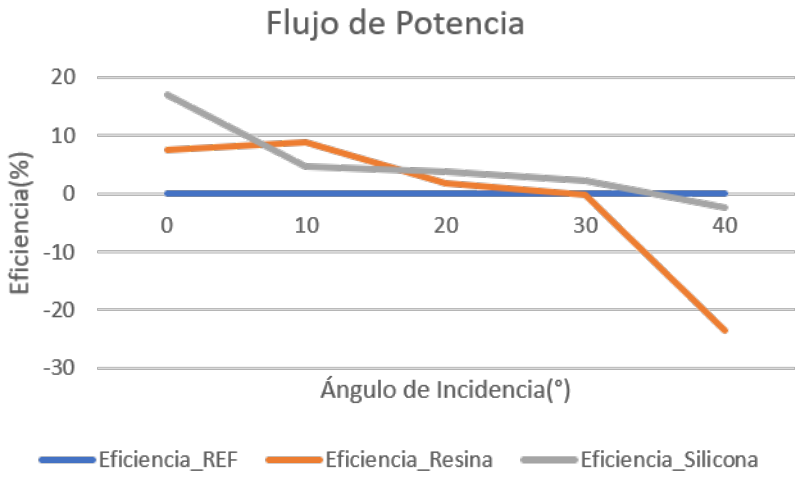

Figure B.19: *Normalized efficiency*

Appendix C

Appendix 3: Mold drawing

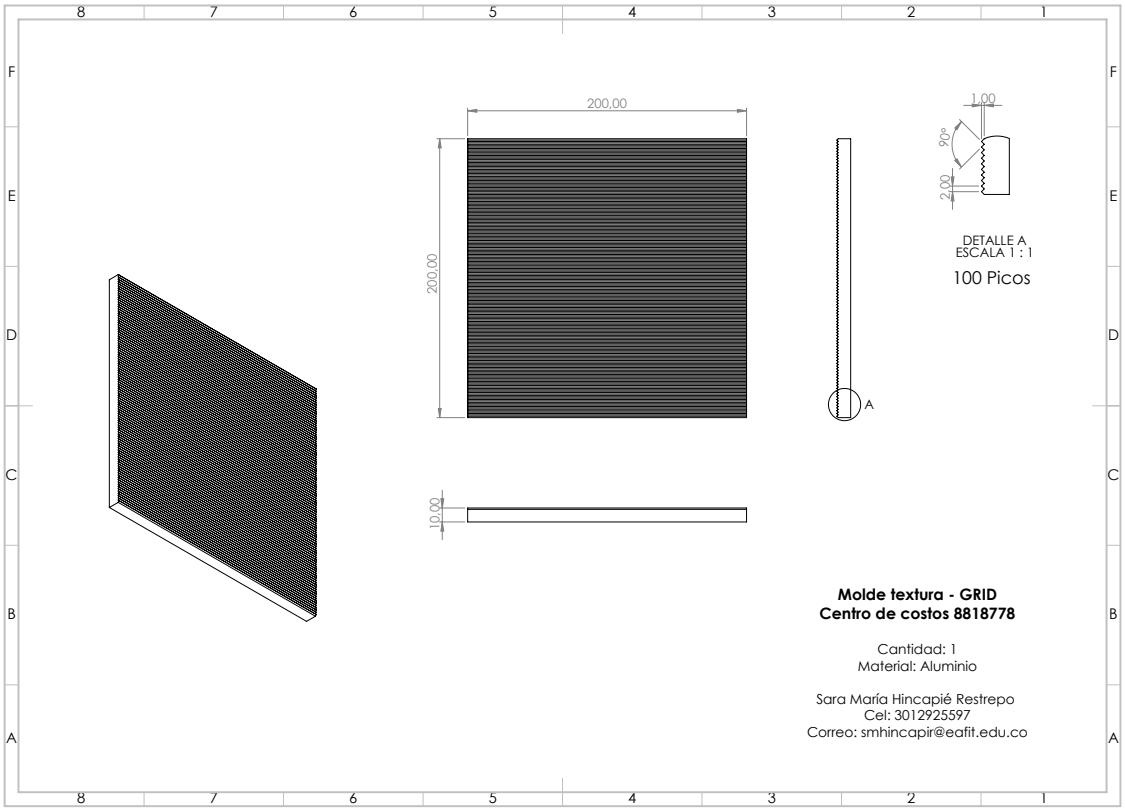

Figure C.1: *Textura 45°*

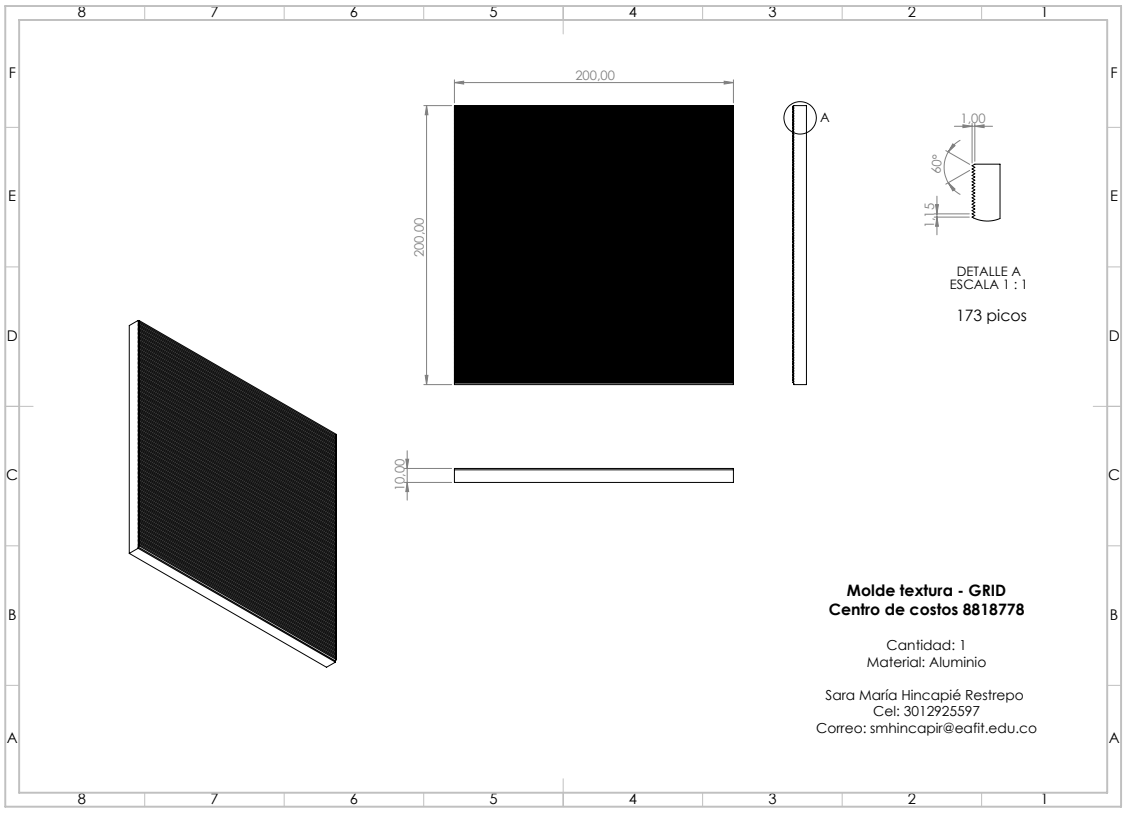

Figure C.2: *Textura 60°*

Appendix D

Appendix 4: Anova assumptions

This appendix explains compliance with the assumptions of the Anova, showing the assumptions of homoscedasticity, normality and independence of the residuals, for which a value greater than alpha, i.e. 0.5, must be guaranteed. Mainly, it must be guaranteed that the normality assumption is met, which shows that the data show a normal distribution, so they can be analyzed in the Anova.

D.1 45º Texture

Treatment	Anova's assumptions			Anova P-Value	Mean Efficiency	
	Homocedastisity	Waste Normality	Independence of Residuals		Control	Texure
9_55	0,78	0,096	2,20E-16	2,20E-16	1,41	6,33
10_23	5,10E-05	0,1	0,0005	2,20E-16	-0,08	2,68
10_26	0,884	0,15	2,20E-16	2,20E-16	1,1	2,47
10_37	0,38	0,07683	0,05452	2,20E-16	1,16	1,95
10_41	0,84	0,29	8,27E-07	9,80E-01	1,51	1,51
10_42	0,95	0,15	5,12E-05	6,00E-01	1,52	1,56
10_48	0,002	0,056	2,20E-16	2,20E+16	1,22	2,99
10_53	0,79	0,123	5,40E-02	2,20E-16	-0,03	0,9521
11_05	0,0615	0,59	6,70E-04	2,20E-16	0,54	4,08
11_21	0,56	0,071	2,00E-03	2,20E-16	1,27	4,08
11_32	0,1797	0,3378	3,60E-03	4,21E-17	1,63	1,94
11_35	1,E-08	0,0810	2,E-11	2,20E-16	2,68	0,89
11_48	0,058	0,0702	4,00E-03	2,20E-16	2,66	1,44
11_51	0,5593	0,1088	2,17E-06	2,20E-16	1,86	3,85
11_53	0,6077	0,2803	3,70E-03	2,20E-16	1,55	3,75
11_55	0,1127	0,1058	2,20E-16	2,20E-16	1,87	3,78
12_03	0,8636	0,182	2,53E-03	2,20E-16	0,85	2,14
12_11	0,00387	0,1131	4,63E-01	2,76E-02	1,99	1,05
12_31	0,3009	0,1393	6,50E-02	2,20E+16	0,639	2,731
12_34	0,5896	0,7969	8,28E-05	2,99E-04	2,237	2,73
12_44	0,03803	0,06859	8,83E-01	6,82E-09	3,4111	2,6632
12_45	0,09325	0,8016	6,50E-02	1,65E-07	3,412	2,6353
12_46	0,054	0,4584	3,26E-04	7,84E-10	3,5422	2,2581
13_07	0,6698	0,5949	7,68E-06	2,20E+16	1,19	5,69
13_31	0,84	0,0004	2,20E-16	2,20E+16	2,31	0,61
13_41	1,32E-05	0,2359	3,30E-14	1,30E-03	2,4	2,77
13_50	0,6675	0,1091	2,08E-05	2,47E-07	0,58	1,25

Table D.1: *Main results for the tests of Anova, Anova assumptions and average efficiencies of the control and 45º texture.*

D.1.1 09_55

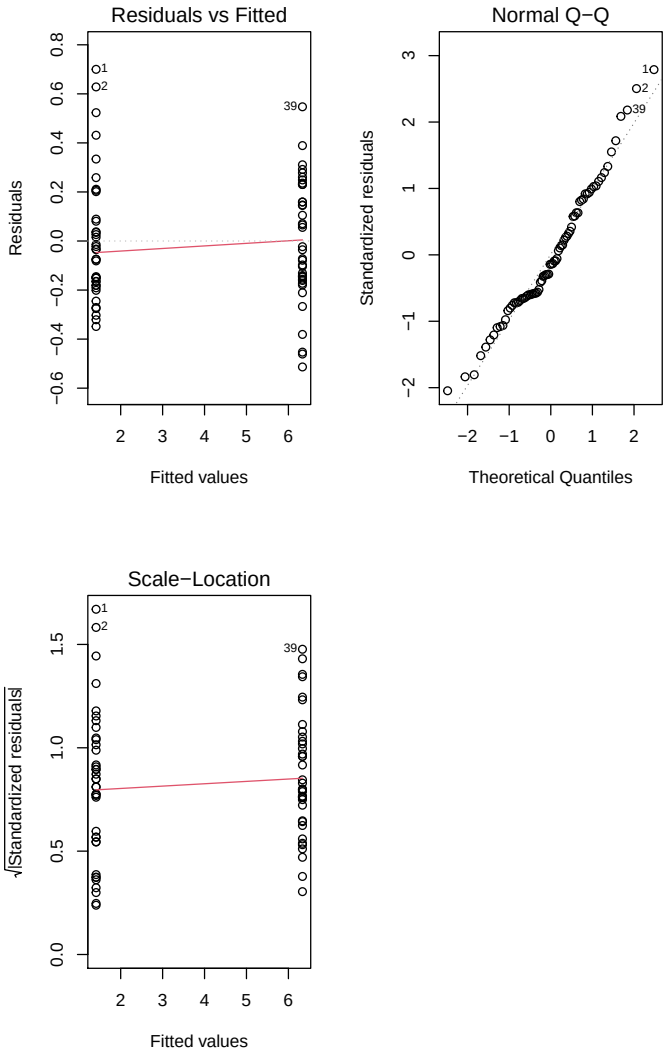

(a) ANOVA assumptions

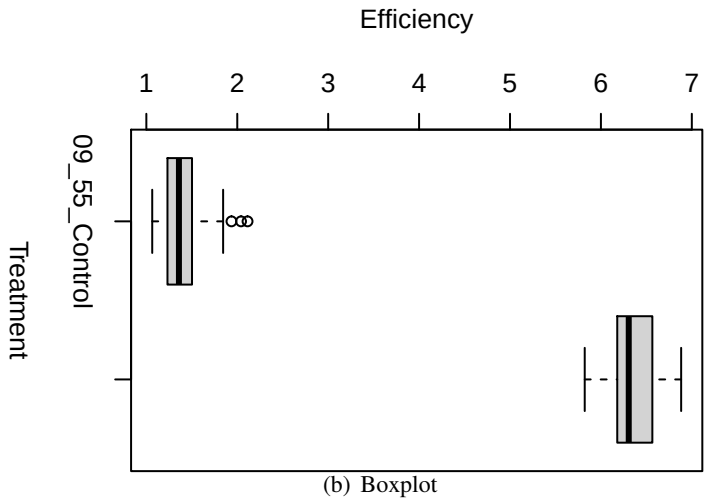

(b) Boxplot

Figure D.1: *09_55 Treatment*

D.1.2 10_23

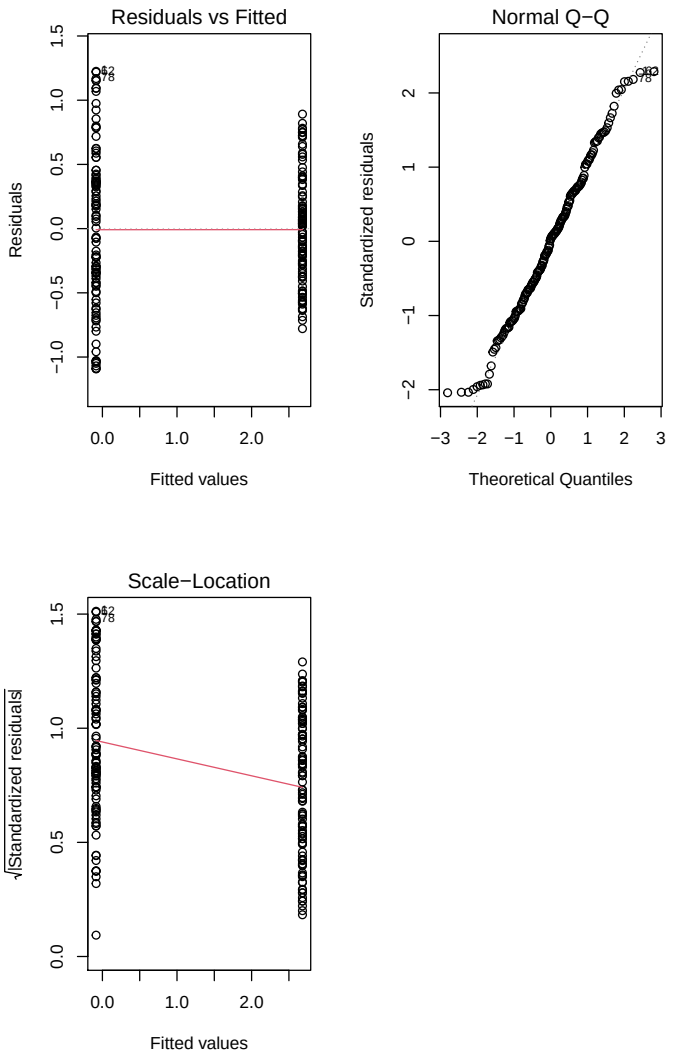

(a) ANOVA assumptions

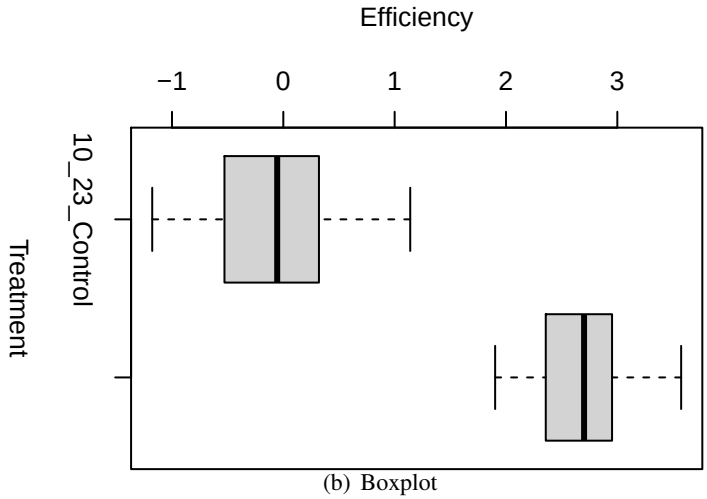

(b) Boxplot

Figure D.2: *10_23 Treatment*

D.1.3 10_26

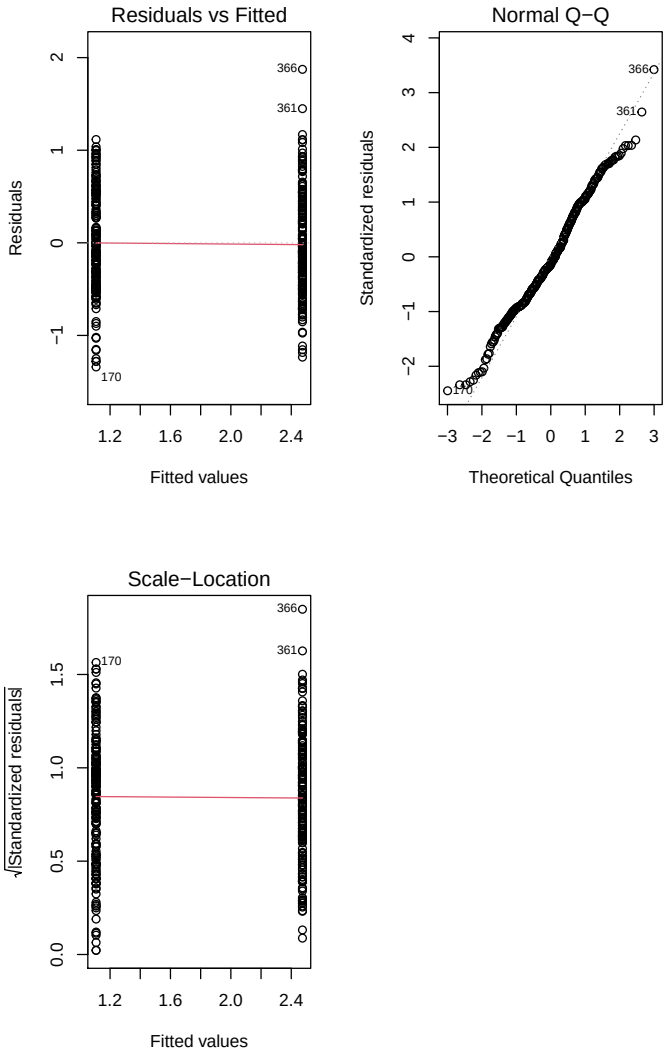

(a) ANOVA assumptions

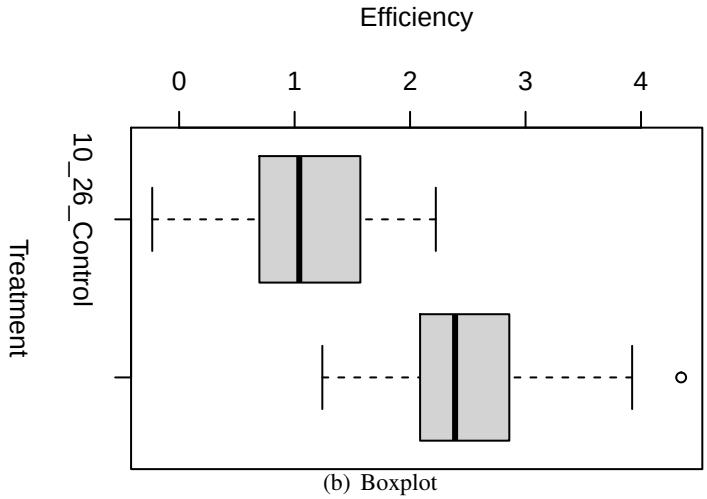

(b) Boxplot

Figure D.3: *10_26 Treatment*

D.1.4 10_37

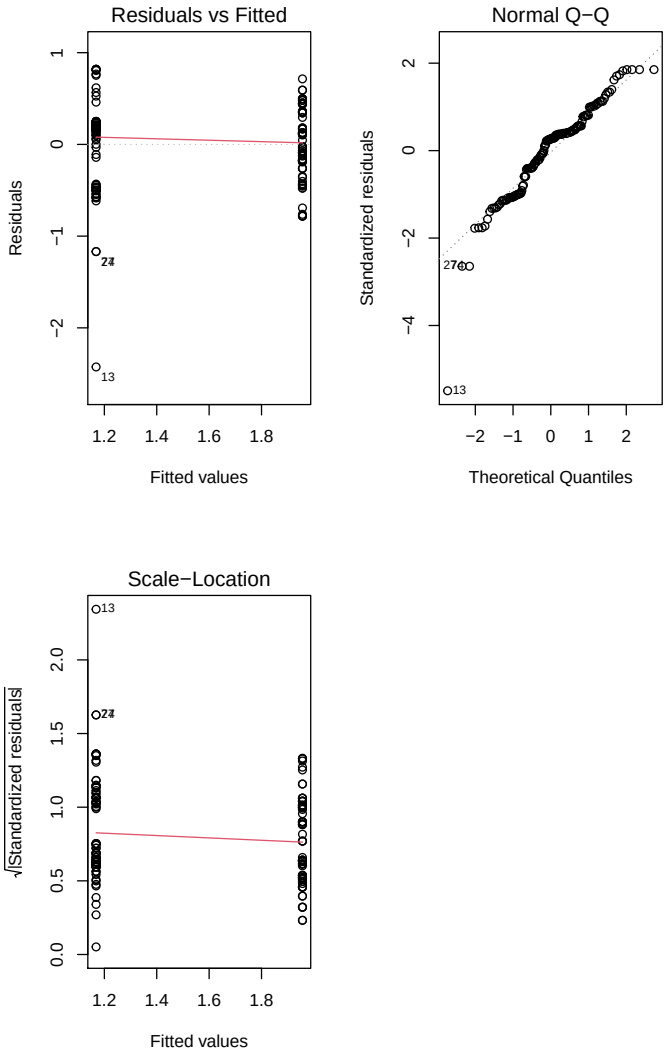

(a) ANOVA assumptions

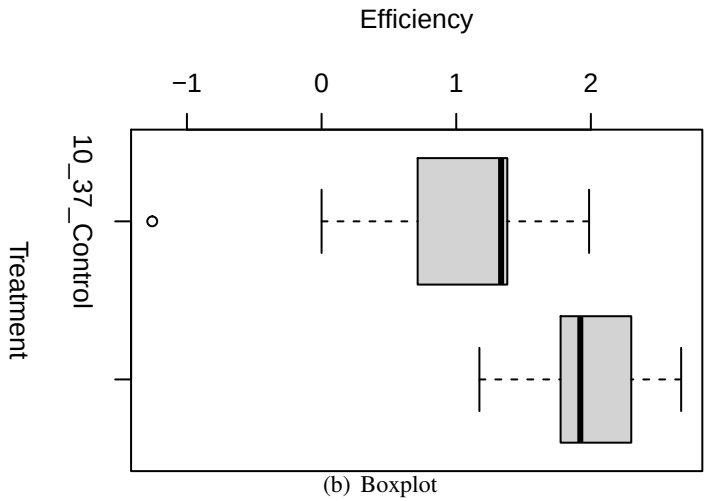

(b) Boxplot

Figure D.4: *10_37 Treatment*

D.1.5 10_41

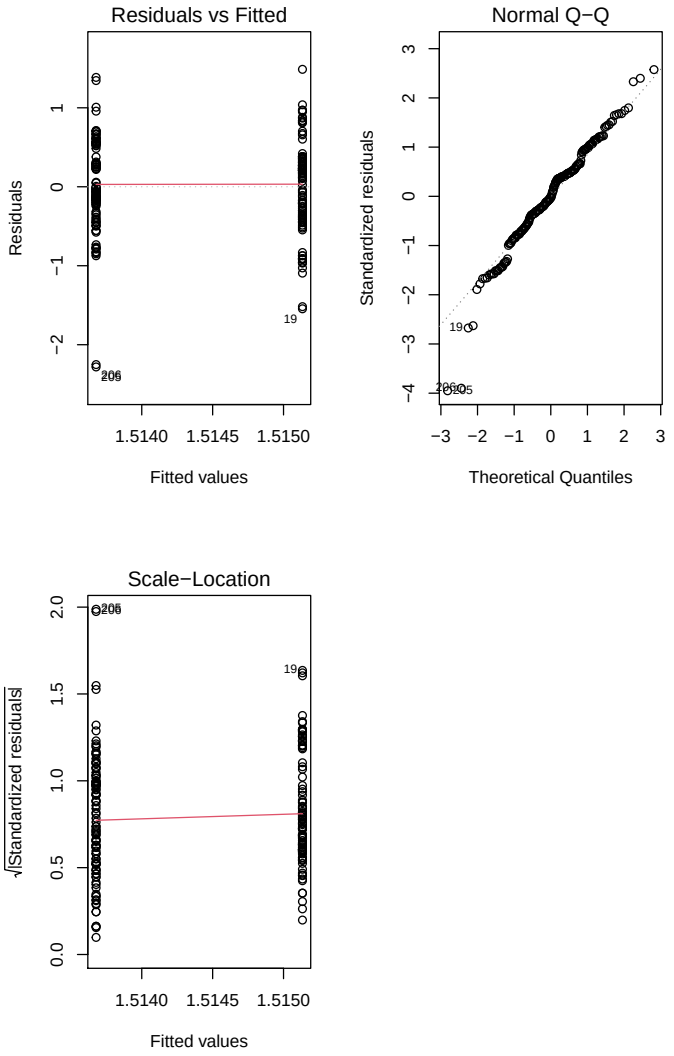

(a) ANOVA assumptions

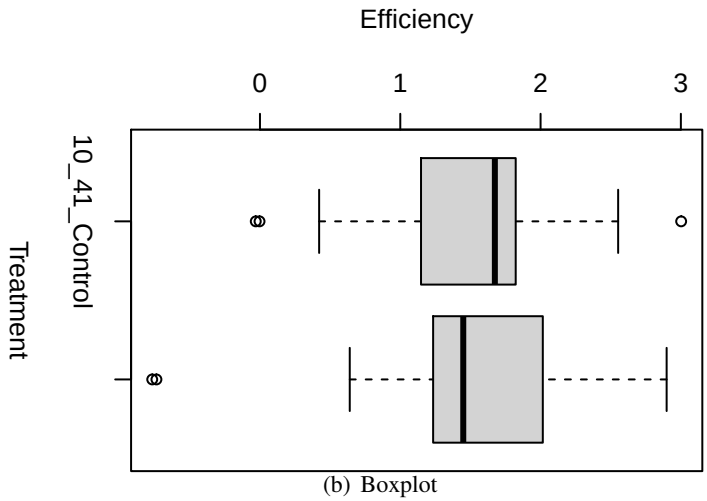

(b) Boxplot

Figure D.5: *10_41 Treatment*

D.1.6 10_42

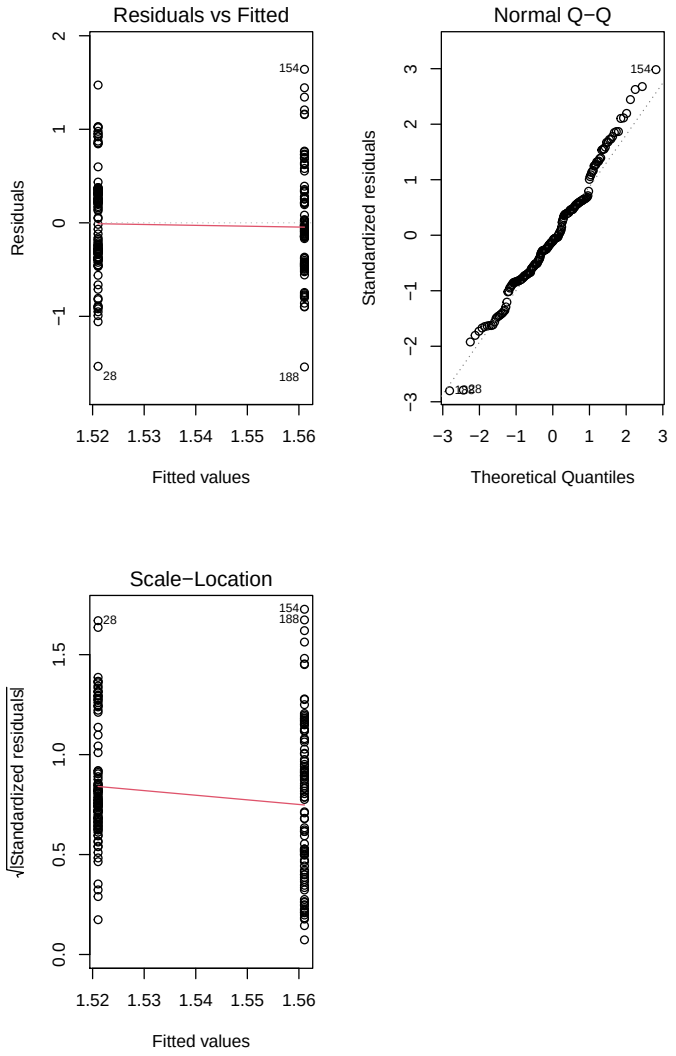

(a) ANOVA assumptions

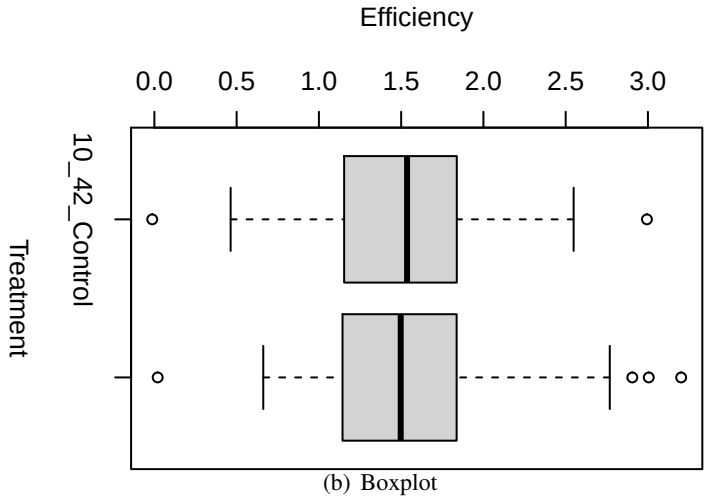

(b) Boxplot

Figure D.6: *10_42 Treatment*

D.1.7 10_48

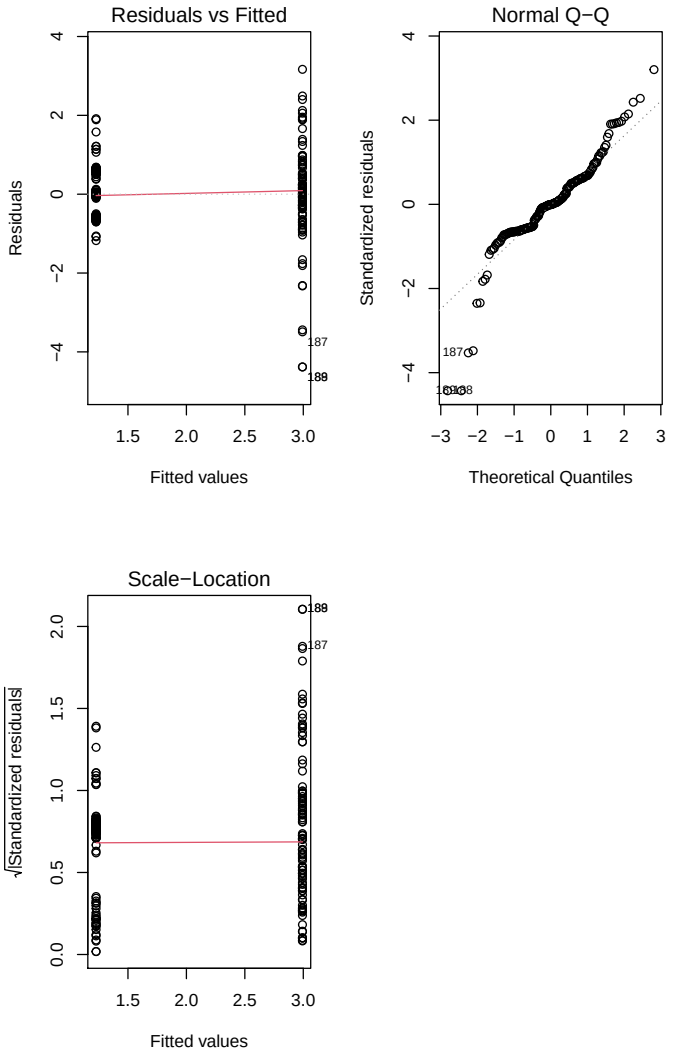

(a) ANOVA assumptions

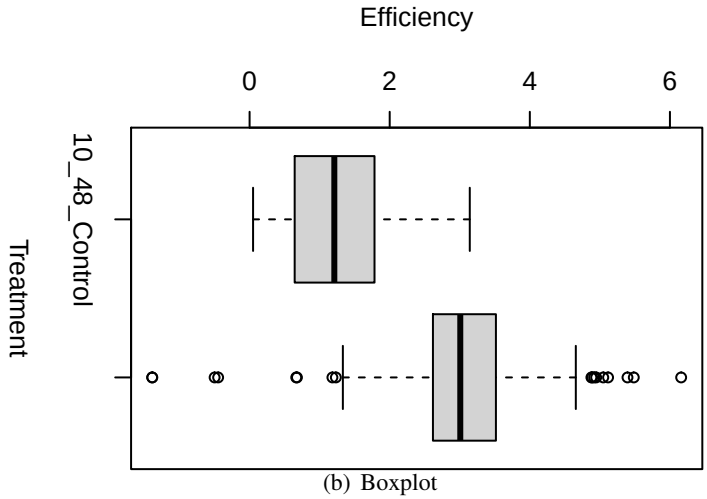

(b) Boxplot

Figure D.7: *10_48 Treatment*

D.1.8 10_53

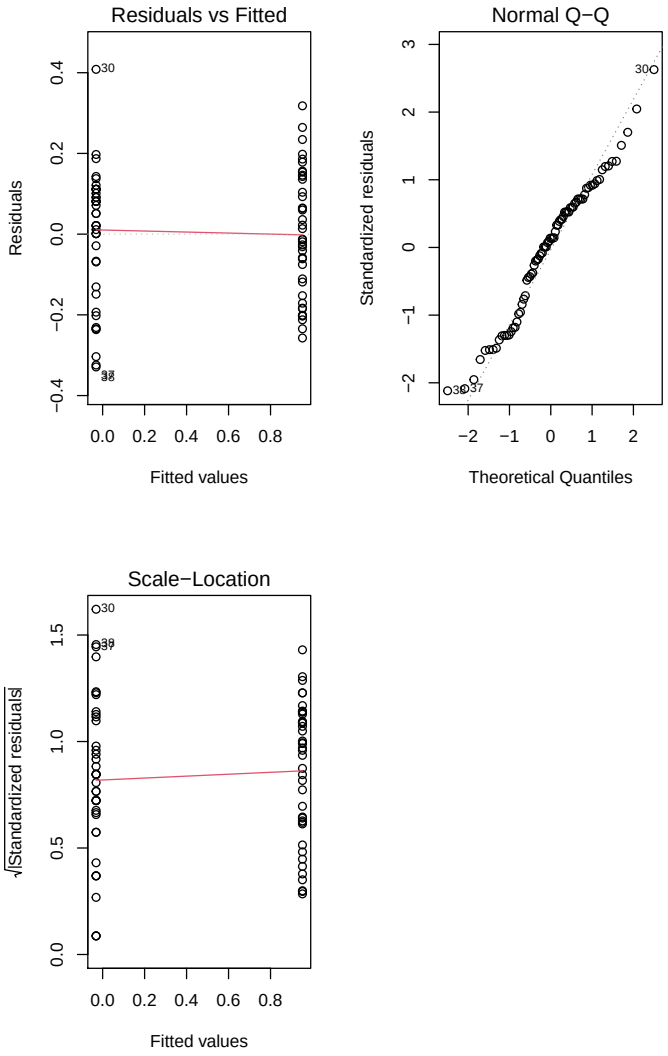

(a) ANOVA assumptions

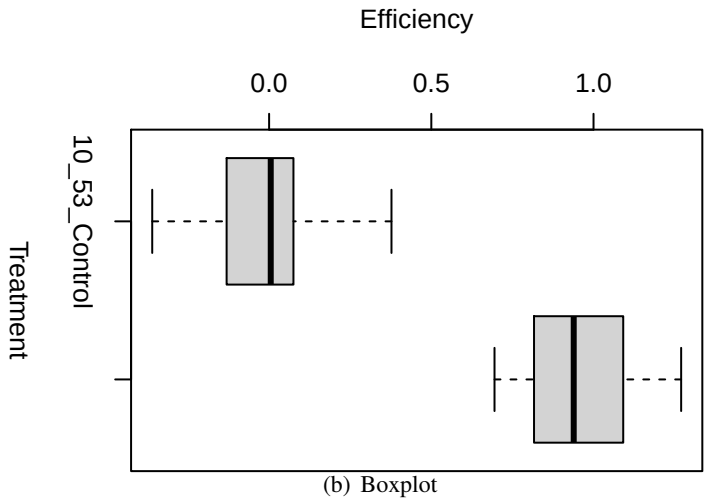

(b) Boxplot

Figure D.8: *10_53 Treatment*

D.1.9 11_05

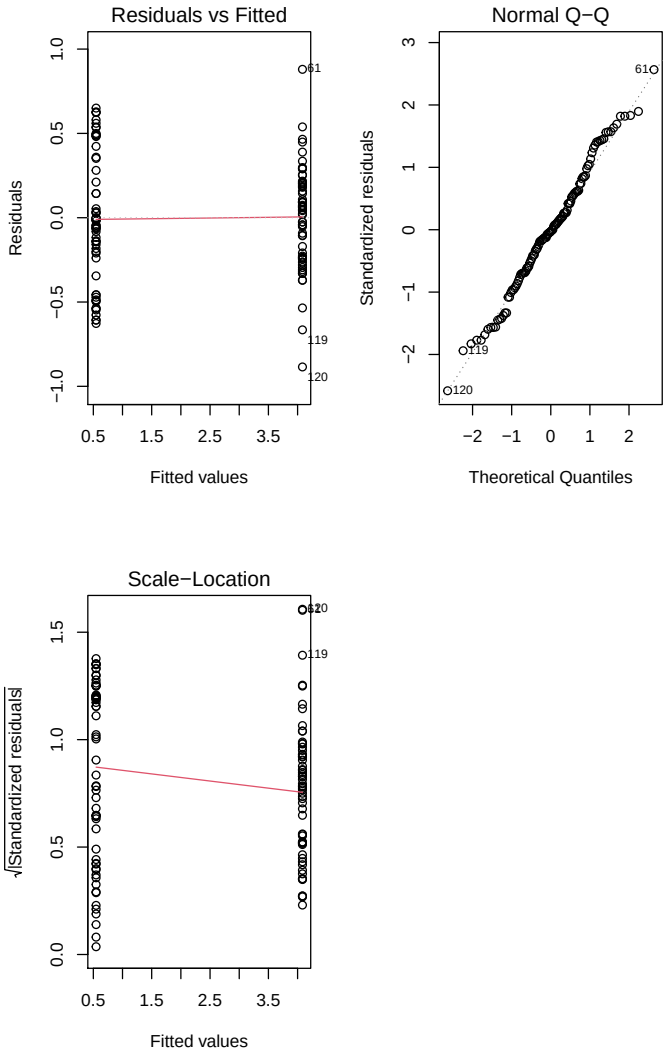

(a) ANOVA assumptions

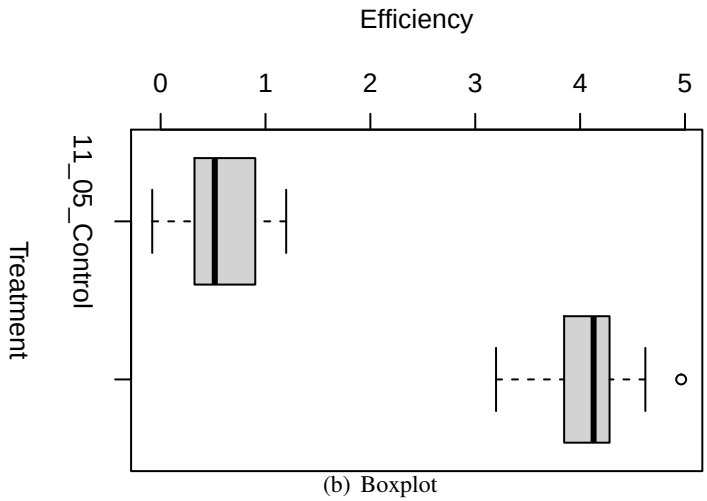

(b) Boxplot

Figure D.9: *11_05 Treatment*

D.1.10 11_05

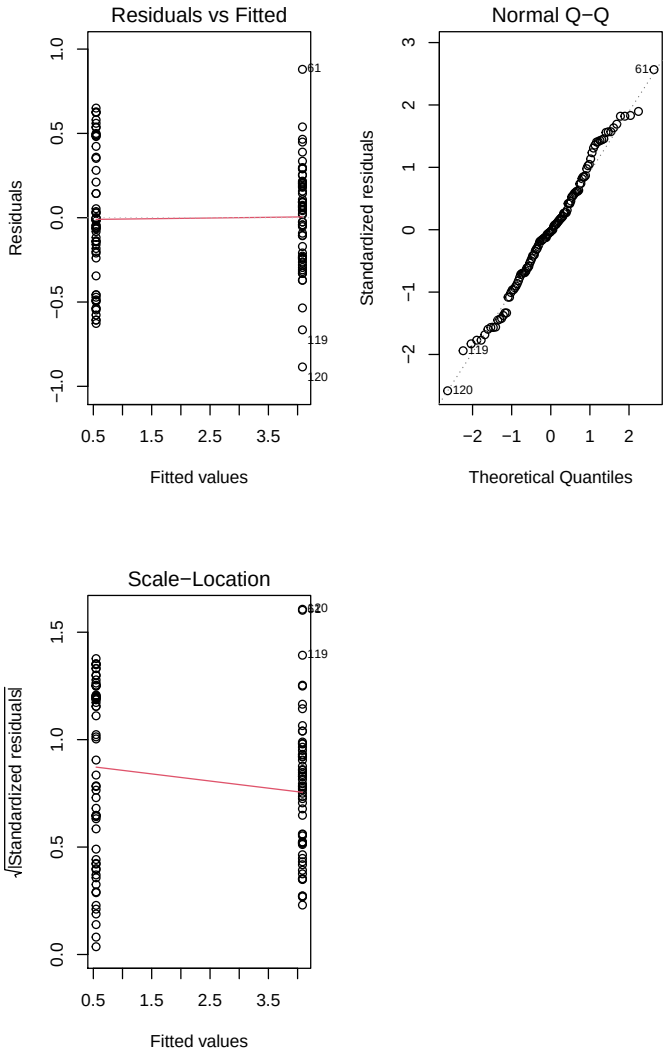

(a) ANOVA assumptions

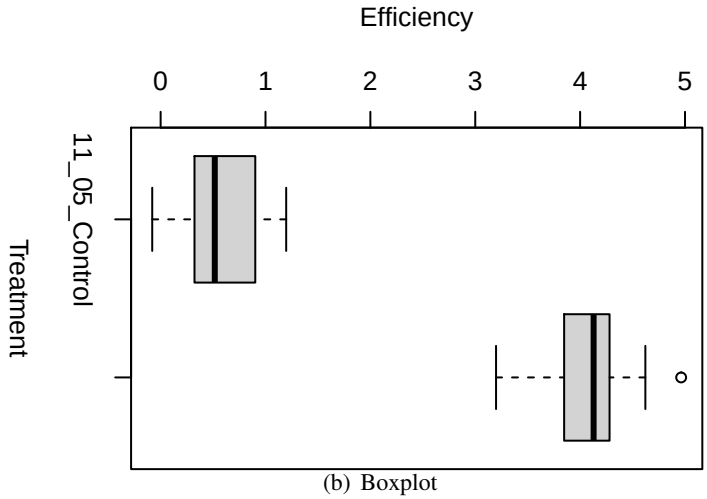

(b) Boxplot

Figure D.10: *11_05 Treatment*

D.1.11 11_21

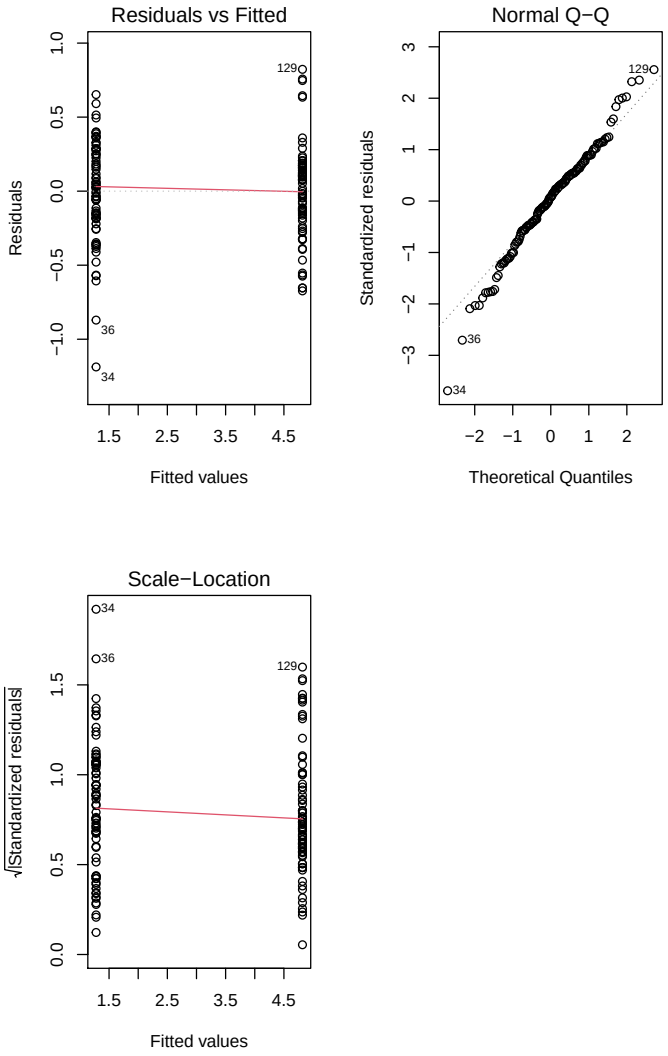

(a) ANOVA assumptions

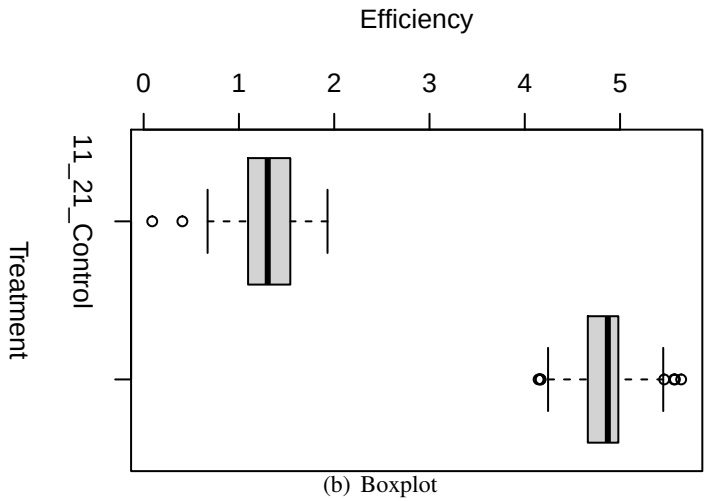

(b) Boxplot

Figure D.11: *11_21 Treatment*

D.1.12 11_32

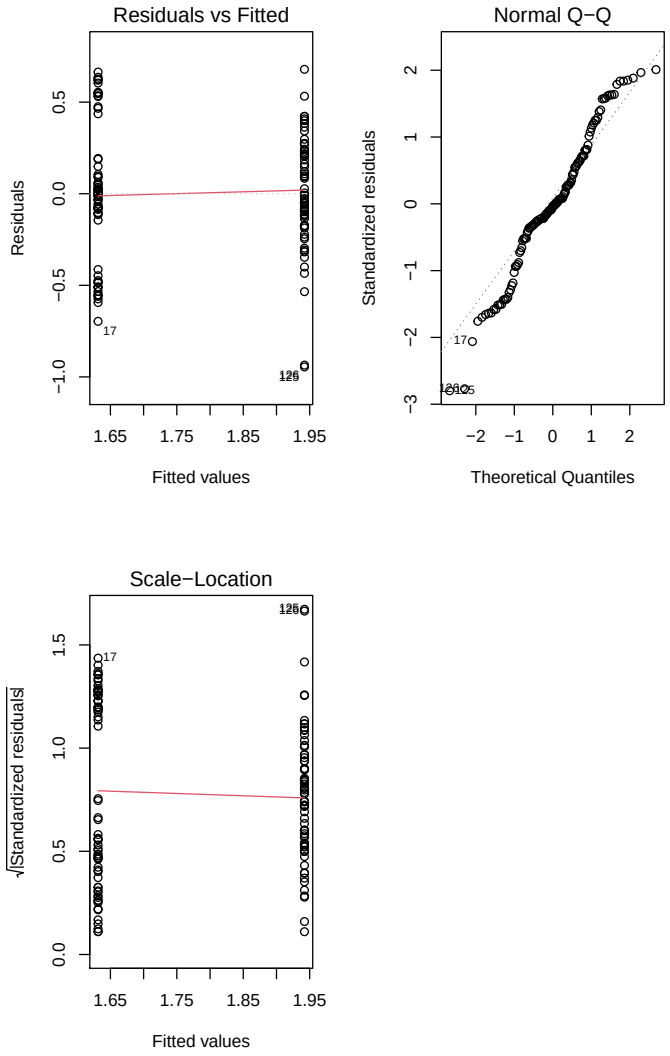

(a) ANOVA assumptions

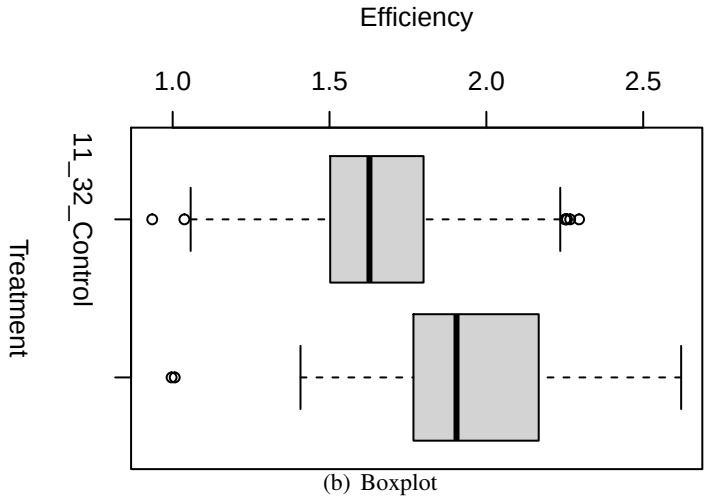

(b) Boxplot

Figure D.12: *11_32 Treatment*

D.1.13 11_35

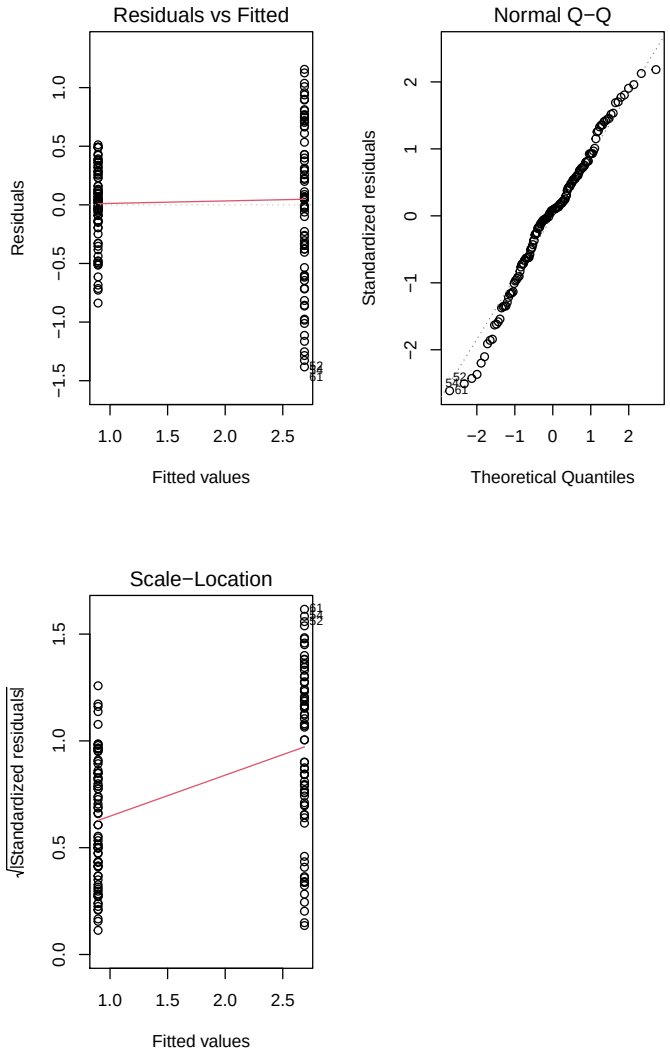

(a) ANOVA assumptions

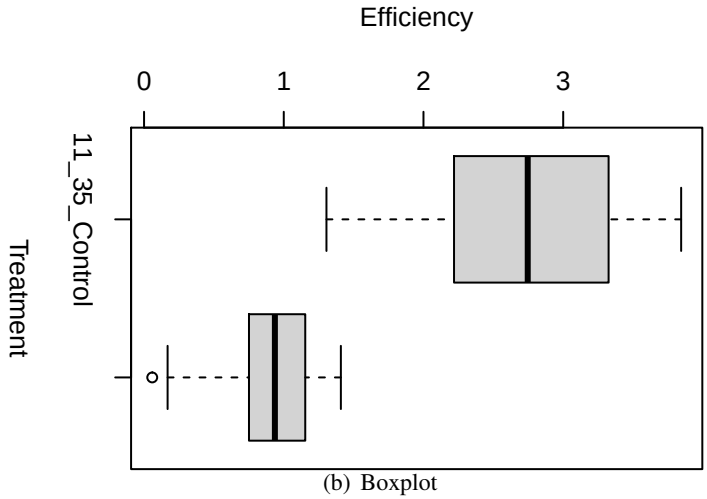

(b) Boxplot

Figure D.13: *11_35 Treatment*

D.1.14 11_48

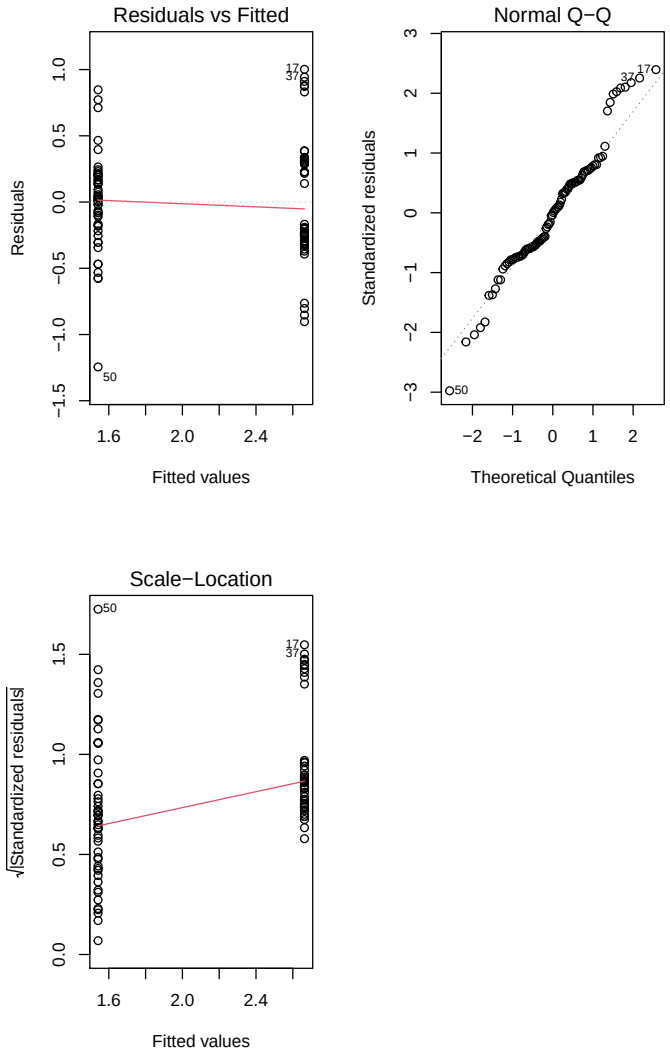

(a) ANOVA assumptions

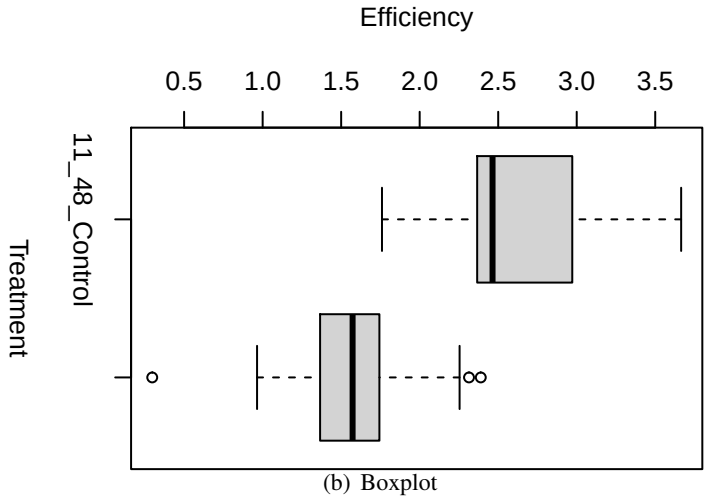

(b) Boxplot

Figure D.14: *11_48 Treatment*

D.1.15 11_51

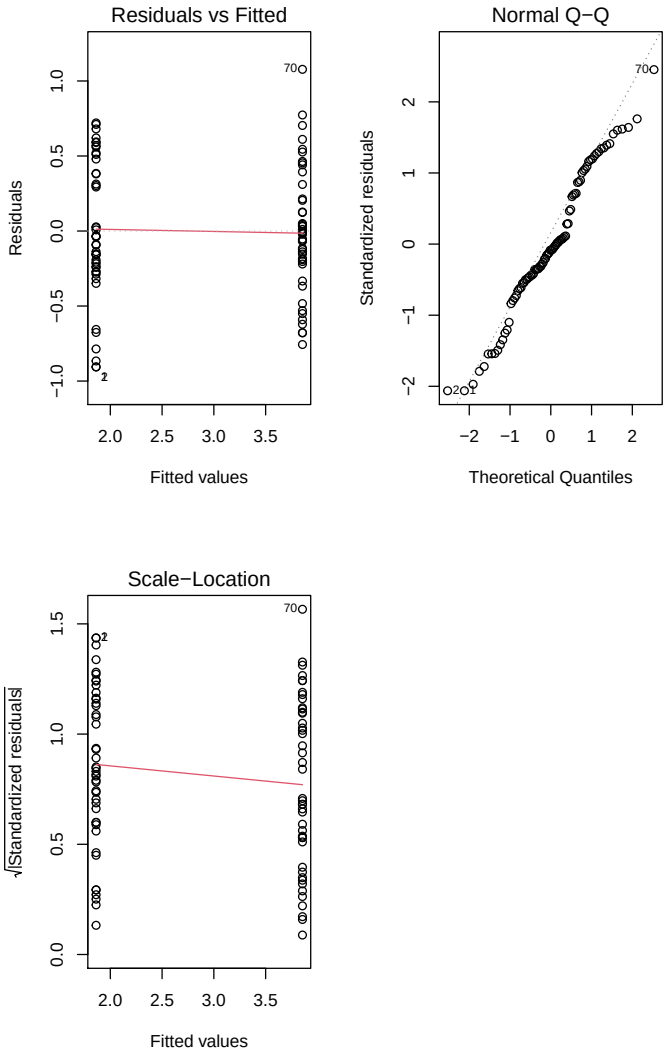

(a) ANOVA assumptions

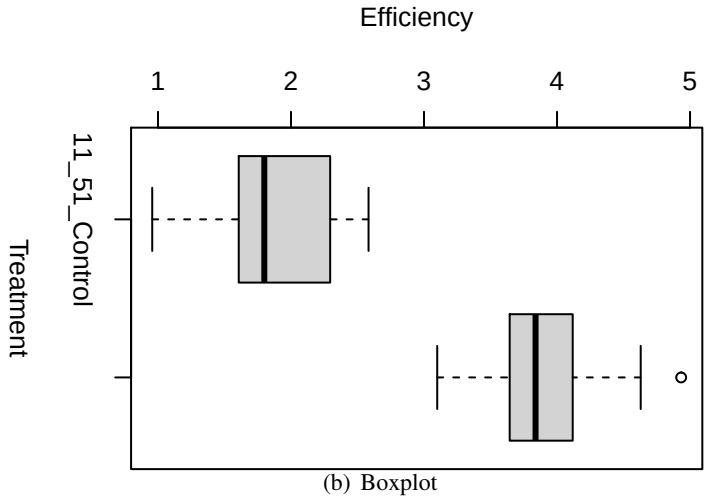

(b) Boxplot

Figure D.15: *11_51 Treatment*

D.1.16 11_53

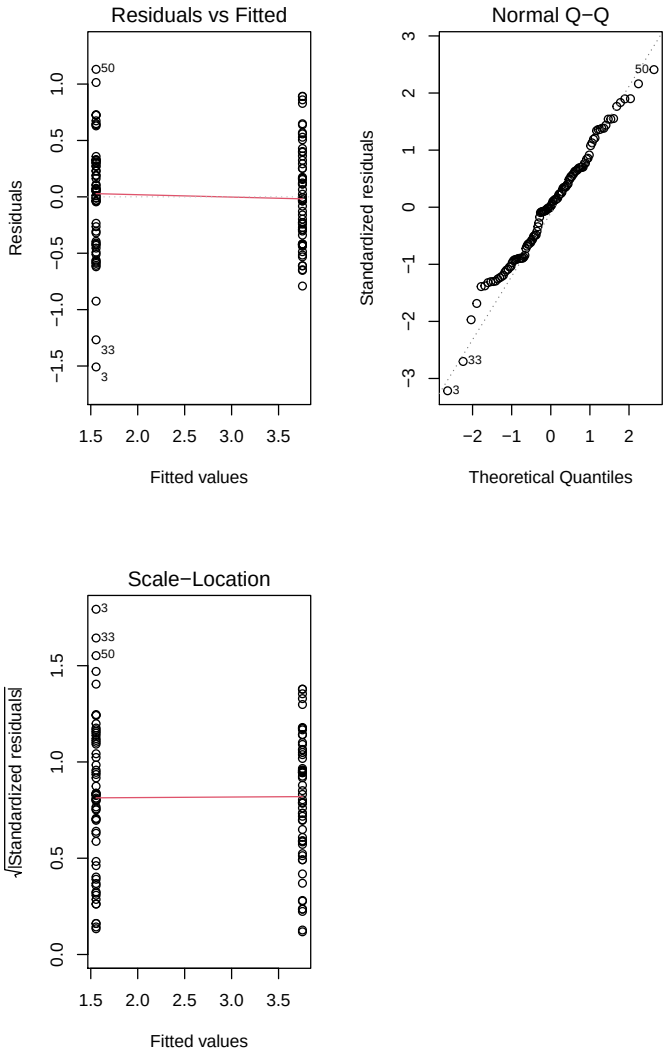

(a) ANOVA assumptions

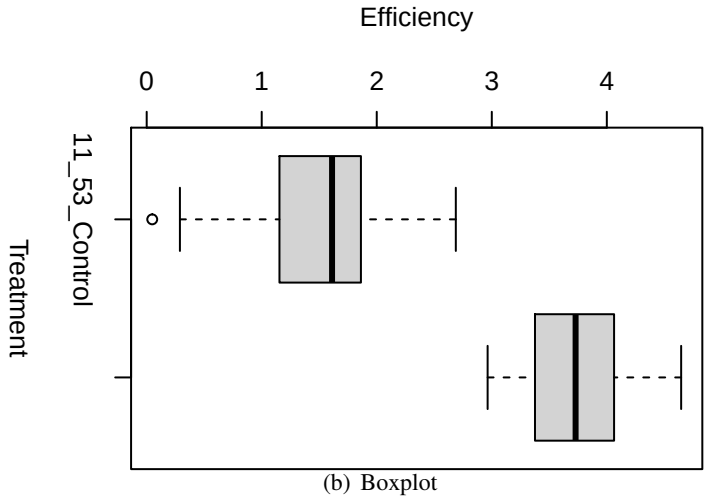

(b) Boxplot

Figure D.16: *11_53 Treatment*

D.1.17 11_55

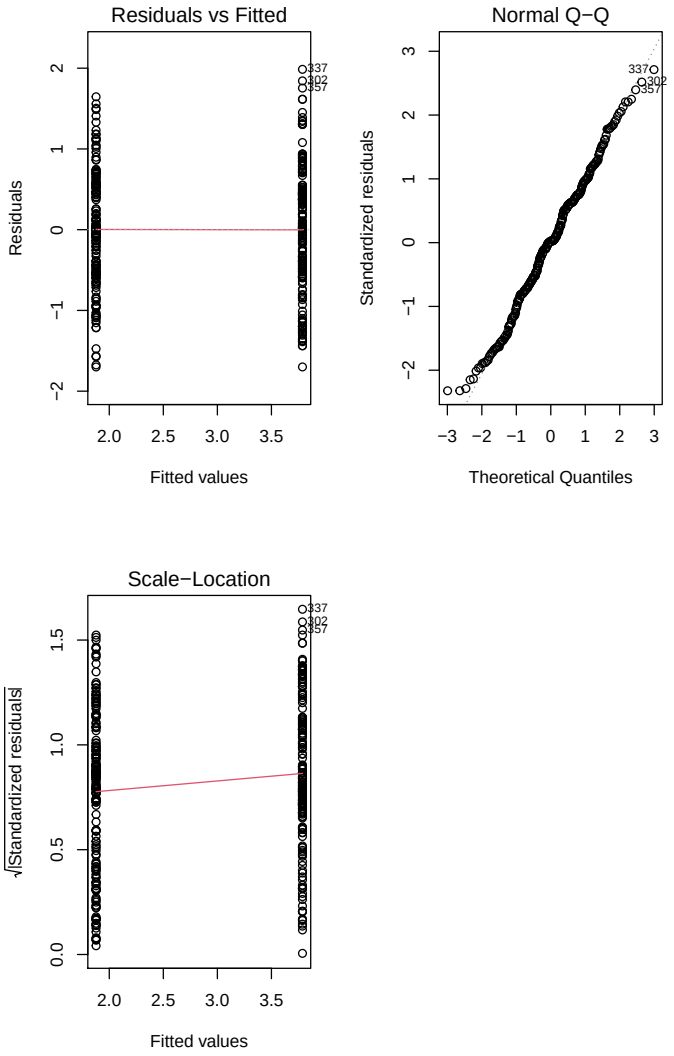

(a) ANOVA assumptions

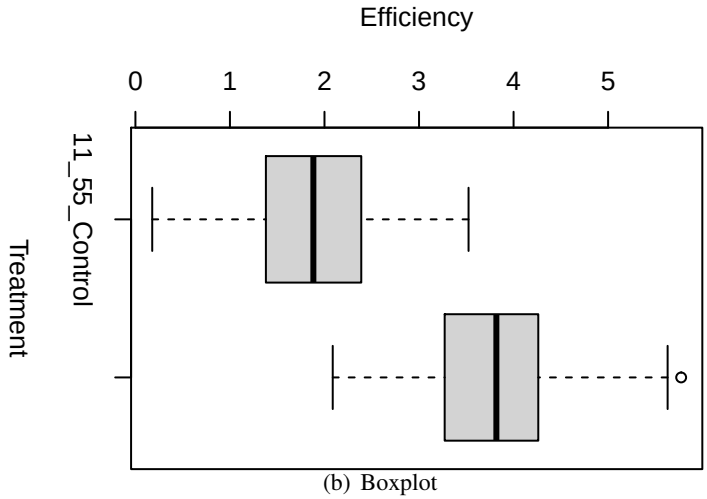

(b) Boxplot

Figure D.17: *11_55 Treatment*

D.1.18 12_03

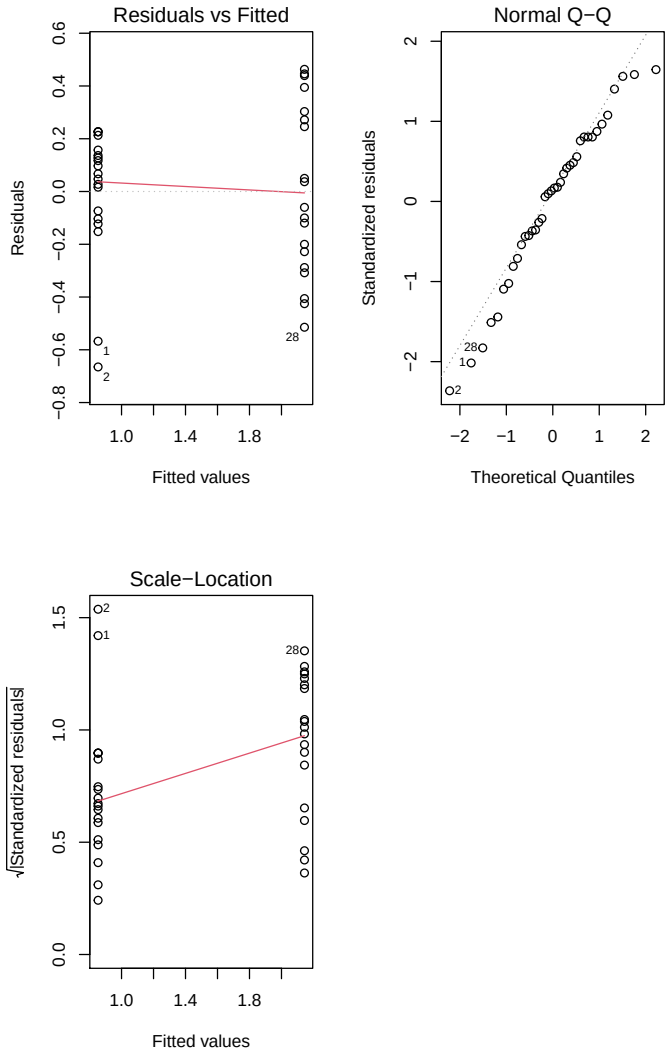

(a) ANOVA assumptions

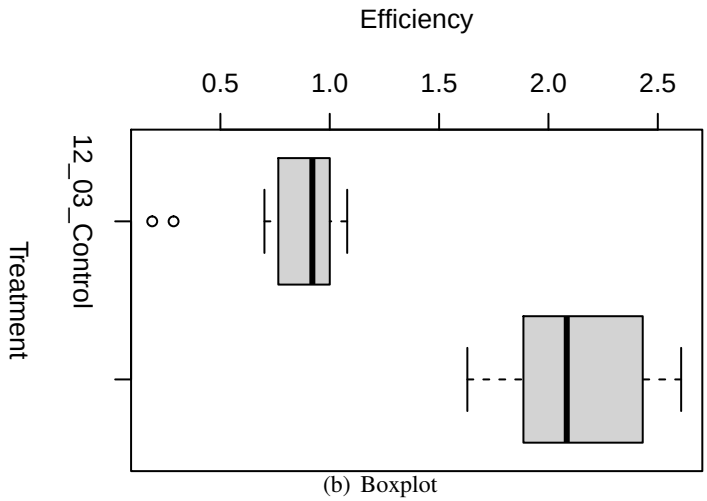

(b) Boxplot

Figure D.18: *12_03 Treatment*

D.1.19 12_11

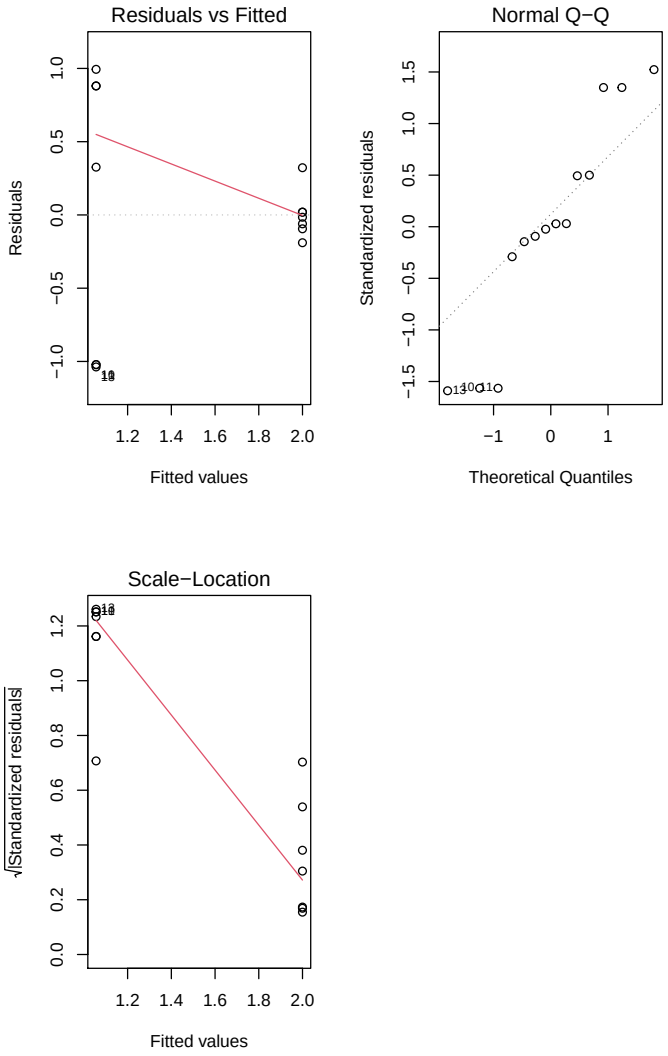

(a) ANOVA assumptions

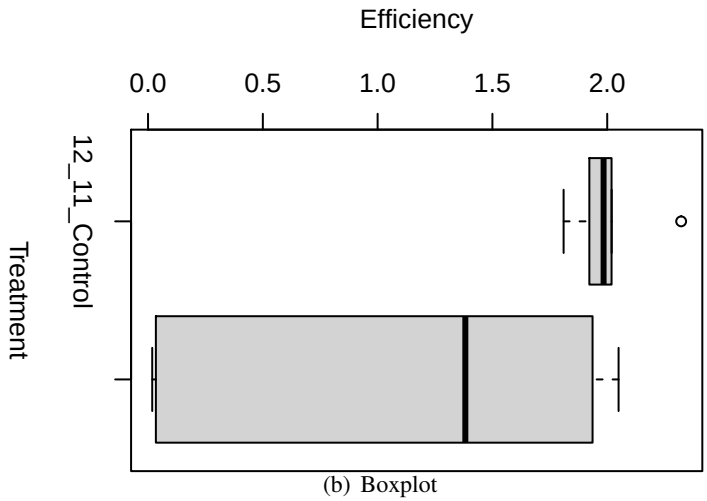

(b) Boxplot

Figure D.19: *12_11 Treatment*

D.1.20 12_31

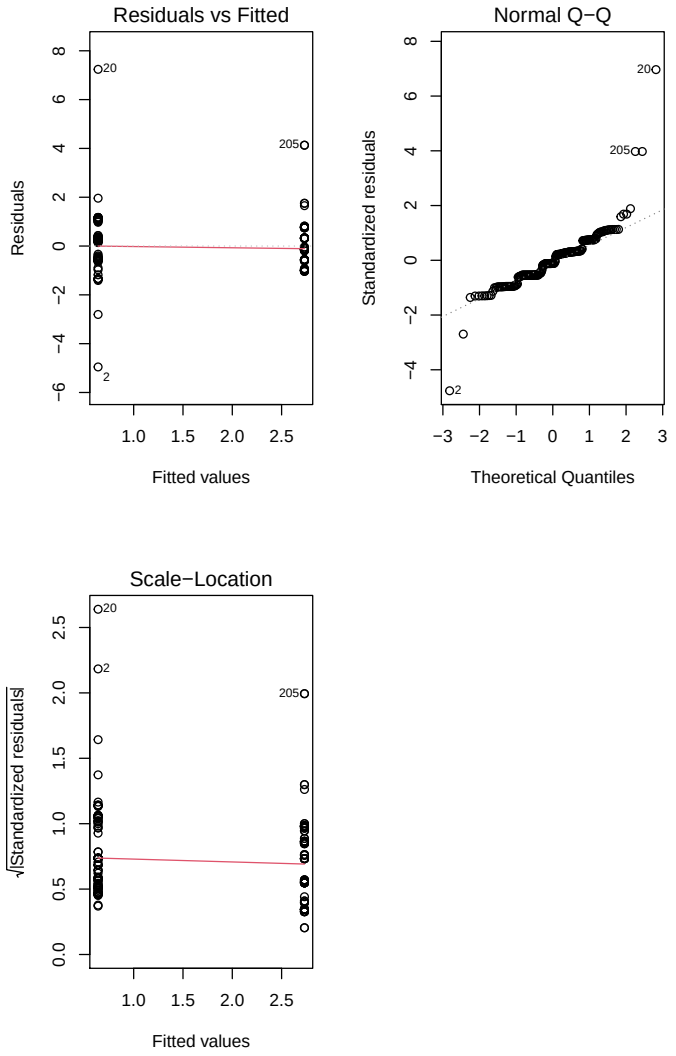

(a) ANOVA assumptions

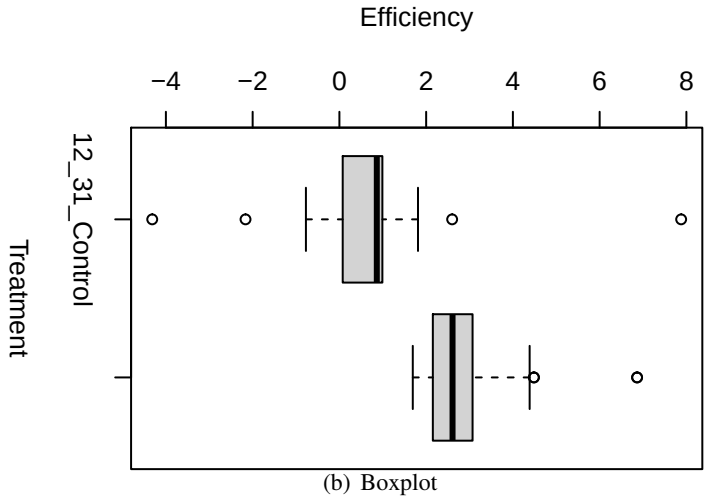

(b) Boxplot

Figure D.20: *12_31 Treatment*

D.1.21 12_34

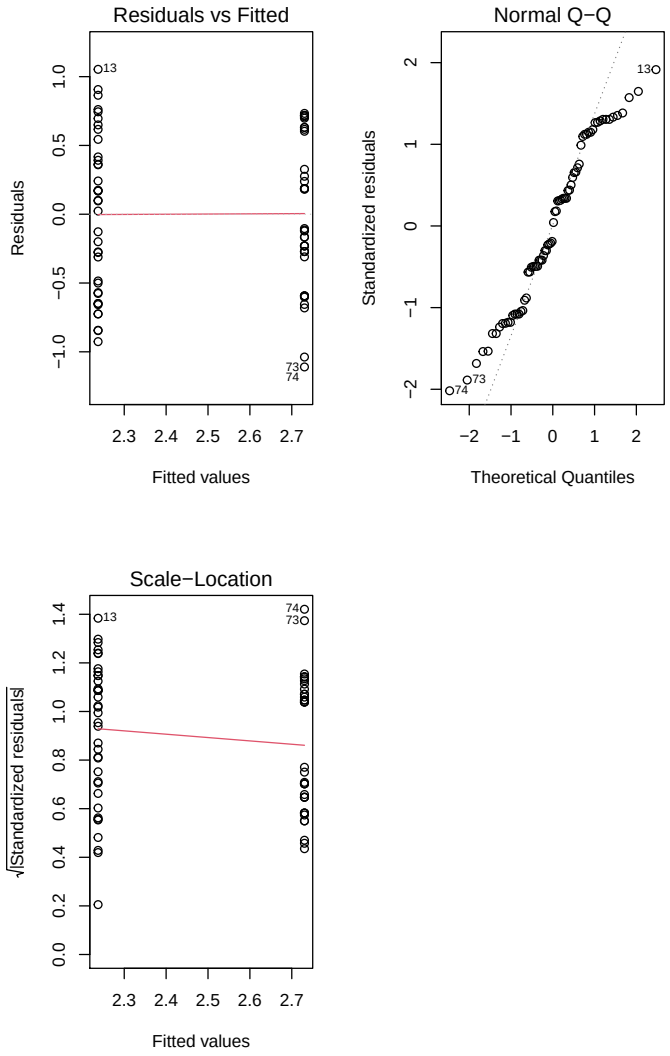

(a) ANOVA assumptions

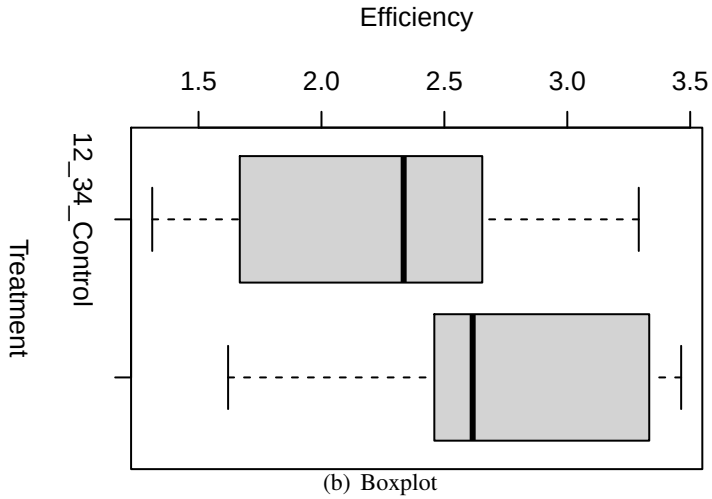

(b) Boxplot

Figure D.21: *12_34 Treatment*

D.1.22 12_44

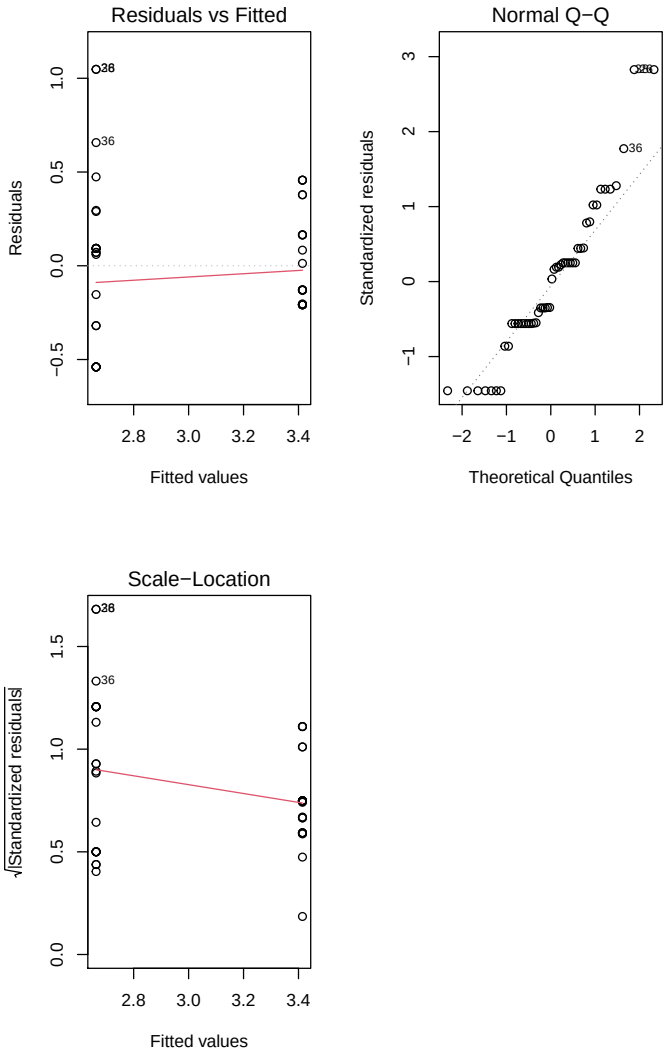

(a) ANOVA assumptions

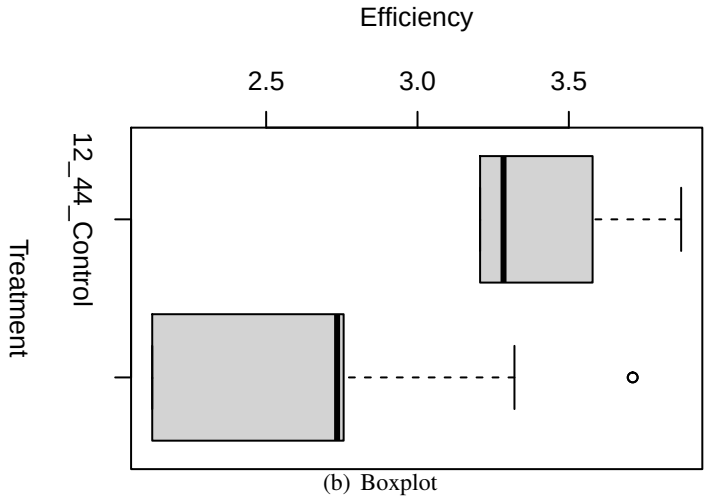

(b) Boxplot

Figure D.22: *12_44 Treatment*

D.1.23 12_45

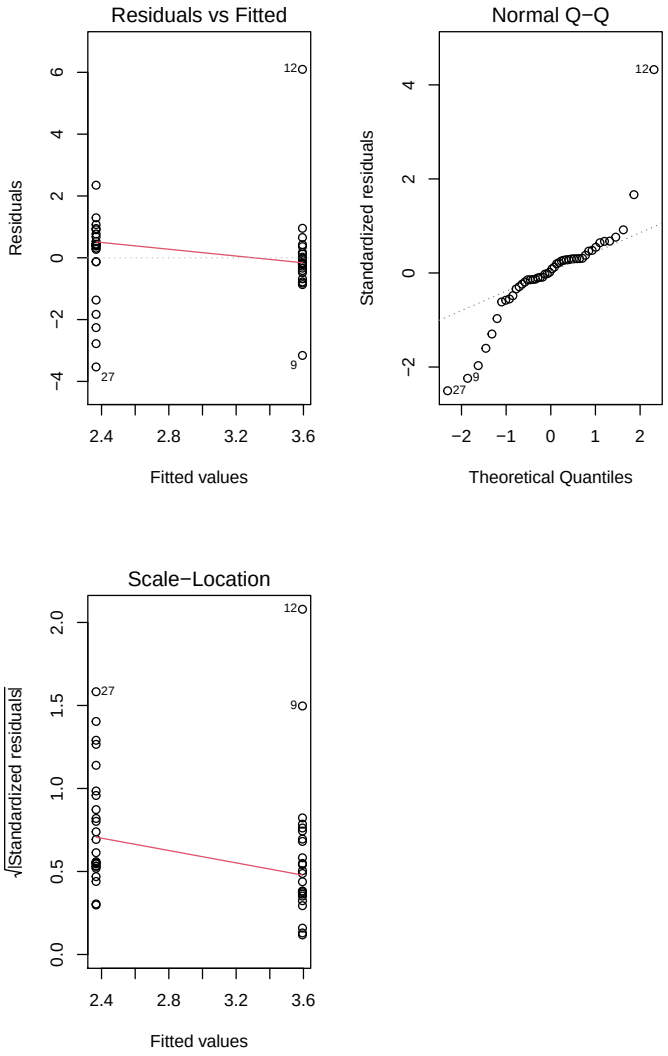

(a) ANOVA assumptions

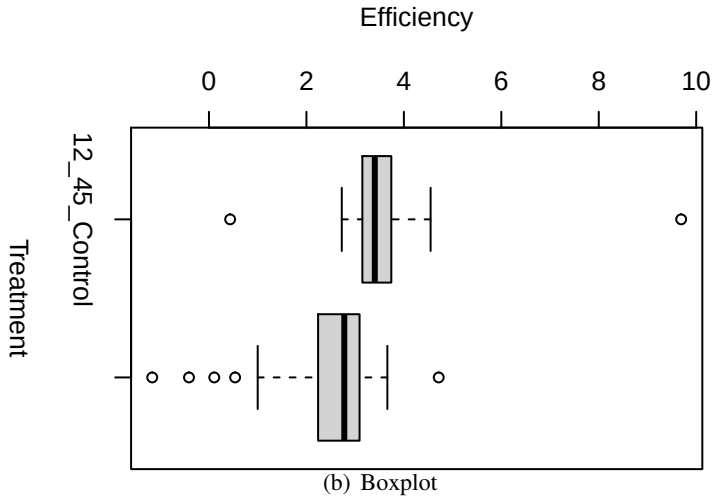

(b) Boxplot

Figure D.23: *12_45 Treatment*

D.1.24 12_46

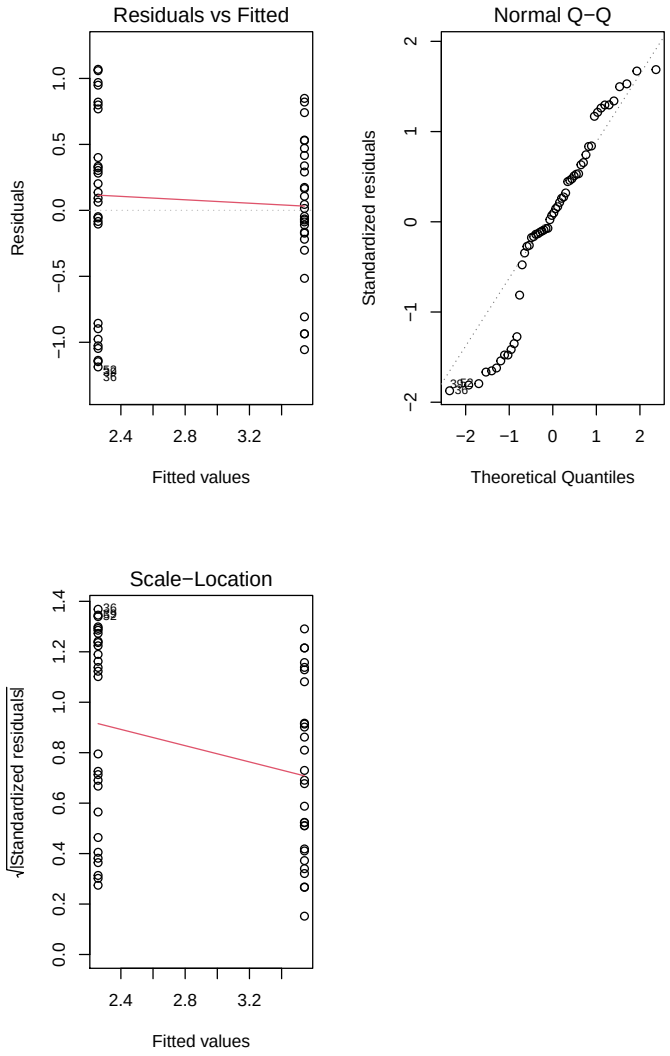

(a) ANOVA assumptions

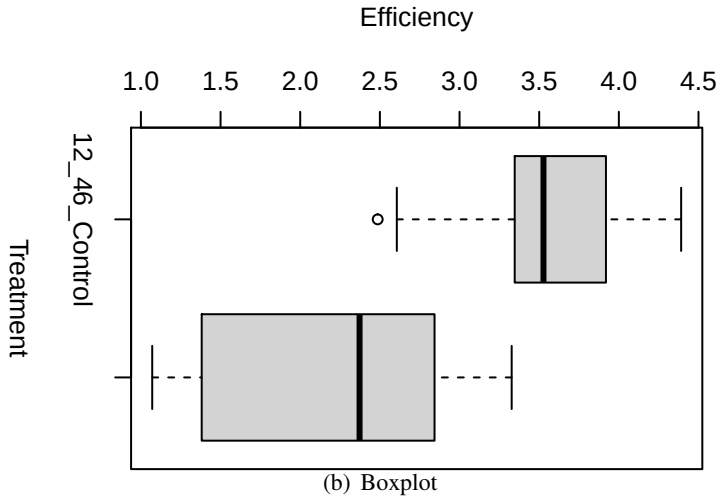

(b) Boxplot

Figure D.24: *12_46 Treatment*

D.1.25 13_07

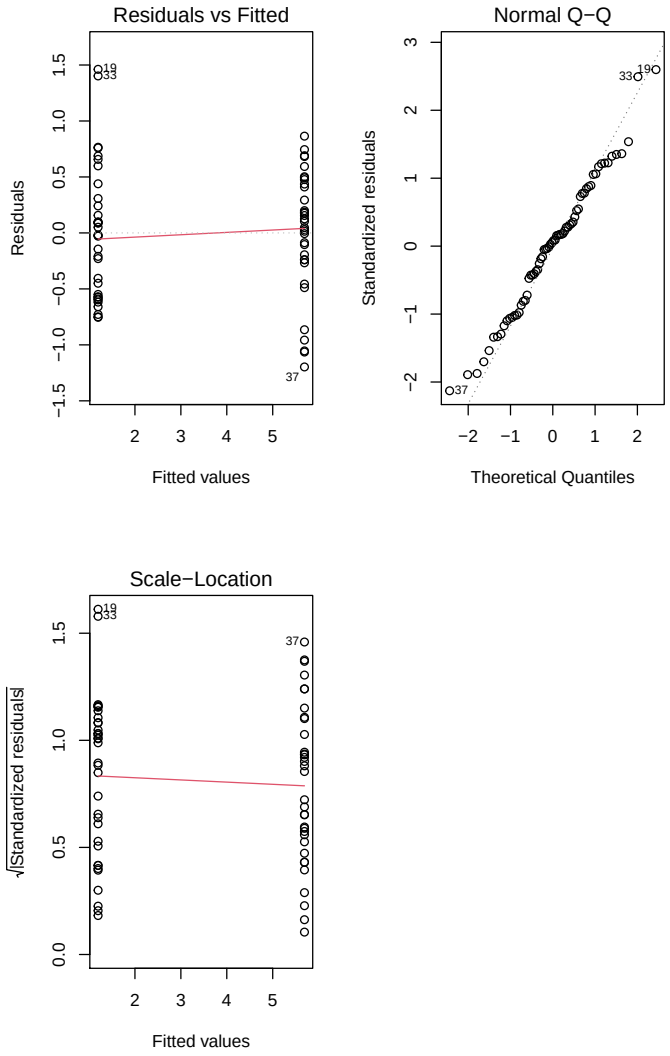

(a) ANOVA assumptions

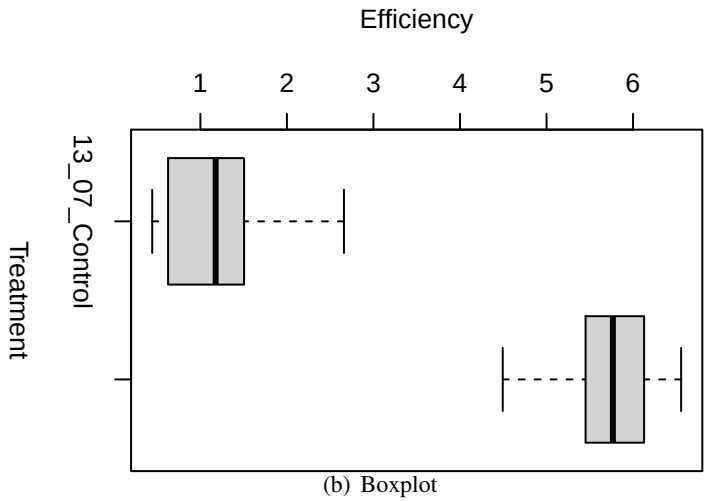

(b) Boxplot

Figure D.25: *13_07 Treatment*

D.1.26 13_31

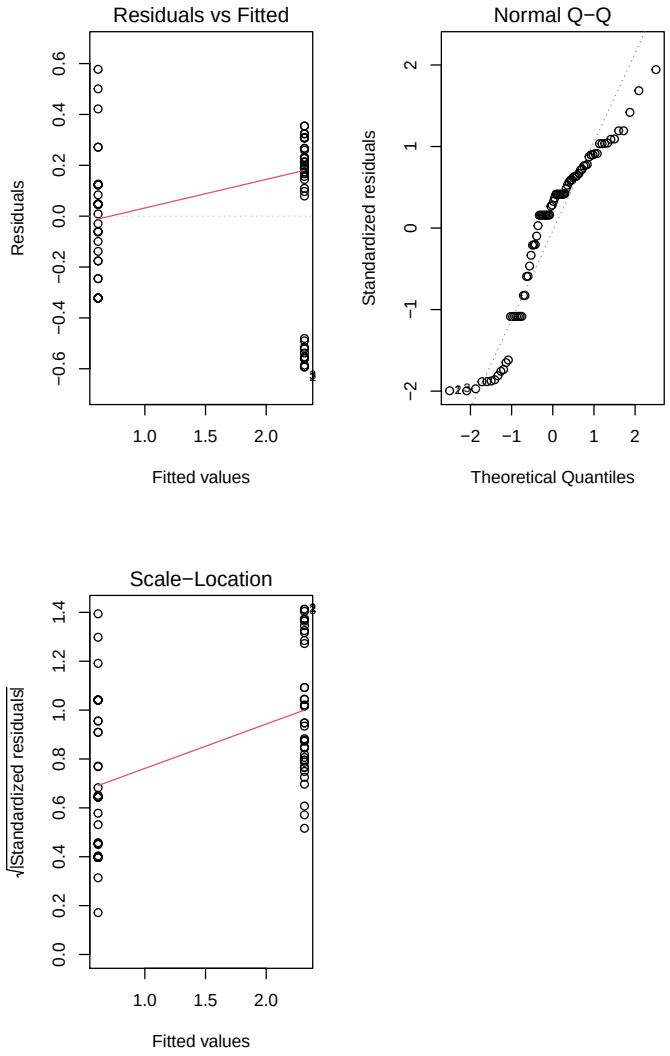

(a) ANOVA assumptions

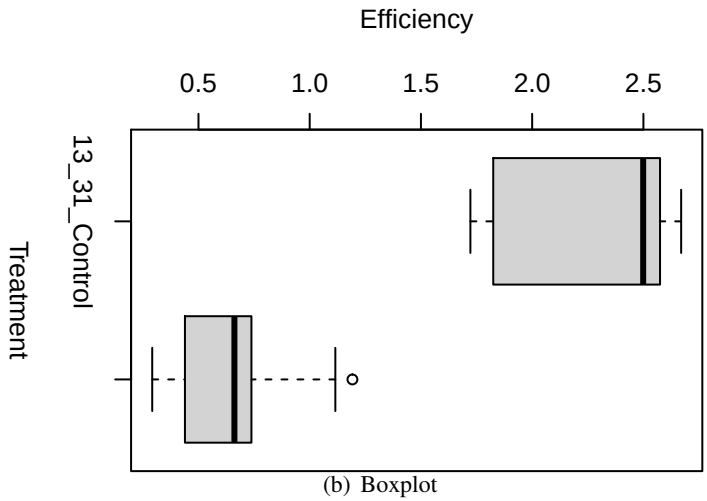

(b) Boxplot

Figure D.26: *13_31 Treatment*

D.1.27 13_41

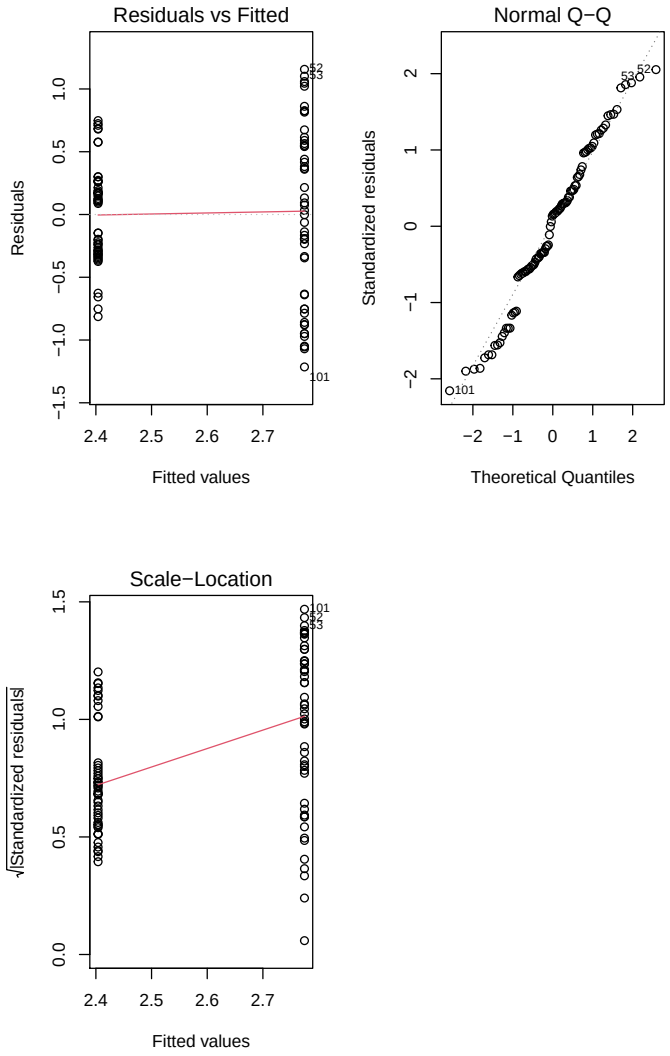

(a) ANOVA assumptions

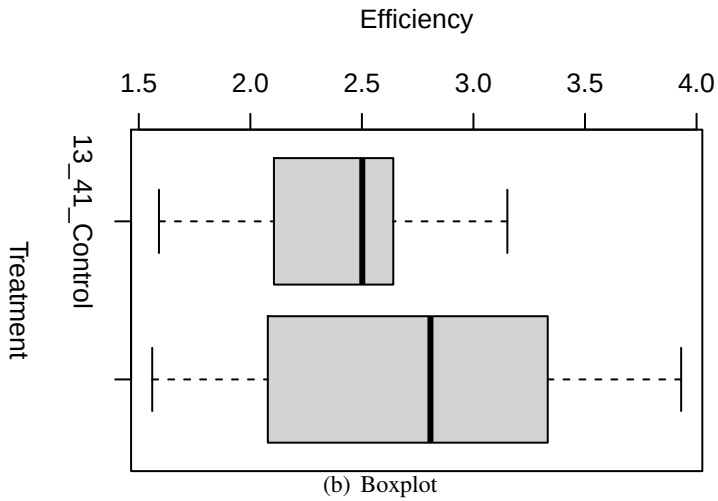

(b) Boxplot

Figure D.27: *13_41 Treatment*

D.1.28 13_50

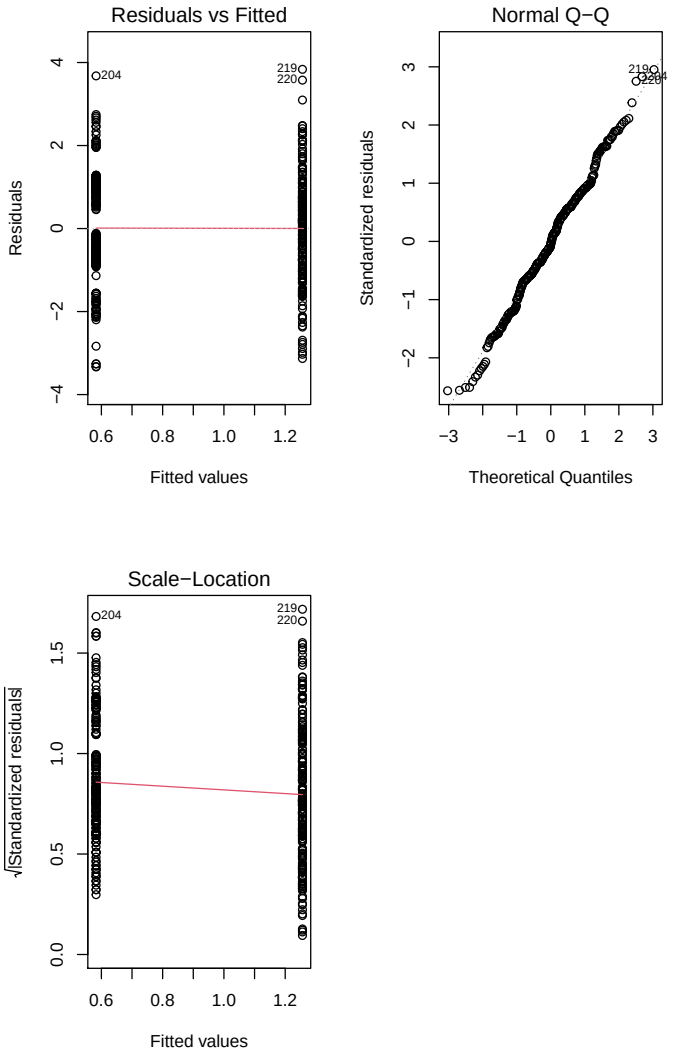

(a) ANOVA assumptions

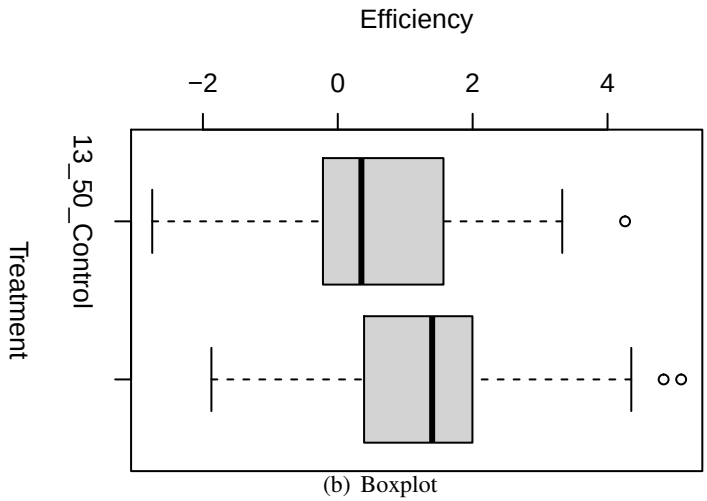

(b) Boxplot

Figure D.28: *13_50 Treatment*

D.2 60º Texture

Treatment	Anova's assumptions			Anova P-Value	Mean Efficiency	
	Homocedastisity	Waste Normality	Independence of Residuals		Control	Texure
09_37	0,49	0,2068	4,93E-05	2,20E-16	4,94	26
10_06	0,72	0,13	2,19E-16	2,20E-16	0,46	3,88
10_36	0,24	0,27	0,002	3,63E-14	1,29	2,38
10_37	0,33	0,49	0,01	1,49E-09	1,57	2,52
10_38	0,38	0,22	2,20E-16	2,20E-16	2,26	0,8
10_41	0,14	0,052	0,008	1,90E-02	1,84	1,97
10_42	0,45	0,00016	2,09E-11	3,93E-12	1,58	2,01
10_47	0,67	0,2	0,09	4,65E-07	1,03	2,09
11_05	0,62	0,06	2,60E-07	2,20E-16	2,16	0,54
11_08	0,039	0,055	2,20E-16	2,20E-16	2,29	1,55
11_09	0,12	0,54	1,00E-02	2,20E-16	1,21	2,09
11_11	0,006	0,36	8,50E-02	2,00E-02	1,91	2,77
11_16	0,58	0,0001	0,0030	2,60E-01	2,26	2,50
11_21	0,001	0,007	5,00E-04	2,25E-07	1,24	1,81
11_22	0,11	0,57	5,90E-01	8,12E-08	1,39	5,02
11_25	0,27	0,2	1,73E-06	2,20E-16	1,62	2,31
12_31	0,41	0,056	3,64E-07	2,20E-16	0,58	2,13
13_18	0,009	0,05137	4,00E-04	2,20E-16	5,13	3,09
13_19	0,67	0,16	3,00E-04	2,15E-07	4,77	2,89
13_27	0,095	0,058	1,90E-02	6,44E-09	3,56	4,45
13_30	0,37	0,2589	3,87E-05	3,20E-02	2,65	3,27
13_31	0,123	0,128	4,72E-01	3,82E-08	4,9	1,99

Table D.2: *Main results for the tests of Anova, Anova assumptions and average efficiencies of the control and 60º texture..*

The assumptions and the distribution of statistical groups are shown graphically below.

D.2.1 09_37

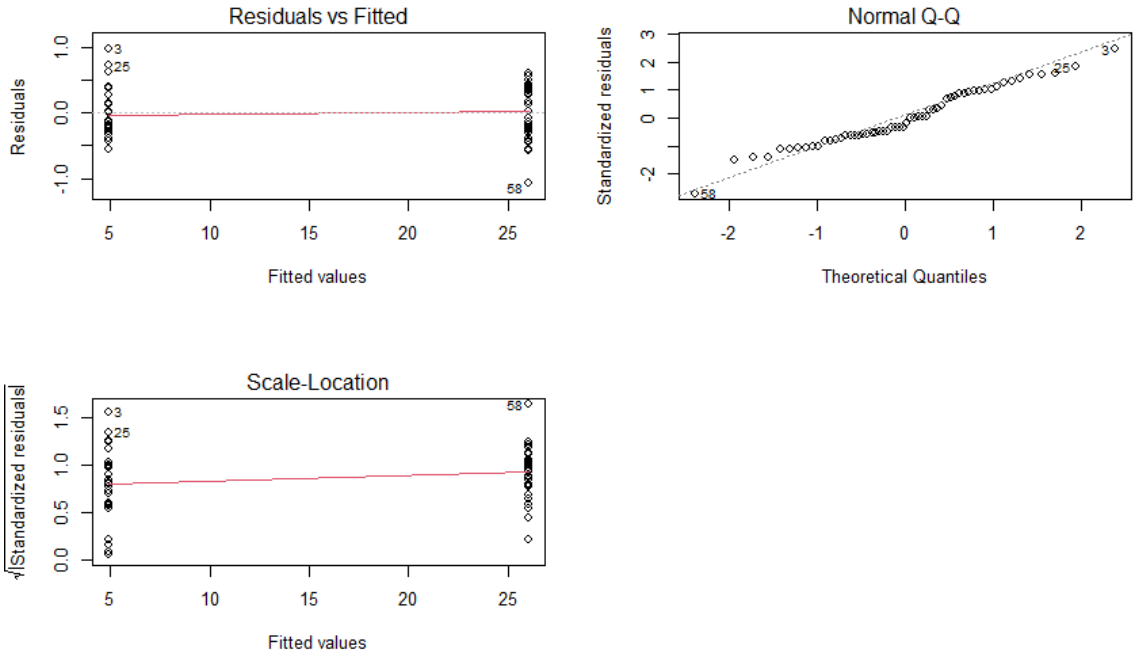

(a) ANOVA assumptions

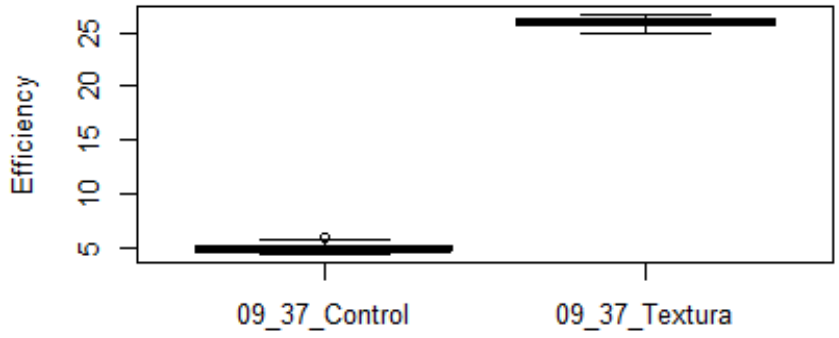

(b) Boxplot

Figure D.29: *09_37 Treatment*

D.2.2 10_06

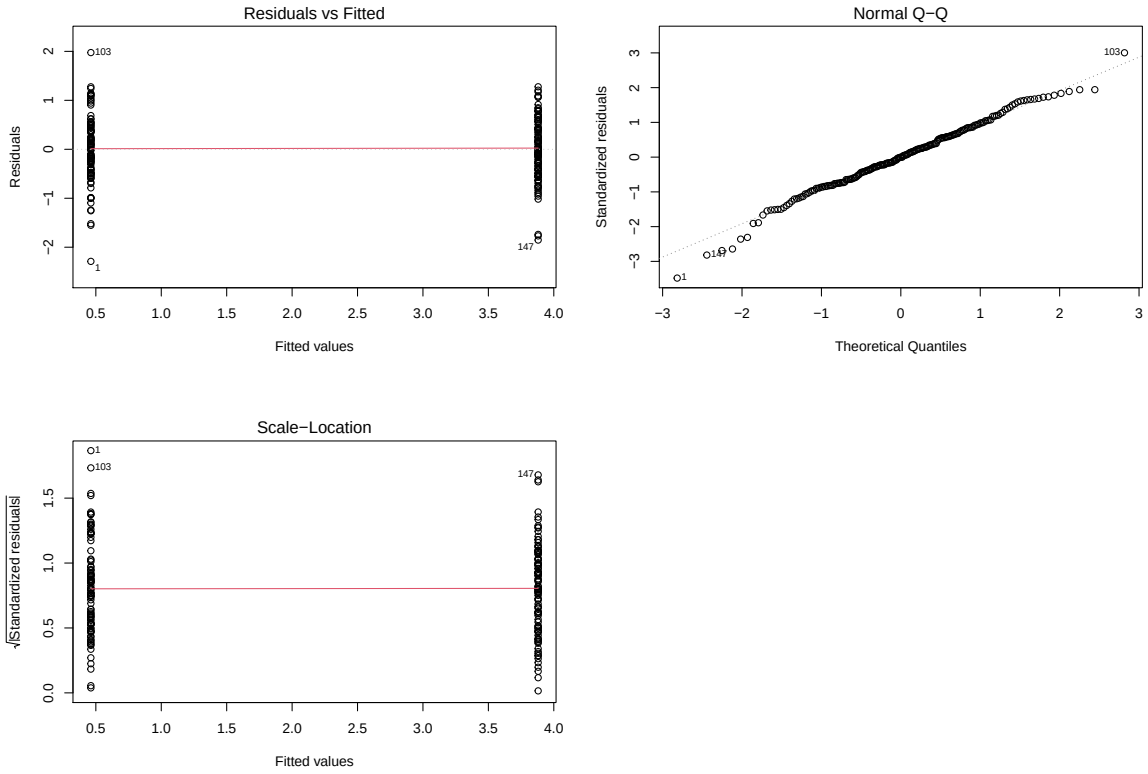

(a) ANOVA assumptions

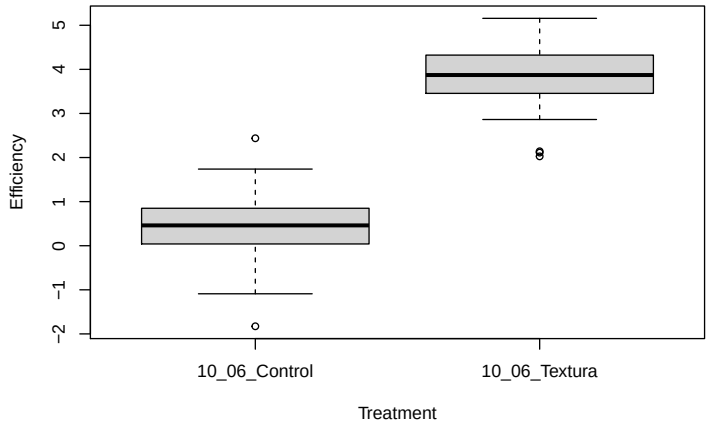

(b) Boxplot

Figure D.30: *10_06 Treatment*

D.2.3 10_36

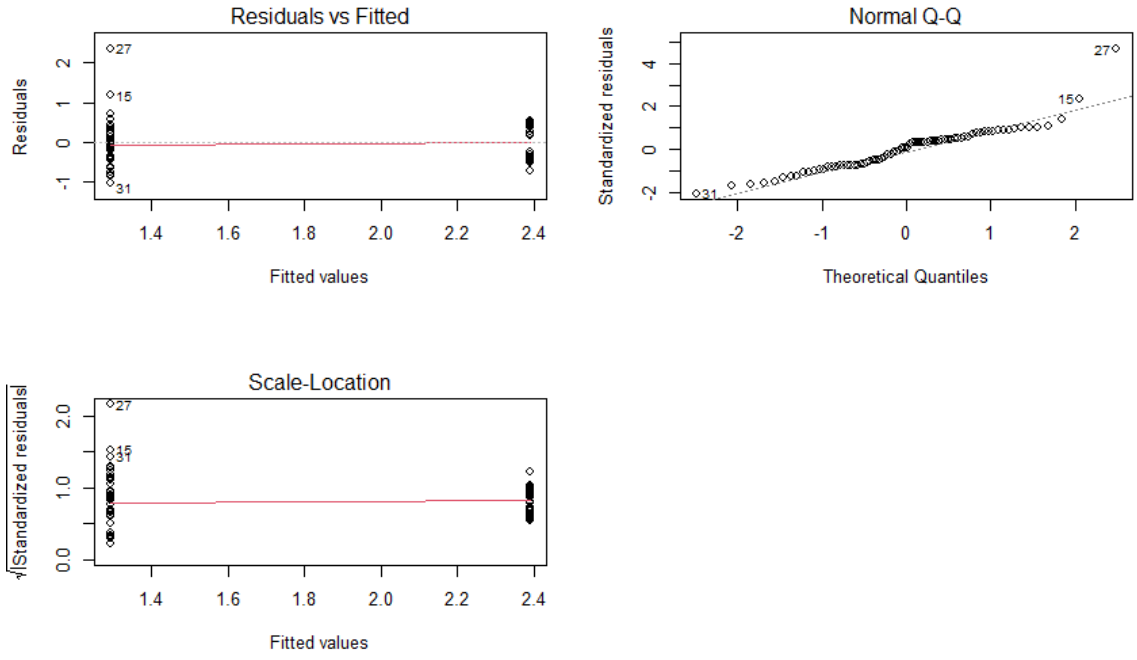

(a) ANOVA assumptions

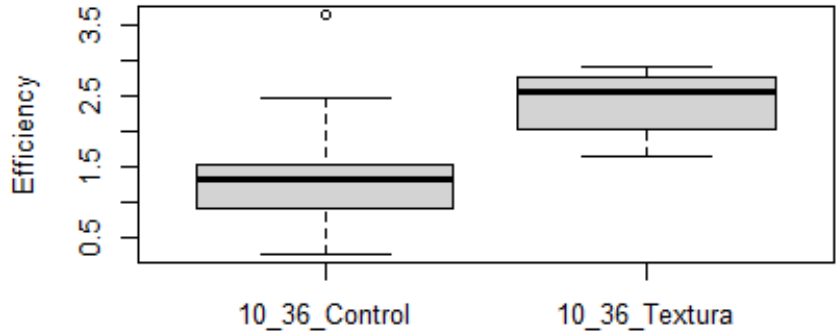

(b) Boxplot

Figure D.31: *10_36 Treatment*

D.2.4 10_37

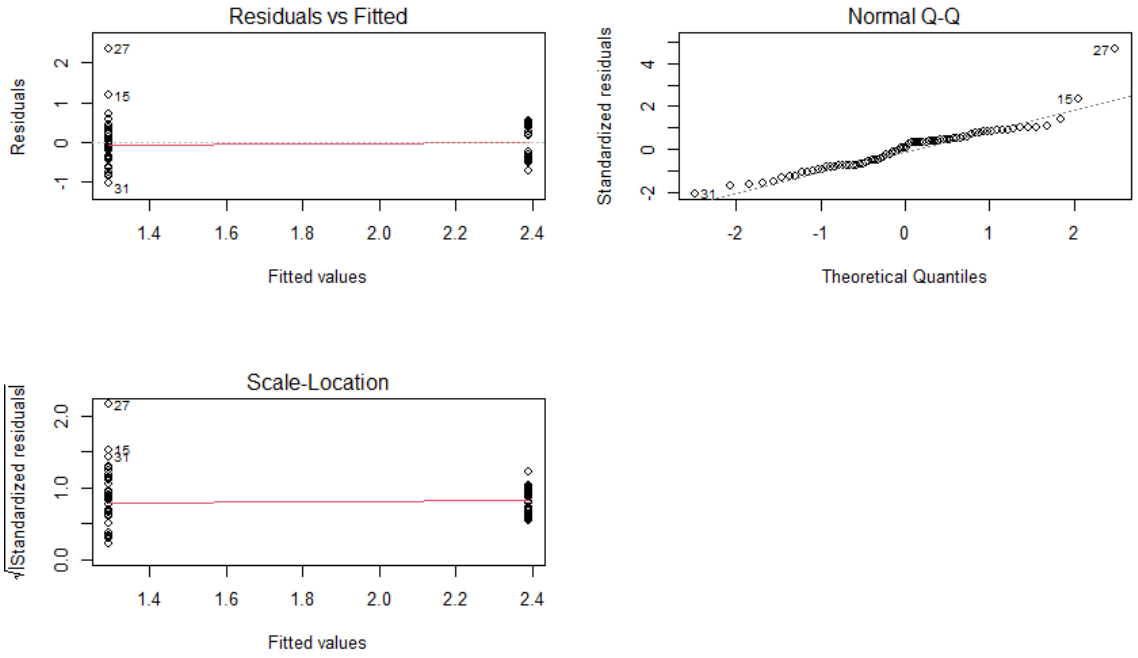

(a) ANOVA assumptions

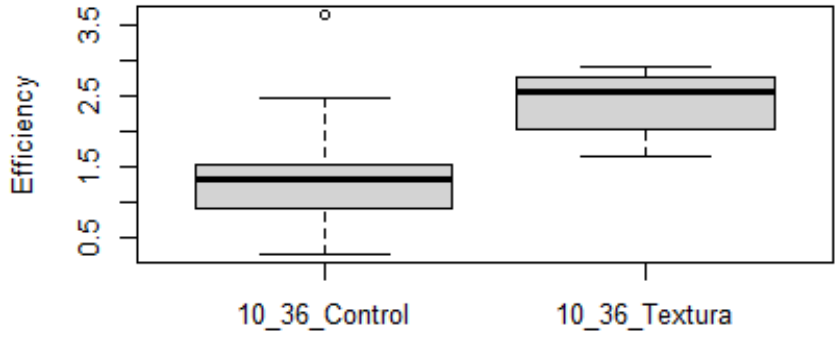

(b) Boxplot

Figure D.32: *10_37 Treatment*

D.2.5 10_38

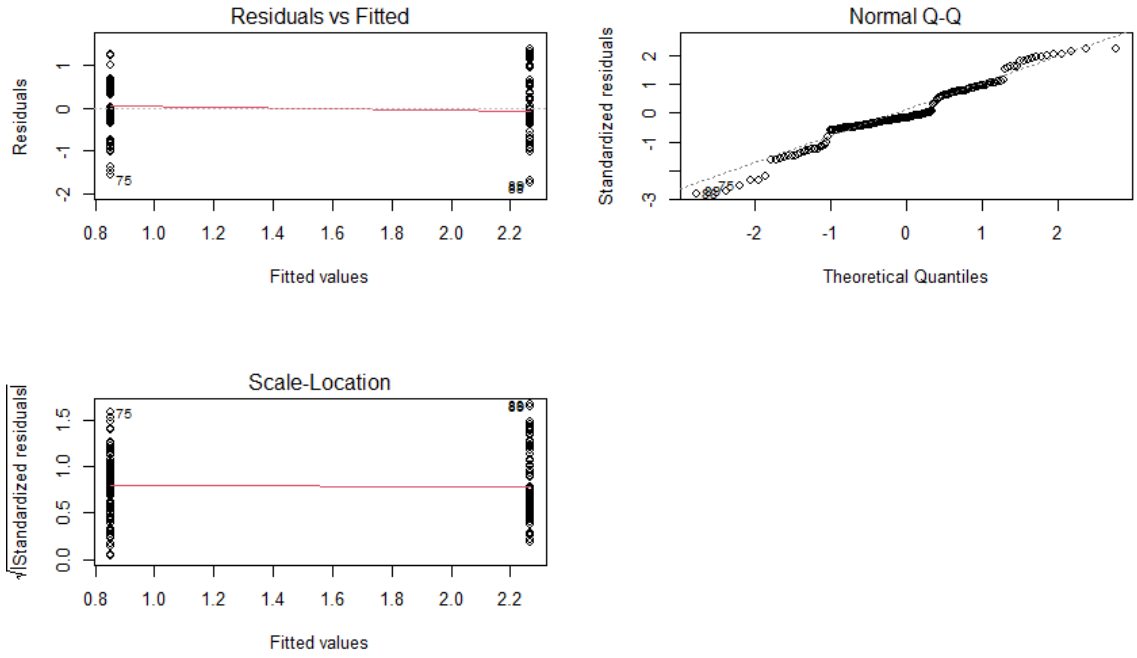

(a) ANOVA assumptions

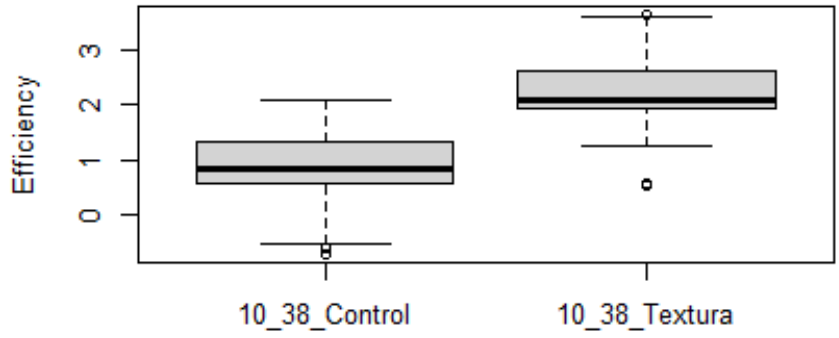

(b) Boxplot

Figure D.33: *10_38 Treatment*

D.2.6 10_41

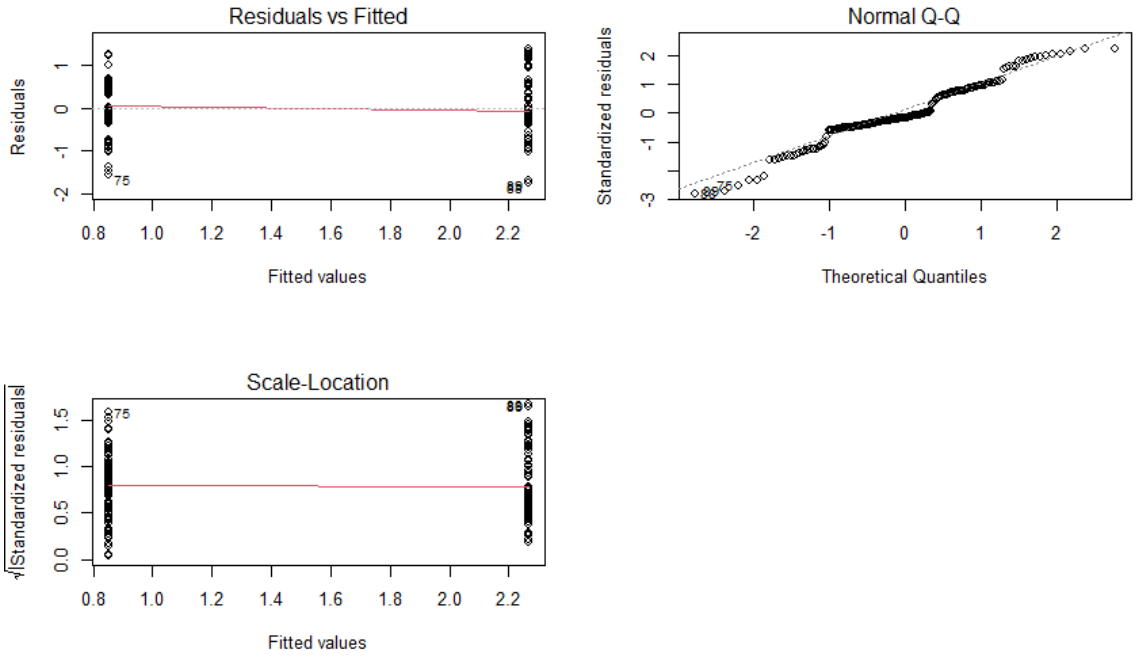

(a) ANOVA assumptions

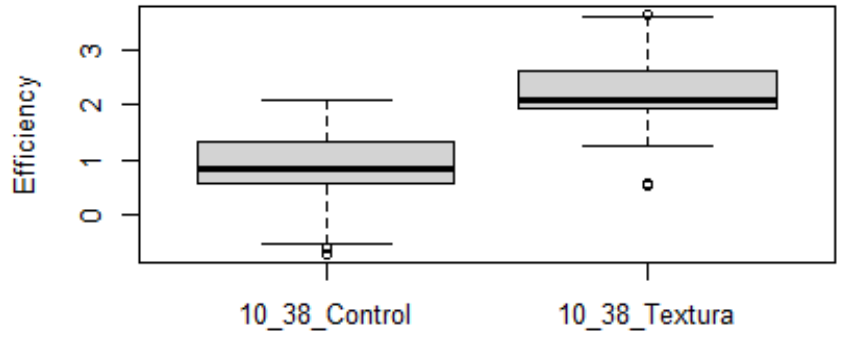

(b) Boxplot

Figure D.34: *10_38 Treatment*

D.2.7 10_41

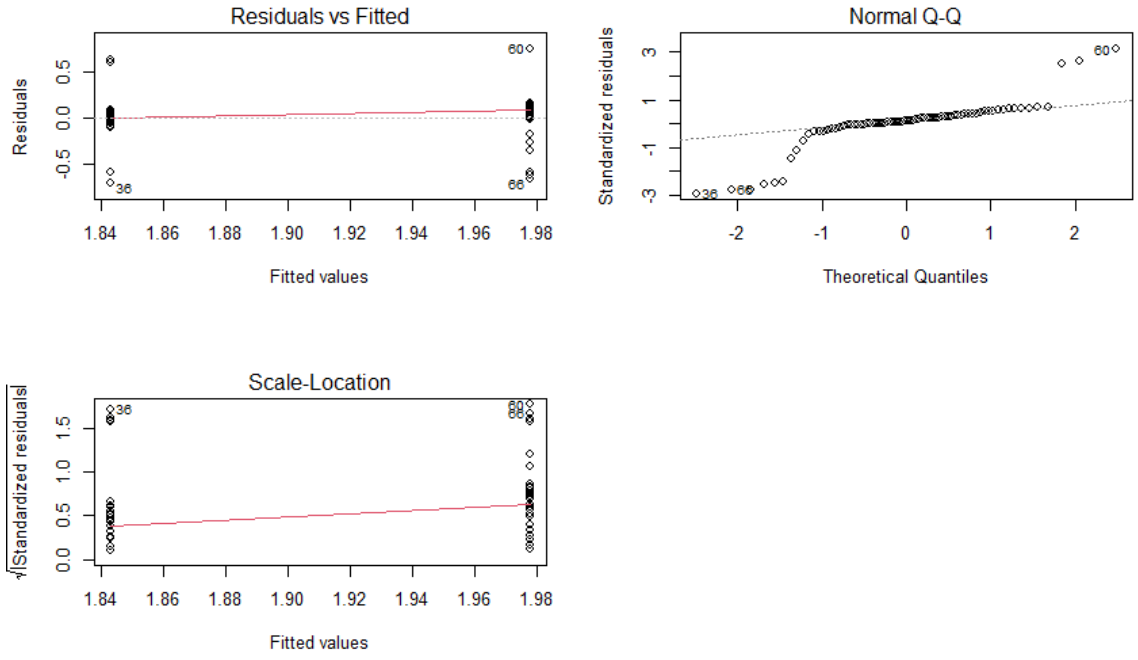

(a) ANOVA assumptions

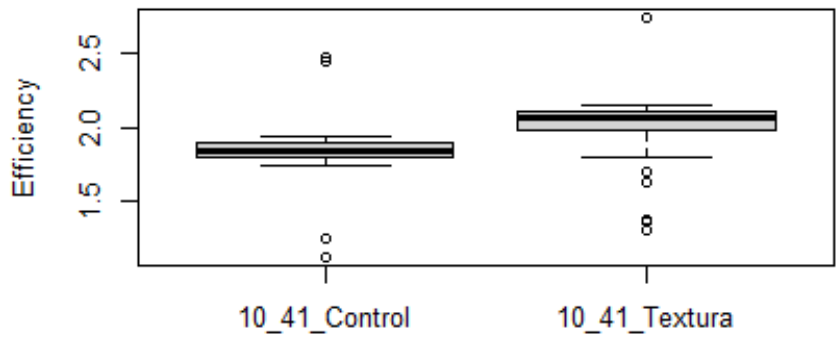

(b) Boxplot

Figure D.35: *10_41 Treatment*

D.2.8 10_47

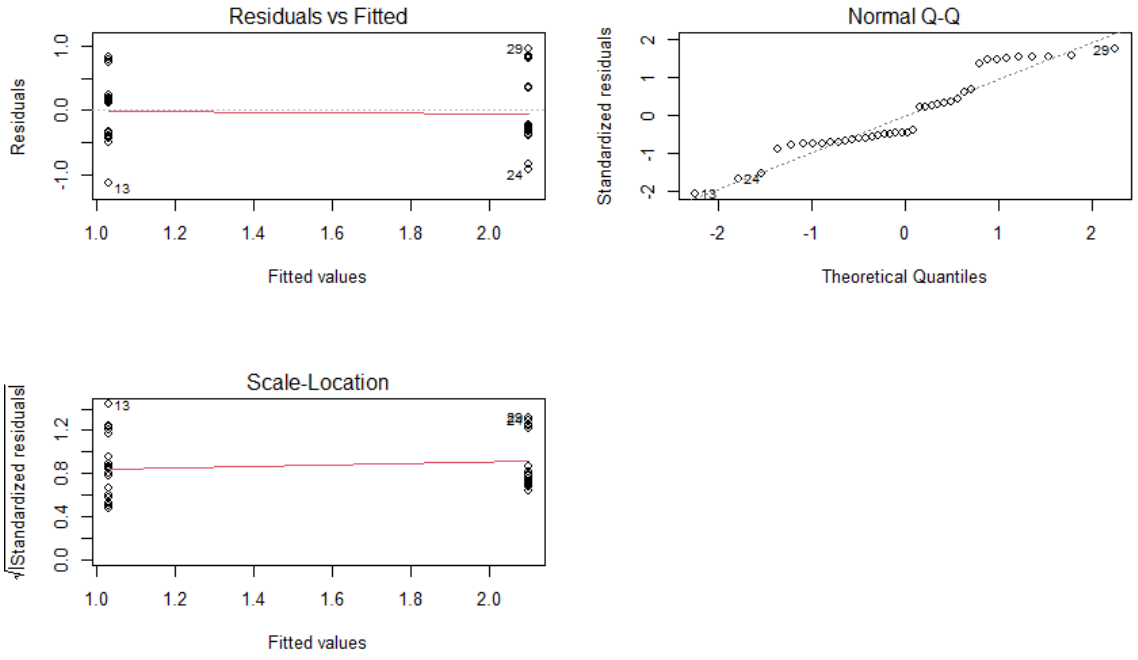

(a) ANOVA assumptions

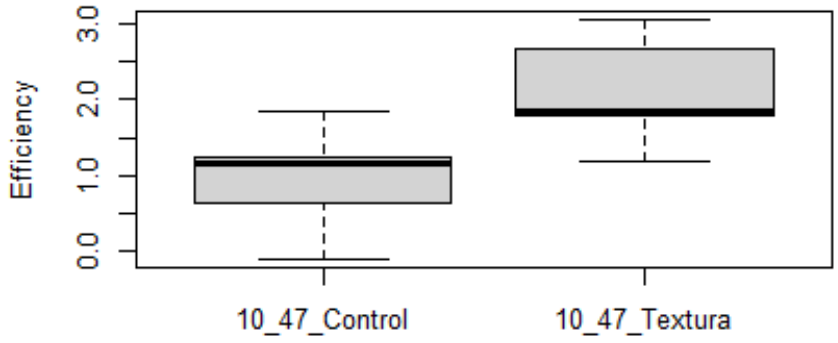

(b) Boxplot

Figure D.36: *10_47 Treatment*

D.2.9 11_05

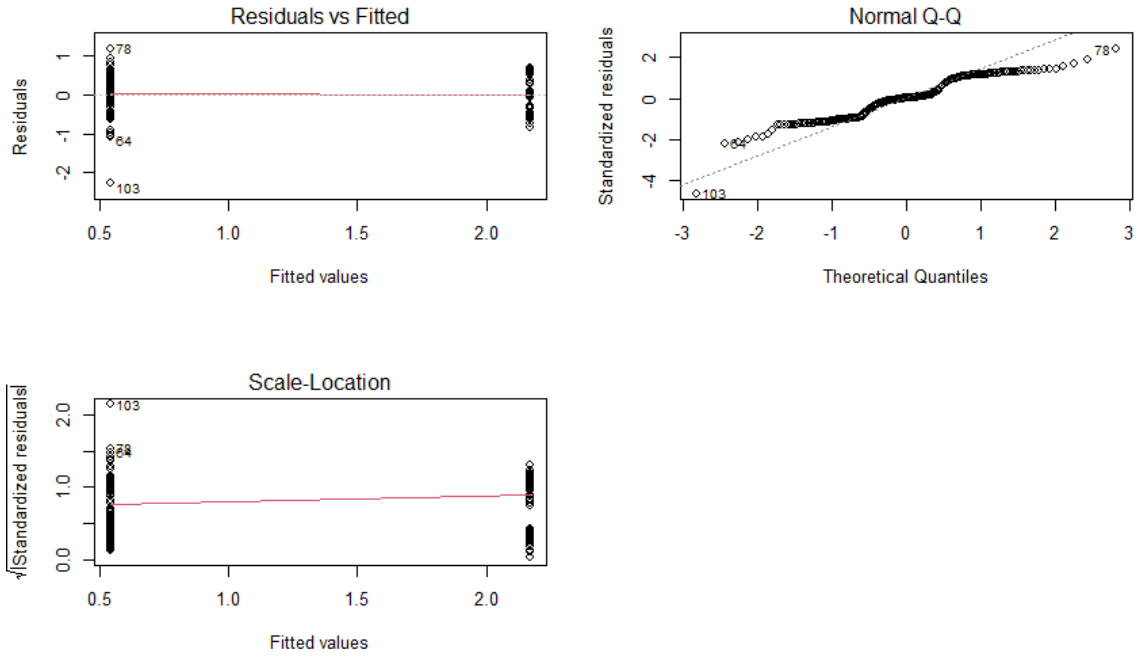

(a) ANOVA assumptions

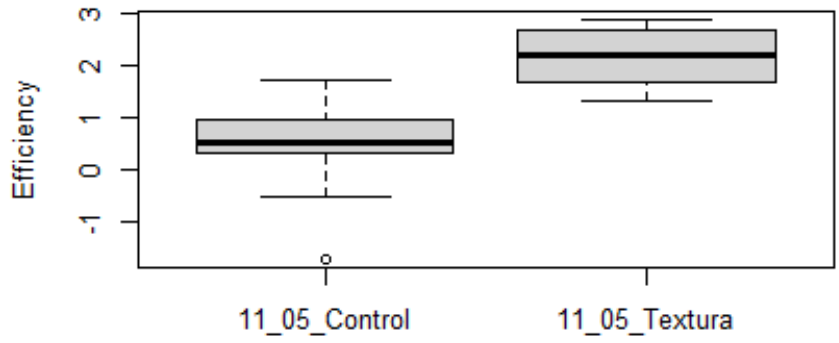

(b) Boxplot

Figure D.37: *11_05 Treatment*

D.2.10 11_08

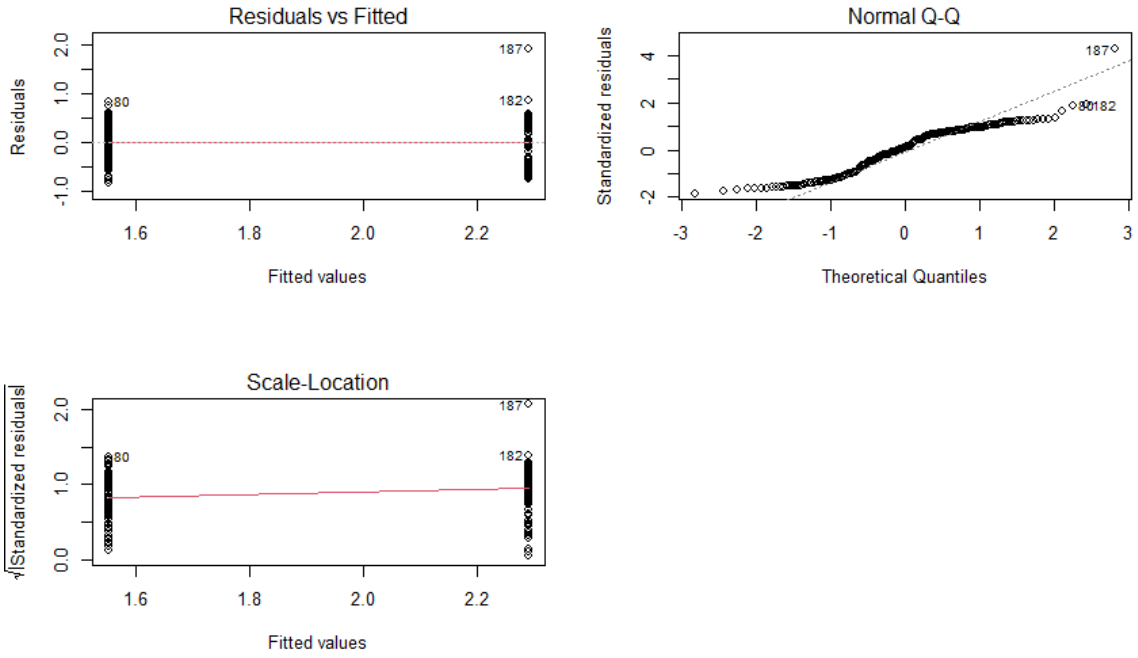

(a) ANOVA assumptions

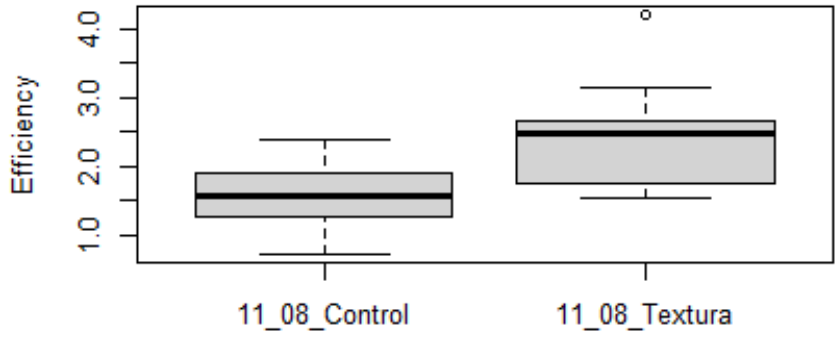

(b) Boxplot

Figure D.38: *11_08 Treatment*

D.2.11 11_09

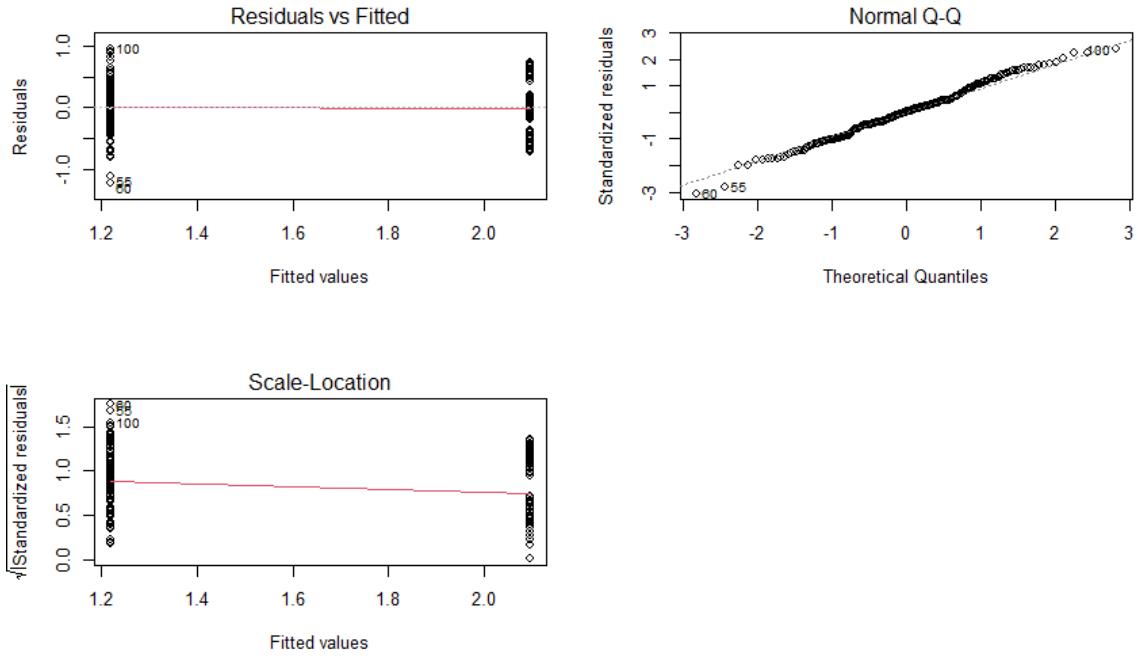

(a) ANOVA assumptions

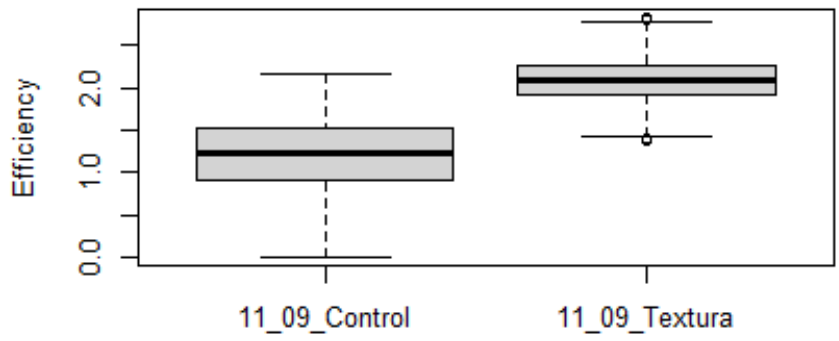

(b) Boxplot

Figure D.39: *11_09 Treatment*

D.2.12 11_11

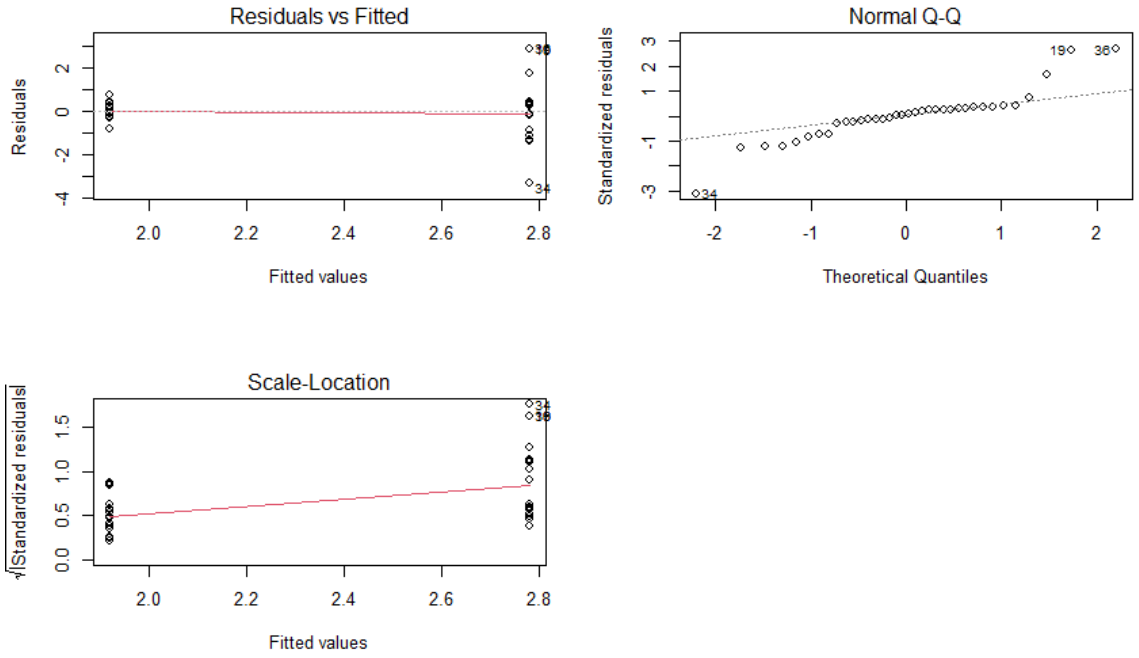

(a) ANOVA assumptions

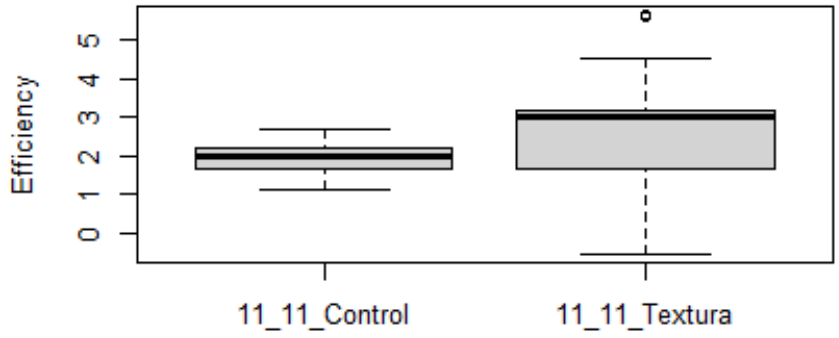

(b) Boxplot

Figure D.40: *11_11 Treatment*

D.2.13 11_16

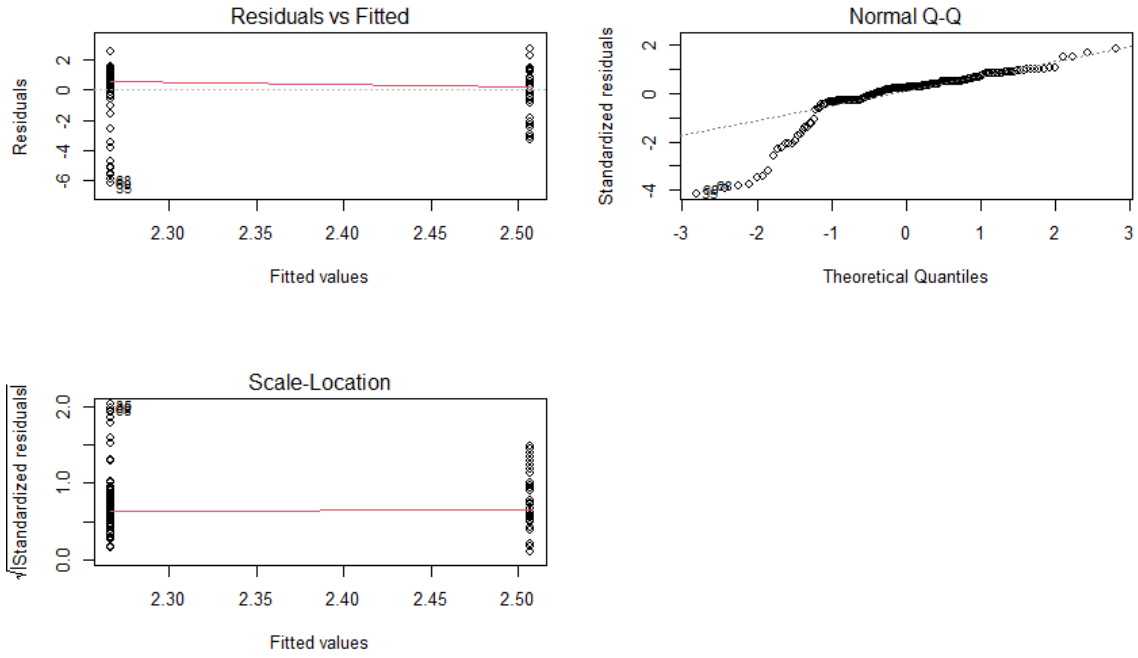

(a) ANOVA assumptions

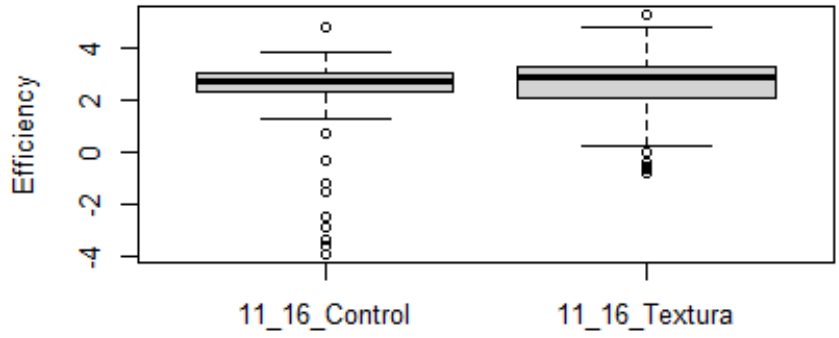

(b) Boxplot

Figure D.41: *11_16 Treatment*

D.2.14 11_21

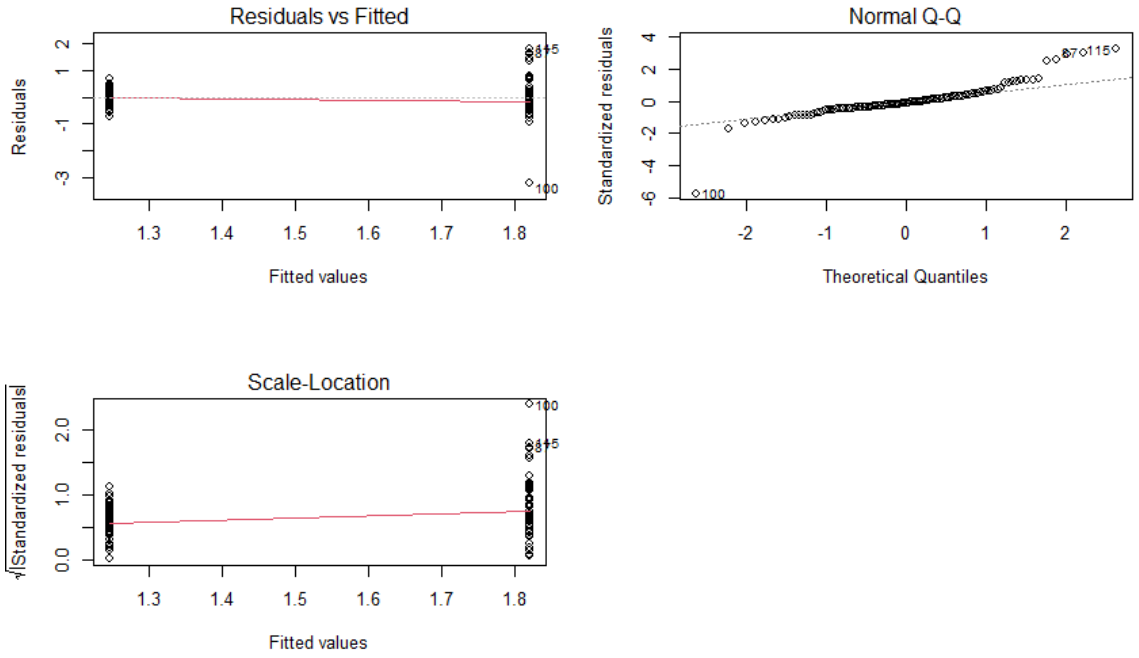

(a) ANOVA assumptions

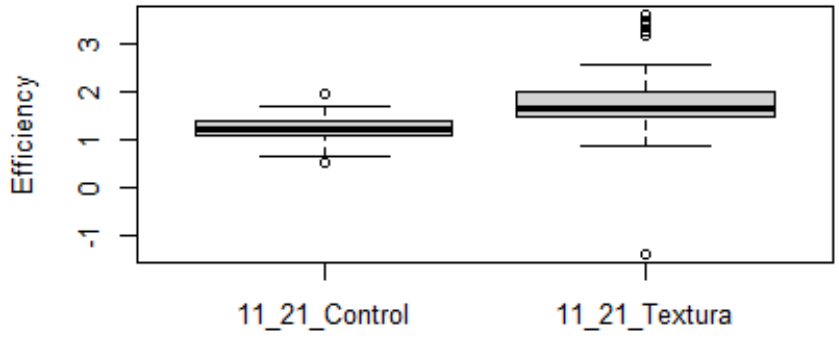

(b) Boxplot

Figure D.42: *11_21 Treatment*

D.2.15 11_22

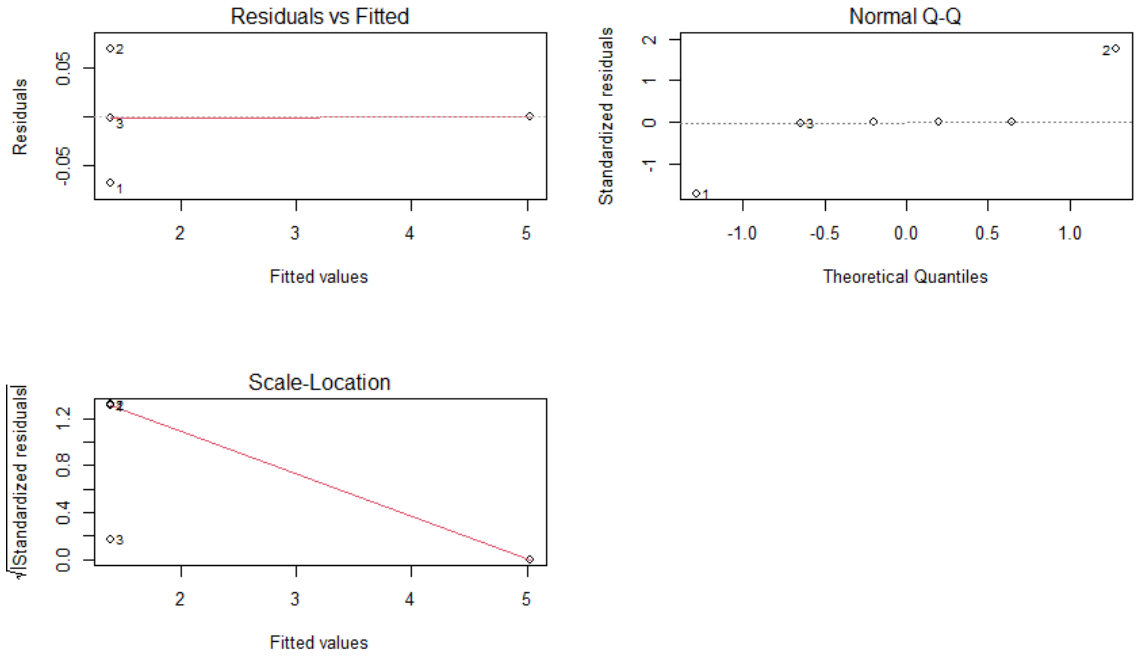

(a) ANOVA assumptions

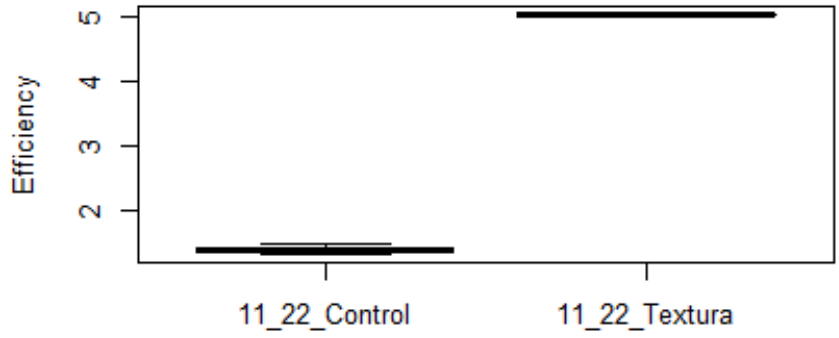

(b) Boxplot

Figure D.43: *11_22 Treatment*

D.2.16 11_25

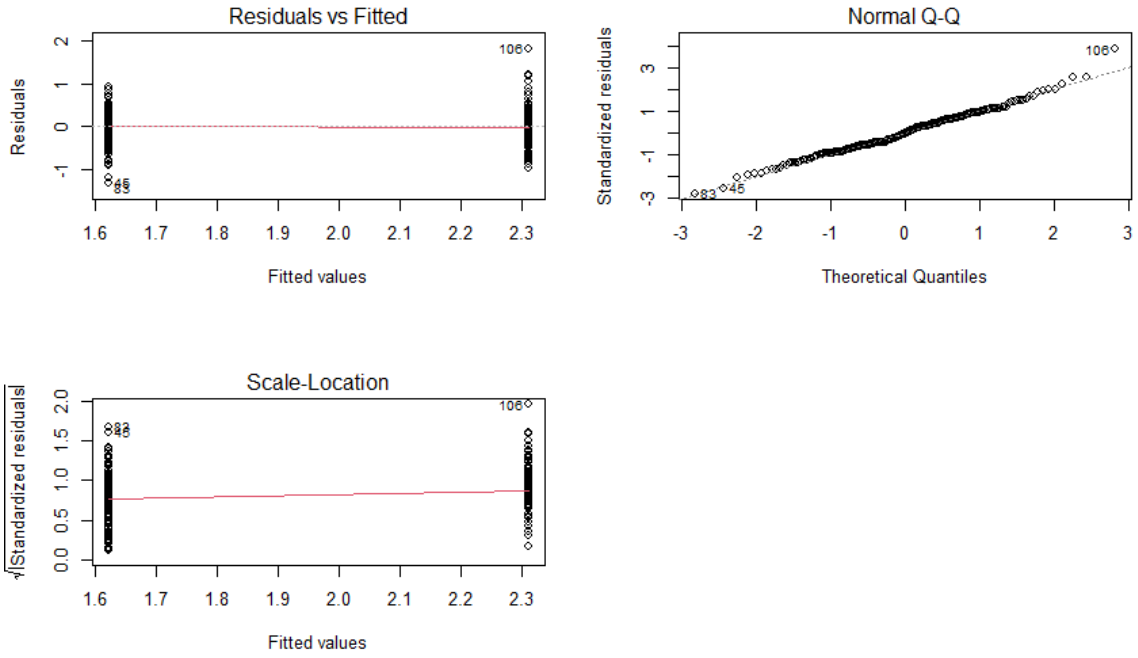

(a) ANOVA assumptions

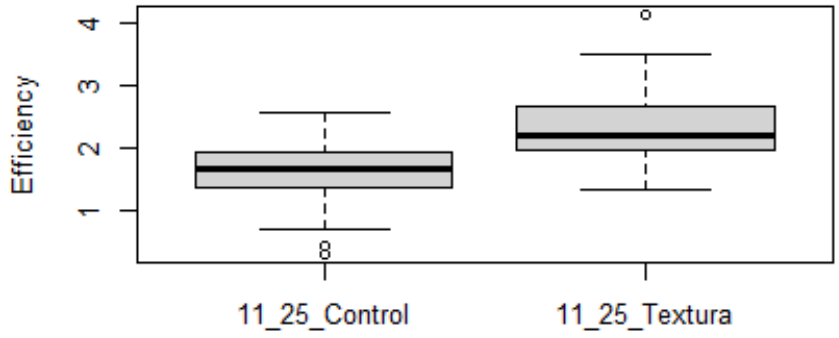

(b) Boxplot

Figure D.44: *11_25 Treatment*

D.2.17 12_31

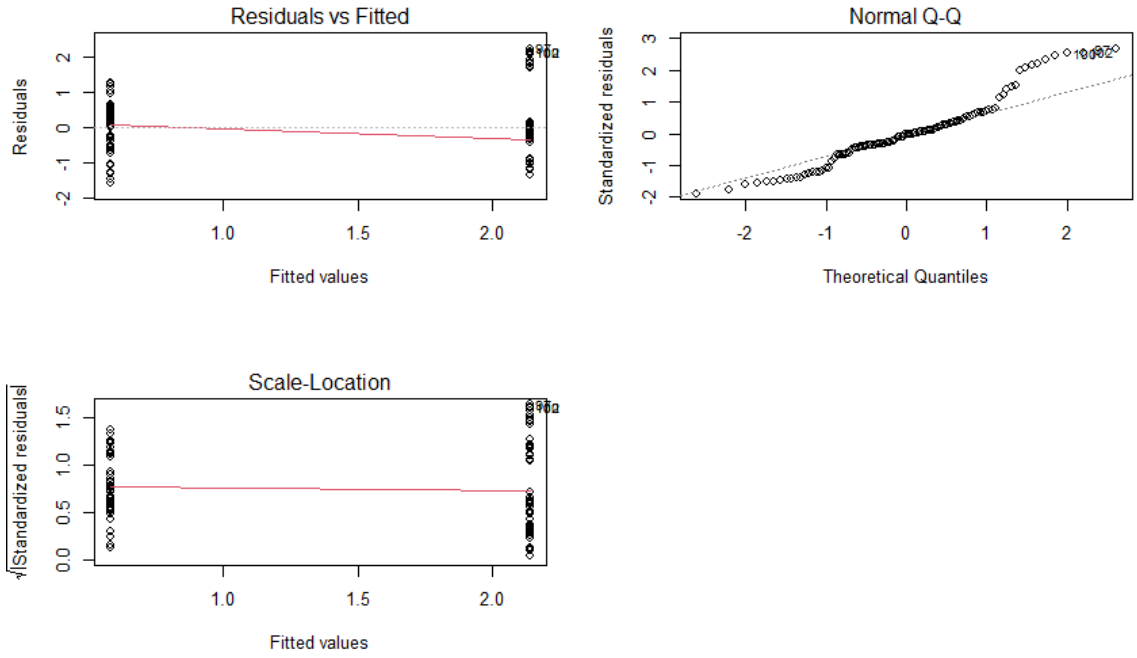

(a) ANOVA assumptions

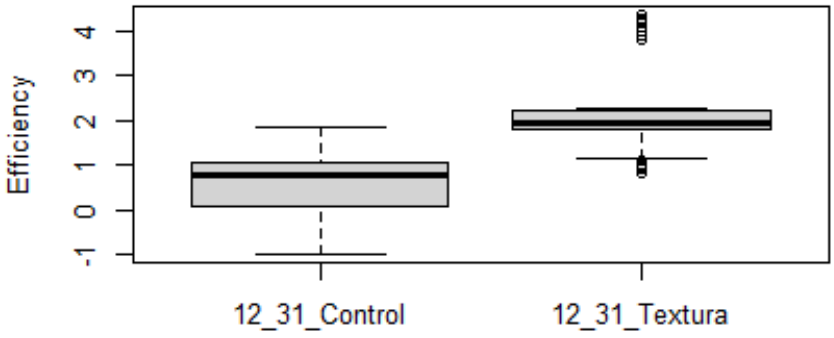

(b) Boxplot

Figure D.45: *12_31 Treatment*

D.2.18 13_18

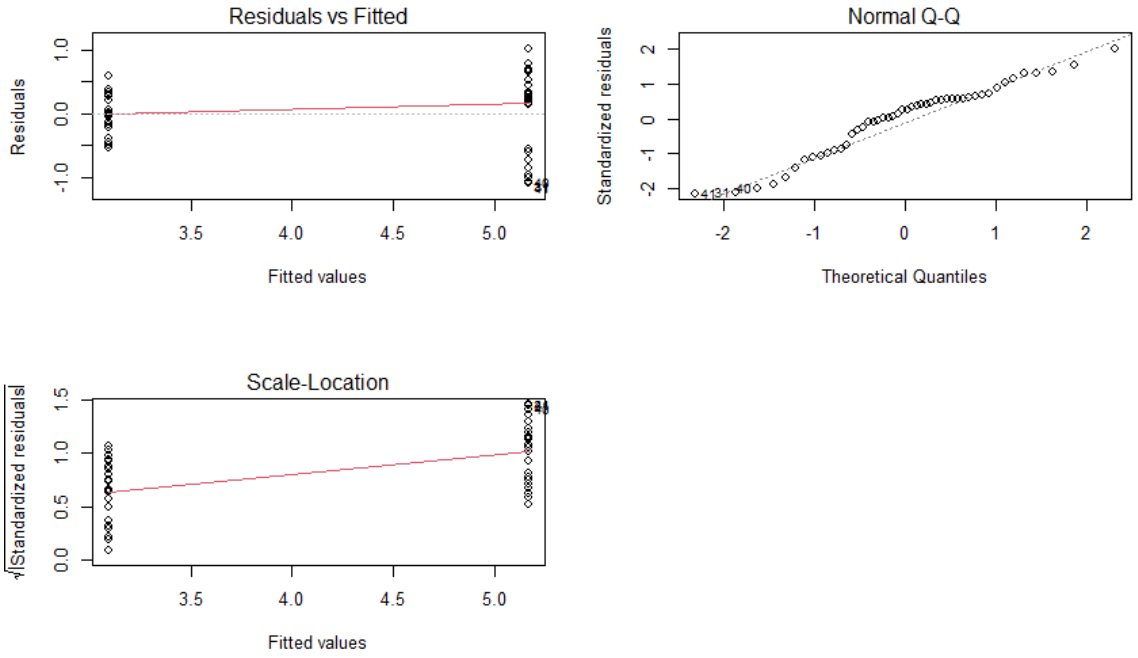

(a) ANOVA assumptions

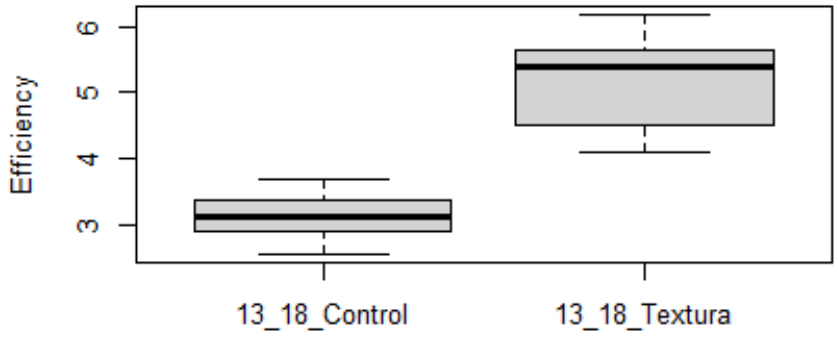

(b) Boxplot

Figure D.46: *13_18 Treatment*

D.2.19 13_19

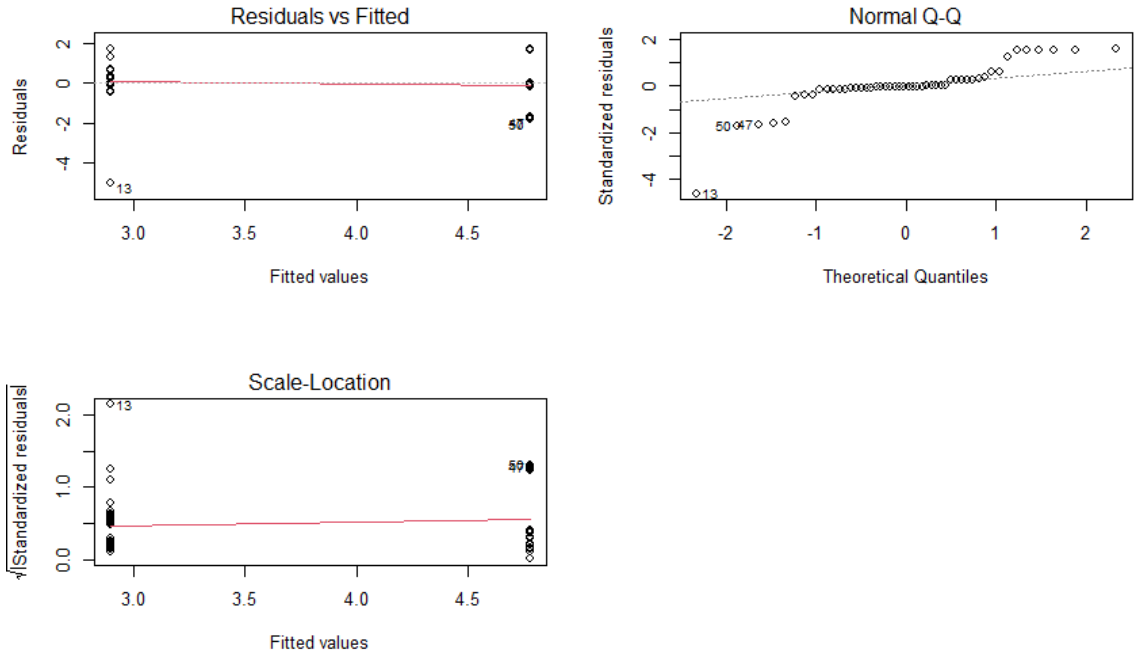

(a) ANOVA assumptions

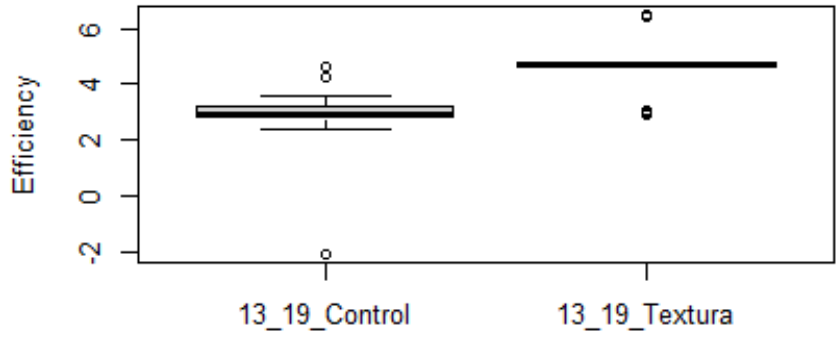

(b) Boxplot

Figure D.47: *13_19 Treatment*

D.2.20 13_27

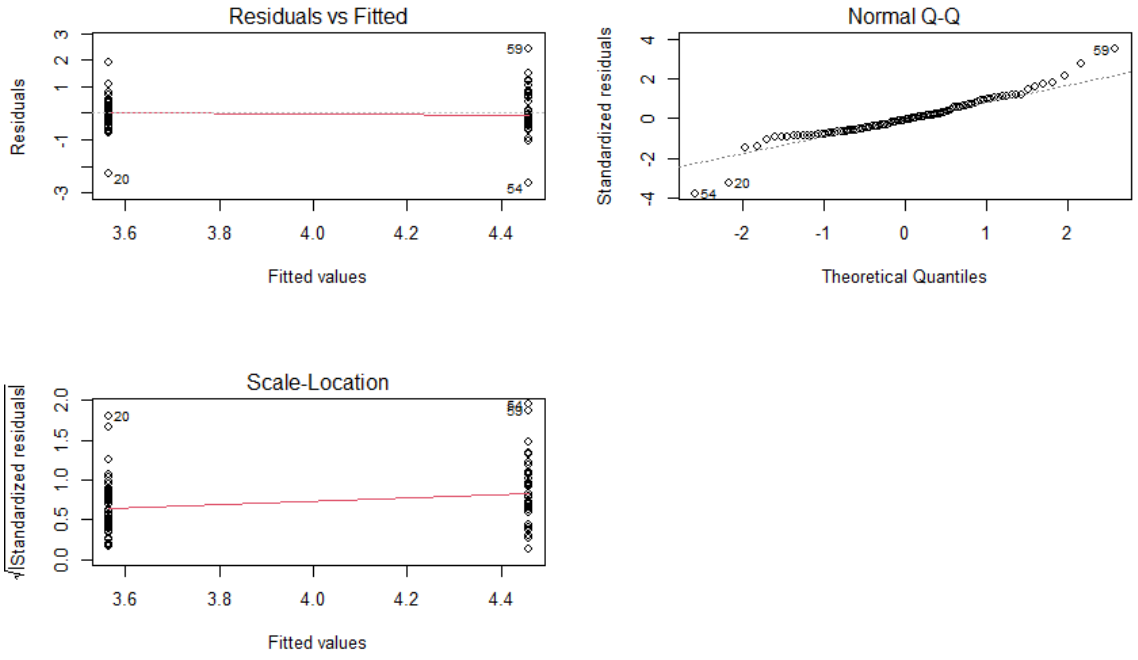

(a) ANOVA assumptions

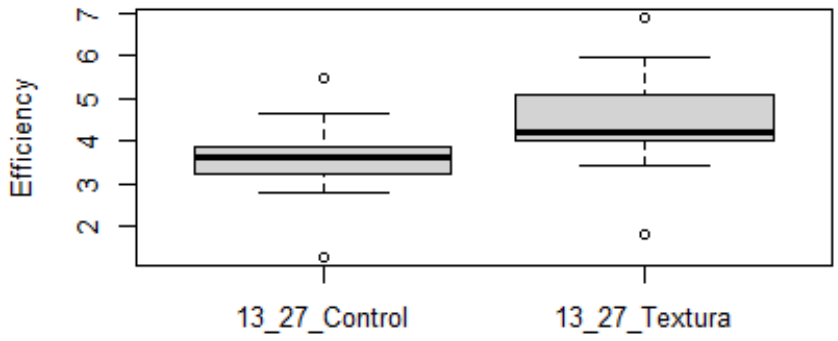

(b) Boxplot

Figure D.48: *13_27 Treatment*

D.2.21 13_30

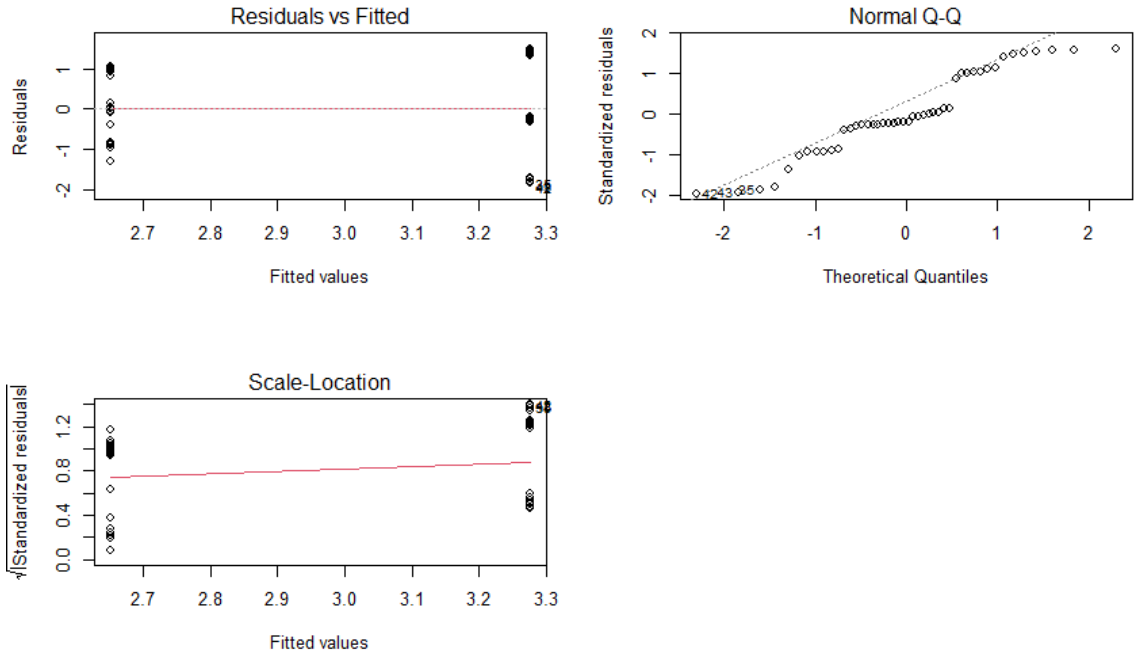

(a) ANOVA assumptions

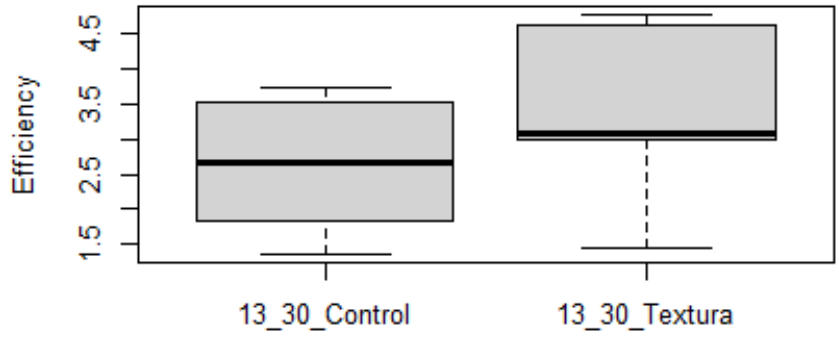

(b) Boxplot

Figure D.49: *13_30 Treatment*

D.2.22 13_31

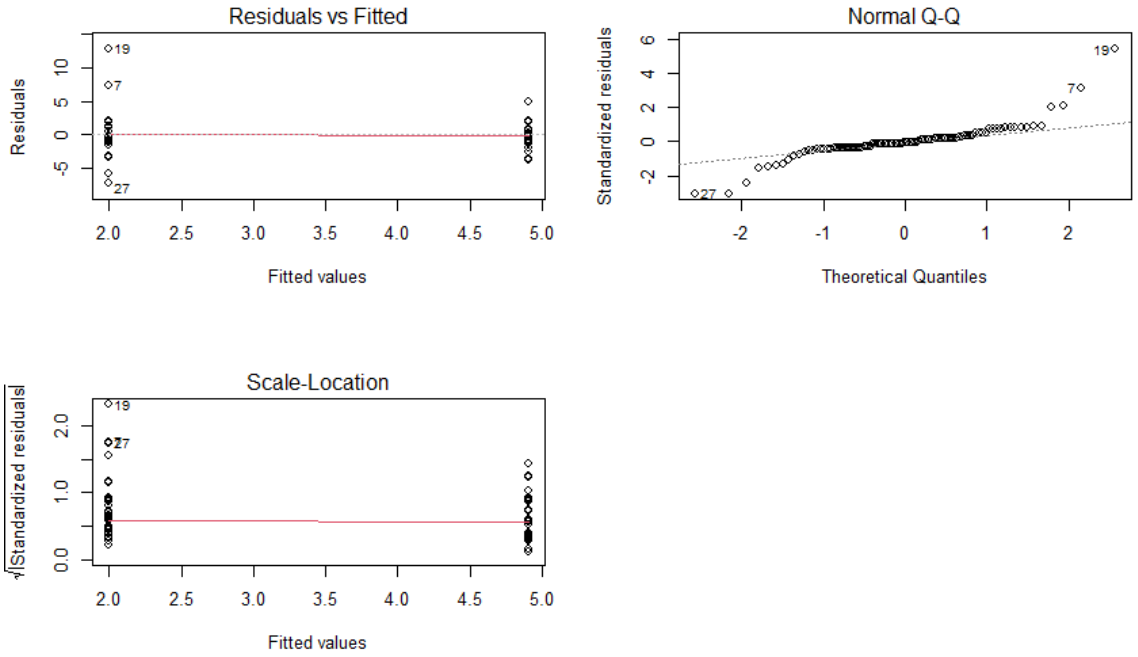

(a) ANOVA assumptions

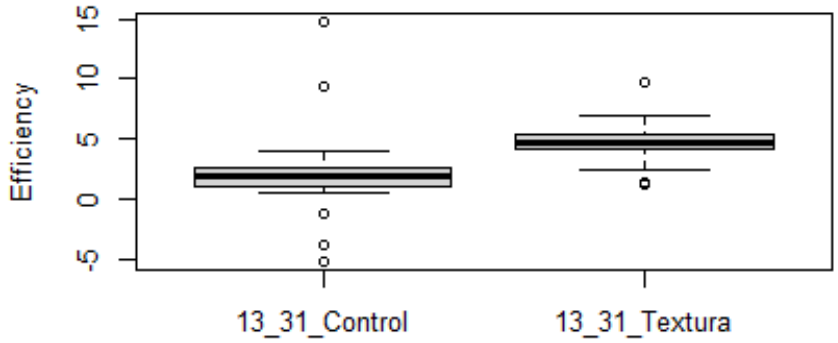

(b) Boxplot

Figure D.50: *13_31 Treatment*